CRANFIELD INSTITUTE OF TECHNOLOGY

SCHOOL OF MECHANICAL ENGINEERING

Ph.D. THESIS

N. MONTAZERIN

EXPERIMENTAL HEAT/MASS TRANSFER STUDIES OF TURBULENT WALL-BOUNDED JETS ASSOCIATED WITH MECHANICALLY VENTILATED ENCLOSURES.

SUPERVISOR

MR. G.P. HAMMOND

MARCH 1986

"Rise up," the Master said, "upon thy feet;
The way is long, and difficult the road,
And now the sun to middle-tierce returns."

Dante Alighieri
The Divine Comedy
Inferno, XXXIV

ABSTRACT

The development and use of an experimental test rig is reported which is capable of modelling two- and three-dimensional wall-bounded air jets. This test rig was primarily produced in order to facilitate the experimental verification of computer codes for calculating convective heat transfer within mechanically-ventilated enclosures. Special attention was therefore given in the design of the rig to heat transfer measurements within such enclosures.

The analogy between heat and mass transfer and the application of the naphthalene sublimation technique are explained. Also use of phase change paints in heat transfer measurements in general, and wall-jets in particular, is discussed and experimentally demonstrated. The boundary conditions for the application of each of the above two methods are then specified. The mass transfer method may be used for the case of a heated plate and a jet at ambient temperature while the phase change paint method is applicable to a heated jet.

Heat/mass transfer studies are carried out for two different geometries. First beneath a plane wall-jet obstructed by a normal flat-plate (Alamdari, Hammond and Montazerin (1986 bound paper)), where the data are compared with the computations of the 'intermediate-level' convection model of Alamdari and Hammond (1982) and the high-level 'elliptic' finite domain flow model of Pun and Spalding (1977). The comparison has been a clear demonstration of the capabilities of the computer codes and has shown that although their results over flat surfaces are in good agreement with the test data, their predictions for jets flowing round corners need further research. Secondly the flow and heat transfer characteristics of a three-dimensional jet parallel to a flat plate has been studied. In this case the flow field and mass transfer are modelled and an equation is finally derived which estimates the average heat transfer over a plate parallel to a bluff-jet for a variety of off-set heights, Reynolds numbers and nozzle aspect ratios and can readily be used by design engineers handling such flows.

ACKNOWLEDGEMENTS

I found working with Mr. G.P. Hammond to be a valuable experience and learnt a lot from his approach towards research work. Help, assistance and encouragement of other SME staff, specially Mr. C.J. Knight and Dr. T.R. Buick is also appreciated.

The bound paper was a collaborative venture between its three authors and my contribution was mainly towards its experimental side. I am grateful for the permission of the other authors to include the paper in this thesis.

Two demonstrations were specially helpful in the early stages of this thesis. First by Mr. T.V. Jones from Oxford University on the application of the phase change paint to heat transfer measurements and then by Messers John Ward and Neville Yeo from the Open University in Wales on the thin-film naphthalene spray. Many thanks for their cooperation.

I am also grateful to the Cranfield Institute of Technology for making this work financially possible.

LIST OF CONTENTS

****

BOUND PAPER

HEAT/MASS TRANSFER BENEATH A TWO-DIMENSIONAL WALL-JET DEFLECTED BY A NORMAL, FLAT-PLATE OBSTRUCTION

LIST OF FIGURES

NOMENCLATURE

A =Slot area

A_n =area sprayed by naphthalene.

b_u =Two-dimensional wall-jet: Cross-stream distance from the wall to the point where: $u/u_m=0.5$.

b_y =Three-dimensional jet: Cross-stream distance from the wall-to the point above the jet centre-line where: $u/u_m=0.5$

b_z =Three-dimensional jet: Cross-stream distance in the lateral direction from jet centre-line and along the peak velocity line to the point where: $u/u_m=0.5$.

b' =Mass transfer coefficient.

B =Slot length.

c_p =Specific heat.

C_v =Vapour concentration.

h =Heat transfer coefficient.

k =Thermal conductivity.

l =Slab thickness.

m =Mass of naphthalene sprayed.

M =Momentum flux.

p_n =Naphthalene partial pressure.

q =Heat transfer per unit area.

R_n =Gas constant for naphthalene vapour.

S =Slot width.

t =time

T =Temperature.

T_n =Naphthalene temperature.

T_o =Initial or ambient temperature.

T_{air} =Local air temperature.

T_m =Temperature at the peak of the temperature profile.

T_s =Local surface temperature.

u =Velocity.

u_m =Local maximum velocity.

u_{mo} =Maximum velocity over the centre-plane

u_e =Slot exit velocity.

u_τ =friction velocity,

ω_x =Uncertainty in the value of x.

x_o =Virtual origin of the jet.

x_r =Distance between the nozzle and the jet reattachment point.

x,y,z =Coordinate directions.

x' =Coordinate for heat penetration.

y_m =Position of the maximum velocity

y_{mo} =Position of the maximum velocity over the centre-plane

ϵ =Momentum eddy diffusivity.

ϵ_H =Heat eddy diffusivity.

ϵ_M =Mass eddy diffusivity.

$\mathcal{D}$ =Mass diffusivity.

α =Thermal diffusivity.

δ =Wall-jet thickness.

τ =Shear stress.

ρ =Density.

ν =Kinematic viscosity.

CONSTANTS AND COEFFICIENTS

a =Constant in averaging the error function.

A =Constant for the Jayatillaka's function.

b =Constant for temperature penetration through a material.

B =Log-law additive constant.

C =Wake function coefficient.

j_M =Chilton-Colburn j-factor for mass transfer.

j_H =Chilton-Colburn j-factor for heat transfer.

k_u =Jet peak velocity decay constant.

k_b =Jet spread parameter.

k_θ =Jet peak temperature decay constant.

n =Jet peak velocity and temperature decay exponent.

κ =von Karmen's constant.

DIMENSIONLESS PARAMETERS

AR =Aspect ratio

Bi =Biot modulus, h.l/k

c_f =local skin-friction coeffient, $\tau / \frac{1}{2} \rho u_m^2$

Fo =Fourier modulus, $\alpha t / l^2$

Le =Lewis number, $\alpha / \mathcal{D}$

Le_t =Turbulent Lewis number, ϵ_H / ϵ_M

OH =Dimensionless off-set height.

Pr =Prandtl number, ν / α

Pr_t =Turbulent Prandtl number, ϵ / ϵ_H

Re_m =Local Reynolds number, $u_m y_m / \nu$

Re_s =Slot Reynolds number, $u_e S / \nu$

Sc =Schmidt number, $\nu / \mathcal{D}$

Sc_t =Turbulent Schmidt number, ϵ / ϵ_M

St =Heat transfer Stanton number, $h / \rho u_e c_p$

$\overline{St}$ =Surface-averaged heat transfer Stanton number

St_m =Mass transfer Stanton number, b' / u_e

$\overline{St}_m$ =Surface averaged mass transfer Stanton number

u^+ $=u/u_\tau$

x^* =Dimensionless penetration depth.

y^+ $=u_\tau y / \nu$

δ^+ $=u_\tau \delta / \nu$

Θ =Boundary-Fourier modulus, $(h/k)^2 . \alpha . t$

CHAPTER 1

INTRODUCTION

CHAPTER 1

INTRODUCTION

"The success of the U.K. energy conservation programme is dependent upon reducing consumption in buildings and their associated services, since these take approximately half of the total U.K. prime energy consumption."(SERC Report for 1979 to 1984)

This has been the motive behind large scale research programmes in energy conservation in buildings since the early 1970's. In 1979 the Science and Engineering Research Council set up a Specially Promoted Programme on Energy in Buildings. This was hoped to increase the fundamental understanding of the dynamic thermal behaviour of buildings and develop the methodology for their prediction.

The direction of a section of the research on this topic which has been carried out at Cranfield is reported by Alamdari and Hammond (1982). They mention that since accurate simulation of the thermal performance of buildings can be a tool for estimating the possible energy savings from alternative building designs and conservation measures, consequently the traditional steady state methods must be replaced by computational techniques for dynamic thermal response of the systems. (see also Clarke 1985). They then continue that in such a replacement, the new models are particularly sensitive to the choice of input data such as air-infiltration and internal heat transfer coefficients. For the latter, the data in ASHRAE (1977) is only for the buoyancy driven convection over the surfaces and no data was available for the more realistic situations in the air-conditioning systems where heat transfer alternates between buoyancy driven and forced convection.

This uncertainty in the values for convective heat transfer coefficients in mechanically ventilated rooms, has led Alamdari and Hammond to develop a hierarchy of programs to calculate the heat transfer rates under different thermal conditions and for various geometries as

part of the above mentioned Energy in Buildings project. They present two calculation procedures which they term "intermediate-level" and "higher-level" models respectively. The intermediate-level procedure uses Hammond's wall-jet profile analysis (1982b) together with empirical data for two- or three-dimensional jets, and has been incorporated in a computer code termed Room-CHT (Room Convective Heat Transfer) program. The "higher-level" flow model, in its present state is a modification of the 'elliptic' computer code of Pun and Spalding (1977) to model the flow for two-dimensional mechanically ventilated rooms. A three-dimensional version of this has recently been developed at Cranfield and is described in the thesis of Mohammed (1986). Although there was some experimental data available to validate these programs for simpler cases, this was inadequate for the more complex configurations.

Alamdari et al (1984) used these computer codes to predict the convective heat transfer coefficients within a two-dimensional mechanically ventilated room. The flow under study was emanating from a grille near the ceiling and then impinged against a backward facing wall. Although the predicted heat transfer coefficients by the two computer codes, averaged along different walls, were usually in good agreement, deviations were evident in the local values after any deflection (figure 1-1). There is a clear gap in the experimental data available on heat/mass transfer in jet:wall interactions. Such flows are not only common in air-conditioning systems but their application extends as far as furnaces and gas-turbines.

The work detailed in this thesis aims at advancing the capability of producing experimental data so that theoretical predictions, such as those mentioned above, can be tested at critical geometries and configurations. Chapter 2 is devoted to a study of the present state of research on wall-bounded jets. The literature survey was not directly applicable to the cases under consideration but provided valuable guidelines for designing the rig and also understanding the flow behaviour for new configurations. A multi-purpose test rig has been developed which can be easily used to model different jet and flat plate configurations. Special attention has been given in the design of the rig to the measurement techniques and the application of the mass transfer method (chapter 3).

For over a decade, heat and mass transfer analogy has been used for many different configurations. Chapter 4 outlines the important points of this analogy. Following that it introduces an alternative technique for convective heat transfer measurement which has found much use in recent years. The phase change paint method is complimentary to the mass transfer technique and facilitates heat transfer measurements for boundary

conditions different to what the first method is applied to.

It was earlier explained that a better knowledge of surface heat transfer coefficients in the buildings can assist building thermal modellers to obtain more accurate simulations. As part of such general outlook, Shute(1984) and Apostolou (1985) studied the heat transfer coefficients of some two- and three-dimensional windows. Many air-conditioned rooms use high wall mounted supply grilles placed near the ceiling. Chapter 5 examines three-dimensional off-set jets for which data is reported that may be used to determine the heat transfered between a ceiling (or floor) and an adjacent heated or cooled air supply jet.

The need to test the data generated by the two computer codes in Alamdari et al (1984) with some experimental data, was the typical instigator for this research. The results of a special study on the behaviour of a similar configuration is now presented in a bound paper at the end of this thesis (Alamdari, Hammond and Montazerin (1986)).

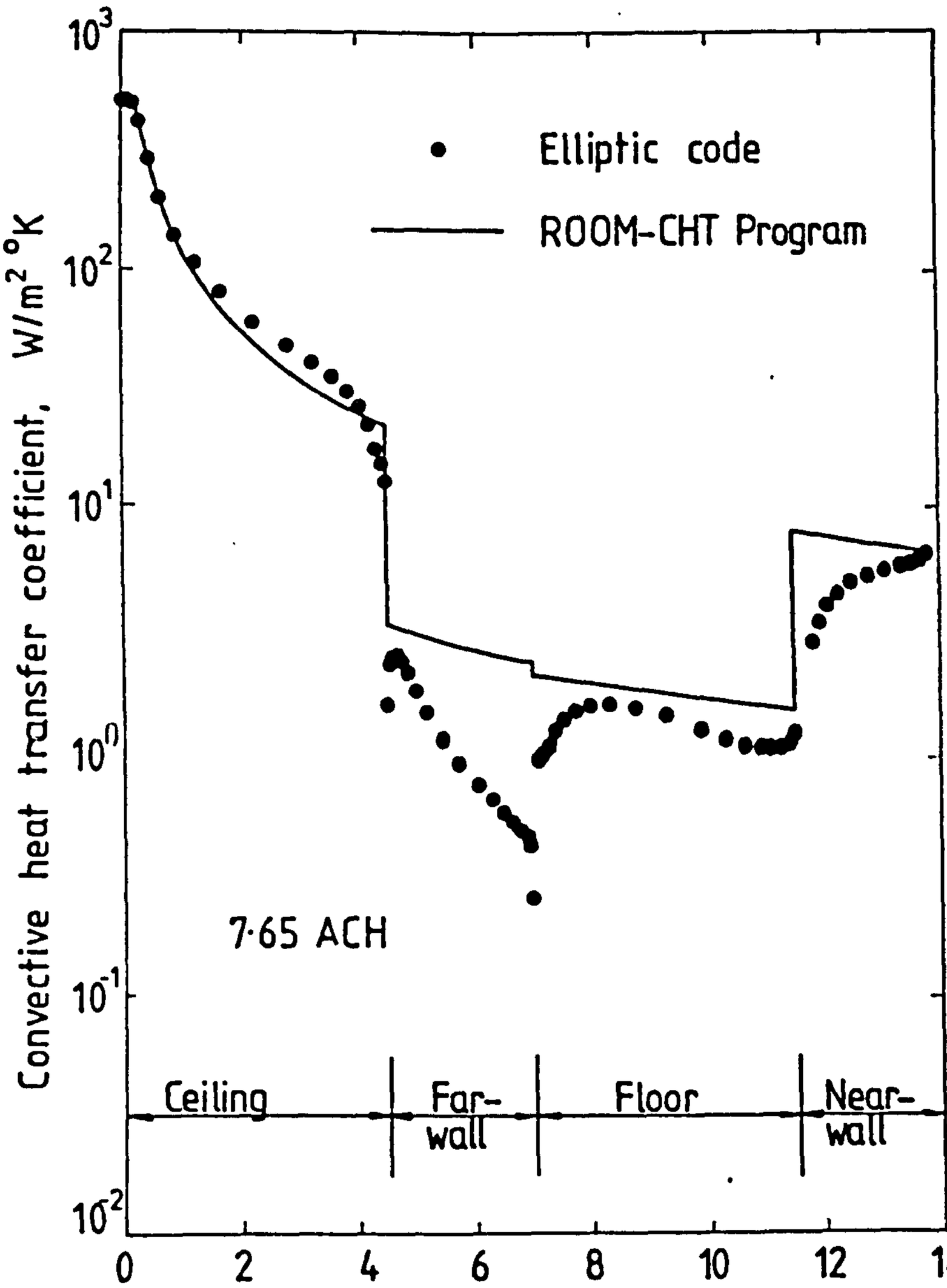

Fig. 1-1 Computed local heat transfer coefficients in mechanically-ventilated rooms. (FROM ALAMDARI ET AL(1984))

CHAPTER 2

JETS PARALLEL TO FLAT BOUNDARIES:LITERATURE REVIEW

CHAPTER 2

JETS PARALLEL TO FLAT BOUNDARIES:LITERATURE REVIEW

2.1 INTRODUCTION

The title to this chapter is taken to imply the case when a solid flat boundary is located in the vicinity of a jet and parallel to the nozzle centre-line. The distance between the wall and the nozzle edge nearest to it, is then referred to as the off-set height. The term wall-jet refers to the particular (limiting) case when the off-set height equals zero. Wall-jets have been studied in both two- and three-dimensional configurations, while only two-dimensional off-set jets appear to have been examined.

A general review of the known research in this field is presented in this chapter to provide some understanding of flow configurations such as impinging wall-jets and three-dimensional off-set jets. These cases are discussed in chapter 5 and the bound paper (Alamdari, Hammond and Montazerin (1986)), where experimental heat/mass transfer studies are reported.

2.2 PLANE WALL-JETS.

Launder and Rodi (1981) defined a plane wall-jet as a shear flow spreading along a flat surface by virtue of some initial momentum. This can happen in a stagnant surrounding or in a moving stream and at any station the stream-wise velocity over some region within the shear flow exceeds that in the external stream.

If the ratio of maximum (or peak) velocity to the free stream velocity for a wall-jet in a moving stream is constant, then the fully-developed jet attains a self-preserving form in which the cross-stream velocity and shear stress profiles are approximately self-similar. Otherwise the wall-jet profiles will vary significantly with streamwise distance, and the jet is termed 'non-similar'. A wall-jet in stagnant surroundings is

therefore self-preserving as the ratio of the peak to free-stream velocities is constant and infinite. Figure 2-1 shows the flow situation for a two-dimensional wall-jet on a plane surface.

The research on the velocity field development of the two-dimensional wall-jet in still air has been independently reviewed by Launder and Rodi (1981) and Hammond (1982a). Launder and Rodi noticed that the lack of two-dimensionality in some experiments was the cause of a significant momentum loss which rendered some of the data sets invalid and thus only 15 papers could be included in their comparison.

Both reviews examined the growth of the jet half-width and found identical mean values, although with rather different standard deviations in the data. Hammond presented this data in the form:

$$\frac{b_u}{s} = k_b \left(\frac{x}{s} + \frac{x_o}{s} \right) \qquad (2-1)$$

where b_u is the velocity half width, x_o is the position of the jet origin and k_b=0.073 for both studies, and Hammond suggested x_o/s=8.1. Hammond further suggests a formula for the local maximum velocity decay as:

$$\frac{u_m}{u_e} = k_u \left(\frac{x}{s} \right)^n \qquad (2-2)$$

where k_u=3.73 and the exponent n=-0.5. This implies a velocity decay that is marginally less rapid than that indicated by the data plotted by Launder and Rodi (see figure 2-2). Hammond also offers an approximate formula for the development of the local Reynolds number as a function of the slot Reynolds number and the downstream distance. This was obtained by combining equations 2-1 and 2-2.

$$Re_m = 0{,}215\ Re_s^{0{,}89} \left(\frac{x}{s} \right)^{0{,}40} \qquad (2-3)$$

A formula for the wall-jet velocity profile was derived by Hammond and this may be presented outside the viscous sublayer in the form:

$$u^+ = \frac{1}{\kappa} \ln y^+ + B + C\omega(y^+/\delta^+) \qquad (2-4)$$

Where coefficients κ, B and C are specified in detail in section 5.4. The wake function (ω) was selected to be a sine function in the above paper but in a more recent report by the same author (1982b) a polynomial has proved more accurate. The coefficients to this function were derived from the complex boundary conditions of the

wall-jet.

Finding a general formula for the skin-friction variation has involved many difficulties. Launder and Rodi discuss the measurements obtained by different researchers using a variety of measurement techniques, and the agreement is generally poor. Hammond (1982a), used profile analysis (above) to develop an optimum log-law for the local skin friction, which he subsequently presented in an approximate form :

$$c_f = 1{,}38\,(Re_s)^{-0{,}23}\,\left(\frac{x}{S}\right)^{-1{,}10} \qquad (2\_5)$$

This was obtained using equations 2-1 and 2-2 and takes into account the initial jet values which as shown by Nizou (1981) have a considerable effect on the skin-friction downstream.

The bound paper, (Alamdari et al (1986)), draws attention to the importance of the thermal boundary conditions on heat transfer beneath wall-jets. For temperature field and heat transfer studies in a wall-jet, two limiting cases have been looked at in different studies. The case where a heated jet is blown parallel to a wall at the ambient temperature, and the heated wall where an ambient jet is blown parallel to a heated wall. In real cases it is likely that all three (the jet, wall and ambient) have different temperatures. This is so, for example, in supply jets emitted into air-conditioned rooms.

Seban and Back (1961) obtained data on the wall-jet temperature profile and heat transfer which is commonly cited. They measured the temperature profiles for a heated jet and an adiabatic plate while the heat transfer tests were for a heated plate and an ambient jet.

No turbulence measurements were made in the present study, and so the interested reader is referred to the review by Launder and Rodi and to a more recent paper by Dakos et al (1984), where the turbulence characteristics of both the plane and curved wall-jets are reported.

2.3 TWO-DIMENSIONAL OFF-SET JETS

Bourque and Newman (1960) were the pioneers in the off-set slot jet studies. They reported that once a two-dimensional jet of air is blown near a solid boundary, the jet entrainment is less on the boundary side and this causes lower pressures which in turn pulls the jet towards the solid boundary and thereby causing reattachment. This phenomena has in recent years become known as Chilowsky effect (Hammond et al (1977)) (figure 2-3).

Bourque and Newman stated that the flow was independent of both the length of the plate and the Reynolds number once these parameters were sufficiently large. Their experimental work largly centred on the measurements of static pressures on the surfaces and the velocity fields for both off-set and inclined jets. Their work on the latter type showed that at inclination angles larger than 45, jets blowing away from the wall may not reattach. This criteria was used in the design of the present test rig(chapter 3).

Kumada et al(1973) carried out some mass transfer measurements beneath a two-dimensional off-set jet. Their data clearly displayed a peak in the local mass transfer rate at a position some distance away from the nozzle. This was attributed to the reattachment of the jet to the flat plate caused by the Chilowsky-effect. An increase in the off-set height clearly reduced the local mass transfer and moved the reattachment point further down-stream. Their results are presented in terms of the mass transfer Sherwood numbers, and no heat/mass transfer analogy was used.

Parameswaran and Alpay(1975) showed the similarity between the off-set jet after reattachment and a plane wall-jet. They suggested that the reattachment point is related to the off-set height by the formula:

$$x_r/S = 0.332(OH) - 0.077(OH)^2 + 0.0169(OH)^3$$

which was shown to be in good agreement with Borque and Newman's data. The slope of the half-width spread rate of the wall-jet following the reattachment point was shown to be 0.066 which is marginally lower than the average value presented earlier in this chapter (see equation 2-1). The decay of the maximum velocity for different off-set heights was shown to behave in a similar fashion to the plane wall-jet but the power law had a marginally higher index of -0.545 rather than -0.5.

Two papers by Hoch and Jiji (1981a and b) give more information regarding the two-dimensional off-set jet and provide some calculation procedures which the interested reader is referred to them.

2.4 THREE-DIMENSIONAL WALL-JETS.

Sforza and Herbst (1969) were the first researchers to report studies on a three-dimensional wall-jet. A practice which they initiated, and which has become well accepted, was to divide the flow field into three major areas (figure 2-4).

First is the Potential Core(PC) region where the flow has a constant maximum velocity equal or very close to the jet exit velocity. This is followed by a Characteristic Decay Region (CDR) where the mixing from near sides of the aperture have joined together in the maximum velocity layer but the mixing from the other two sides are further apart and have not permeated into the entire jet. In the third region, known as the Radial Type Decay (RTD) region, the mixing from all boundaries have joined the maximum velocity line which from then on decays like that of a radial wall-jet generated from normal impingment of a jet on a plate.

One major problem with the experimental configuration employed by Sforza and Herbst was that the jet emanated from a sharp orifice instead of a channel. This caused the formation of horse-shoe vortices and a saddle shape velocity profile for the jet spread in the lateral direction. Some effects of channelling the jet prior to the nozzle exit have been studied in more detail by Sfeir (1979).

Rajaratnam (1976) has reviewed the research undertaken on three-dimensional wall-jets up to the early 1970's. In his account the jets issuing from nozzles with aspect ratios in the region of one are referred to as bluff-jets. His own detailed studies on three-dimensional wall-jets were originally reported in Rajaratnam and Pani (1974) where the velocity field and skin-friction measurements are presented for different exit nozzle geometries. These are shown in figures 2-5 and 2-6 and are useful tools for validating other such jets. The local skin-friction for the bluff wall-jet was approximately 0.0065 after an initial rise and a similar value was found by Narain (1975). Narain used momentum integral techniques to investigate the flow development of three-dimensional wall-jets emanating from bluff orifices.

The centre-line maximum velocity decay may be closely approximated by the relatioship: (Hammond, private communication)

$$\frac{u_m}{u_{slot}} = \left[1+\left(\frac{7.7\sqrt{A}}{x}\right)^{-6}\right]^{-1/6} \qquad (2\_7)$$

A review of three-dimensional wall-jets in stagnant surroundings is given by Launder and Rodi (1981). They suggest two linear relationships for the half-width jet spreads in both directions and show that the inverse of the maximum velocity should grow linearly with distance from the orifice. The rate of the spread normal to the wall, is represented by the formula:

$$db_y/dX = 0.048 \pm 0.003$$

which is in good agreement with various experiments. Rajaratnam (1976) estimates this slope as 0.045 which is within the deviation of Launder and Rodi's work. This rate of growth is considerably less than in the case of the two-dimensional wall-jet and is closely associated with the rapid span-wise spread.

The lateral spreading rate does not generally exhibit a self-preserving behaviour before X/S=130 and, after that the span-wise spreading rate lies within the bounds:

$$db_z/dX = 0.26 \pm 0.02$$

This slope is higher than the one predicted by Rajaratnam (0.20), but does not imply a contradiction since, unlike Launder and Rodi, Rajaratnam tried to take the data near the nozzle into account.

A recent development in three-dimensional wall-jet research is reported by Butterman et al(1983). In this work they first solved the integral form of the mass, momentum and energy conservation equations, to analytically predict the downstream wall-jet development, using assumptions for approximate velocity and temperature profiles and coefficients of the entrainment function. The thermal boundary conditions adopted in this work were that of a heated jet blowing on an adiabatic surface. An experimental investigation was also undertaken with nozzle aspect ratios ranging from 0.1 to 1.0 which agreed with the theory and with previous data reported by Rajaratnam and Pani(1974).

Koso and Ohashi (1982) have measured the turbulence intensities in the three-dimensional wall-jets and their work is recommended to the interested reader.

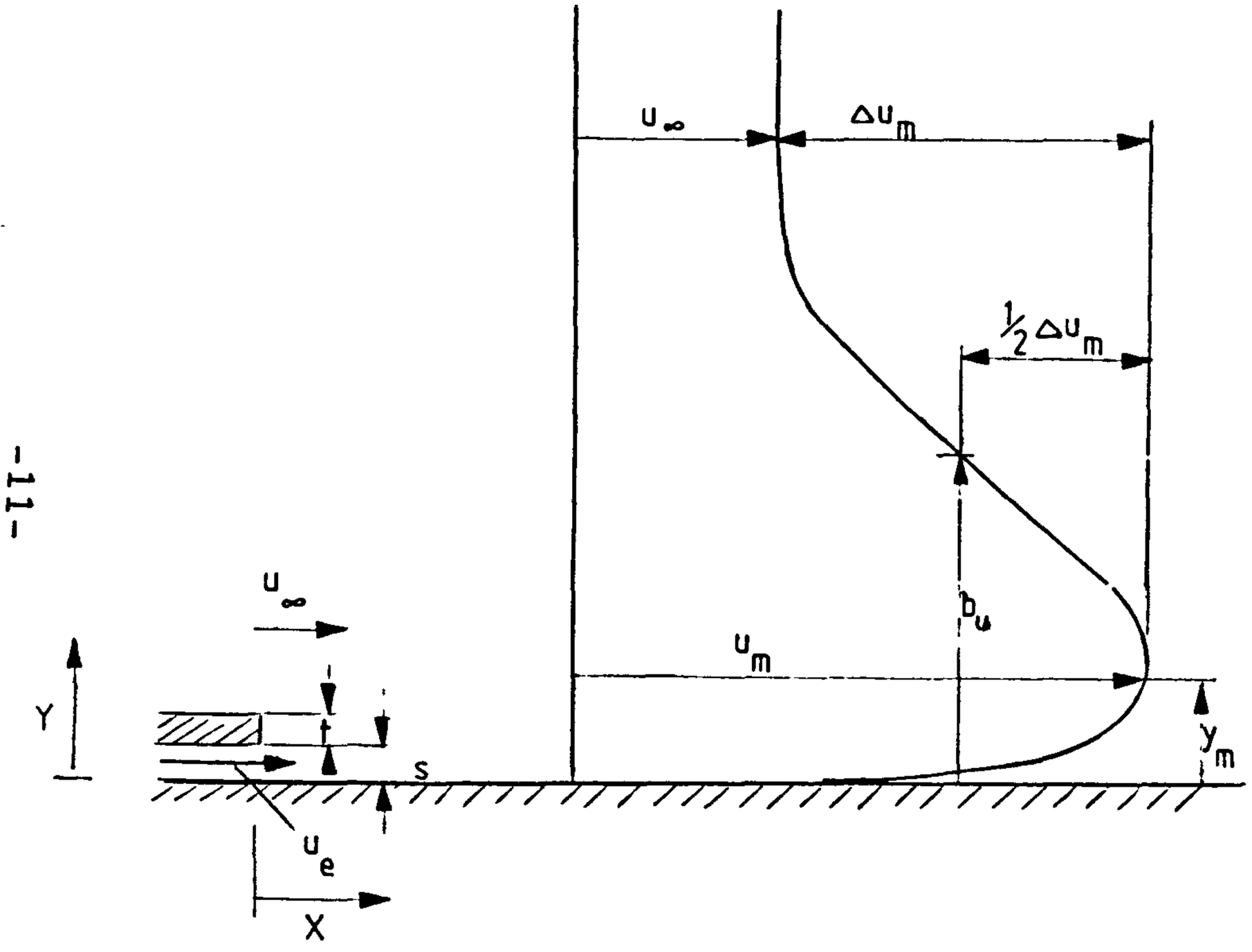

FIGURE 2-1 THE PLANE WALL JET (ADAPTED FROM LAUNDER . RODI «1981-)

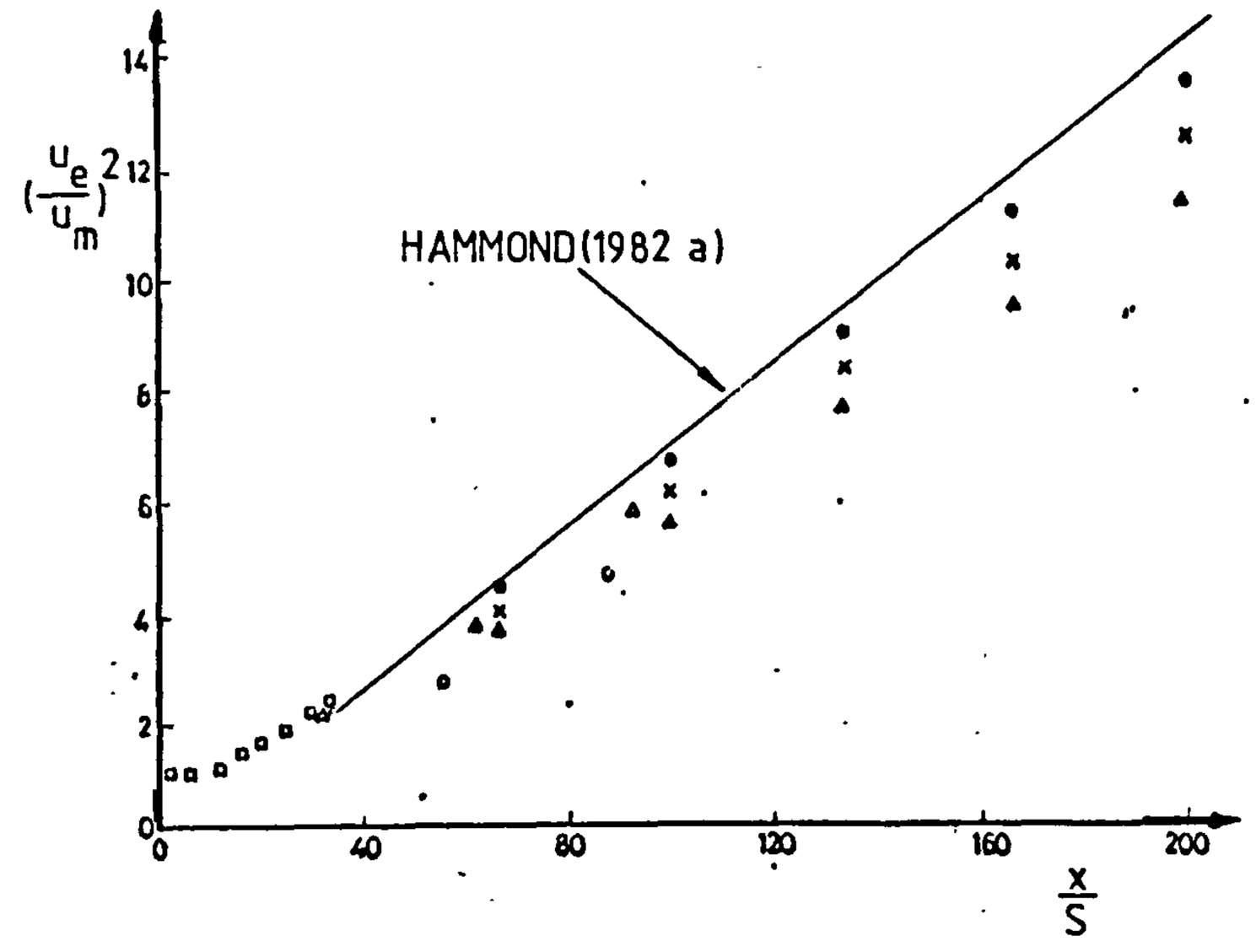

Figure 2_2 Maximum velocity decay for a two_dimensional wall_jet. Hammond's correlation in comparison with a selection of data by Launder & Rodi.

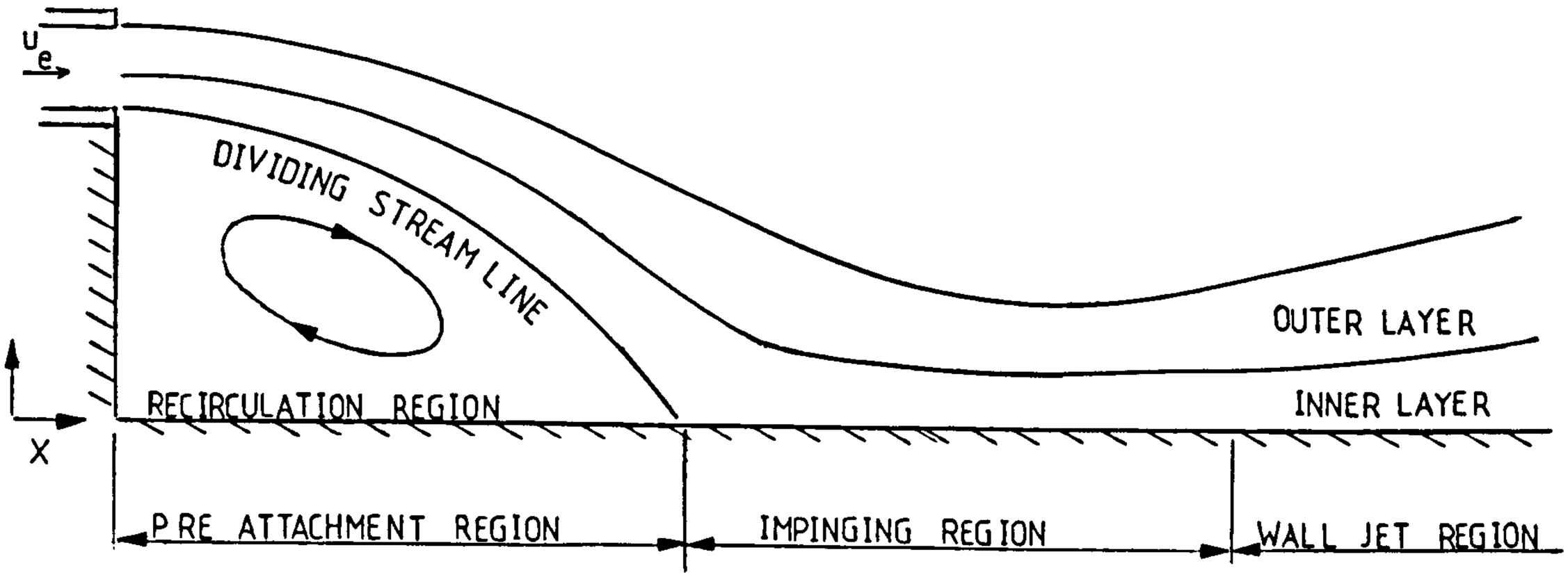

FIGURE 2-3 SCHEMATIC OF THE TWO DIMENSIONAL OFF SET JET (ADAPTED FROM HOCH & JIJI (1981)

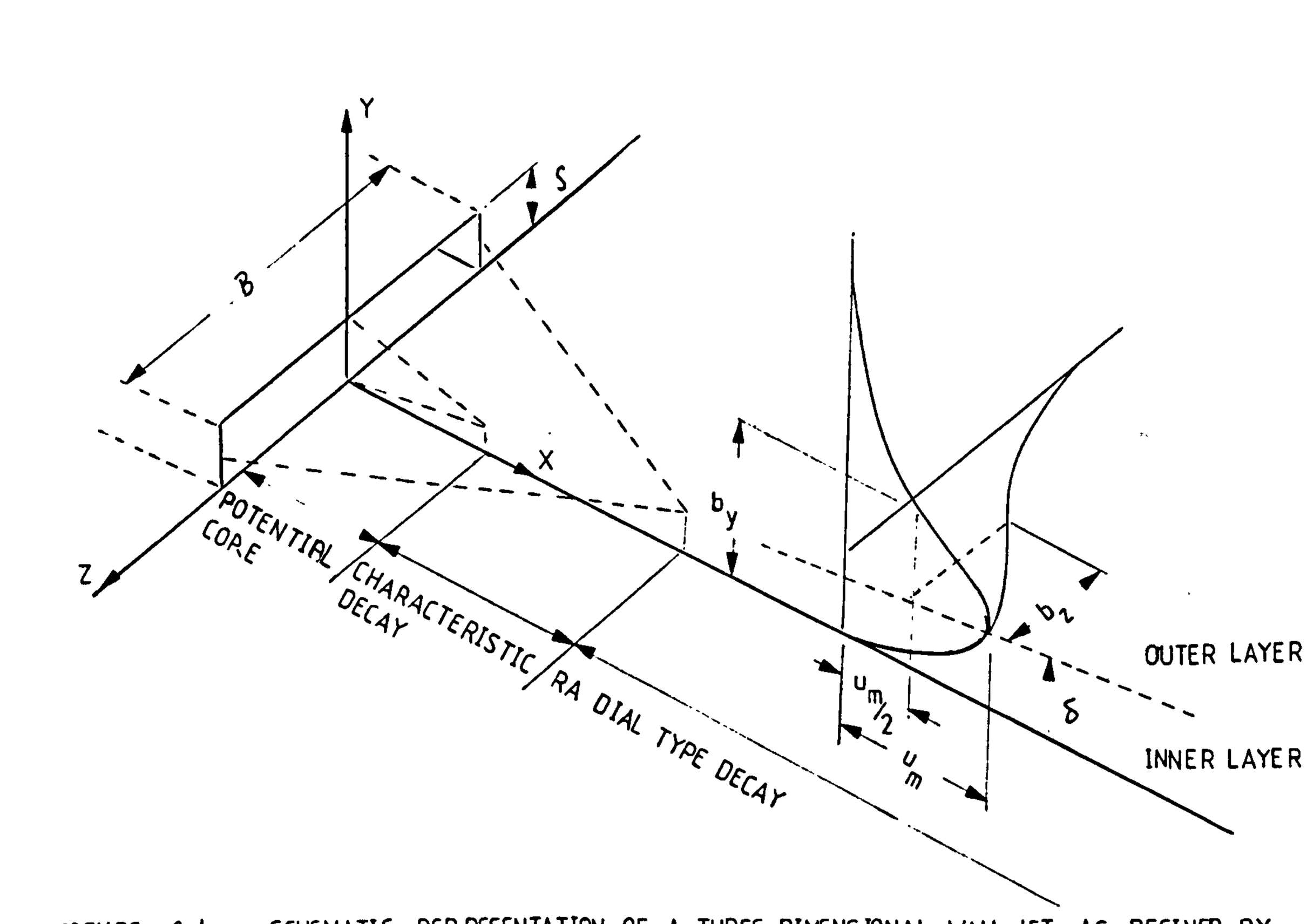

FIGURE 2-4 SCHEMATIC REPRESENTATION OF A THREE DIMENSIONAL WALL JET AS DEFINED BY SFORZA AND HERBST WITH NOTATION FROM RAJARATNAM

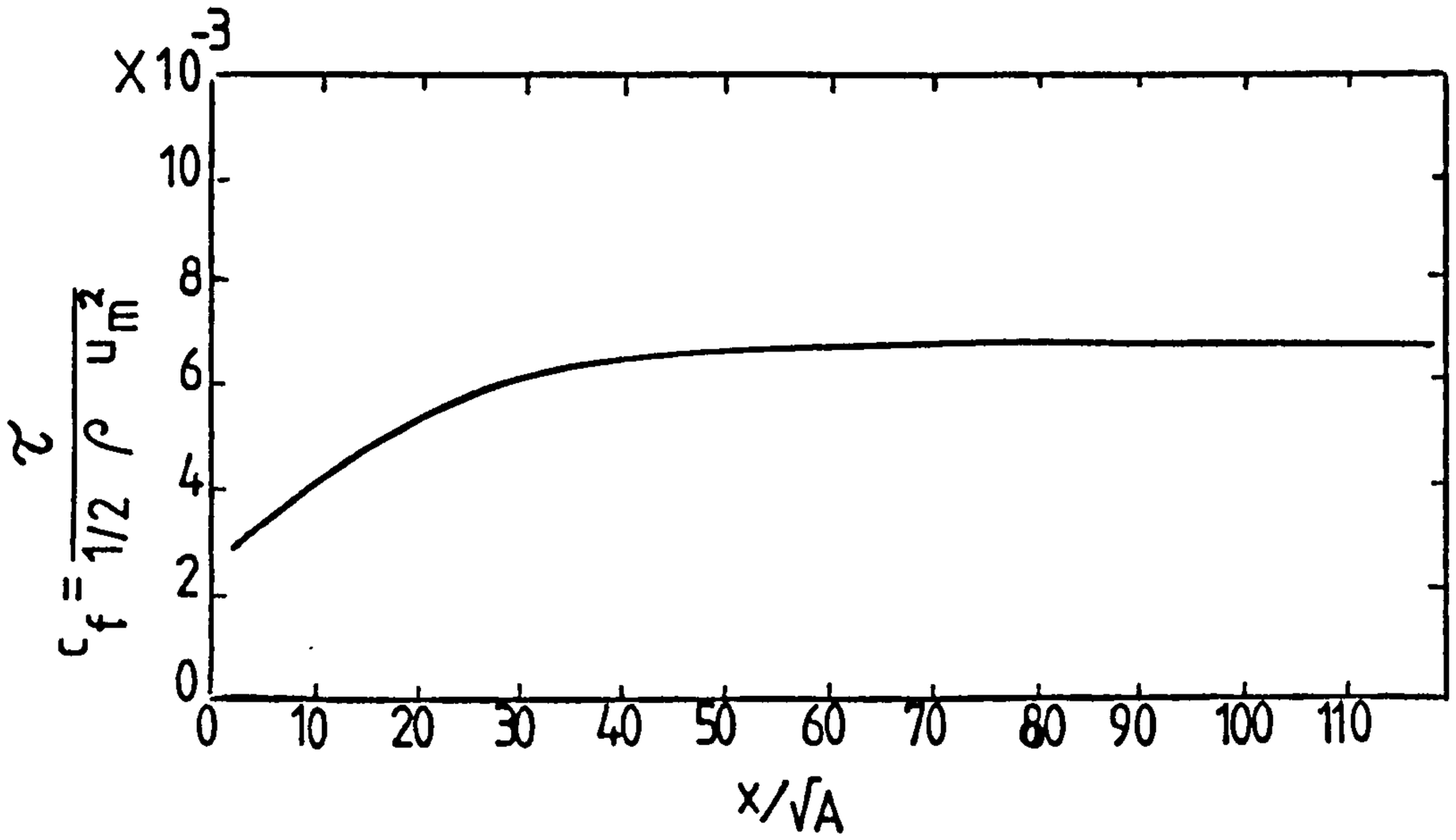

Figure 2-5 Wall shear stress in the centre-plane for a bluff wall-jet (Rajaratnam & Pani(1974))

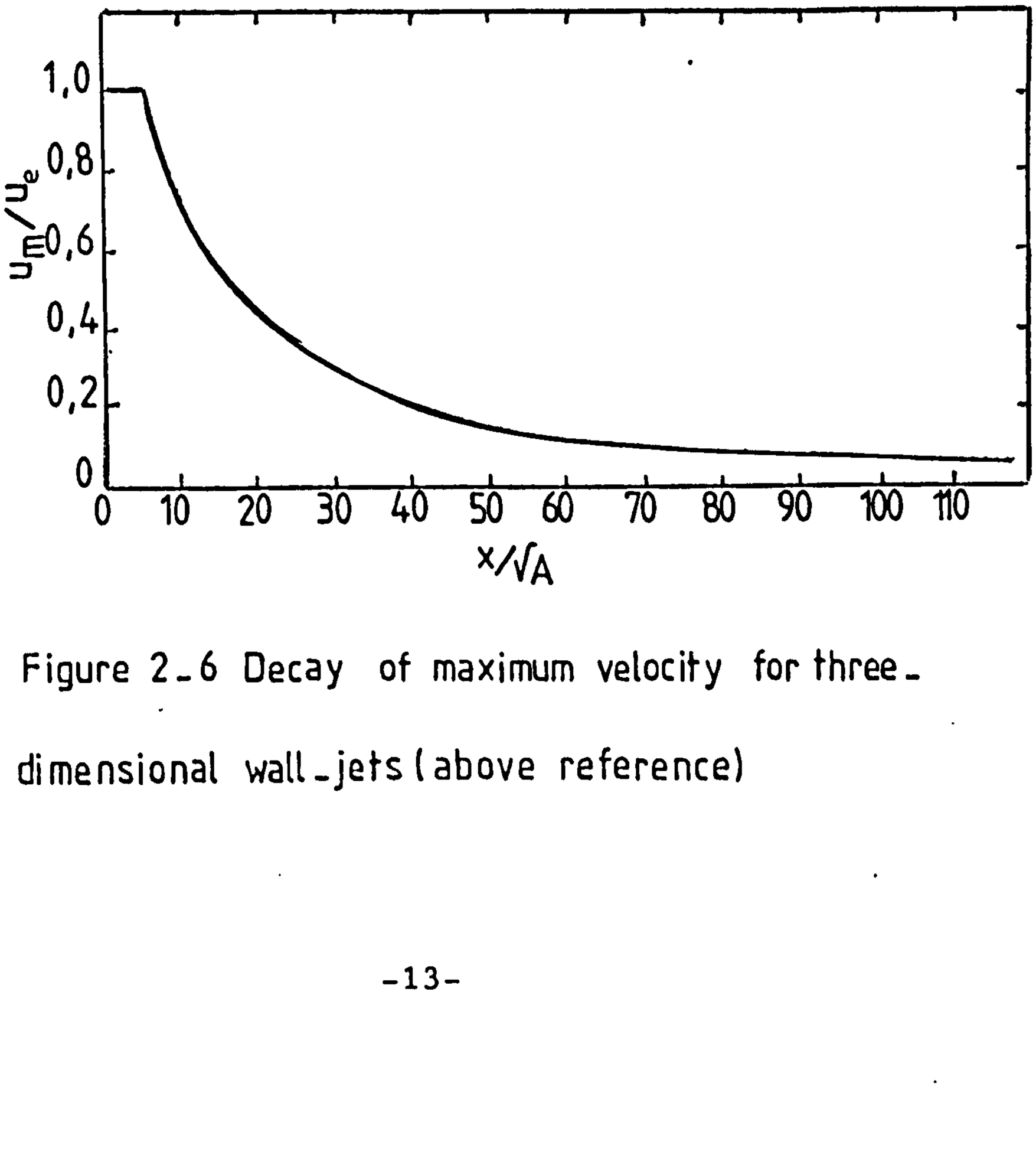

Figure 2-6 Decay of maximum velocity for three-dimensional wall-jets (above reference)

CHAPTER 3

EXPERIMENTAL SYSTEMS

CHAPTER 3

EXPERIMENTAL SYSTEMS

3.1 INTRODUCTION

The research outlook detailed in chapter 1 indicated that there was a need for a test rig which could facilitate a wide range of jet studies. Such outlook covers only part of a wider research programme on turbulent jets which usually involves many different aspects (various measurements for a variety of configurations)and could last for over a decade. The test rig was therefore built to allow a much wider variety of experiments than those reported in this thesis. In the first part of this chapter the design and development of the rig is described.

The use of the thin film naphthalene sublimation technique was made possible by the availability of a spray rig, Ward and Mahmood (1982), as a development of Neal's design (1975). This rig has been used since 1978 by many Cranfield students and has proved a basic facility for the application of the above technique. The second section of this chapter explains the present arrangment of the spray rig and recent improvements to it.

3.2 HEAT TRANSFER RIG

3.2.1 Requirements

The rig was required to produce a jet emanating from either a slot or a rectangular nozzle adjacent to a flat plate. In order to cover the full range of experimental configurations required of the test rig, the following variations on the jet were necessary:

1. Two- or three-dimensionality. This would enable numerical modellers to validate either two- or three-dimensional computer codes and also experimenters to simulate a variety of real,

three-dimensional geometries on the rig.

2. Temperature control. The naphthalene sublimation technique required that the supply air temperature remained constant and equivalent to that of the ambient air, while hot air was necessary for tests using the phase change paint technique.

3. Pulse Jet. This has long been the subject for research at Cranfield, (see for example Sidaway et al (1980)), and has many applications especially in air conditioning and warm air heating systems that are thermostatically controlled.

4. Off-set and/or inclined jets. This is an important area for research and probably where the rig will be most widely used. Outlet diffusers in air-conditioning systems and burners inside industrial furnaces (where the load is heated by the oblique impingement of single or multiple jets) are two industrial applications of such configurations. The configuration adopted was chosen to cover the range of geometries studied by most of the previous researchers. Bourque and Newman(1960), Hammond et al(1977) and Hoch and Jiji(1981a and b) have suggested that for two-dimensional jets the range of inclination angle should be within 30 degrees clockwise and 50 degrees anticlockwise from vertical, and that the maximum off-set height should be within 35 slot heights.

The flat plate needed to be:

1. Covered with pressure tappings for static pressure and skin friction (wall shear stress) measurements.

2. Adiabatic since building materials are insulating and this could more realistically model the geometry. Also the naphthalene sublimation technique requires an accurate temperature control but minor differences between the temperatures of the top and bottom of the plate would not affect the test results.

Added to these requirements for the jet and the flat plate, a few more features were considered desirable in the rig design :

1. A capability for modelling different geometrical configurations (i.e, inside rooms and furnaces) with little modification.

2. The possibility of employing flow visualization.

3. The possibility of using hot-wire or laser-Doppler anemometry.

4. Ease of heat and mass transfer measurements.

Two parameters were key to the design of a rig which would meet the above requirements. Most of the rig dimensions were directly affected by the choice of slot height. A survey of the literature on wall-jets by Launder and Rodi (1981) showed that for most previous jet studies, the slot height was no more than 15 mm and was often less than 10 mm. Since the rig was intended to be capable of utilising hot-wire and laser-Doppler anemometry and flow visualization, a larger value for the slot height was appropriate and therefore specifications were calculated for a slot height of 10 mm. Nevertheless, as the rig is designed, the exit nozzle is a variable component, and smaller or larger slot heights could be accommodated.

The slot Reynolds number has been evaluated in the jet studies using the slot height as the length parameter. Launder and Rodi (1981) and Hammond(1982) give the range of Reynolds numbers used in previous jet studies as generally below 35000. Flow at such a Reynolds number is fully turbulent and so this value was selected as the ceiling for the test rig air flow-rate.

3.2.2 General Layout

Figure 3-1 and plate 3-1 show the general construction of the test rig. The frame was made of 50 mm angle iron bars connected with bolts, nuts and brackets. The air supply was provided by a Keith Blackman 2-stage fan which could produce up to 1000 cfm at 50 in wg. (Keith Blackman Ltd. London N17). Although this fan was more powerful than necessary, it was chosen simply because it was freely available. An inlet throttling valve was connected to the fan, and this provided a blockage to the excess air which the fan was capable of pumping into the test rig.

An air to water heat exchanger, modified from an aircraft oil cooler, was used to reduce the air temperature downstream of the fan. No data was available on its performance but a few 'dummy' runs proved that it was suitable for this duty. The heater selected for the rig was an 18 KW SECOMAK industrial heater (SECOMAK Air Products, Stanmore, Middx, model 15) which exibited a pressure drop of 3.5 in wg at 800 cfm.

A diversion valve was designed, built and located downstream of the air heater, which provided an easy and accurate control of the air flow into the chamber and to the jet. The flow was roughly adjusted using the inlet trottling valve, and the excess air was exhausted into the laboratory using the diversion valve to provide fine adjustments. Since it took a fairly long time to stabilize the air temperature, once the flow was set, the diversion valve was used to bypass the heated or cooled air allowing the experiment to be set up and the test conditions to be quickly re-established.

The valve could also be used in a similar way to assist in generating a pulse jet. The front plate of the settling chamber is inter-changeable, and also a rather large space is available behind that plate and inside the chamber. For more elaborate pulse generation, suitable nozzle and pulse generating system can simply be accommodated into the chamber.

A flexible pipe, (Flexible Tubing and Fittings Ltd. Birmingham, Flexflyte U1) provided the connection between the diversion valve and the settling chamber. This was a neoprene coated, woven glass-fibre cloth, on a galvanised spring steel helix and could withstand temperatures of up to 150 C.

The settling chamber was constructed from 16 swg light aluminium alloy, and was fitted with detachable back and front plates. Both the jet nozzle and the front plate on which it was mounted were inter-changeable and thus permitted the selection of a variety of two- or three-dimensional nozzles. The chamber can both rotate and move vertically in a 25 mm angle iron frame hinged to the main frame. There was a baffle plate in the middle of the chamber, blocking half the chamber height, to prevent the entering jet to affect the exit flow. There also was a perforated plate within the chamber to produce a more uniform flow turbulence distribution.

All the jets studied were emitted from nozzles with contraction ratios of at least 4 (i.e. figure 5-1). After passing through the contraction in the nozzle, the flow passed through a straight channel at least 4 cms long. Tests in chapters 5 and the bound paper indicated that this arrangement produced uniform velocity profiles.

The flat plate was fabricated from a 'Melamine' coated chip-board ('White-Plas') resting on bars which provided both a base for the plate and ensured the rigidity of the main-frame structure. Pressure tappings on the plate facilitated static pressure measurements (see appendix A).

The test section measured 2440 mm X 800 mmX 850 mm (LXWXH). This was chosen to enable jet studies within the range as indicated by the papers reviewed in the second chapter. Constructional stability and practical aspects of working on the rig were other factors in the choice of the above dimensions. A three-dimensional traverse mechanism could span this volume for the purpose of obtaining total pressure and temperature measurements. The sides of the test section could be covered by Perspex side panels in order to prevent spanwise dispersion of the flow.

3.2.3 Accessories

Two systems were designed in conjunction with the test rig, and each one was essential for part of the tests intended on the rig.

3.2.3.1 The Traverse Mechanism -

Measuring the velocity and temperature profiles is a standard procedure for any jet studies. A mechanism was required which could traverse every point in the test section while holding a pitot tube, a temperature sensor or any similar measurement device. In addition to three-dimensional movement, some degree of stability was necessary to ensure the accuracy of the measurements.

The traverse mechanism is presented on plate 3-1 as mounted on the test rig. The probe holder, traversed in the vertical direction (normal to the test plate surface) by means of a handle and screw. Two bars and a slide mechanism provide the necessary rigidity for the structure and restrict any twist. This system could be slid in the spanwise direction along two 25 mm diameter bars, which themselves could be moved in the jet axial direction on another two 25 mm bars. This system although simple in construction, satisfied all the traverse requirements for the present studies. It was always possible to locate the probe within 0.5 mm of the desired position for each reading in any of the three directions.

3.2.3.2 The Roller Blind -

An important requirement for using phase change paint in the heat transfer measurement was that the paint coated plate could experience a pulse of hot air (Chapter 4). The roller blind was not used for the present research as in the early stages, the importance of the boundary conditions in heat and mass transfer(Alamdari et al (1986,

bound paper)) was not yet recognised. It was then planned to conduct tests on three-dimensional jets using the phase change paint and compare the results with the tests presented in chapter 5 and also the computer codes being developed at Cranfield.

The above paper demonstrates that a change in the wall-jet boundary conditions results in a different temperature profile and consequently affects the heat transfer behaviour. While the thin film naphthalene technique resembles a heated plate facing an ambient jet, the phase change paint method models the heat transfer between a hot jet of air and a plate at ambient temperature. The difference in the boundary conditions allows no direct comparison between the two methods although both of them are useful tools for obtaining experimental data. It is hoped that the roller blind shall eventually be used once computer codes are capable of modelling different three-dimensional flows with appropriate boundary conditions (Mohammed(1986)).

The roller blind was designed to cover the test plate while the test was being set up. A few seconds was adequate for the jet to stabilize. Releasing the blind marked the start of the test as the paint was exposed to the hot air. Figure 3-2 shows the general features of the roller blind mechanism as mounted on the test rig. The spring mechanism was a modification to a domestically used roller blind and the material for the blind was the "silver/silver" solar sheet (Solar X, U.K. Ltd., Solar X House, 8-12 Stockport Road, Stockport, Cheshire SK3 OHZ) which had high temperature resistance and was flexible enough to be wrapped round the roller. Two 9.5 mm bars mounted along the sides of the rig provided the guides for the blind and a catch held the blind at the nozzle exit plane.

3.2.4 Recommendations

The tests conducted in this research in addition to those reported by Shute (1984), Apostolou (1985) and Mok (1985) demonstrated that the rig satisfies all requirements. In the following recommendations the first one is concerned with the safety of the rig and the rest are minor adjustments which may ease the future research.

Careless handling of the air heater could cause extensive damage to the elements. As the rig is wired, the fan must be working before the heater can be loaded, but a minimum mass flow-rate through the heater is necessary to ensure that the elements are kept adequately cool. The air heater was restricted to a maximum exit temperature of 300 C with a minimum flow rate of 200 cfm. The temperature of the air at the exit of the heater was

monitored but this reading did not provide sufficient information on the safety of the heater under all conditions. A simple device which could provide protection against conditions of inadequate air flow, would be a simple flap operating a mercury tilt switch. If more air than that required for the experiment had to be heated, the excess could be dumped through the diversion valve.

The settling chamber had a large heating capacity which took a long time to overcome at low mass-flow rates (one hour). Provision of a by-pass valve on the settling chamber would allow a higher mass flow rate into the chamber and therefore reduce the heating up time. The valve should be positioned such that the higher mass flow passes through most of the chamber without disturbing the uniform flow out of the exit nozzle taking the flow pattern inside the chamber into account.

The allignment of the junction between the nozzle and the flat plate was usually very difficult and time consuming. The future nozzles for the wall-jets should have a lip which extends over the flat plate (figure 3-3) and therefore uses it as part of the nozzle.

Simplicity of the tests performed by Shute (1984) in applying the mass transfer technique compared with the tests presented in the bound paper of this thesis, advocates modelling of the two-dimensional geometries to smaller dimensions than the total width of the rig. The width of the rig was decided to allow for three-dimensional jet expansion in its early part but only an aspect ratio of 20 is adequate to ensure two-dimensionality.

3.3 SPRAY RIG

3.3.1 Background

The rig was designed and built by Mahmood(1980), and is shown in Plate 3-2. It consisted of two different systems:

1. Electronically controlled traversing system which provided the two-dimensional motion necessary for the spray action on the plate.

2. Naphthalene/inhibisol solution pipe system, and associated compressed air, which provided the spray.

3.3.2 Electronically Controlled Traversing System

A D.C. motor moved the spray nozzle along one horizontal axis, while a stepper motor provided the plate motion perpendicular to the nozzle movements. The action and frequency of the motors were manually set on a control box. The parameters governing the movement of the nozzle were arbitrary and needed optimisation in each individual case.

The D.C. motor, which moved the nozzle across the plate, was required to operate at the minimum possible speed for the rig so as to reduce the acceleration/deceleration times and thus produce a more uniform spray across the plate by increasing the density of deposit on the plate.

The setting of the stepper motor governed the number of times each point on the plate was sprayed. It could produce naphthalene strips (strictly a sinusoidal density variation) on the plate if the number of the steps were high (adjacent passes further apart). Consequently, a thick layer could be generated using a small number of steps. This would have needed a longer time to clear, and therefore make each test run unnecessarily time-consuming. Mahmood (1980) found that 400 steps per pass proved satisfactory in providing a thin layer of naphthalene.

3.3.3 Flow System

The piping consisted of a pipe from a source of compressed air set at 60 psi that directed the air through a needle valve and then into the nozzle. The naphthalene/Inhibisol solution pipeline passed the solution from a tank pressurized by dry nitrogen, a flow-meter and a needle valve to the nozzle. The nozzle details were as in figure 3-4. It is an atomiser where the solution exit is into the turbulent high pressure air which quickly turns it into droplets and forms a fine spray.

The maximum flow for the solution was achieved when the time between each two passes of the nozzle was just adequate for the Inhibisol on the plate to evaporate. This was approximately equivalent to 50% of the flow-meter capacity. The shape of the spray emitted from the nozzle was very dependent upon the ratio of air and solution flow rates. The best spray was obtained once the solution was broken into droplets immediately after leaving the nozzle.

Mahmood(1980) and Oladiran(1982) reported that the nozzle suffered from clogging, and 4 factors were thought to have contributed to this:

1. Stopping procedure. Once the system was stopped, the solution exposed to the air would lose its inhibisol, and naphthalene would be deposited in the pipe, especially in the smaller sections.

2. Narrow passages. Sections like the needle valve and the nozzle, were prone to blockage and needed constant attention.

3. Concentration of naphthalene in inhibisol. Although the two were mixed untill no naphthalene particles were visible in the solution, the ratio of 10 gr of naphthalene for each 100 cc of inhibisol, as suggested by Mahmood, was very near saturation and it was believed that this could cause naphthalene deposition on parts of the system.

4. Foreign particles in the system. There was no filter in the solution pipe-line and therefore dirt could enter the system and cause blockage. Closer inspection revealed excessive dirt inside the tank, which had accumulated through the years. Further it was observed that the solution reacted with the tank itself, causing a greasy sediment to be deposited on the tank surface and colouration of the charge.

One problem which was previously undetected with the flow system was the insensitivity of the flow-meter. Small changes in the flow capacity could directly affect the uniformity of the naphthalene on the plate. These changes at times occurred due to minor blockages whithin the system and were usually unnoticed since they had no significant effect on the flow-meter reading.

The needle valve used for the flow control in the pipes presented a major problem when minor changes in the flow were detected. Small modifications to the setting of either the needle valve or the valve on the flow meter caused major fluctuations in the flow rate, rendering the run invalid.

3.3.4 Present Modifications

Many of the problems mentioned in the previous section were discovered through the period of two years of experiments with the spray rig. It was necessary to correct some of them in order to be able to continue the test work. Possible solutions to some others are suggested in the next section, but are left for future researchers to impliment.

The tank was dismounted, cleaned thoroughly and sealed inside with Petseal (Auster Design, P.O. Box 4, Shirly, Solihull, West Midlands, B90 3TD) which stoped any reaction between the solution and the tank. A more accurate flow meter was employed in the solution pipe-line. The regulator on the nitrogen bottle was used for small adjustments to the flow rate. The concentration of naphthalene in the inhibisol was reduced to 60 gr of naphthalene in 800 cc inhibisol and the resulting solution was then discharged into the tank through filter paper.

A new procedure was employed for stopping the system which allowed the air flow to continue while the solution flow was shut off. This cleared the nozzle and reduced the chance of naphthalene deposition inside it.

The steps taken above proved to overcome the clogging in the nozzle without requiring any changes to its design. Occasional blockages occured in the needle valve, which could easily be changed if it caused significant problems in the future.

3.3.5 Recommendations

Fine adjustment to overcome the sudden changes in the solution flow rate was only possible through changes in the nitrogen pressure. A control system which monitors the solution flow, and is capable of automatically adjusting the nitrogen pressure in the tank could ensure the uniformity of the spray and therefore greatly enhance the reliability of the spray rig.

The bracket which held the pipes leading to the spray nozzle was susceptible to fracture and a new simple design for this part is strongly recommended.

There is little improvement which could be made to the electronic control of the rig however the uniformity of the spray on the sides of the plate (i.e. at each end of the traverse sweep) could be improved if slower traverse speeds were possible.

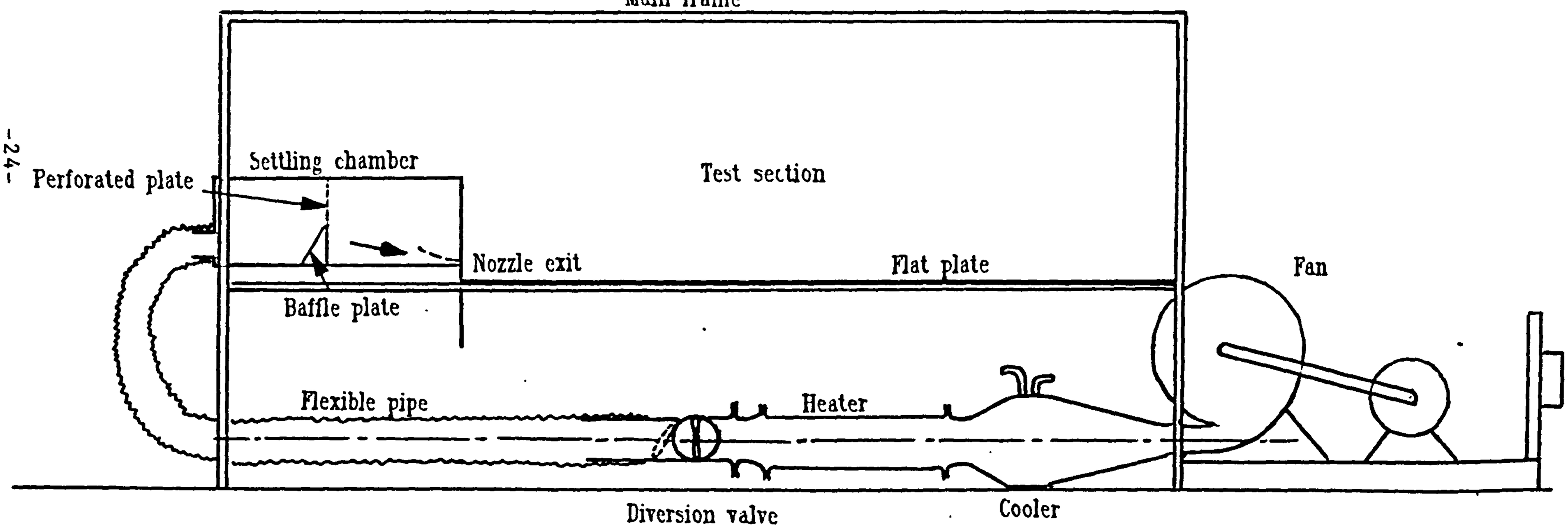

Figure 3-1 General assembly of the test rig

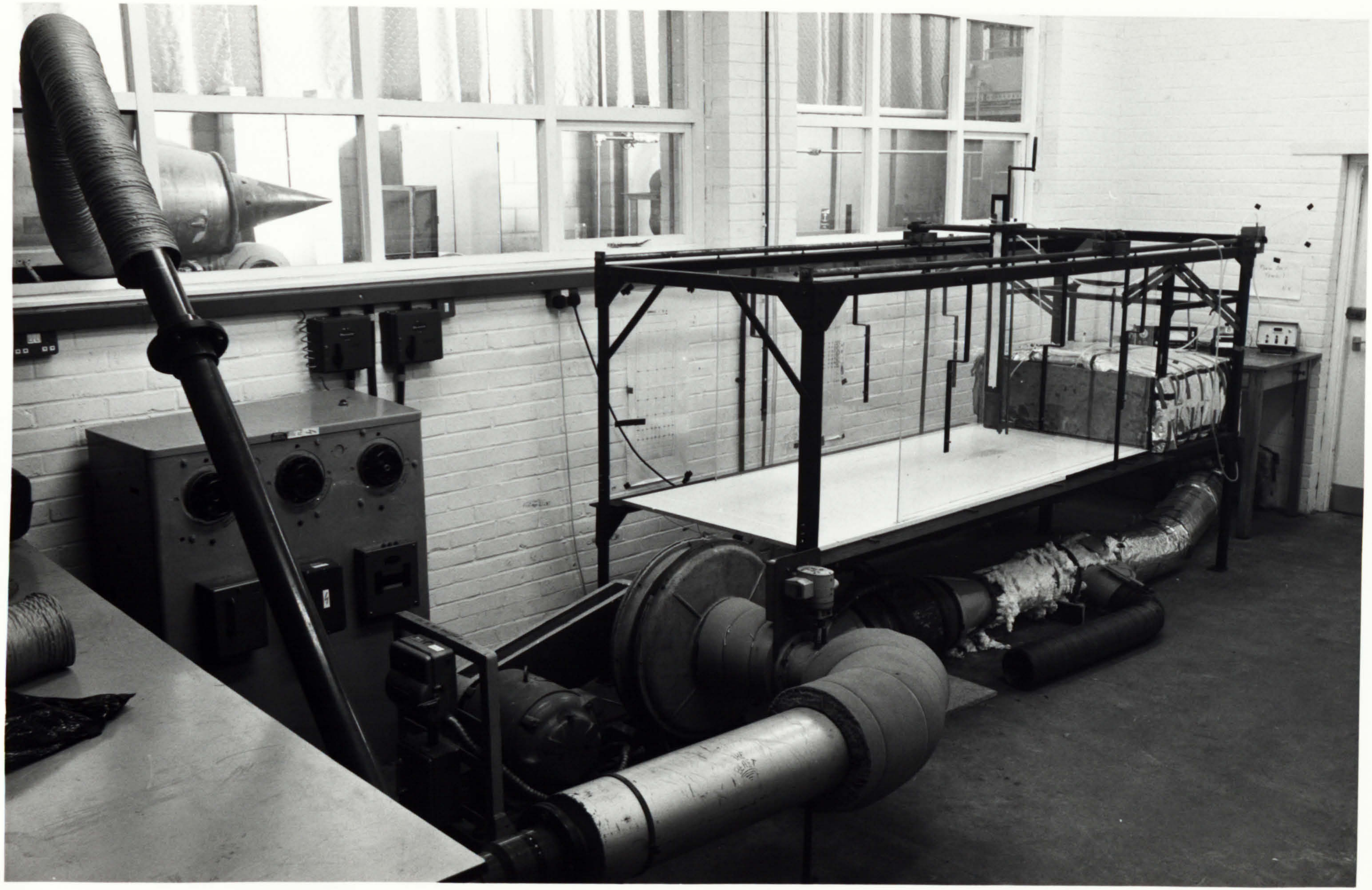

Plate 3_1 Heat Transfer Test Rig

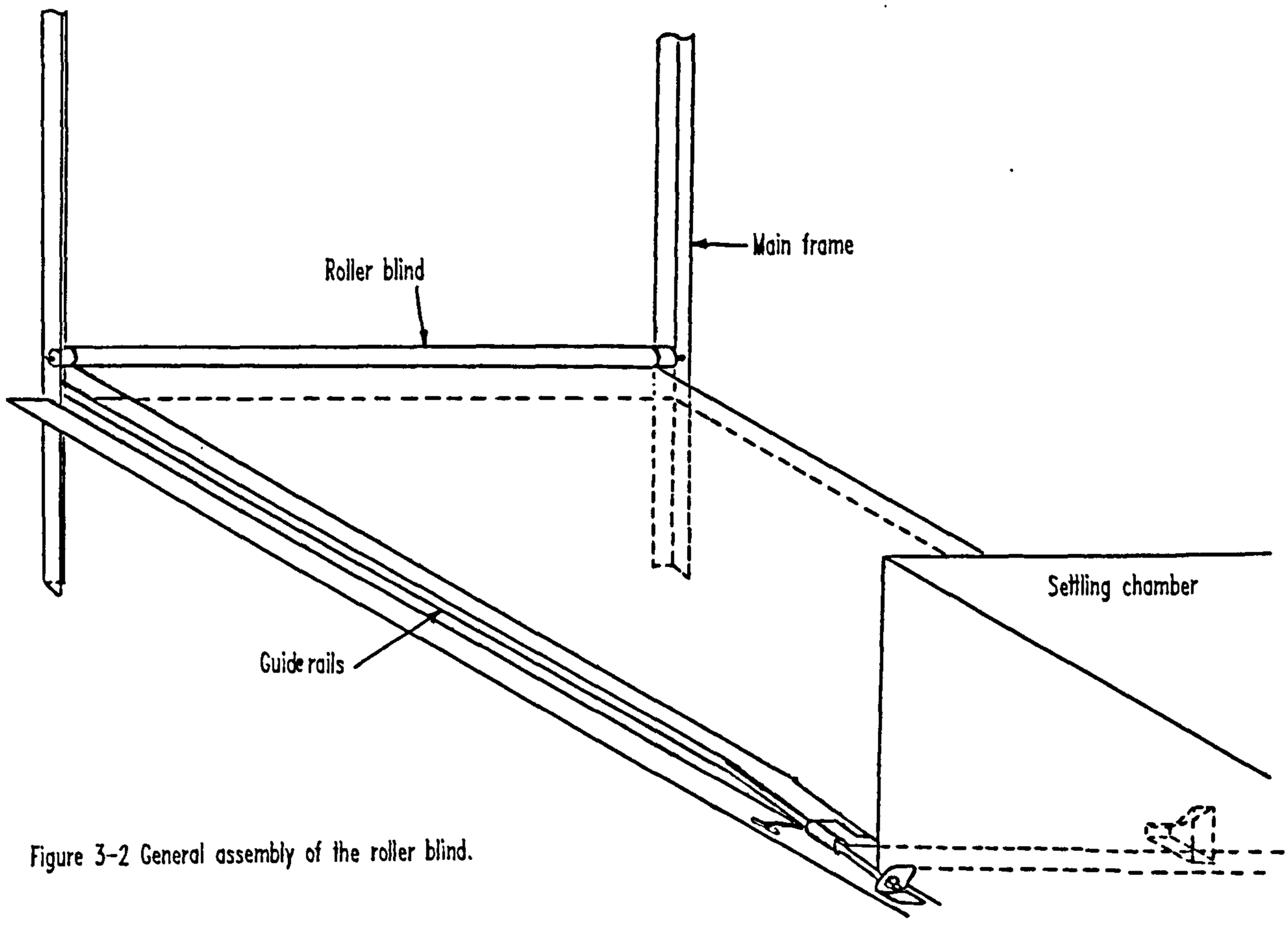

Figure 3-2 General assembly of the roller blind.

a) Suggestion for future designs

b) Present designs.

Figure 3-3 Suggestion for design of the wall-jet nozzles.

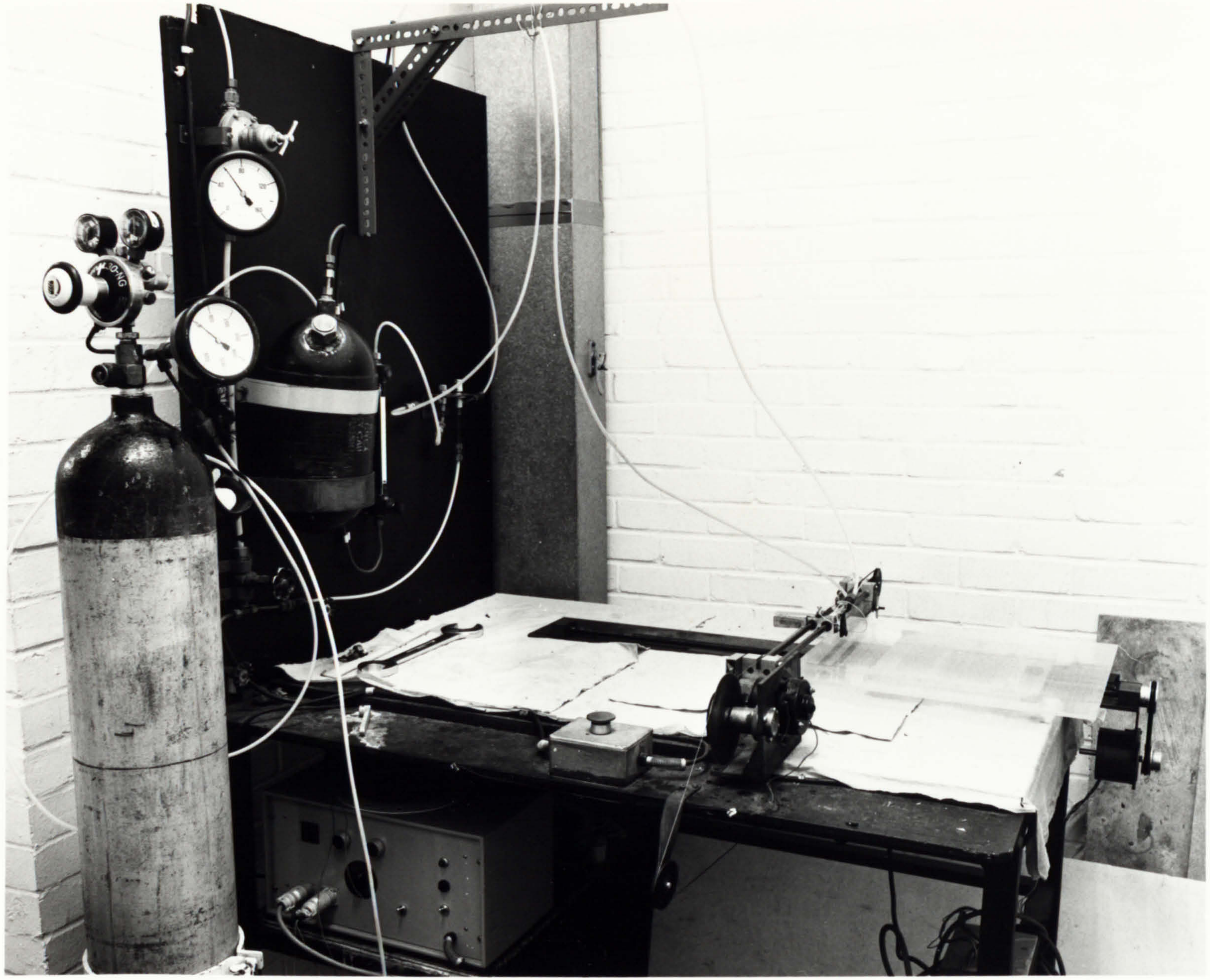

PLATE 3_2 THE SPRAY RIG

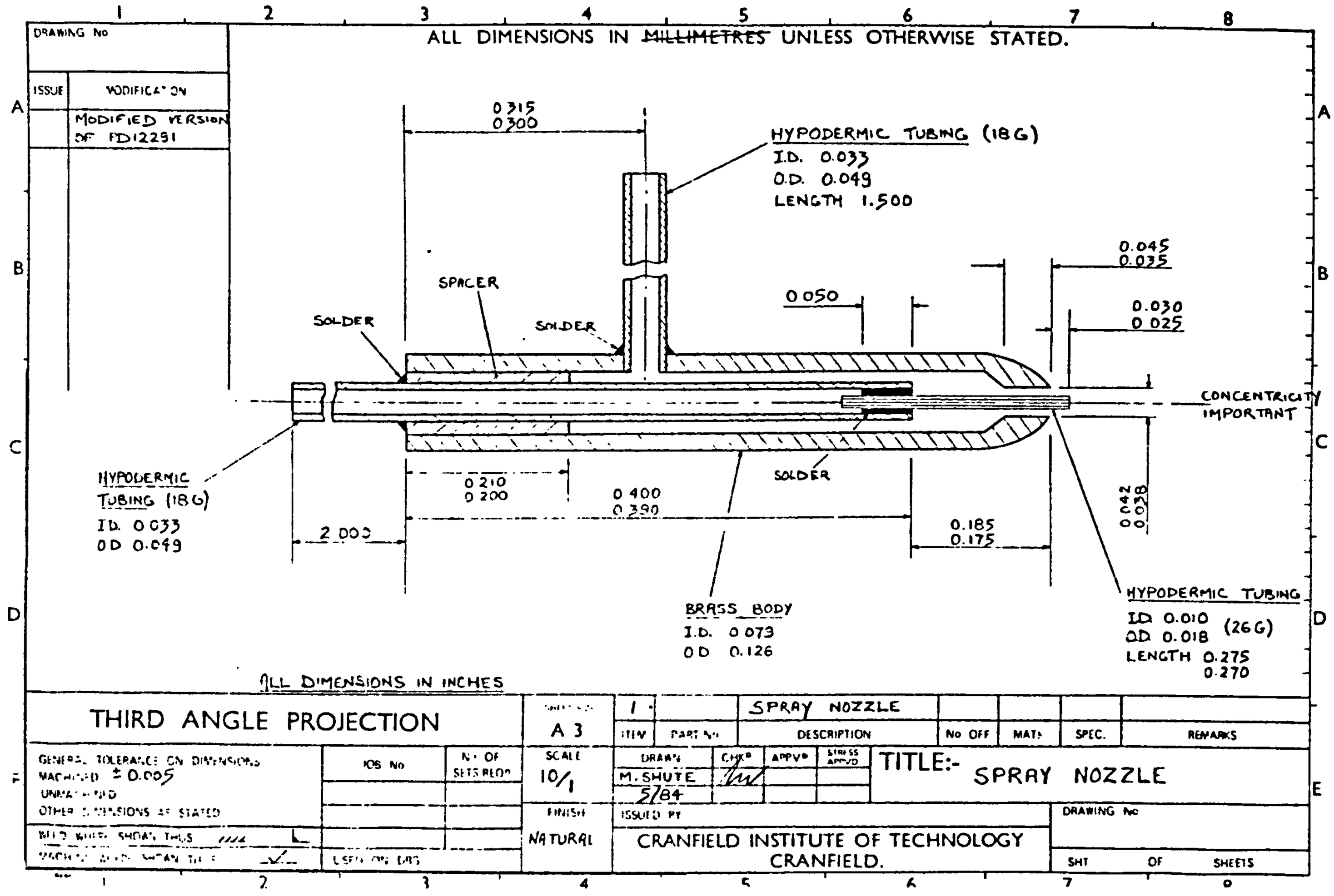

Figure 3-4 Details of spray gun on the naphthalene spray rig.

CHAPTER 4

HEAT TRANSFER MEASUREMENT TECHNIQUES

CHAPTER 4

HEAT TRANSFER MEASUREMENT TECHNIQUES.

4.1 INTRODUCTION

Direct measurement of the convective heat transfer coefficients usually requires an accurate knowledge of heat input/output and sensitive temperature measurements. Errors can occur in such experiments from three different sources. First is the positioning of the thermo-couples, if such devices are used. They should be flushed with the surfaces, otherwise the boundary conditions will be affected. The conduction within the heated surface and the thermo-couple leads themselves can also have a significant impact on measurement accuracy. Finally it is difficult to determine thermal radiation effects since surface emissivities and shape factors may not be accurately known. The two methods presented in this chapter avoid the above complications, while being simpler and cheaper to employ.

4.2 HEAT/MASS TRANSFER

4.2.1 General Theory

The similarity between heat, mass and momentum transfer in a turbulent flow over a flat plate can be demonstrated by consideration of their physical processes, commonly expressed in the classical Boussinesq formulations.

For momentum transfer:

$$\tau = \rho (\nu + \epsilon) \frac{\partial u}{\partial y} \qquad (4\_1)$$

where ρ is the density, ν is the kinematic viscosity, and ϵ is the momentum eddy diffusivity, a measure of the momentum flux within the turbulent flow. While ν is a property of the fluid, ϵ depends on its motion. This

formulation implies that the momentum transfer for both laminar and turbulent flow can be represented as a gradient diffusion process. Although this is not strictly correct, it is an adequate approximation for the present purposes.

For heat transfer, the analogous expression implies that the amount of heat is a function of the temperature gradient:

$$q = \rho c_p (\alpha + \epsilon_H) \frac{\partial T}{\partial y} \qquad (4\_2)$$

where α and ϵ_H are molecular and turbulent diffusivities for heat transfer within the flow and c_p is the specific heat. Finally, mass transfer may be assumed to be a function of the concentration gradient.

$$N = (\mathcal{D} + \epsilon_M) \frac{\partial C}{\partial y} \qquad (4\_3)$$

where $\mathcal{D}$ and ϵ_M represent the molecular and turbulent mass diffusivities.

An analogy between any two of the above processes enables values for one to be deducted from a knowledge of the other. The pre-condition for the validity of any analogy is the provision of similar geometric and boundary conditions, equality between the Reynolds numbers and between the turbulent and molecular diffusivities. The first three can be achieved by correct and accurate experimental set up. $Pr = \nu/\alpha$ and $Sc = \nu/\mathcal{D}$ and $Le = \alpha/\mathcal{D}$ represent the molecular flux ratios between momentum, heat and mass, and a knowledge of their values is important to the application of any analogy. Since they are physical properties their values are usually known for any specific case.

Two analogies have been widely employed. One is simple to apply (Chilton-Colburn analogy(1934)) while the other (Jayatillaka (1969)) is complex, although more accurate. Parallel to this project, the development of wall-jet profile analysis (Hammond(1982)) provided a third method for obtaining analogy factors. This is explained in more detail in the bound paper by Alamdari, Hammond and Montazerin (1986), where the profile analysis has been used to deduce heat transfer coefficients from mass transfer data.

Chilton and Colburn (1934) devised two similar non-dimensional products for heat and mass transfer, and termed them j-factors. For mass transfer the factor has the form:

$$St_m \cdot (Sc)^{2/3} = j_M \qquad (4\_4)$$

while for heat transfer it becomes:

$$St \cdot (Pr)^{2/3} = j_H \qquad (4\_5)$$

They then experimentally showed that $j_m = j_H$, which means:

$$\frac{St}{St_m} = \left(\frac{Sc}{Pr}\right)^{2/3} = \phi \qquad (4\_6)$$

where ϕ is the analogy factor. Therefore:

$$h = b' c_p \rho \, (Sc/Pr)^{2/3} \qquad (4\_7)$$

where h and b' are the convective heat and mass transfer coefficients.

The above analysis has been used by, among others, Kabari (1977), Sparrow and Lovell (1980), Oladiran (1981), Fletcher et al (1982), Dixon (1984) and Shute (1984). The analogy factor in equation 4-6 is constant, and therefore does not allow for variations in the heat and mass diffusivities.

Jayatillaka (1969) proposed an empirical expression to describe the heat transfer in the near-wall region of a shear flow. He undertook an extensive review of previous distributions proposed for the turbulent/molecular momentum diffusivities across boundary layers, and recommended the following expression (transformed in terms of the Stanton number):

$$\frac{1}{St} = \left(c_f/2\right)^{\frac{1}{2}}\left[Pr_t \left(2/c_f\right)^{\frac{1}{2}} + A\left[\left(\frac{Pr}{Pr_t}\right)^{\frac{3}{4}} - 1\right]\left[1 + 0{,}28\exp\left(-0{,}007\frac{Pr}{Pr_t}\right)\right]\right] \qquad (4\_8)$$

$$A = 8{,}32 \quad \text{for} \quad Pr_t = 0{,}9$$

$$A = 9{,}00 \quad \text{for} \quad Pr_t = 1{,}0$$

Mass transfer Stanton number may similarly be obtained when Sc and Sc_t are substituted for Pr and Pr_t respectively. The analogy factors resulting from this equation unlike the constant one obtained from the Chilton-Colburn analogy, have slightly lower values at low Reynolds numbers, with the disparity widening as the local Reynolds number increases (figure 4-1).

The validity of the above analogies is still subject to discussion. The simplicity of applying the Chilton-Colburn analogy has encouraged the experimenters to employ it and then discuss its validity. Profile

analysis (Alamdari et al (1986,bound paper)) has shown that the Chilton-Colburn analogy can over estimate heat transfer rates by up to 30%. In this thesis, mass transfer Stanton numbers are presented for every case. Heat transfer data is subsequently derived using any of the available analogy factor expressions, bearing in mind the deficiencies in the various formula.

4.2.2 Thin Film Naphthalene Sublimation Technique.

In the thin film naphthalene technique, the surface of the test plate is first covered with a uniform layer of naphthalene and its density is accurately measured. Density is here referred to as the mass of naphthalene per unit area. The plate is then positioned in the test section and then the test started. Naphthalene gradually sublimates into the air and the rate of sublimation at each point is directly proportional to the heat transfer rate. The clearance patterns therefore represent the heat transfer coefficient contours on the plate. Each test can last between 30 mins and two hours, depending on the specific geometry under consideration and the flow Reynolds number.

The choice of naphthalene has some advantages with regard to the molecular and turbulent diffusivities. Naphthalene diffusion in air is a reasonable analogue for heat transfer in air, since Sc=2.44 for the former case while Pr=0.7 for the latter. This is in contrast to the electrochemical mass transfer technique which is also popularly used to obtain heat transfer data and for which Sc=1500. The turbulent diffusivities are difficult to measure and the data available are scarce, but most investigators (such as those referred to in the previous section) have agreed that the turbulent Prandtl number and the turbulent Lewis number in the case of naphthalene and air are close to unity. (A more detailed and recent treatment of the turbulent Prandtl number near the surfaces is given by Hammond(1985)).

4.2.3 Calculation Of Heat Transfer Coefficients.

The coefficient b' in equation (4-7), the mean mass transfer coefficient, may be obtained from:

$$\frac{m}{t} = b' A_n (C_n - C_\infty) \qquad (4-9)$$

where t is the time for the mass of naphthalene (m) to clear, and C_n and C_∞ represent the concentration of naphthalene on the plate and in the air. The naphthalene vapour can be regarded as a perfect gas at temperature T_n,

as the partial pressure of naphthalene vapour may normally be assumed negligibly small. Then:

$$C_n = \frac{p_n}{R_n T_n} \qquad (4\_10)$$

where p_n and T_n are vapour-solid equilibrium values. Wilkie (1982) mentions the effect of the naphthalene concentration build up in the bulk fluid, but since the air intake in all present experiments was from outside the lab, the lab was ventilated as much as possible and the flow over the test plate was expanding into the open air, the vapour concentration of the naphthalene in the free stream could usually be neglected, i.e., $C_a = 0$. Therefore:

$$b' = \frac{m}{A_n t} \cdot \frac{R_n T_n}{p_n} \qquad (4\_11)$$

Consequently, the heat transfer coefficient may be obtained from:

$$h = \left(\frac{m}{A_n t}\right) \cdot \rho \cdot c_p \cdot \frac{R_n T_n}{p_n} \cdot \left(\frac{Sc}{Pr}\right)^{2/3} \qquad (4\_12)$$

if equality in Chilton-Colburn j-factors is assumed.

4.2.4 The Application Of The Thin Film Naphthalene Technique.

The provision of similar geometric and temperature/concentration boundary conditions are pre-conditions for the validity of the heat/mass transfer analogy, as discussed in section 4.2.1 above. Since the naphthalene thin film technique is based on the clearance patterns on the subject plate, a changing concentration boundary condition during the test is inevitable. This so called "bare patch effect" was originally studied by Neal(1975) and he found the error to be negligible from comparison of his data with the other heat transfer measurements. He reasoned that the bare patch effect is time dependent and affects a given measurement point for only a relatively short period. More recently Oladiran (1981) used boundary layer heat transfer calculations for a flat plate to study this effect. He calculated the local heat transfer rates at different time steps allowing for the bare patch effect to start at the front of the plate and then progress. It was then demonstrated that the error in the time-averaged local heat transfers with and without the bare patch effect was no more than 2.5%.

Buoyancy-driven, or 'natural' convection, causes some sublimation of naphthalene before the test starts. This had two effects on the present experiments. Firstly, it

induced a density gradient along the plate, since it took approximately one hour to coat the plate with naphthalene, and subsequently naphthalene was able to sublimate during the time between the end of spraying and the start of the test. Mahmood (1980) showed that the natural sublimation along the test plate was linear, but dependent on the temperature.

For each experiment, a dummy plug was sprayed parallel to the plate and weighed twice to provide the naphthalene density and the natural sublimation rate. Glass slides of dimensions 76 mm X 25.4 mm X 1 mm were used by the previous investigators at Cranfield to sample the density of the naphthalene on the plate. The mass deposited on such slabs was so small that a balance with accuracy of 0.1 of a milligram was used. The balance, presently available at Cranfield, was accurate only up to a milligram. To off-set this reduction in weighing accuracy, it was decided to use a larger perspex slab with dimensions 297 mmX 24.5 mm X 3 mm. Positioning these slabs on the test plate could cause two types of error. Generally the spray had to travel some 30 mm from the spray nozzle to the test plate. When the slab was present, this distance was reduced to 27 mm. A simple test demonstrated that the extra mass lost to the surrounding air due to this 3 mm change was negligible. The slab thickness was changed from 1 to 3 mm and the diffenence in the naphthalene density over it was less than 1%.

The other source of error was the naphthalene deposited on the sides of the slab, which could cause over estimation of the naphthalene density. This can be approximated by comparing the surface area of the sides of the slab with the surface area under experiment. Some allowance should be made for the direction of the nozzle and its movement which reduces the naphthalene spray on the sides. It was found that the over estimation for both the smaller and the larger slabs was approximately 3%, which resulted in a 3% increase in the measured Stanton number.

4.3 THE USE OF THE PHASE CHANGE PAINT FOR HEAT TRANSFER MEASUREMENTS.

4.3.1 Introduction

An approach to heat transfer measurement is presented in this section which could be employed for heat transfer between hot air and a plate at a lower temperature. This utilizes paints which change colour at a predetermined temperature. They are commercially available from Tempilaq (Tempil division, Big three industries Inc, So, Plainfield, NJ 07080. U.S.A.). The minimum colour change

temperature in the range of their products was 43 C, and this was accurate to within a degree centigrade.

The surface under examination, covered with paint, is suddenly exposed to hot air at the start of the experiment. The colour change is closely monitored. Points on the surface where the heat transfer rate is highest, experience a fastest temperature rise, and therefore a more rapid change in the paint colour. The local heat transfer coefficients may subsequently be calculated from the measurement of the colour change time.

It is important to emphasize that the thin-film naphthalene sublimation and phase change paint techniques are not always directly comparable in every case since the boundary conditions may be different. For example in the case of wall-jet flows, In the former method the mass transfer is from the plate to the air stream, while in the latter the heat is transfered from the air jet to the plate (see Alamdari, Hammond and Montazerin (1986, bound paper for further discussion of these differences). Nevertheless, data acquired using both methods could assist in the development and verification of the computer codes mentioned in chapter 1, as well as providing experimental data for different heat transfer configurations.

4.3.2 Calculation Procedure.

Most heat transfer text books have discussed the unsteady conductive heat transfer through a slab when the fluid adjacent to it experiences a sudden temperature rise, figure 4-2,(i,e, Krieth(1965)). Three methods for approaching this problem are presented in this section. The first method is used for a slab of finite thickness and its detailed derivation is presented in the above reference. The second and third methods are both for a semi-infinite plate. The second method which is also cited by Krieth, uses the charts to obtain the heat transfer coefficients. The third method can be used independently and its full derivation is explained here.

Method 1:

If the slab has a finite thickness (figure 4-2a) and is insulated on the cooler side, then the temperature history within the slab is a function of time and distance from the slab surface.

$$T(x',t) = X(x').\theta(t) \qquad (4\_13)$$

The above two time and distance functions should satisfy the one dimensional conduction equation,

$$\frac{1}{\alpha}\cdot\frac{\partial T}{\partial t} = \frac{\partial^2 T}{\partial x'^2} \qquad 0 \le x' \le 1 \qquad (4\_14)$$

They should also meet the following requirements:

$$1)\ \partial T/\partial x' = 0 \qquad \text{at} \qquad x' = l$$

$$2)\ -\partial T/\partial x' = \frac{h}{k}.dT \qquad \text{at} \qquad x' = 0$$

$$3)\ T = T_{\circ} \qquad \text{at} \qquad t = 0$$

where dT is the temperature difference for the convective heat transfer at the surface. The calculation procedure for this case has been presented in the form of charts which have been used for convenience. In the charts, the temperature history through the slab is drawn against two dimensionless parameters(chart 1). First is the dimensionless time, Fourier modulus: $Fo = \alpha.t/l^2$ where $\alpha = k/\rho.c_p$, k=slab thermal conductivity, ρ =slab density and c_p =slab specific heat and "t" and "l" represent the time and length parameters. The second is the dimensionless thermal resistance of the material, Biot modulus: Bi=h.l/k where h is the convective heat transfer coefficient. When the surface temperature after a certain time is determined by the test, the Fourier modulus and the temperature ratio $(T_{air} - T_s)/(T_{air} - T_{\circ})$ can be calculated and then the Biot modulus may be read from the charts.

Method 2:

If the slab is thick enough to be assumed semi-infinite, (figure 4-2b), the temperature history through it is known to follow the Gaussian error function.

$$\frac{T_{air} - T_{x'}}{T_{air} - T_{\circ}} = G\left(x'/2\sqrt{\alpha t}\right) \qquad (4\text{-}15)$$

where G is the error function, and $x'/2\sqrt{\alpha.t}$ is the dimensionless penetration depth x^*,(figure 4-3). For $x^* > 2$ the error function is one. A plate may be assumed semi-infinite if the penetration depth(x') corresponding to $x^* = 2$ remains less than the plate thickness during the test. The solution to this problem has also been presented in form of charts (i.e. chart 2), where the temperature ratio is drawn against two dimensionless variables. First is the local Biot modulus, $h.x'/k$, while the second is the boundary-Fourier modulus: $\Theta = (h/k)^2.\alpha.t$. In the phase change paint method the local Biot modulus is always zero since the paint measures the plate temperature at the surface. The temperature ratio (defined as in method 1) shall also be known at the colour change moment. The boundary-Fourier modulus may then be taken from the chart and then the heat transfer coefficient is only a simple function of the time for the colour change.

Method 3:

A simple calculation method may also be used to simplify the solution for the semi-infinite plate (figure 4-2b). Writing Newton's law of cooling for every position on the plate and for a short length of time:

$$c_p \cdot \rho \cdot x' \cdot dT = -h(T_s - T_{air})\, dt \qquad (4\_16)$$

Attention must be given in the above formula to the application of every parameter. T_s is the surface temperature at any time which varies from that of the ambient temperature at the start of the test to the phase change temperature. T_{air} is the local air temperature. dt is the time interval which is set to zero at the start of the test, and recorded for every point when the paint changes colour.

The left hand side of the equation (4-16) represents the local energy rise in the flat plate. x′ is the penetration depth at which $x^*=2$, and dT is the average temperature rise for the penetration depth. If the temperature history inside the plate is Gaussian, then the average penetration depth (x") is always a fixed portion of the penetration depth (x′), for $x^*=2$. The coefficient can be calculated by averaging the Gaussian function. Therefore:

$$dT \Rightarrow dT_s \qquad x' \Rightarrow x'' \qquad x' = x'/a \qquad a = 3{,}596 \qquad (4\_17)$$

Applying this to equation 4-16 gives:

$$c_p \cdot \rho \cdot x'\, dT_s = -a.h.(T_s - T_{air})\, dt \qquad (4\_18)$$

$$\frac{d(T_s - T_{air})}{(T_s - T_{air})} = \frac{-a.h}{c_p \cdot \rho \cdot x'}\, dt$$

$$h = \frac{c_p \cdot \rho \cdot x'}{a \,.\, t} \,.\, \ln \frac{T_{air} - T_\bullet}{T_{air} - T_s} \qquad (4\_19)$$

If the value of $x' = 4\sqrt{\alpha \,.\, t}$ is substituted into the above formula:

$$h = b' \cdot \frac{\sqrt{\rho\, c_p\, k}}{\sqrt{t}} \cdot \left(\ln \frac{T_{air} - T_\bullet}{T_{air} - T_s} \right) \qquad (4\_20)$$

or

$$\frac{T_s - T_{air}}{T_\bullet - T_{air}} = e^{\left(\frac{-b.h}{\sqrt{c_p \cdot \rho \cdot k}}\right)\sqrt{t}} \qquad (4\_21)$$

where b=1.112. If replacing $\rho.c_p$ with k/α this will be the identical relationship to the boundary-Fourier modulus avoiding the need for any charts. In equations 4-20 and 4-21, three parameters are unknown, namely: T_s, h and t. At the time in the experiment when the paint changes colour, T_s and t are known and therefore h may be calculated from equation 4-20. If h is constant throughout the test, then T_s may be calculated at any time from equation 4-21.

4.3.3 Experimental Set Up.

The study of heat transfer beneath a two-dimensional wall-jet was selected to illustrate the use of the phase change paint method for wall-jet flows. This choice was made since there was already some data available for comparison purposes and the geometry was relatively easy to set up on the present test rig. The jet slot dimensions chosen were 5 mm X 840 mm which, together with confining side walls, ensured two-dimensionality.

Hot air was provided by employing an equal load on all elements of the heater battery, enabling the nozzle exit temperature to be brought up to 110 C. The nozzle exit velocity was set at 17.9 m/s resulting in a slot Reynolds number of 3730. The target plate was from perspex which is a good insulant. As will be explained this was important for the assumption of one-dimensional conductive heat transfer through the slab.

The rig was first heated up to the desired nozzle exit temperature. In order to avoid heater burn out, the heater was not loaded without an air flow, and the heater exit temperature was held below 170 C. After stabilising the rig temperature, the hot air was directed to the laboratory through the by-pass valve so that the experiment could be set up. The flow was subsequently directed back to the plenum chamber/nozzle box, but was deflected away from the target plate as indicated in figure 4-4. Removing the diversion plate initiated the test, and the heated jet then flowed over the target plate which had been covered with a thin layer of the phase change paint. The time taken for the paint on the plate to change colour was recorded for points 4 cm apart starting from the nozzle.

Figure 4-5 shows the temperature profile at any downstream position. This profile is expected to follow curve (a) at t=0. Gradually as the plate warms up, the profile changes to (b) and finally it is expected to become normal to the plate, curve (c), which is the boundary condition for the adiabatic plate. It takes a very short time (approximately one minute) before the profile changes from (a) to (c). Therefore reported temperature profile measurements (Seban and Back(1961) and MoK(1984) show trends similar to curve (c).

The air temperature adjacent to the surface was measured along the plate at the peak temperature location(figure 4-6). The maximum temperature decay, downstream of the nozzle may be correlated in a similar way to the maximum velocity decay (chapter 2):

$$\frac{T_m - T_\infty}{T_{slot} - T_\infty} = k_\theta \left(\frac{x}{S}\right)^{-0,5} \qquad (4\_22)$$

where $k_\theta = 3.08$.

This configuration utilised the method in a different way to that adopted by Jones and Russell (1978 and 1980). The latter employed insulated wind tunnels where the air temperature was maintained constant in the streamwise direction. The variable streamwise air temperature characteristic of a wall-jet, adds complications to the use of the method. Any common insulant used for the target plate will deform after 80 C and the paint changes colour at 43 C. This is a severe restriction on the air temperature as it must be held between 60 and 70 C. In the present experiment the jet temperature at the nozzle was 110 C. The jet lost heat very rapidly and so the data was only obtained for a limited downstream distance. This problem was ignored for the present experiment since only one test was carried out and it was aimed at demonstrating the application of the phase change paint in the wall-jet flows.

4.3.4 Results And Discussion

The assumptions in the application of this method to the present experiment are as follows:

1. The heat transfer rate through the slab is assumed one-dimensional. , Using the principal of superposition, the heat flow inside perspex in directions X and X′ can be treated individually. The heat penetration is negligible after $x^*=2$ in any direction. This shows that it takes heat about 100 seconds to travel every centimetre through the

perspex. The experiment lasted only 102 seconds which allowed heat to travel for one centimetre in any direction. The temperature decay for the wall-jet was less than three degrees centigrade for every centimetre. Comparing the distance between every two reading stations (4 cm) and the plate thickness (0.58 cm) and the temperature gradients in X and X′ directions, (2 degrees compared with at least 34 degrees for every 6 mm), it is clear that the heat transfer in the X direction may be ignored.

2. It was necessary to insulate the colder side of the slab to meet one of the boundary conditions. The perspex was therefore placed on a second sheet of perspex and then on plywood. The air gaps between the plates also provided some insulation.

3. This method assumes uniform heat transfer coefficient (h) throughout the test and ignores its possible variations due to the increase in the slab surface temperature. This convection coefficient is therefore an average value for the duration of the test.

4. The other condition for the application of this method is that the plate should suddenly be exposed to heat. This was achieved here by employing the deflection plate.

Table 4-1 shows the step by step calculation procedure for every point. Three heat transfer coefficients are presented where each is obtained using one of the above mentioned methods. The resulting heat transfer coefficients are compared with the data of Seban and Back(1961) and the profile analysis results of Hammond(1982b) (figure 4-7). The figure also includes the vlaues for heat transfer Stanton numbers calculated using the slot parameters. The agreement is reasonable and demonstrates that realistic results may be obtained from this method. Seban and Back (1961) do not clearly explain the boundary conditions in their experiments but it is understood that their test was for a heated plate and an ambient jet. This is possibly the reason for the difference in their heat transfer coeffients compared with other data.

As the values for the penetration depth in the table 4-1 show, the plate may be assumed semi-infinite only for the first three measurement stations from the nozzle. The results show that there is limited allowance for the choice of the method even if the plate is not thick enough to be semi-infinite. For the point furthest away from the nozzle(x/S=56), the results from different methods show little difference although the penetration depth is more than twice the plate thickness.

The presence of the paint over the plate may introduce some resistance to the heat flow and also disturb the boundary layer. These two effects may both be reduced by careful application of a uniform and thin layer of paint. This is perhaps the main drawback to the method. Other similar techniques which effectively avoid the surface irregularities are considerably more difficult and expensive to employ (Ainsworth and Jones(1979)).

A simple calculation compared the thermal radiation between the plate and its surroundings and the heat transferred from the jet to the plate. This showed that the former at its highest is only two to five perecent of the latter at its lowest and therefore radiation effects may be ignored.

The experimental uncertainty in the present heat transfer data was estimated to be 9% (at 20:1 odds) at the point nearest to the nozzle (x/S=8), using the method of Kline and McClintock(1953). This reduces to 4% for the point furthest away from the nozzle(x/S=56). The error in time measurement was the main contributor to the former, while the error in the perspex plate thickness (which varies from 0.56 to 0.6 mm) was the main cause for the latter. In experiments lasting less than 10 seconds, the time measurement can be a major source of error. Using a camera to freeze the clock and the patterns on the test surface in the same picture, can eliminate this error. Unlike the present test, where the clearance patterns were straight lines, the use of a camera is essential in the cases of three-dimensional flows.

This experiment was the first attempt to use phase change paints for heat transfer measurements at Cranfield. It will obviously take some time before the technique is established and applied to different geometrical configurations. Present experiments and the tests by Jones and Russell (1978 and 1980) demonstrate the potential for the application of the phase change paint to the heat transfer measurements. Once set up properly, the tests are simple and can be applied to many configurations.

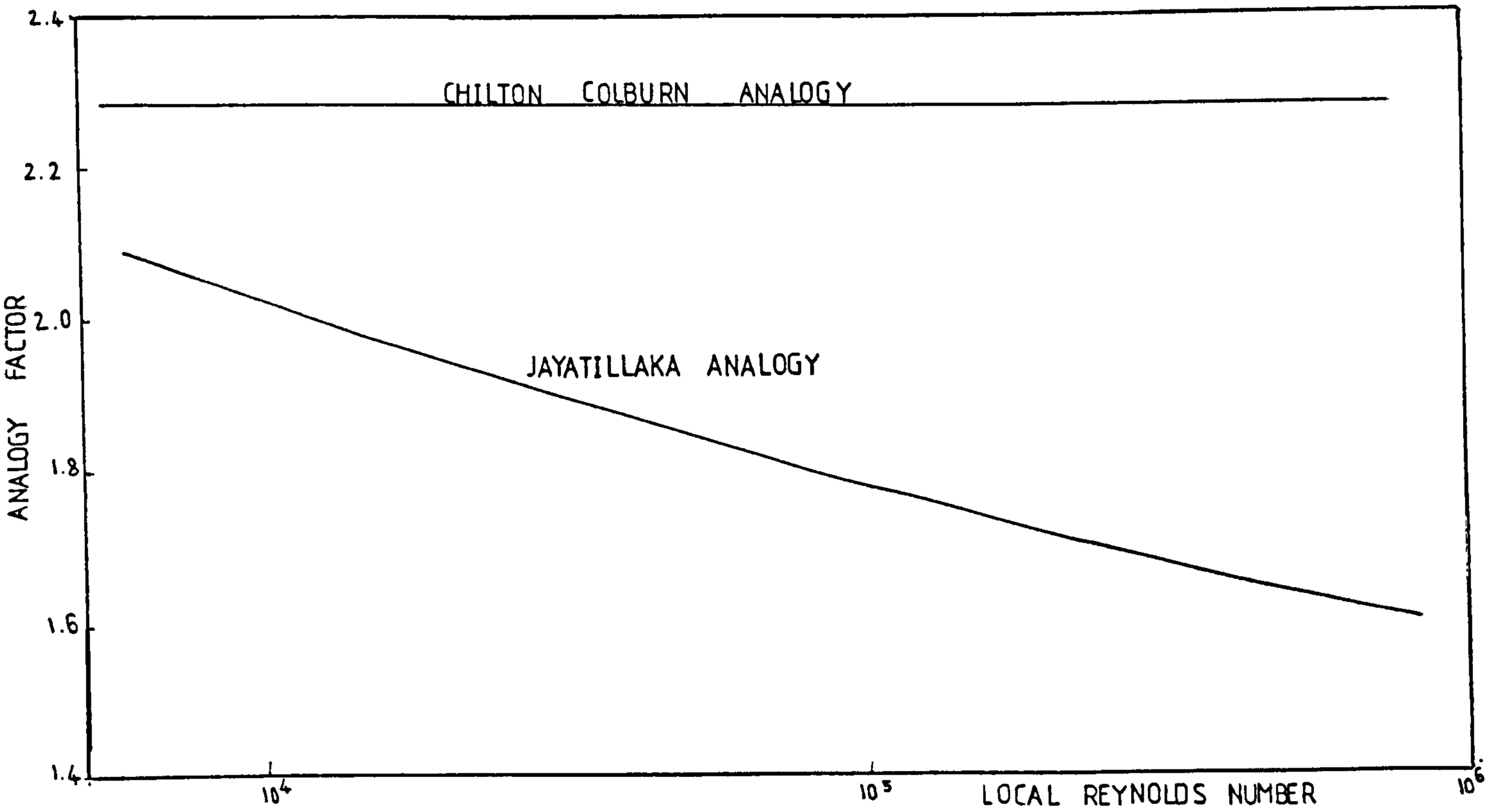

FIGURE 4-1 COMPARISON BETWEEN THE ANALOGY FACTORS(MAHMOOD 1981)

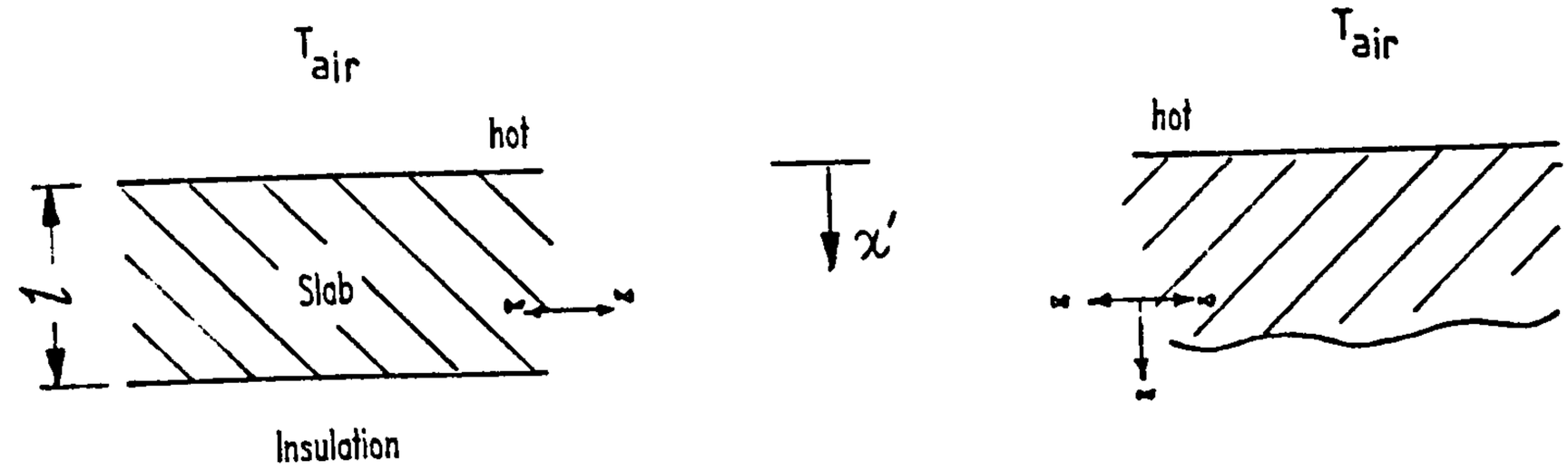

a) Slab of finite thickness. b) Semi-infinite plate

Figure 4-2 Geometrical configuration for the three calculation methods.

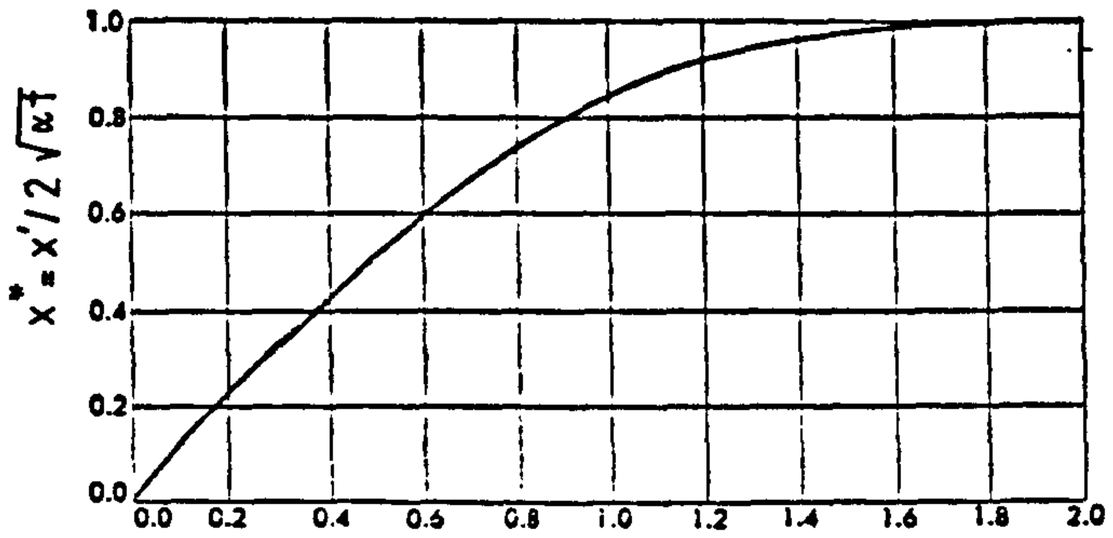

$$\frac{T_{air} - T_{x'}}{T_{air} - T_{\bullet}}$$

Figure 4-3 The Gaussian error function. (from Krieth 1965)

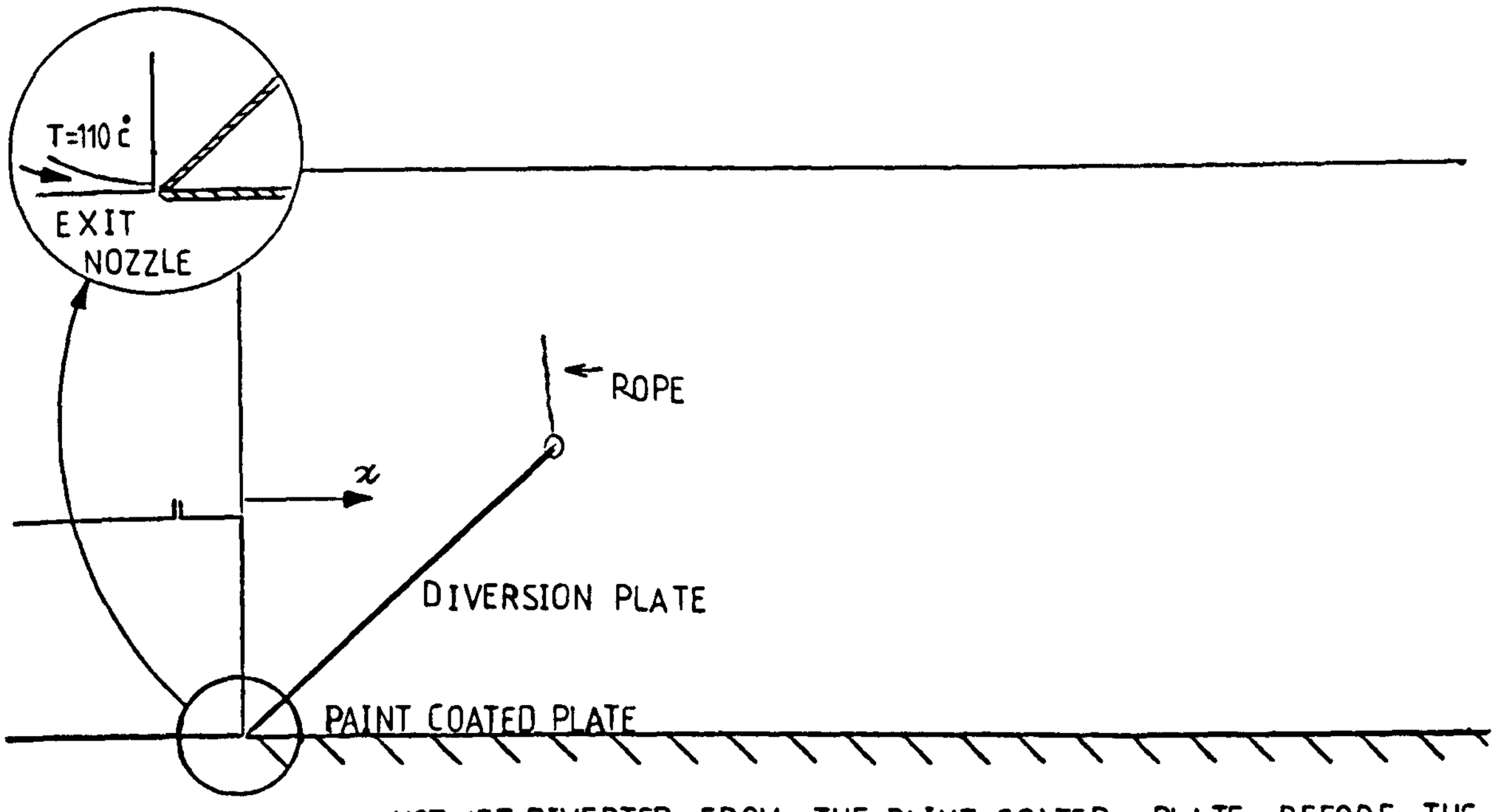

FIGURE 4-4 HOT JET DIVERTED FROM THE PAINT COATED PLATE BEFORE THE TEST START

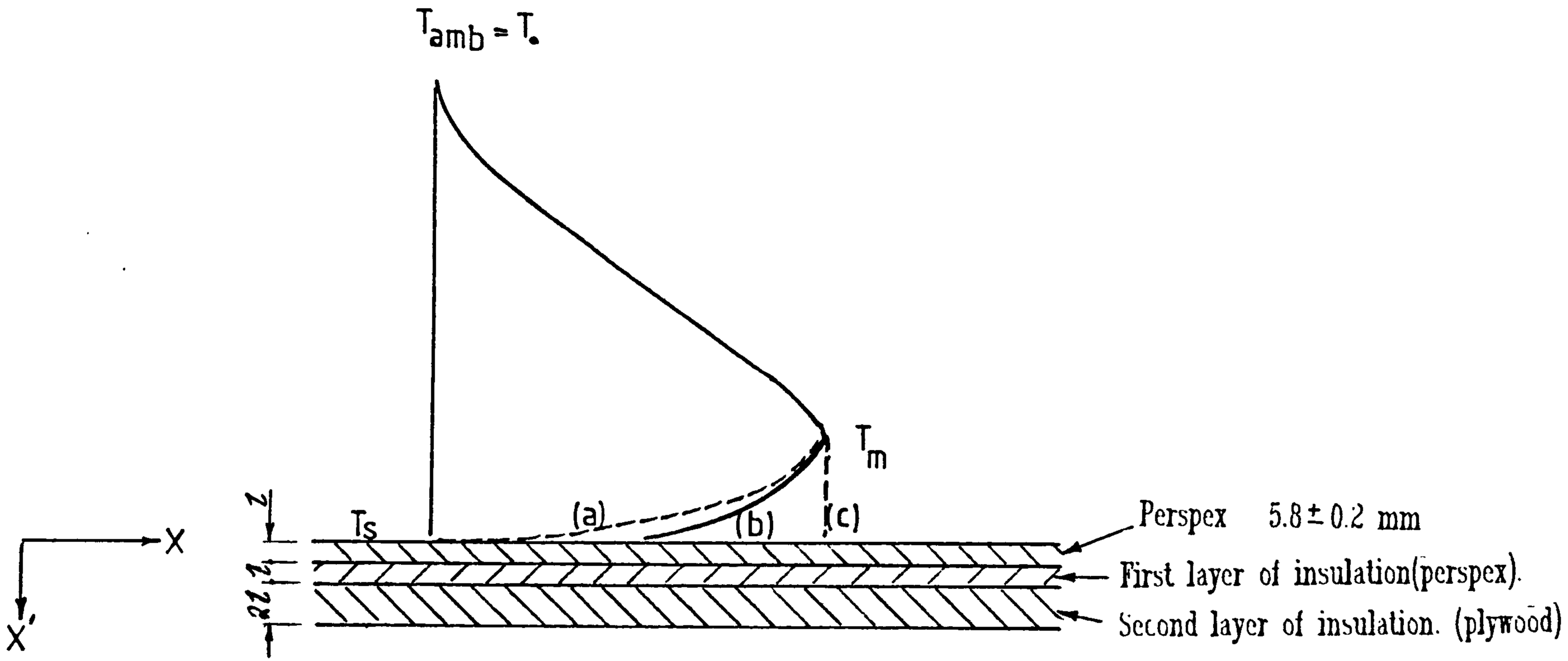

Figure 4-5 Wall-jet temperature profile and the insulated perspex plate at any downstream position.

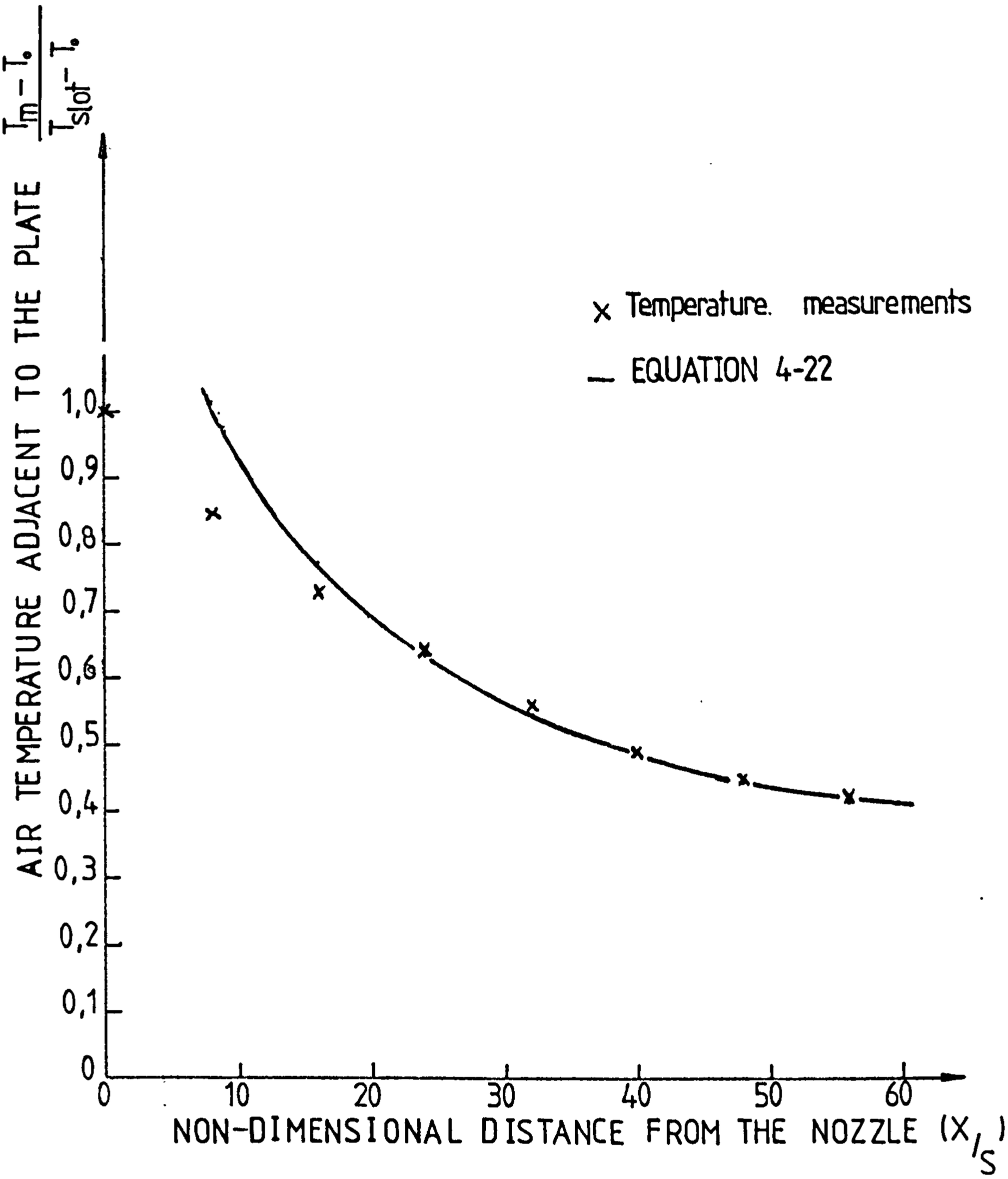

FIGURE 4-6 MAXIMUM TEMPERATURE DECAY ALONG THE WALL-JET

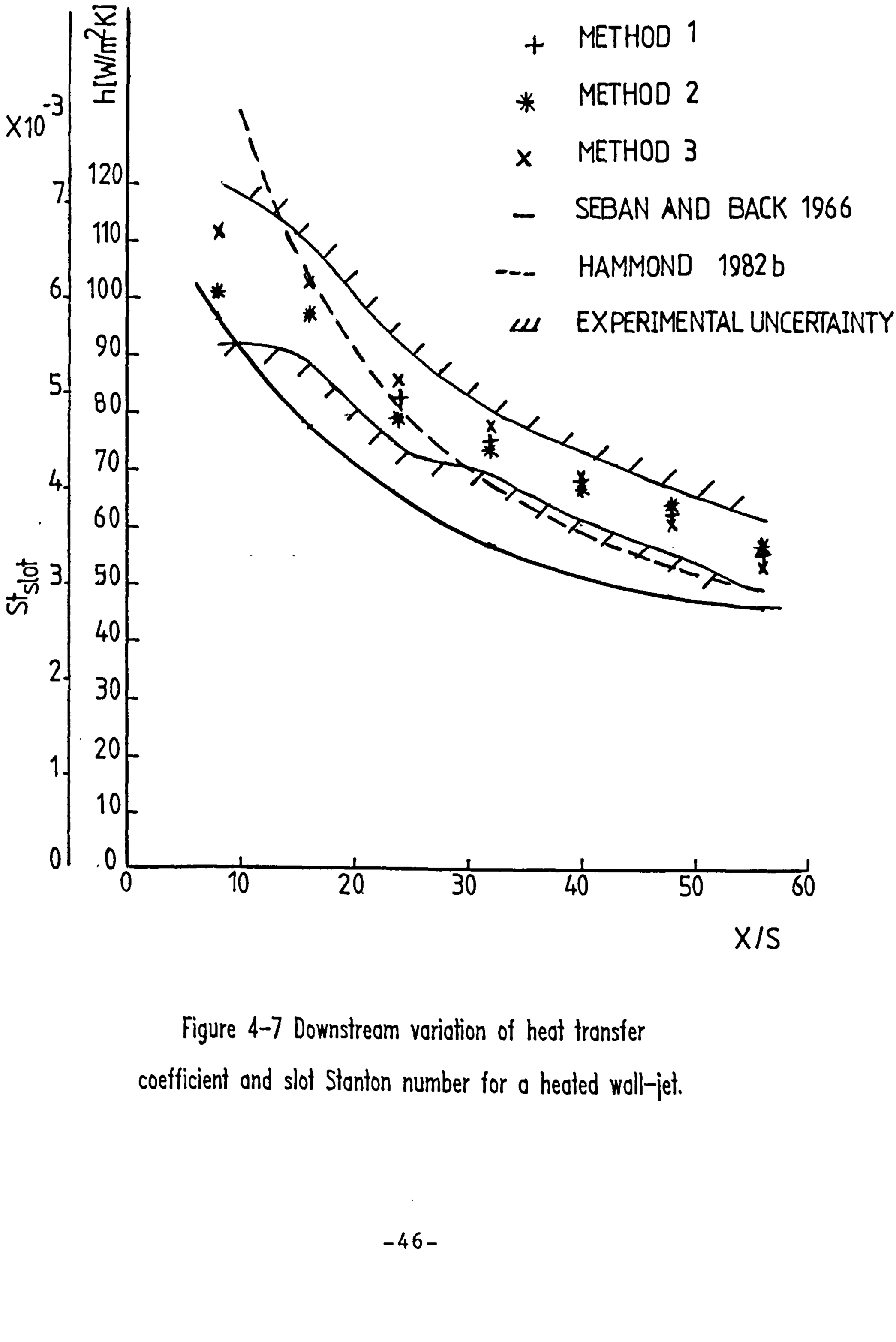

Figure 4-7 Downstream variation of heat transfer coefficient and slot Stanton number for a heated wall-jet.

					FIRST METHOD			SECOND METHOD		THIRD METHOD
DISTANCE FROM THE NOZZLE, X/S	PHASE CHANGE TIME t[Sec]	LOCAL AIR TEMPERATURE °C	PENETRATION DEPTH $x^*=2$ x' [cm]	$\frac{T_m - T_p}{T_m - T_s}$	FOURIER MODULUS Fo	$(\frac{h.l}{k})^{-1}$	h [W/m² K]	BOUNDARY FOURIER MODULUS	h [W/m² K]	h [W/m² K]
8	3.6	96.5	0.25	0.717	0.0116	-	_	0.112	101.1	111.7
16	6.0	86	0.32	0.671	0.0193	-	-	0.173	97.3	103.8
24	12.1	78	0.46	0.624	0.0388	0.409	79.4	0.252	82.7	86.1
32	21	71	0.60	0.57	0.0674	0.439	74	0.363	75.4	78.2
40	38.8	65	0.82	0.51	0.125	0.484	67.1	0.56	68.9	68.9
48	63.2	61.5	1.05	0.467	0.203	0.502	64.7	0.75	62.5	61
56	102	59	1.33	0.431	0.327	0.571	56.9	1.0	56.7	53.1

For Perspex: k=0.1884 W/m °K, c_p=1465 W.Sec/Kg °K, ρ=1190 Kg/m³, α= 1.08X10^{-7} m²/Sec

++++++++++

Re =3730 , Plate thickness(l)= 0.58 ± 0.02 cm , T_{amb} =T_s =21.9 °C,

T_p :Phase change temperature= 43 °C , Nozzle exit temperature=110 °C.

Table 4-1 Step by step calculation of heat transfer coefficient in the phase change paint method

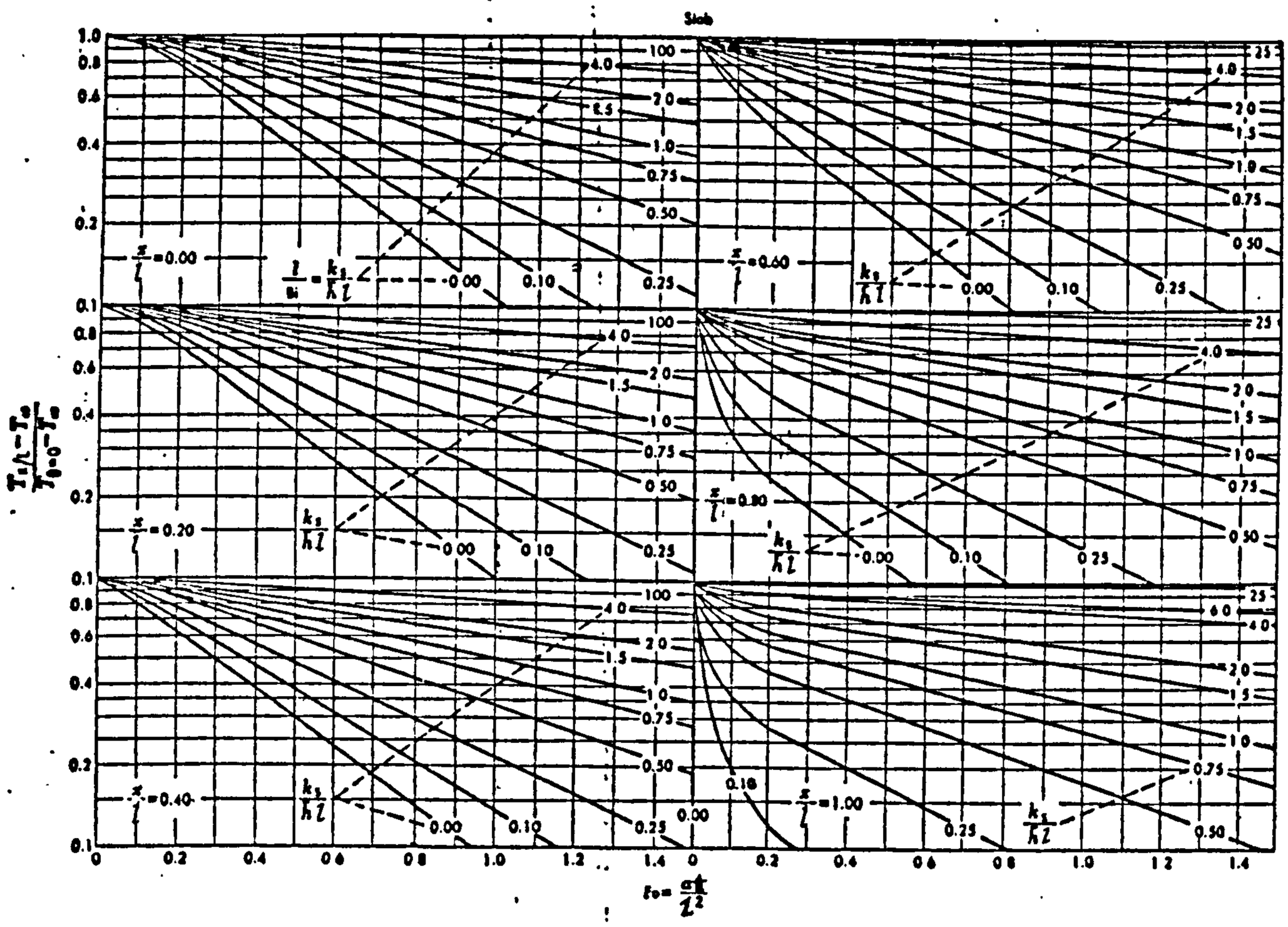

Chart 1 , Dimensionless temperature distribution in a slab (from Krieth 1965)

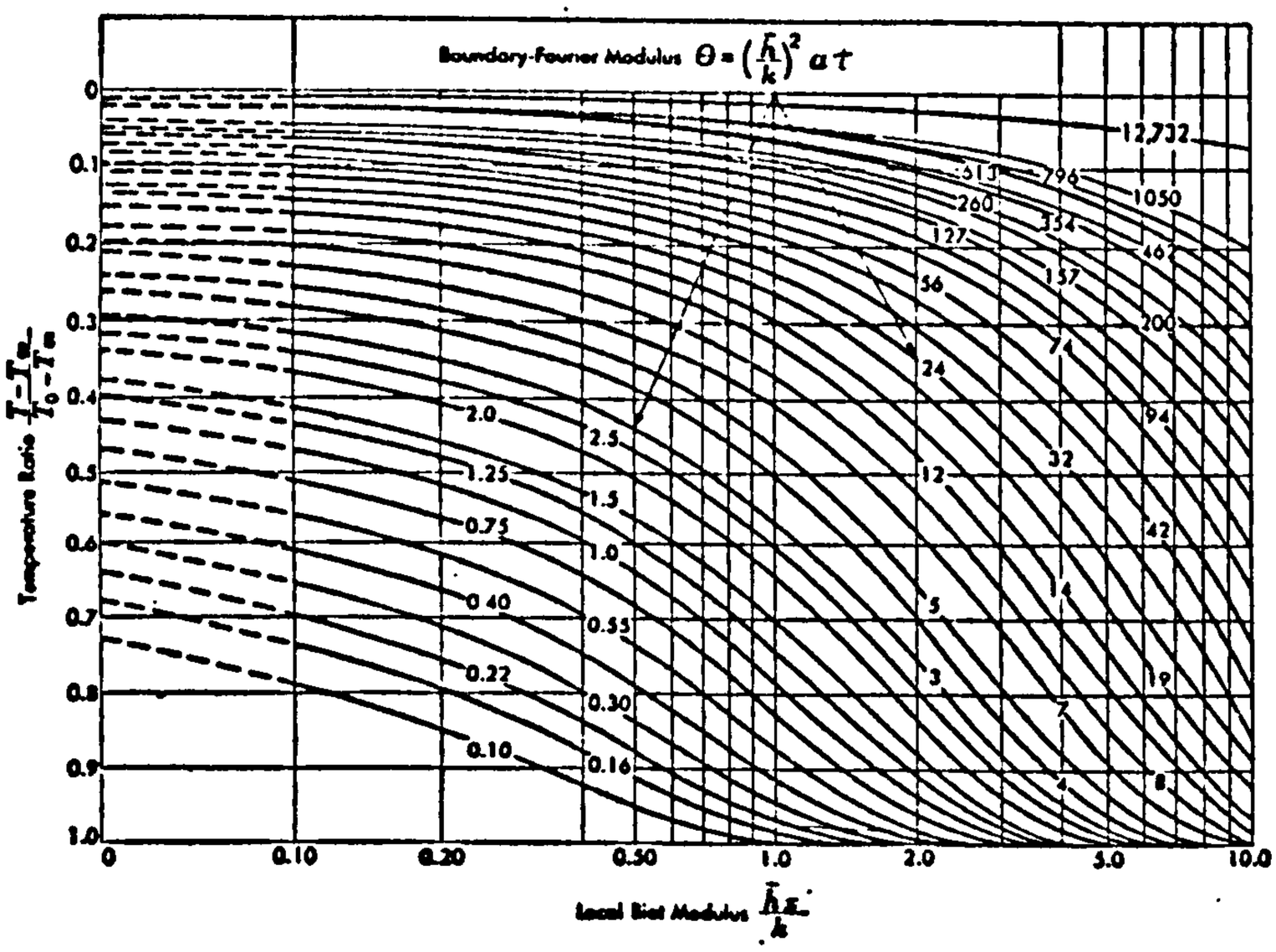

Chart 2 , Dimensionless temperature distribution in a semi-infinite plate. (from Krieth 1965)

CHAPTER 5

THREE-DIMENSIONAL PARALLEL WALL-BOUNDED JET HEAT TRANSFER

CHAPTER 5

THREE-DIMENSIONAL PARALLEL WALL-BOUNDED JET HEAT TRANSFER

5.1 INTRODUCTION

Study of the three-dimensional jets parallel to flat boundaries demonstrates many differences between this configuration and its two-dimensional counterpart. The presence of spanwise mixing, reduces the vertical spread compared to that of a plane jet. Similarly, the absence of the Chilowsky effect in the three-dimensional off-set jet leaves the jet to approximately follow along the nozzle axis. The spread is then only affected by the plate after the jet impinges upon it.

In this chapter velocity field measurements for three-dimensional wall-jets and off-set jets are presented. The mass transfer method has been employed to simulate the heat transfer from a constant temperature wall to the jet. The data covers the range of jet configurations from the wall-jet to jet with an off-set height of 7.4. An 'intermediate level' calculation procedure has been used to study the effect of the slot Reynolds number and aspect ratio on the average heat exchange from the plate. A simple correlation is then presented that enables the calculation of the surface averaged Stanton number from a knowledge of the slot parameters and plate length.

5.2 THE FLOW FIELD.

5.2.1 General Arrangements.

An outlet nozzle of dimensions 20 mm X 10 mm (W X H) was chosen, as this constitutes a bluff-jet according to Rajaratnam's definition (Rajaratnam 1974). The air velocity at the nozzle exit was determined by means of a pitot tube at different Reynolds numbers. Pitot tube traverses across the aperture indicated that the exit velocity profiles were essentially uniform in every

direction. The mean exit velocity was calibrated against the plenum chamber static pressure, so that the latter could subsequently be used to set the former. Downstream of the nozzle the jet was found to spread symmetrically about the X-axis. This was regularly monitored during the experiments, and visually demonstrated by the mass transfer clearance patterns. The required off-set was achieved by vertical movement of the settling chamber.

The general experimental set-up and the co-ordinates for these flow field and mass transfer experiments are shown in figure 5-1. The Reynolds number at the nozzle exit (based on nozzle height) was maintained nominally at 25000. This value was selected near the maximum design Reynolds number of the test rig to increase the accuracy in both the velocity field measurements and the mass transfer tests.

Cross-stream (Y direction) velocity profiles for the three-dimensional wall-jets and off-set jets, were measured along the centre-plane for six dimensionless off-set heights, ranging from 0 to 3.8. In three of the cases examined, measurements were also made in the lateral direction (Z). A number of streamwise stations were selected for each case in order to enable the general flow patterns to be studied. These measurements were obtained both before and after the jet impinges upon the plate. In the spanwise direction the profiles were measured at stations which started from the centre-plane and were spaced such that 4 to 6 stations covered the spanwise spread of the jet.

The pitot tube used in the velocity profile measurements was made out of hypodermic tubes, 19 swg at the tip gradually expanding to 10 swg, and was connected to a micro-manometer with a range of 0.01-100 mmwg. At low air velocities, (less than 10 m/s) the experimental uncertainty was estimated to be 20% (at 20:1 odds) using the method of Kline and McClintock(1953) (see Appendix C). Therefore, measured velocities below 5 m/s are likely to be very inaccurate. This agrees with White's suggestion (White 1979) that only at Reynolds numbers (based on the local velocity and the pitot tube tip diameter) greater than 1000, the velocity can be predicted from the difference between static and stagnation pressure according to Bernoulli equation.

The cross-stream velocity profiles are presented in Appendix D along with the details of the measurements where symbol (x) represents the experimental measured data for which the average uncertainty is estimated to be 3%. If the height and velocity values are non-dimensionalised using the velocity half-width and the local maximum velocity respectively, the profiles will all collapse into one. A selection of these is plotted in figure 5-2 where these are compared with the profile analysis of Hammond

(1982 b). The maximum velocity decay and spread rates obtained from the above profiles are presented in table 5-1. In the following sections, the three-dimensional wall-jet is compared with experimental data obtained in previous studies (section 2.4). The off-set jet values are also included where appropriate. The equations are obtained by Hammond (private communication) from an evaluation of the data presented by Launder and Rodi (1981) and Rajaratnam (1974). The parameters characterising the three-dimensional wall-jet (such as b_y and b_z and y_m) are defined in figure 2-4. Similar definitions are used for the off-set jet and the dimensionless off-set height is given the symbol OH.

5.2.2 Position Of The Maximum Velocity.

Generally the height of the velocity peak (y_m) appears to remain constant over the centre-plane for downstream distances ($0 \leq x/S \leq 40$) considered in the present study. Launder and Rodi(1981) concluded, from two sets of wall-jet measurements by previous experimenters, that this peak rises with downstream distance. Figure 5-3 compares the previous data with that obtained in the current study. The upward trend in the maximum velocity height is not apparent before about 40 dimensionless distances downstream of the nozzle. There is only one set of data available for positions further downstream for which an upward trend is observed. The velocity peak height data may be correlated with the following expression:

$$y_m/S = 0.16 + 0.0082\ x/S \qquad (5\text{-}1)$$

Although this agrees with the general trend as demonstrated by Launder and Rodi, the scatter in the data is high for points closer to the nozzle than x/S=40. This is not surprising for bluff-jets, as their mixing characteristics differ at points near the nozzle compared with positions further away. In any case there is considerable difficulty in locating the maximum velocity accurately, especially near the nozzle. This uncertainty is comparable in most measurements with the scatter in the above figure. It might be expected that the position of the maximum velocity would start from the nozzle axis and move upwards. The above correlation (equation 5-1) does not indicate a value of y_m greater than the nozzle axis until x/S=41, although the majority of the present and previous measurements are indeed for distances closer to the nozzle.

Linear increase of y_m as correlated by equation 5-1, has been confirmed indirectly, since Launder and Rodi have noted that as $y_m \propto x$ and $u_m \propto x^{-1}$, $u_m y_m/\nu$ remains constant and therefore a uniform value of skin-friction downstream the bluff wall-jet is to be expected. Measurements by

Rajaratnam and pani (1976) confirm such constant coefficient of friction and this indirectly demonstrates the linear rise in the position of the maximum velocity.

In the off-set jet, the velocity peak location remained constant downstream and no significant deviations from the nozzle axis was noticed. The same occured in the spanwise direction before the jet impingment upon the plate. After that the peak moved towards the plate and reached the wall almost at the last lateral measurement station (Table 5-1). Koso and Ohashi (1982) have proposed a relationship for the spanwise variation of the above in the form:

$$\frac{y_m}{y_{mo}} = e^{\left[(-\ln 2).(\alpha)^{\left\{\left(\frac{0.4}{\alpha+0.4}\right)+1\right\}}\right]} \qquad \alpha = \frac{z}{b_z} \qquad (5-2)$$

where y_{mo} is the position of the maximum velocity over the centre-plane.

5.2.3 Decay Of The Maximum Velocity.

The decay of the maximum velocity is shown in figure 5-4. The data for different off-set heights are compared with equation 2-7 which in a dimensionless form may be written as:

$$\frac{u_m}{u_{slot}} = \left[1+\left(\frac{7.7\sqrt{AR}}{x/S}\right)^{-6}\right]^{-1/6} \qquad (5-3)$$

where AR is the slot aspect ratio. The velocity decay for larger off-set heights is marginally faster. This may be attributed to the extra entrainment of the jet on its wall-side when the separation distance is greater. Nevertheless, the equation is an equally good approximation to all the cases. Spanwise velocity decay expression was expressed by Koso and Ohashi similar to equation 5-2 in the form:

$$\frac{u_m}{u_{mo}} = e^{\left[(-\ln 2).(\alpha)^{\left\{\left(\frac{0.4}{\alpha+0.4}\right)+1\right\}}\right]} \qquad \alpha = \frac{z}{b_z} \qquad (5-4)$$

where u_{mo} is the maximum local velocity over the centre-plane.

5.2.4 Jet Spread.

Figure 5-5 shows the vertical half-width spreading rate which has a similar trend for all off-set heights. b_y/S increases with distance from the nozzle due to the jet entrainment and vertical diffusion. For $x/S \geq 18.9$, the data is rather sparse and uncertain. This is due to the

lack of measurement accuracy as previously discussed. This data is in good agreement with the correlation:

$$b_y/S = 0.93 + 0.045\ x/S \qquad (5\text{-}5)$$

The slope of which was in the range ($db_y/dx = 0.048 \pm 0.003$) mentioned in section 2.4.

The peak of the velocity profile moves towards the wall by moving from the centre-plane in the Z-direction. b_z is measured along contours of the u_m values at lateral stations. This was in contrast to the previous practices reviewed in section 2.4, to bring the movement of the peak of the velocity profile into attention, (The reviews in section 2.4 have measured b_z at a constant height from the flat plate). The values of the lateral half-width spread are presented in table 5-1. Figure 5-6 shows the downstream changes of b_z/B. No deviation due to the off-set height is evident in figure 5-6. Therefore the lateral spread may be expressed using the present data and that of Rajaratnam (1974) and Launder and Rodi (1981) as:

$$\begin{aligned}
b_z/B &= 0.5 && && x/B \leq 3.5 \\
b_z/B &= 0.073\ x/B + 0.26 && && 3.5 \leq x/B \leq 11.9 \\
b_z/B &= 0.20\ x/B - 1.25 && && 11.9 \leq x/B \leq 130 \\
b_z/B &= 0.26\ x/B - 9.05 && && 130 \leq x/B
\end{aligned} \qquad (5\text{-}6)$$

5.2.5 Momentum Loss.

The final mean-flow test criteria used, was the conservation of momentum flux evaluated from the product ($M = u_m^2 b_y b_z$), as suggested by Launder and Rodi (1981). The ratio of M at the downstream distances (x/S) of 18.9 and 9.4 was found to be 0.68. Using the above correlations (equation 5-3, 5-5 and 5-6) for the flow field, the corresponding value was calculated to be 0.75.

5.3 MASS TRANSFER MEASUREMENTS.

Mass transfer tests were carried out to study the effect of off-set height on the heat transfer from the plate to the bluff-jet.

5.3.1 Experimental Procedure.

The rig was switched on at least 30 minutes prior to each test run, while the test plate was being simultaneously sprayed. This allowed the temperature to

reach equilibrium conditions. The water cooler was used to cool the air down to the ambient temperature after being heated by the fan.

The naphthalene was sprayed on a perspex plate of dimensions 470X420X6 mm which was positioned over the melamine coated plate during the test (figure 5-1). While the sprayed plate was being positioned in the test rig, the conditioned air was diverted into the laboratory. The paralellism between the jet nozzle and the perspex plate was checked using a spirit level for every test run. When the sprayed plate was secured in its position, the flow was redirected over the target plate, thereby marking the start of the test.

During the tests it was possible to distinguish clearance patterns for dimensionless off-set heights of up to 3.8 and at greater heights the target plate cleared simultaneously. Two test plates, each 47 cm long, were required to cover the full streamwise length (x/S=94) under study. The plate immediately located after the nozzle is referred to as the first plate while the other plate, located further downstream, is the second plate.

For the tests on the second plate, a naphthalene coated dummy plate was placed upstream. This was done in order to retain the initial boundary conditions and was a similar practice to that adopted for the study reported in the bound paper (Alamdari, Hammond and Montazerin (1986)), where test runs performed without naphthalene sprayed dummy plates displayed discontinuities in the mass transfer rates. Such phenomenon was analogous to that experienced in boundary layer heat transfer with an unheated starting length.

Clearance contours were drawn on the perspex plate during the test at different time intervals. These were then transferred to drawing paper. Each test was continued until the clearance patterns recorded were close to the physically distinguished jet boundaries. For each test, the timer was started at the commencement of the target plate spraying.

The clearance contours did not represent constant mass transfer rates since the spray thickness was not uniform (due to the time lapse necessary to spray the whole plate). Different points on the plate were selected to obtain a distribution of the Stanton numbers. Using such a distribution, contours of constant Stanton numbers were drawn.

Daily changes in the ambient conditions were taken into account in the calculations. The average value for various test parameters were as follows: density=1.196 Kg/m^3, specific heat=1004.5 J/Kg K, viscosity=0.18X10 Kg/m^2 s, Reynolds number=24910, Schmidt

number=2.45 and Prandtl number=0.709.

5.3.2 Heat And Mass Transfer Results.

Constant mass transfer contours for selected off-set heights ranging from the wall-jet case up to a dimensionless off-set height of 3.8 are presented in Appendix D with and without the local values. The contours are generally for the first plate since the effect of the off-set height on mass transfer rate was reduced over the second plate. This is illustrated in figure 5-7, where the centre-plane mass transfer distributions for different off-set heights are compared. Heat transfer values obtained using the Chilton-Colburn analogy, are also presented in the same graph. The mass transfer rates for the second target plate were measured for the wall-jet and for the jet with an off-set height of 3.8. It was just possible to distinguish the clearance contours for the wall-jet case. However, in the off-set jet no distinct clearance patterns were discernible, and the naphthalene appeared to clear along the whole plate at the same time. The mass transfer distributions in both cases were very similar.

The test with an off-set height of 7.4 produced only one data point (the plate appeared to clear simultaneouly) which is taken as the maximum value. This is shown in figure 5-8, where the effect of the off-set height on the peak Stanton number is displayed. The data points in this figure suggest a hyperbolic curve which has its maximum value for the wall-jet and reduces with increasing off-set height. This curve may be expressed as:

$$St_m = \frac{1{,}65X10^{-3}}{(OH)^{0{,}75}} \qquad (5\text{-}7)$$

Figure 5-9 shows the effect of the off-set height on the downstream location of the peak mass transfer coefficient. This was obviously located at the nozzle exit ($X_r=0$) for the wall-jet case and when the off-set height was increased it moved gradually downstream. It may be assumed that this corresponded with the point at which the jet impinges over the plate. The approximate position of this impingement point was detectable for smaller off-set heights, but this became increasingly more difficult for higher ones. The data seems to suggest a straight-line ($x_r=7.42$ X OH) which may be expected to pass through the origin. This is far beyond the attachment line for an off-set two-dimensional jet. The side-wise entrainment precludes the creation of a low pressure closed 'vortex' underneath the jet, as occures with the latter type of jets.

Figure 5-10 shows the surface averaged heat transfer rate from the plate as a function of downstream distance for different off-set heights. This average was obtained in a corridor which starts from the nozzle edges and spreads with a slope of dz/dx=3.1. This was an arbitrary choice which seemed to adequately encompass the spread of the wall-jet and the off-set jets. The computer program presented in section 5.4 calculates the limits of the jet spanwise spread which was in good agreement with this line. Simple multiples of the half-width spread, neither agreed with the spread rate predicted by the program nor provided a more accurate prediction of the jet boundaries as shown by the mass transfer experiments. The grid points used for averaging purposes were located at the intersections between the constant mass transfer contours and the centre-line. Doubling the number of these grids produced only a 1% change in the surface averaged values. The real error in averaging is likely to be slightly higher than 1%, since the Stanton numbers near the outer boundaries were not accurately measurable and therefore had to be approximated. The averages were also sensitive to the interpretation of the contours at points near the nozzle, especially in the case of the wall-jet. This effect is further discussed in section 5.4.

To obtain a curve fit to the data reported in figure 5-10, a two part formulation was employed: the first part representing the wall-jet case, while the multiple reflected the influence of off-set height, viz:

$$\bar{St}_m = \bar{St}_{m|_{WJ}} \cdot N(OH, x/S) \qquad (5\text{-}8)$$

A curve fit to the wall-jet data was then derived which showed that the downstream distance has a logarithmic effect on the surface averaged Stanton number, which could be represented by:

$$\bar{St}_m = [0.00328 - 0.000637 \ln(x/S)] \qquad (5\text{-}9)$$

The shape of the $\bar{St}_m$ curves show that N is a function of both OH and x/S, where the dependence of OH is exponential. This was formulated linearly using a computer package (Al-Zafarani, private communication) and may finally be expressed as:

$$N = \mathrm{erf}[-1.19 + 0.42\ln(x/S) + 1.81e^{-OH}] \qquad (5\text{-}10)$$

This is only a dimensionless coefficient, always less than or equal one, which allows for the effects of off-set height. Figure 5-11 shows the actual data points and their comparison with equation 5-8. This curve fit is only valid within the limits of the experiments.

The experimental uncertainty in the mass transfer data presented in this chapter is estimated to be 7% at 20:1 odds (Appendix C). The uncertainty in the clearance

time and temperature measurements are believed to be the main contributors.

5.4 CALCULATION OF HEAT AND MASS TRANSFER BENEATH BLUFF WALL-JETS.

The above expressions for the surface-averaged Stanton number (equations 5-8 to 5-10) are only valid for the particular test conditions examined in the present study (Re =24910 and AR=2.0). The wall-jet profile analysis of Hammond (1982 b) was therefore used to study the effect of the slot Reynolds number and aspect ratio on the bluff wall-jet heat/mass transfer. The bound paper discusses the extension of this analysis to wall-jet flows where the transfer phenomenon is from wall to the jet. In this case the mass transfer analogy factor may be expressed as:

$$\frac{St}{0{,}5\,c_f} = \frac{K_\theta / K}{1+\left[\frac{\ln\{(\delta_\theta/\delta)(\delta/y_m)\}+K_\theta B_\theta - KB - Kg(y_m/\delta)}{K}\right](c_f/2)^{0.5}} \qquad (5\text{-}11)$$

where $K_\theta = 0.48$, $B_\theta = 12.5(Sc)^{2/3} - 5.8$, δ =wall-jet thickness and δ_θ is the thickness of the concentration boundary layer. The log-law for skin-friction was derived from equation 2-4, and this may be expressed as:

$$(2/c_f)^{0.5} = \frac{1}{K}\ln[Re_m(c_f/2)^{0.5}] + B + C.\omega(y_m^+/b_u^+) \qquad (5\text{-}12)$$

where $K = 0.41$, $B=5.2$, $C=-[-\frac{1}{K}\ln(D.b_u^+)+B]$, $b_u^+ = 0.283\ Re_m$, $D=2.43$, $y_m^+ = Re_m(c_f/2)^{1/2}$,

$$g = C.\omega \qquad \omega(y^+/b_u^+) = \sum_{n=1}^{n=4} a_n (y^+/b_u^+)^n$$

where $a_1 = 0.841\ Re_m^{-0.1040}$, $a_2 = 0.223\ Re_m^{0.0917}$, $a_3 = -0.180\ Re_m^{0.0627}$, $a = 0.030\ Re_m^{0.0555}$.

Therefore given the values for the local Reynolds number (Re_m), profile analysis calculates all the terms in the above equation except $\bar{St}_m$ and the ratio (δ_θ / δ). For a single slot Reynolds number the values for the mass transfer Stanton number over the flat plate are known from the experiments. Using the data in figure D-17 in conjunction with the above equation, the downstream variation of the thickness ratio was obtained. This variation is shown in figure 5-12 along with a curve fit using an error function. Figure 5-13 shows the downstream development of the velocity and concentration field. The cross-stream variations in (δ_θ/δ) were not significant compared to those downstream and showed no distinct trend. These were then cross-stream averaged (except the one indicated with a circle in figure 5-12) to obtain the ratio for every position from the nozzle. The rapid rise

in the thickness ratio near the nozzle is expected as the concentration boundary layer grows from zero thickness. Downstream, nevertheless, the derived data indicate a thickness ratio which is higher than one. The rate of turbulent diffusion of naphthalene in air is expected to be very similar to the spread of the velocity field. A rise in the thickness ratio to values higher than one was not therefore plausible. A more realistic curve was therefore selected that asymptotes to one after an initial rise. The growth of the thickness ratio therefore may be expressed as:

$$\ln[(\delta_0/\delta)\times 1000] = 3{,}45\,[1+\mathrm{erf}(1/35)(x/S-70)] \qquad (5\text{-}13)$$

The sensitivity of the surface-averaged and local Stanton numbers to the particular choice of variation in the thickness ratio was subsequently checked. A 20% change in the latter was found to cause less than a 2% alteration in the former.

The Stanton number variation beneath bluff wall-jets may therefore be calculated using the empirical equations given in the section 5.2 for the flow field, together with the wall-jet profile analysis, for every position on the plate. This was undertaken using a FORTRAN computer program which modelled the development of three-dimensional wall-jets for a range of Reynolds numbers between 1000 and 150000, and nozzle aspect ratios between 0.25 to 2.5. This program is called the WALJET computer code, and may be regarded as an 'intermediate-level' calculation procedure in the sense used by Alamdari et al (1984). The only requirement to start the calculations and to progress downstream was the specification of values for the nozzle Reynolds number and aspect ratio.

Stanton numbers were calculated based on the nozzle exit velocity. The cross-stream spread of each jet was computed up to the point where the local Reynolds number was less than 100 which practically signalled the jet boundary. The streamwise grid lines were single increments in the dimensionless distance from the nozzle, while the cross-stream grids were selected such that (z/B)*AR*4 increased in single increments. The mass transfer Stanton numbers were first averaged across each cross-stream segment in the streamwise position. The result was then used in conjunction with the preceding upstream values to obtain an overall surface-averaged Stanton number up to the line under consideration.

The program was initially run for the nozzle aspect ratio of 2 and Reynolds number of 24910, similar to the conditions for the mass transfer experiments. The decay of the centre-plane Stanton number predicted by the WALJET program from the above run is compared with the

experimental data in figure 5-14 where agreement is shown to be very good. This is not unexpected as the same Stanton number data was used to derive the thickness ratio expression (equation 5-13) employed in the calculation procedure. However the thickness ratio values adopted for points away from the nozzle was not the same value as that obtained from the heat transfer data. This confirms the high degree of insensitivity in the wall-jet profile analysis to the choice of thickness ratio and therefore a knowledge of the velocity field for the wall-jet and a rough approximation for the thickness ratio, permits accurate calculation of heat and mass transfer.

A comparison between the surface-averaged mass transfer Stanton number predicted by the computer program and the measurements is shown in figure 5-15. Agreement is seen to be reasonable for practical purposes. The differences are due to the approximations made for the position of the jet boundaries and the local Stanton numbers near them which are required for the integration of the experimental data.

The mass transfer coefficient for the bluff wall-jet may be expressed by:

$$\bar{St}_m = B\,[\,A - \ln(x/S)] \qquad (5\text{-}14)$$

The WALJET program was run for a range of Reynolds numbers between 1000 and 150000, and the resultant curves are shown in figure 5-16. Increasing Reynolds number clearly reduces the surface averaged mass transfer Stanton number and this effect diminishes at higher values of the former (appendix E). All curves in figure 5-16 seem to asymptote to a common trend and imply that the second constant in equation 5-14 has a value A=6 which also suggests that the Stanton number is negligibly small after x/S>400. In reality these curves are likely to asymptote to the horizontal axis, but the above assumption is plausible within the limits of this study, and simplifies the curve-fitting. The other constant, B, may then be represented as a function of Reynolds number having the form:

$$B = \frac{1,3905}{[\ln(Re_S)]^{3,5}} \qquad (5\text{-}15)$$

The WALJET program was then used to evaluate the effect of the aspect ratio on the surface-averaged Stanton number. This assessment was carried out for five nozzle aspect ratios between 0.5 to 2.5. Figure 5-17 shows that for the bluff wall-jets the aspect ratio has less of an effect compared to that of the Reynolds number. An increase in the latter only gives a marginal increase in the former. This may be included in the general Stanton number formula by adding a coefficient in the form

(0.175AR+0.65). Hence the surface-averaged mass transfer Stanton number for a bluff wall-bounded jet may finally be calculated from the expression:

$$\overline{St}_m = \frac{1,3905(0,175AR+0,65)}{[\ln(Re_s)]^{3,5}} [6-\ln(x/S)].erf[-1,19+0,42\ln(x/S)+1,81e^{-OH}] \qquad (5-16)$$

To deduct heat transfer data from this equation, it may be multiplied by the Chilton-Colburn analogy factor (~2.28). Alternatively, the more accurate analogy factor for the wall-jets derived from the profile analysis (as presented in the bound paper) gives a factor of ~1.63. The latter may be used to yield:

$$\overline{St} = \frac{0,4(AR+3,71)}{[\ln(Re_s)]^{3,5}} [6-\ln(x/S)].erf[-1,19+0,42\ln(x/S)+1,81e^{-OH}] \qquad (5-17)$$

which is valid for the range of parameters $2000 \leq Re \leq 150000$, $0.5 \leq AR \leq 2.5$, $0 \leq OH \leq 3.8$ and $5 \leq x/S \leq 95$.

5.5 SKIN-FRICTION COEFFICIENT.

The local skin-friction coeffient may also be calculated over the plate using the WALJET program. The computed centre-plane values are presented in figure 5-18 for a range of nozzle Reynolds numbers. The experimental data of previous researchers are also included. These data (as mentioned in section 2.4) agree on a similar value for skin-friction (0.0065), due to a similar choice of the nozzle Reynolds number. The figure shows that curves shift as a result of a change in the nozzle Reynolds number. The agreement between the data and the results of the WALJET program is good.

5.6 RECOMMENDATIONS FOR FURTHER WORK.

This study has covered only a small section of the series of tests necessary to ascertain the heat transfer behaviour between a jet of air and a flat plate. Previous investigators have shown that in bluff jets the shape of the nozzle does not seriously effect the jet behaviour. It is predicted that slender and multiple jets will require different equations for the surface-averaged Stanton numbers than those indicated above. Added to this is the effect of nozzle inclination in both directions, which would make the data applicable to other industrial applications, such as furnaces.

The configuration studied in this chapter, was similar to that of a supply grille near a wall or a ceiling in a mechanically-ventilated enclosure. In the bound paper, it is argued that the jet behaviour can be

affected by surrounding surfaces (a normal flat wall in the case of that study). It would be useful in the future to model the behaviour of the present three-dimensional jet within an appropriate geometry in order to simulate a room ventilated by a bluff-jet.

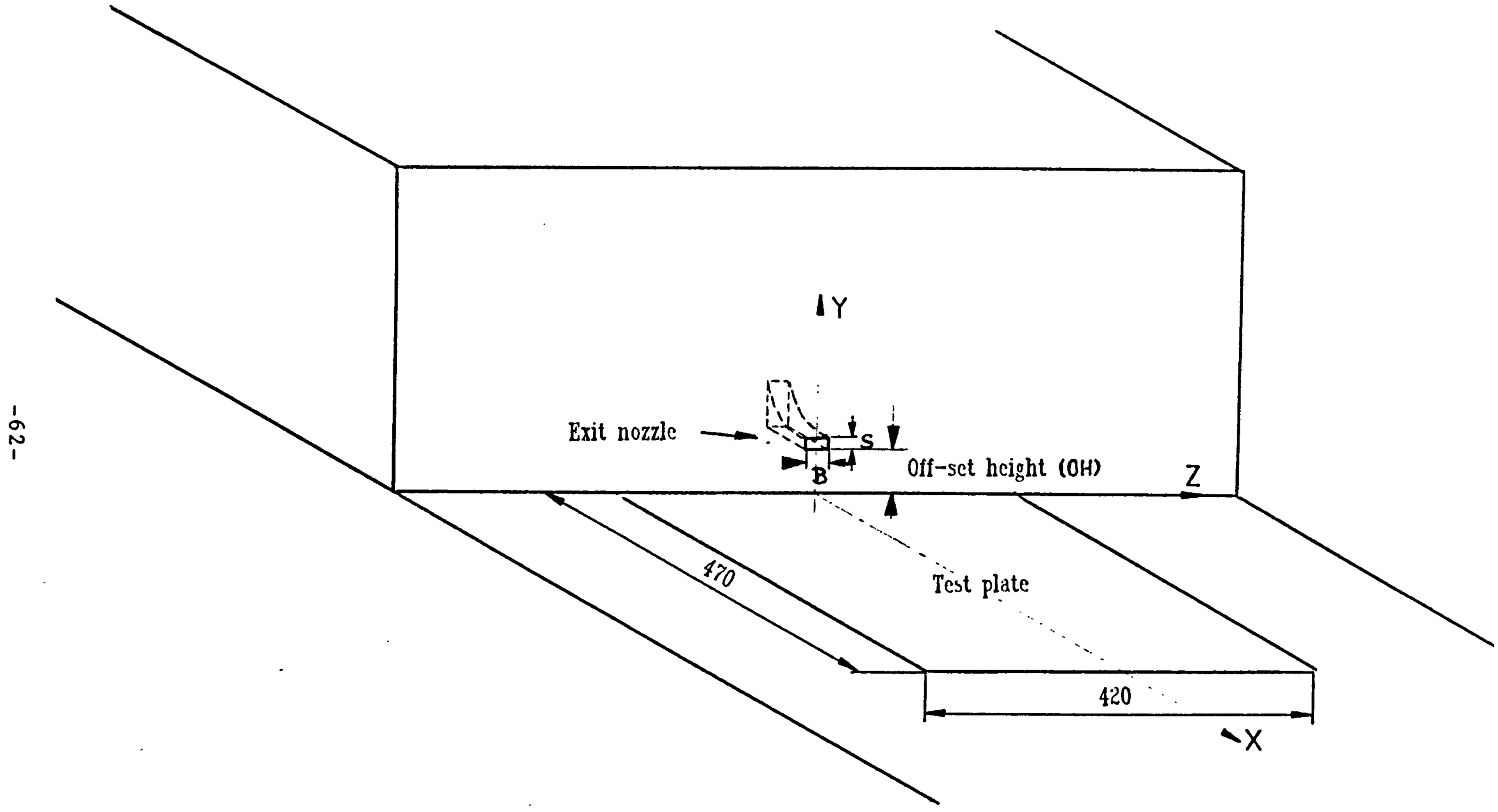

Figure 5-1 General arrangement for the three-dimensional off-set jet.

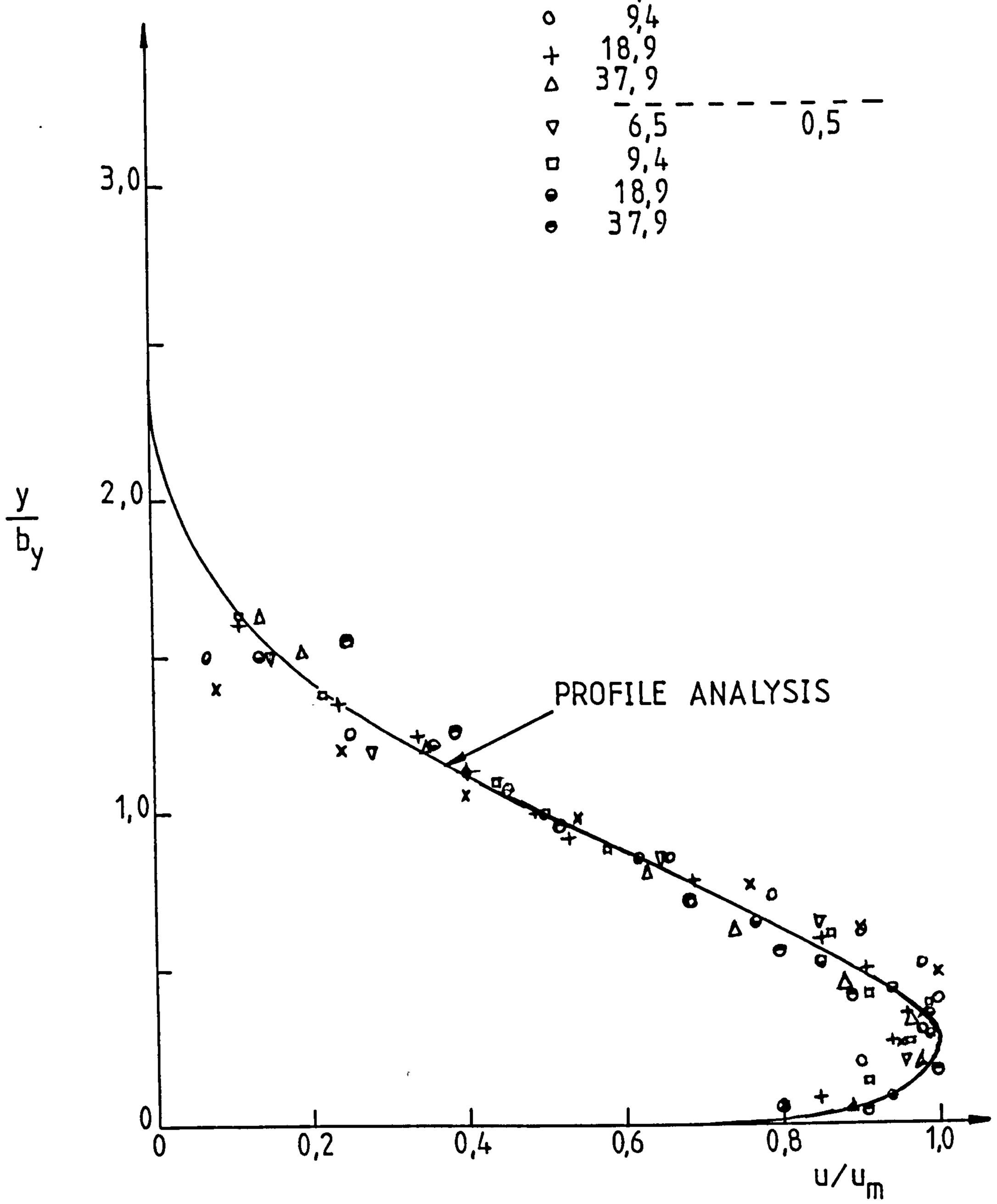

Figure 5.2 Comparison between the profile analysis and the data for the bluff wall-jet

WALL-JET b_z=12.5 x/S=6.5 x/B=3.25 $x/\sqrt{A}$=4.6				WALL-JET x/S=9.4 x/B=4.7 $x/\sqrt{A}$=6.7			
z/B	u_m/u_e	b_y/S	y_m/S	z/B	u_m/u_e	b_y/S	y_m/S
0	0.98	1.55	0.7	0	0.89	1.75	0.7
0.25	0.94	1.15	0.4	0.25	0.83	1.5	0.6
0.5	0.7	1.0	0.35	0.5	0.6	1.45	0.5
0.75	0.34	0.8	0.1	0.75	0.36	1.35	0.25

WALL-JET b_z=18.5 x/S=18.9 x/B= 9.45 $x/\sqrt{A}$=13.4				WALL-JET x/S=37.9 x/B=18.95 $x/\sqrt{A}$=26.8			
z/B	u_m/u_e	b_y/S	y_m/S	z/B	u_m/u_e	b_y/S	y_m/S
0	0.62	2.2	0.6	0	0.32	3.1	0.45
0.25	0.61	2.2	0.7	0.5	0.32	2.5	0.4
0.5	0.52	2.2	0.65	1.0	0.27	2.5	-
0.75	0.41	2.2	0.35	1.5	0.23	2.1	-

Table 5-1 Dimensionless values of the three-dimensional jet spread.

OH=1.6 b_z=12.5
x/S=6.5
x/B=3.25
$x/\sqrt{A}$=4.6

z/B	u_m/u_e	b_y/S	y_m/S
0	0.96	3.0	2.1
0.25	0.95	3.0	2.1
0.5	0.71	2.85	2.2
0.75	0.41	2.6	2.1

OH=1.6 b_z=13.5
x/S=9.4
x/B=4.7
$x/\sqrt{A}$=6.7

z/B	u_m/u_e	b_y/S	y_m/S
0	0.85	3.15	2.1
0.25	0.77	3.0	2.1
0.5	0.54	3.1	2.1
0.75	0.34	2.9	1.6

OH=1.6 b_z=15
x/S=13.4
x/B= 7.7
$x/\sqrt{A}$= 9.5

z/B	u_m/u_e	b_y/S	y_m/S
0	0.66	3.5	2.1
0.25	0.45	3.4	2.1
0.5	0.3	3.35	2.1
0.75	0.23	3.0	-

OH=1.6 b_z=20
x/S=18.9
x/B= 9.45
$x/\sqrt{A}$=13.4

z/B	u_m/u_e	b_y/S	y_m/S
0	0.46	4.15	2.1
0.25	0.46	3.85	2.0
0.5	0.39	3.9	1.9
0.75	0.3	3.9	-

Table 5-1 continued

OH=3.8 b_z=13
x/S=6.5
x/B=3.25
x/$\sqrt{A}$=4.6

z/B	u_m/u_e	b_y/S	y_m/S
0	0.93	5.2	4.3
0.25	0.9	5.1	4.3
0.5	0.76	4.9	4.3
0.75	0.23	5.1	4.2

OH=3.8 b_z=15
x/S=13.4
x/B= 7.7
x/$\sqrt{A}$= 9.5

z/B	u_m/u_e	b_y/S	y_m/S
0	0.65	5.85	4.4
0.25	0.62	5.7	4.3
0.5	0.5	5.6	4.3
0.75	0.31	5.5	4.3

OH=3.8 b_z=25
x/S=27.1
x/B=13.55
x/$\sqrt{A}$=19.2

z/B	u_m/u_e	b_y/S	y_m/S
0	0.35	6.7	4.3
0.25	0.34	6.7	4.3
0.5	0.3	6.7	4.2
0.75	0.25	6.7	-

OH=3.8
x/S=37.9
x/B=18.95
x/$\sqrt{A}$=26.8

z/B	u_m/u_e	b_y/S	y_m/S
0	0.25	7.4	-
0.5	0.25	7.4	-
1.0	0.23	7.2	-
2.0	0.2	7.3	-

Table 5-1 Continued

		OH=0.7 z=0			OH=2.2 z=0			OH=3.1 z=0		
x/S	$x/\sqrt{A}$	u_m/u_e	b_y/S	y_m/S	u_m/u_e	b_y/S	y_m/S	u_m/u_e	b_y/S	y_m/S
3.4	2.4	1	1.75	-	-	-	-	-	-	-
6.5	4.6	0.96	1.95	1.2	0.89	3.6	2.7	0.85	4.55	3.6
9.4	6.7	0.83	2.2	1.2	0.75	3.8	2.9	-	-	-
13.4	9.5	0.68	2.4	1.2	0.61	4.25	2.8	-	-	-
18.9	13.4	0.55	2.65	0.9	0.46	4.8	2.8	0.44	6.25	3.9
27.1	19.2	0.41	3.2	0.7	0.32	-	-	0.28	-	-
37.9	26.8	0.3	-	-	-	-	-	-	-	-

Table 5-1 Continued

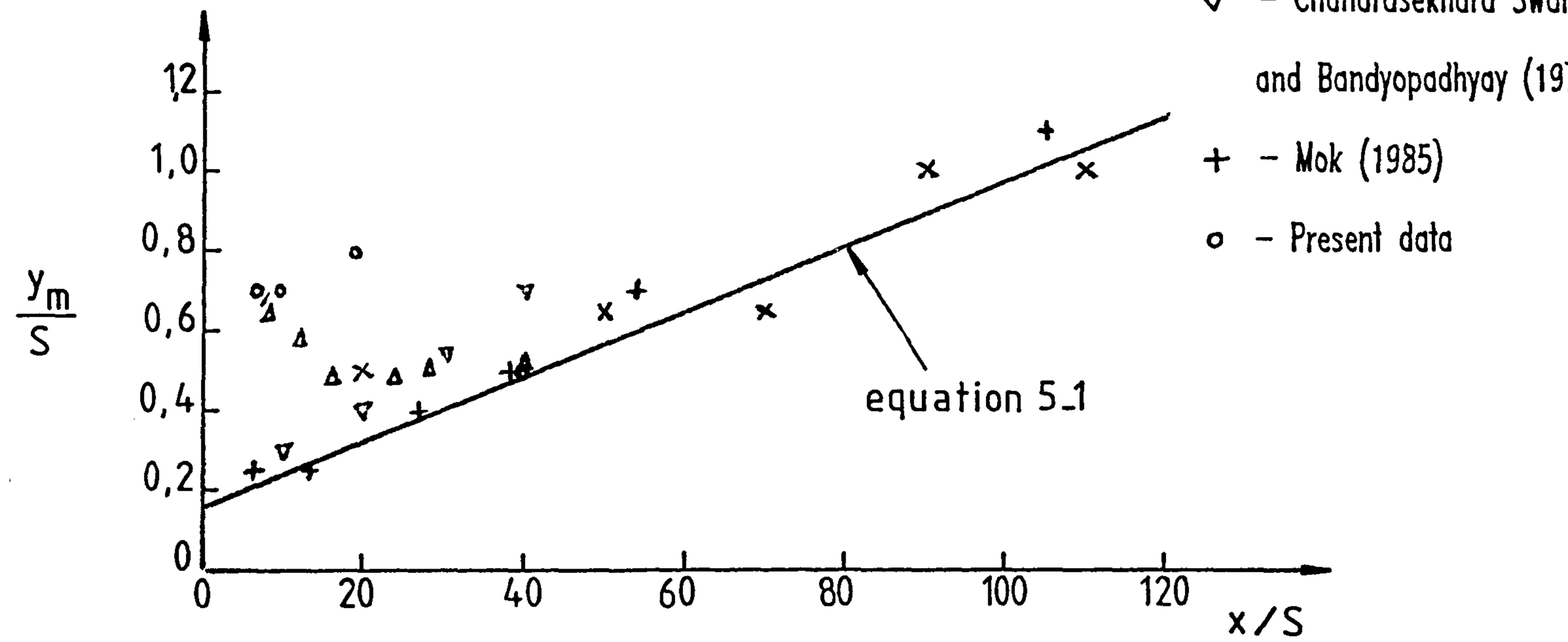

Figure 5-3 Growth of the maximum velocity height along the centre-plane of the three-dimensional wall-jet

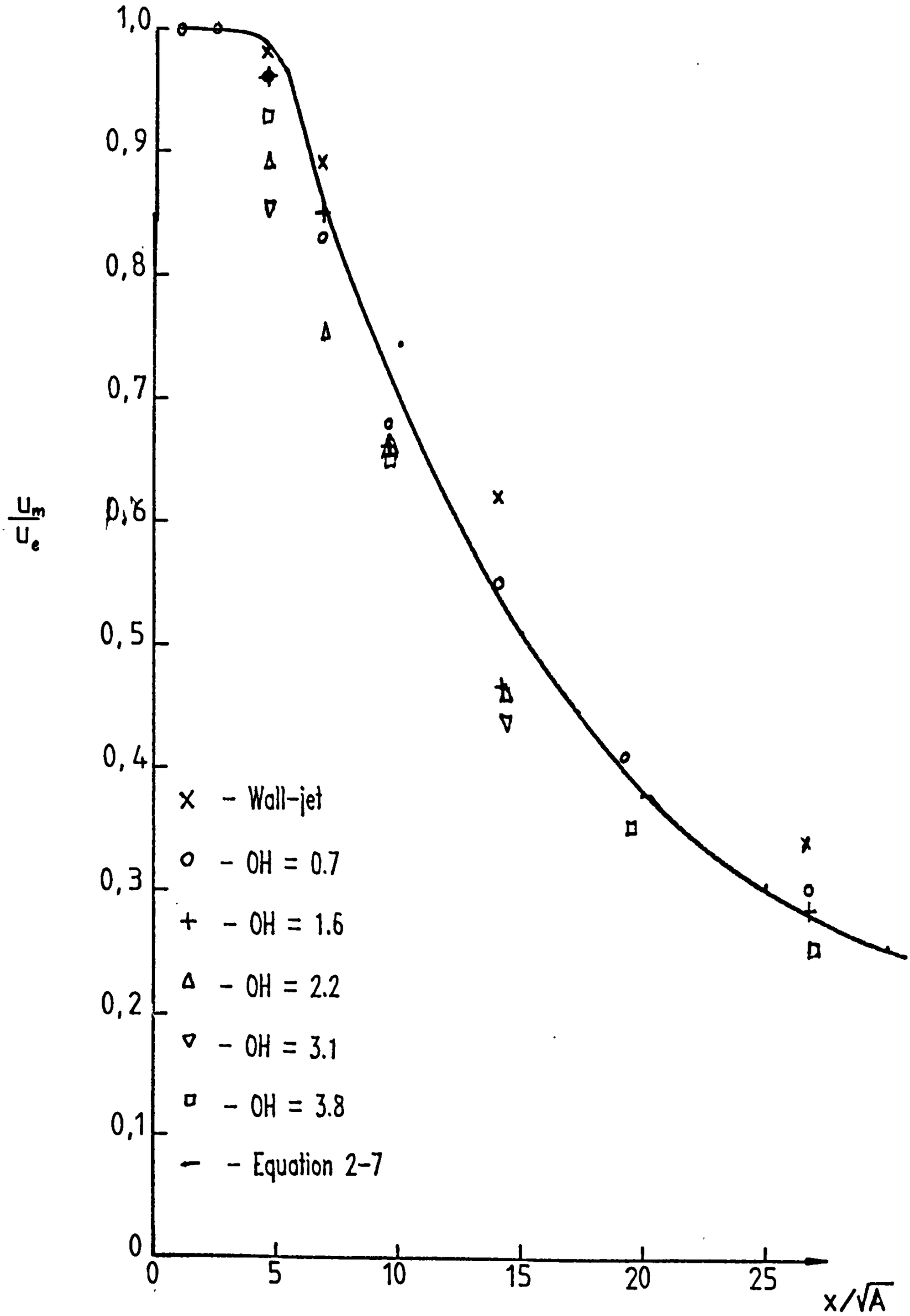

Figure 5-4 Decay of the maximum velocity for the centre-plane of the three-dimensional wall-bounded jet.

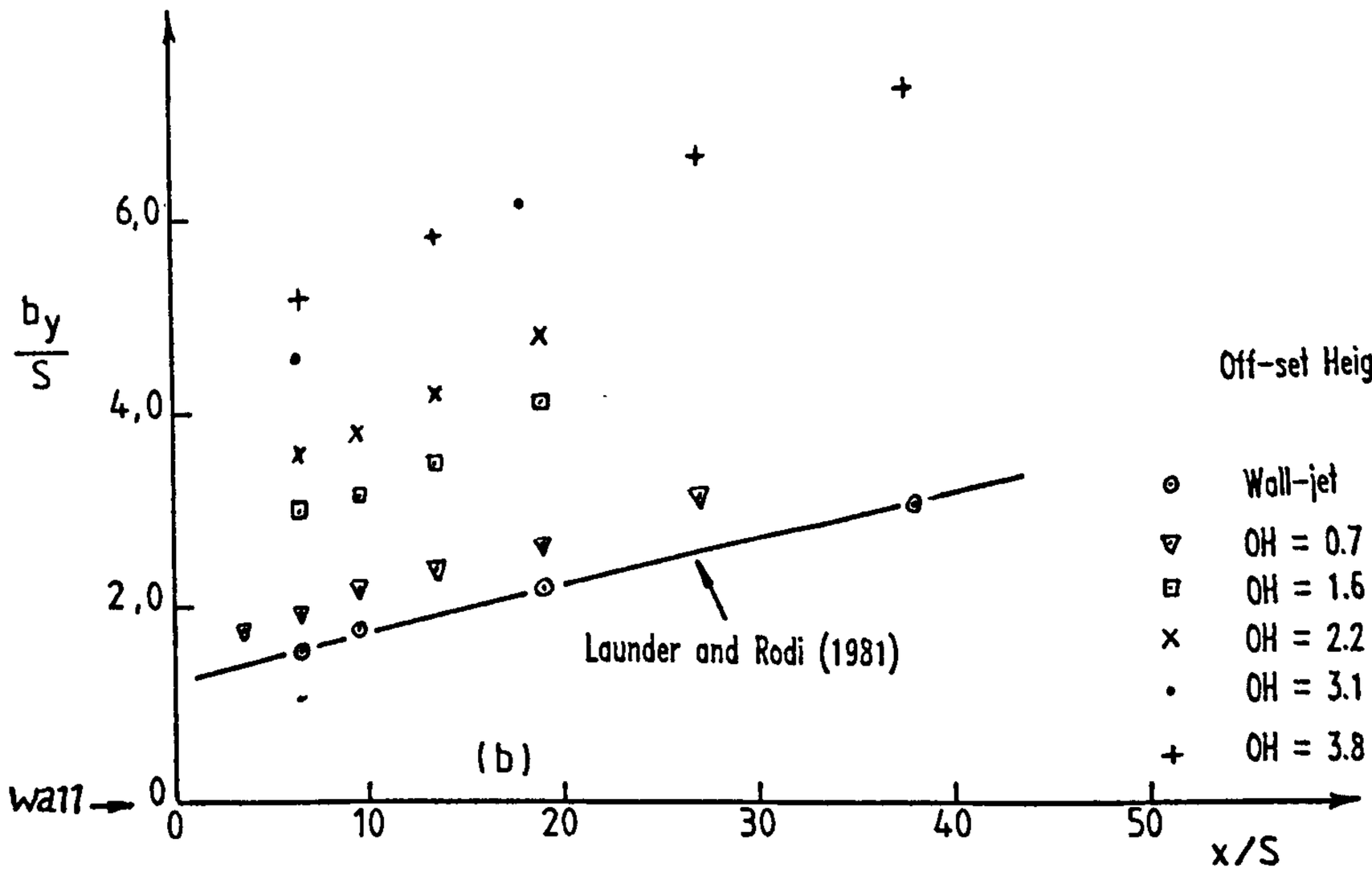

Figure 5-5 Vertical spread rate for the three-dimensional wall-bounded jet in the centre-plane.

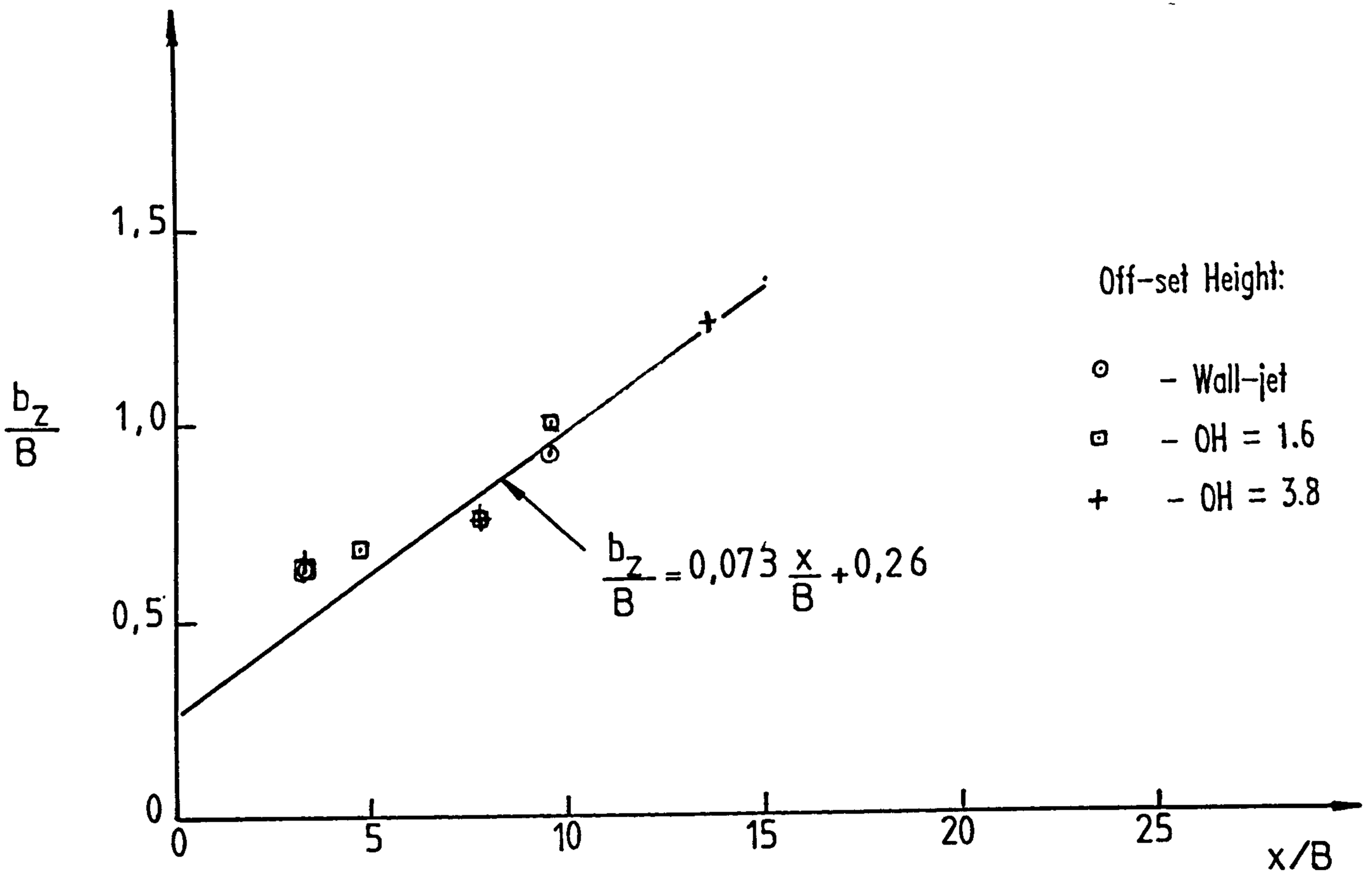

Figure 5-6 Lateral spreading rate for the three- dimensional wall-bounded jet.

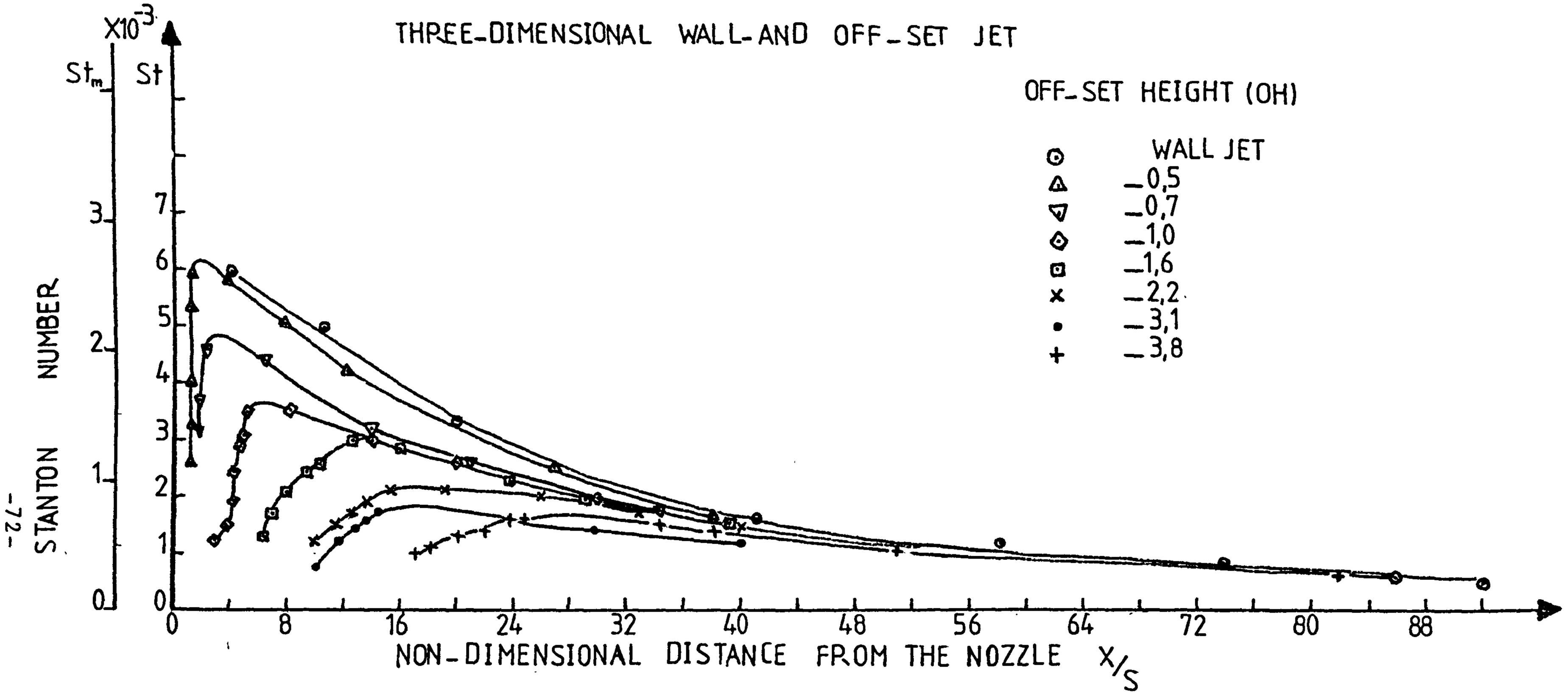

Figure 5-7 CHANGE OF CENTRE-LINE STANTON NUMBER WITH OFF-SET HEIGHT (ANALOGY FACTOR - 2,28)

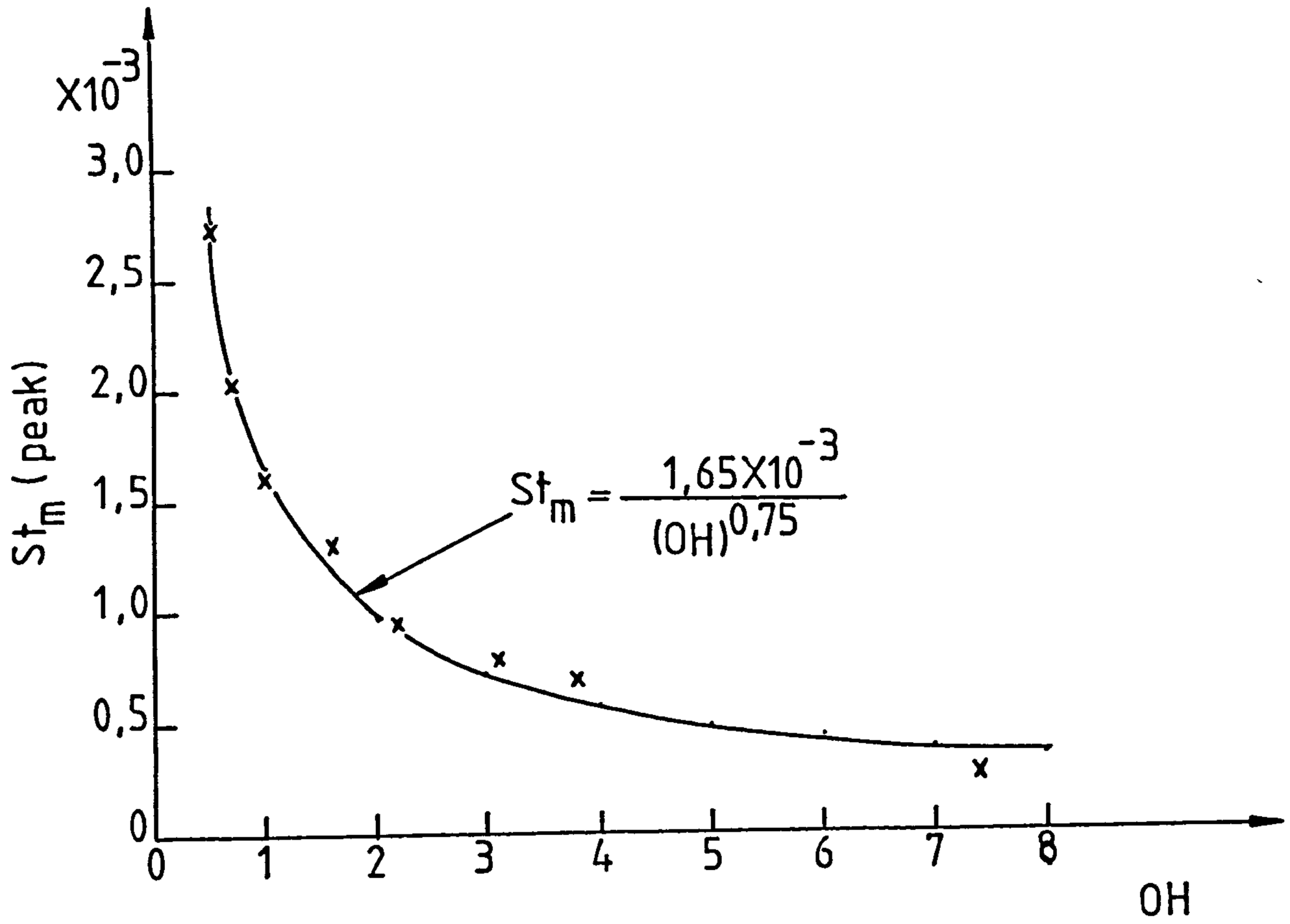

Figure 5-8 Change of peak Stanton number with off-set height.

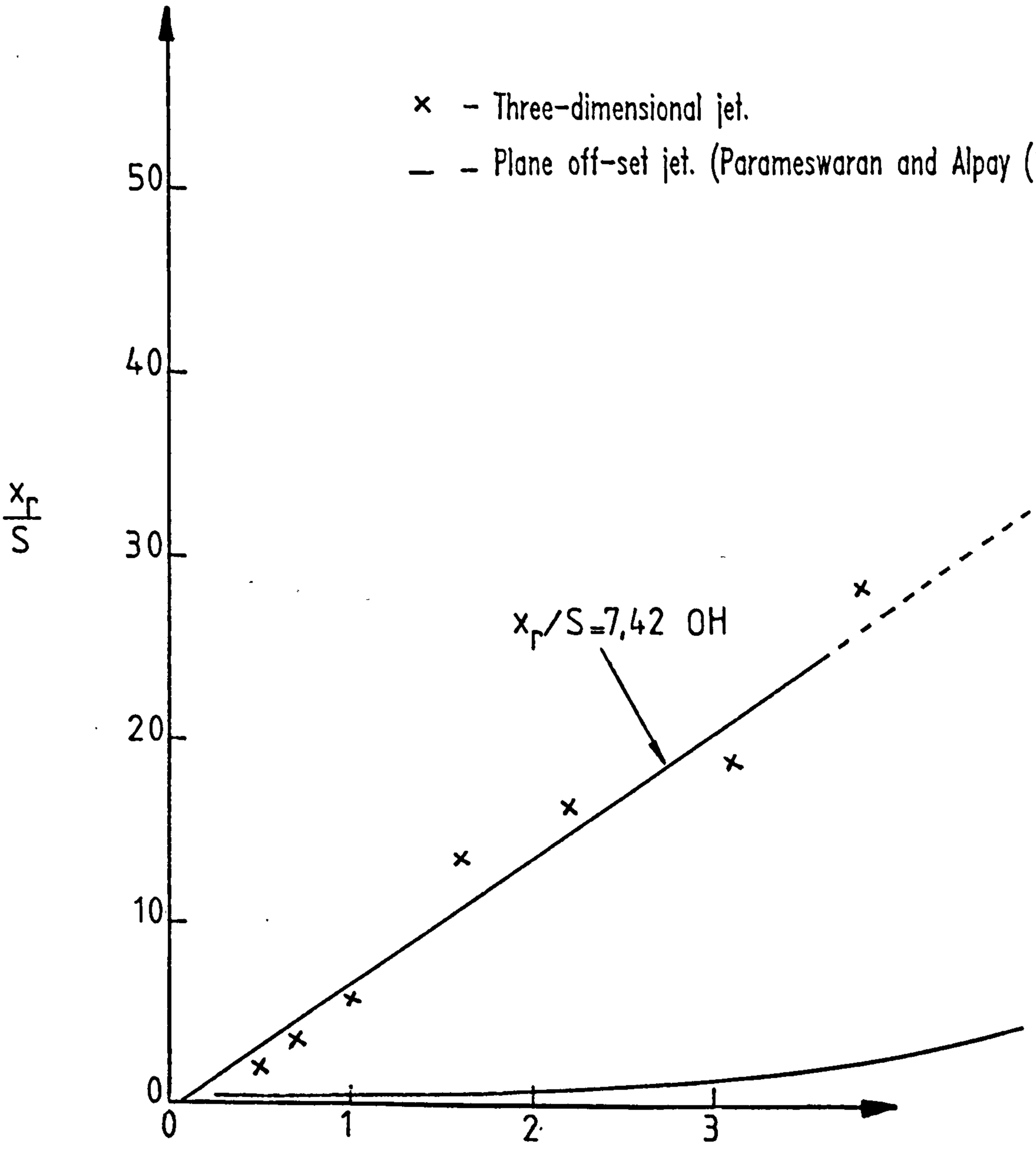

Figure 5.9 Position of jet impingement on a parallel adjacent plate over the centre-plane for two and three-dimensional off-set jets.

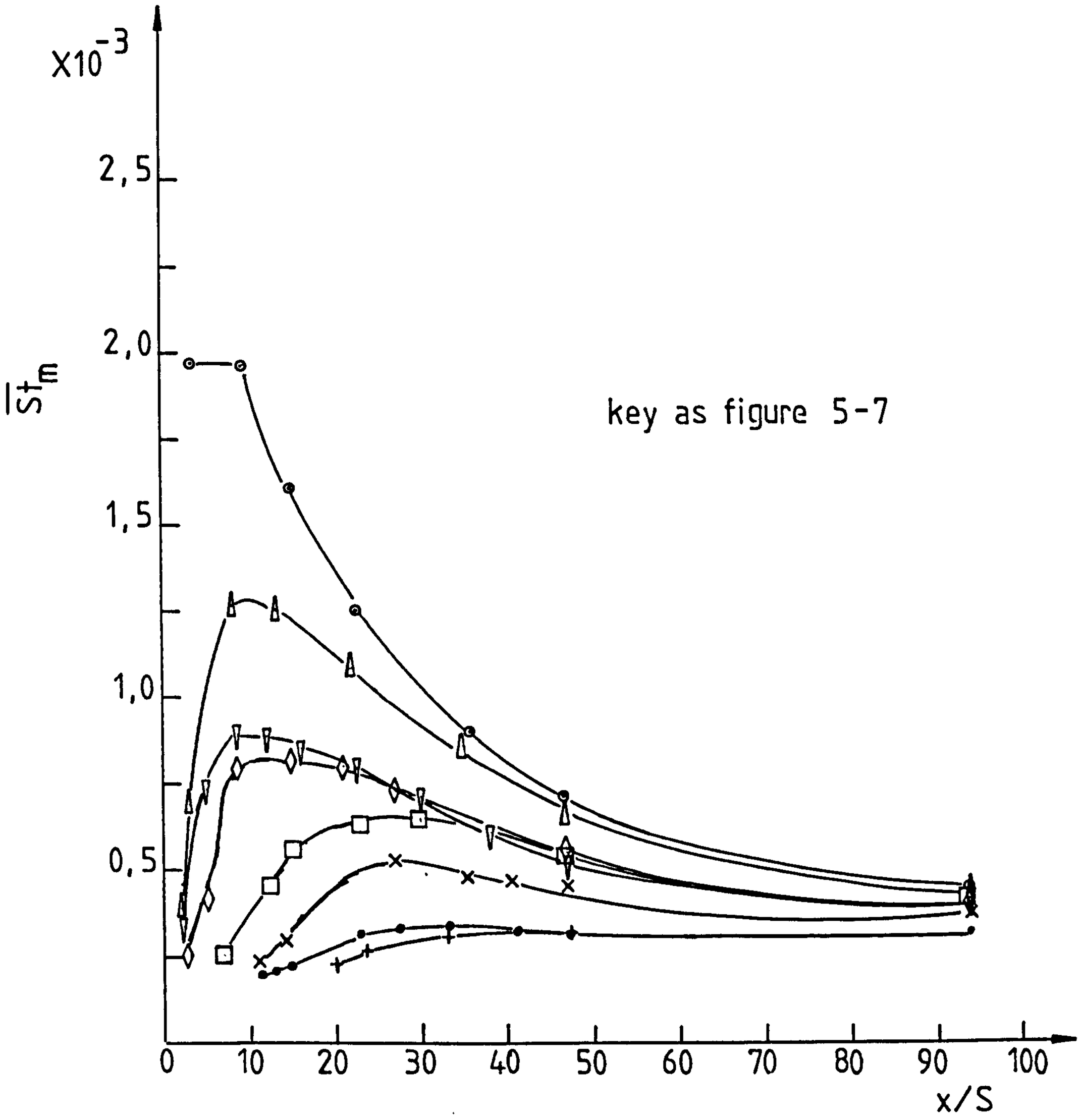

key as figure 5-7

Figure 5.10 Change of surface averaged mass transfer with downstream distance and off-set height.

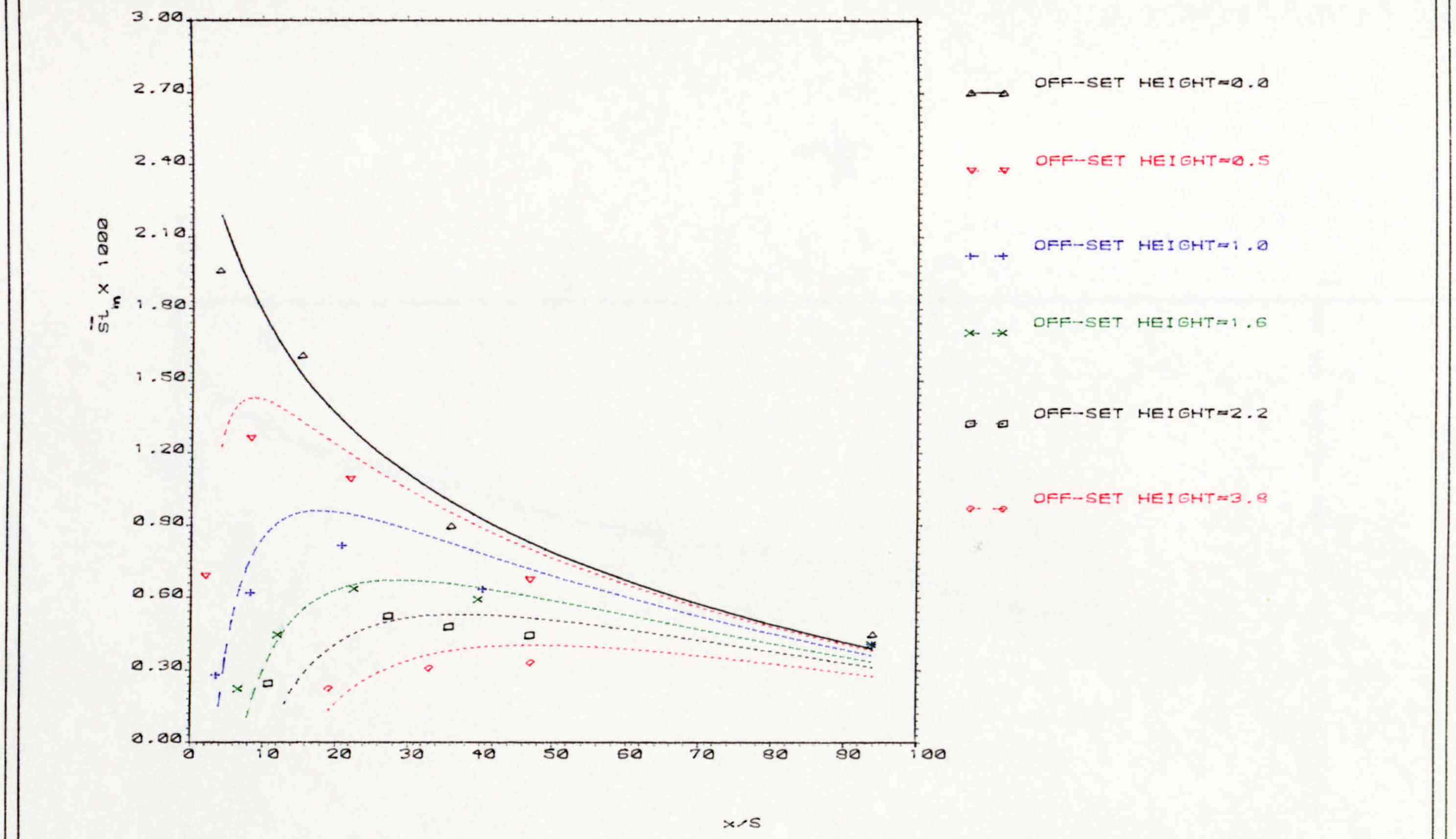

FIGURE 5-11 CHANGE OF SURFACE-AVERAGED MASS STANTON NUMBER WITH DOWN-STREAM DISTANCE AND OFF-SET HEIGHT AND THE CURVE FIT OF EQUATION 5-8

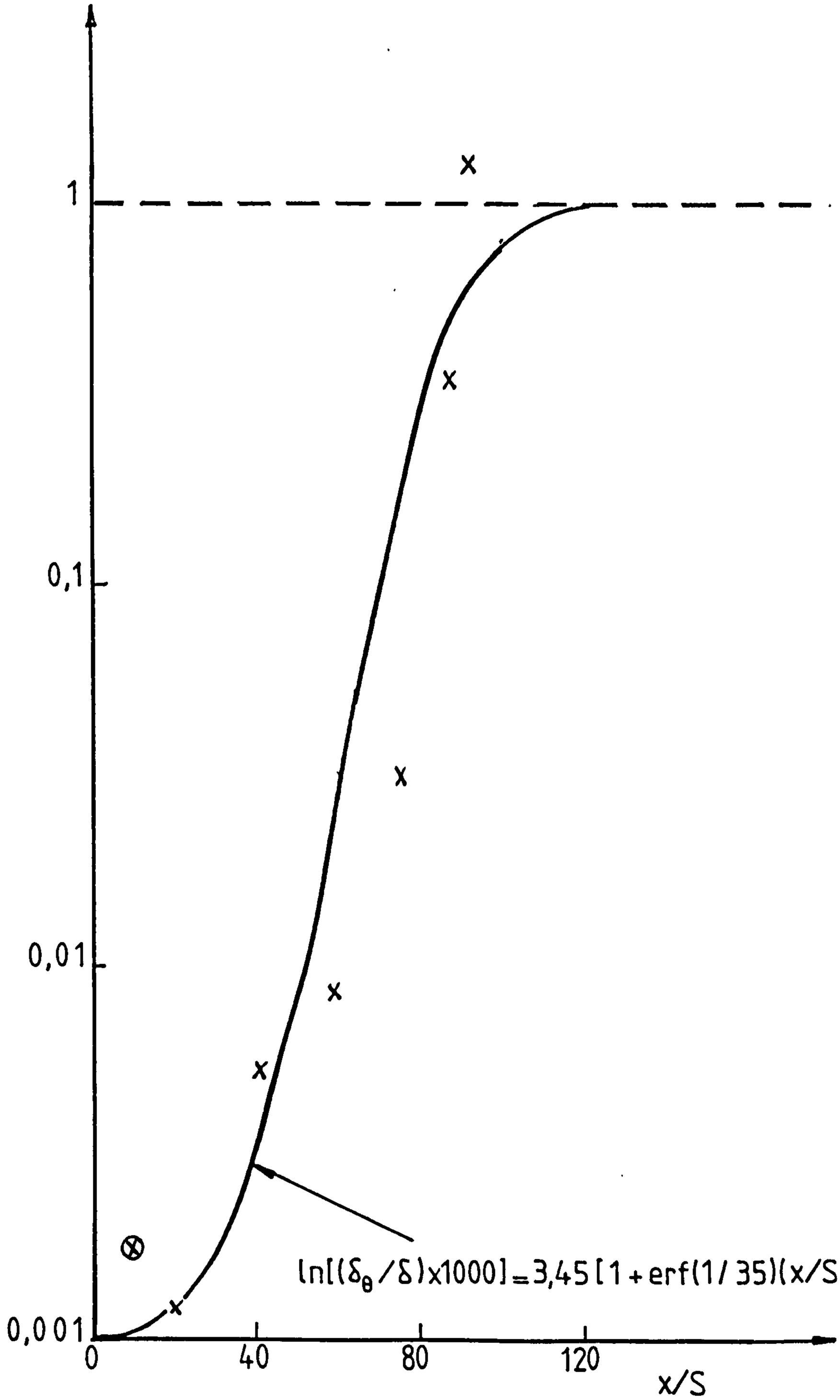

Figure 5.12 Downstream variation of the thickness ratio

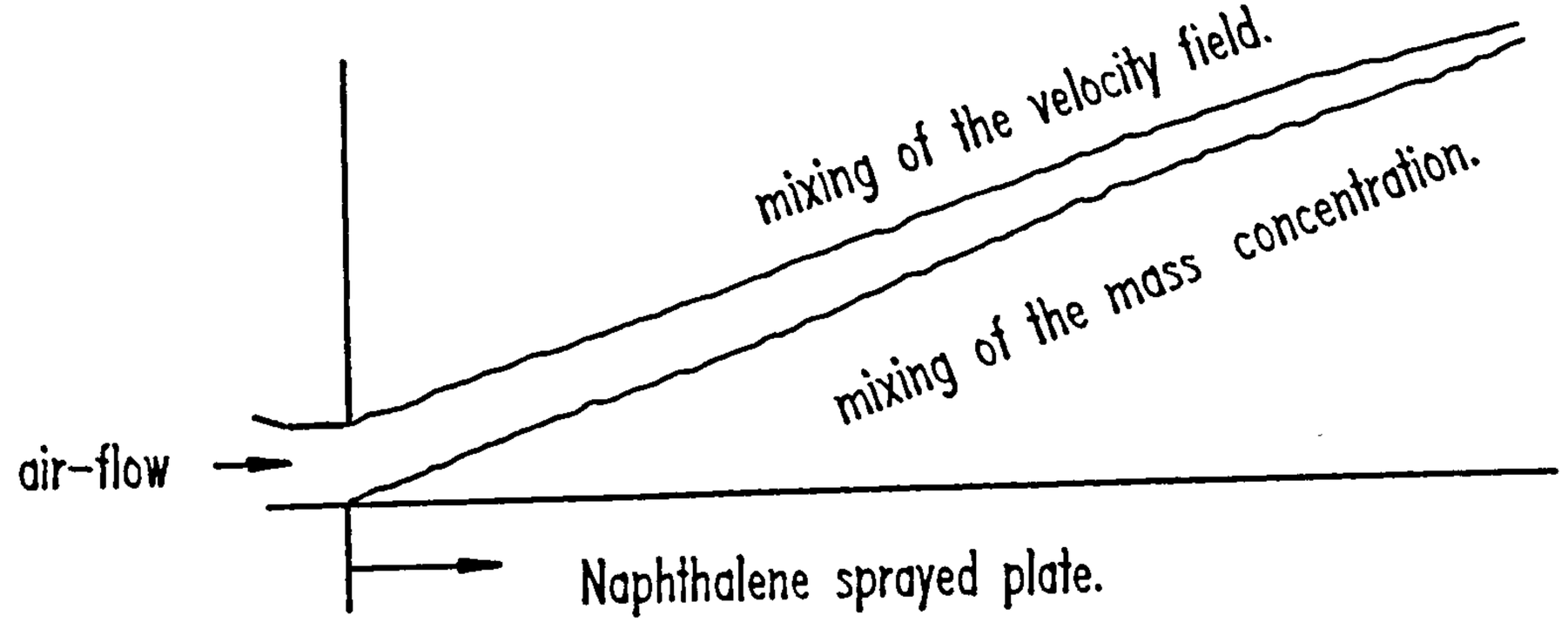

Figure 5.13 Naphthalene mixing in the air

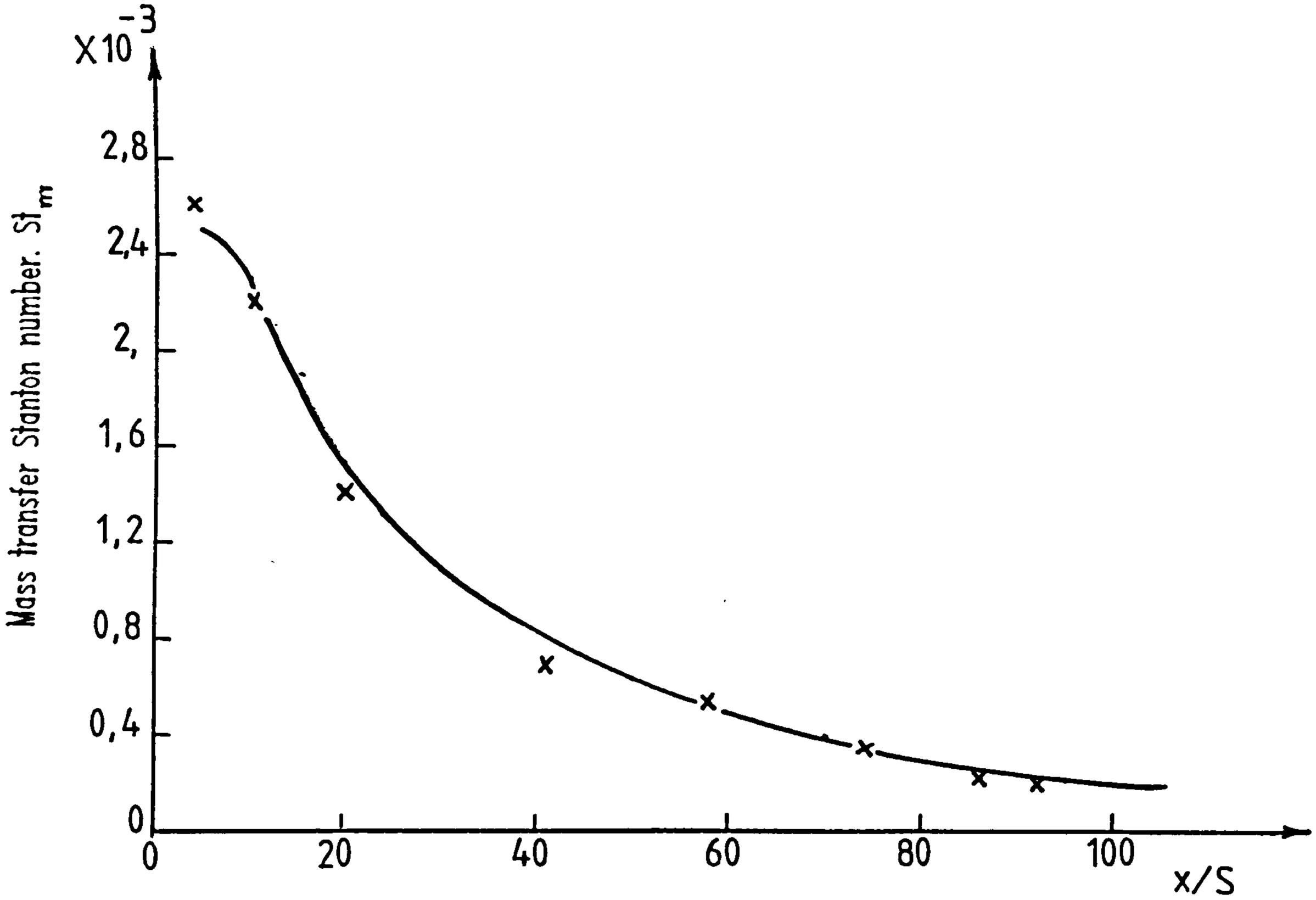

Figure 5.14 Comparison between the centre-line mass Stanton numbers as predicted by the WALJET program and the experimental data.

AR=2.0 Re_S=24910.

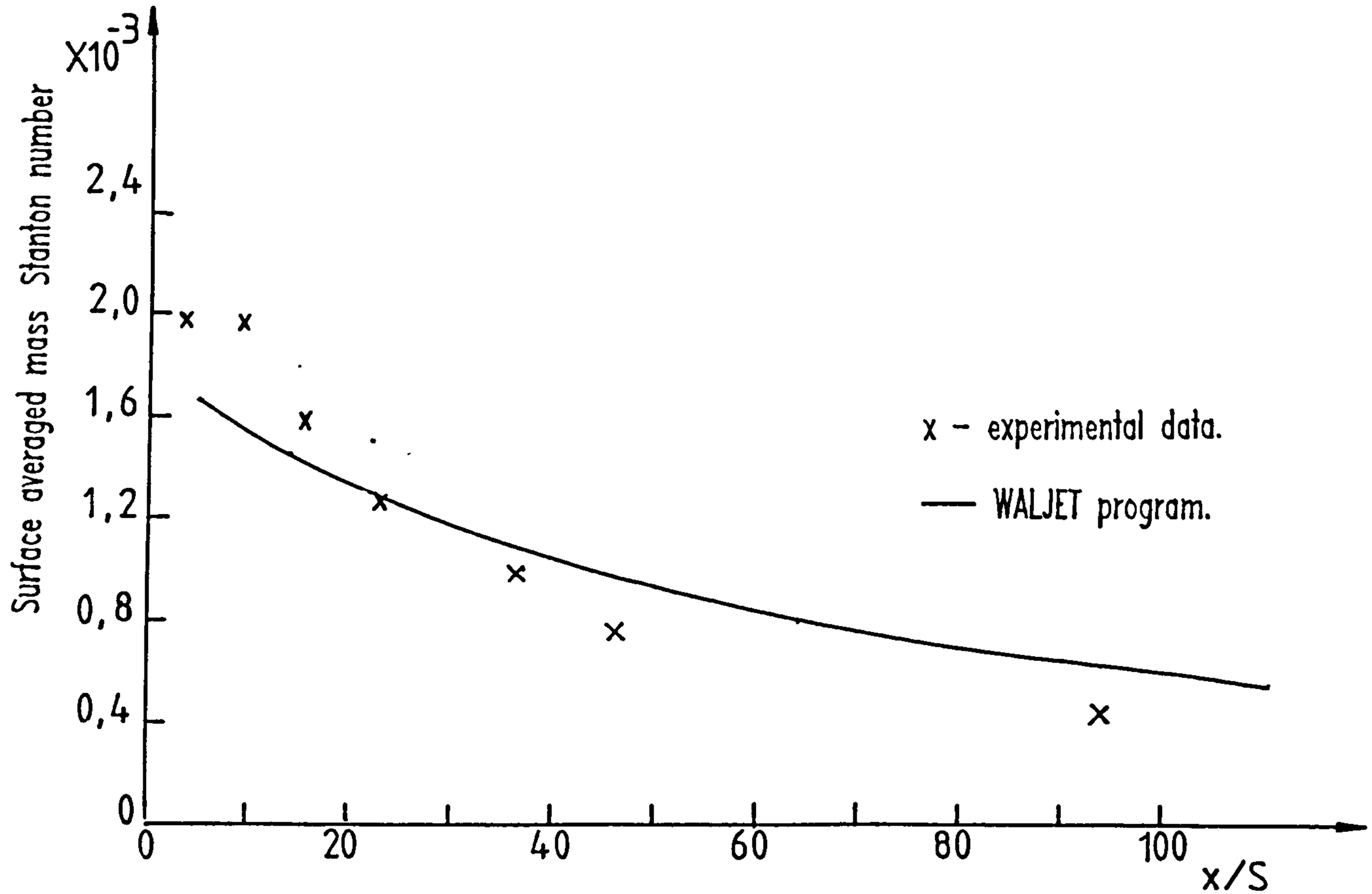

Figure 5.15 Comparison of the surface-averaged Stanton number predicted by the WALJET program and the experimental data

AR=2.0 Re_s=24910

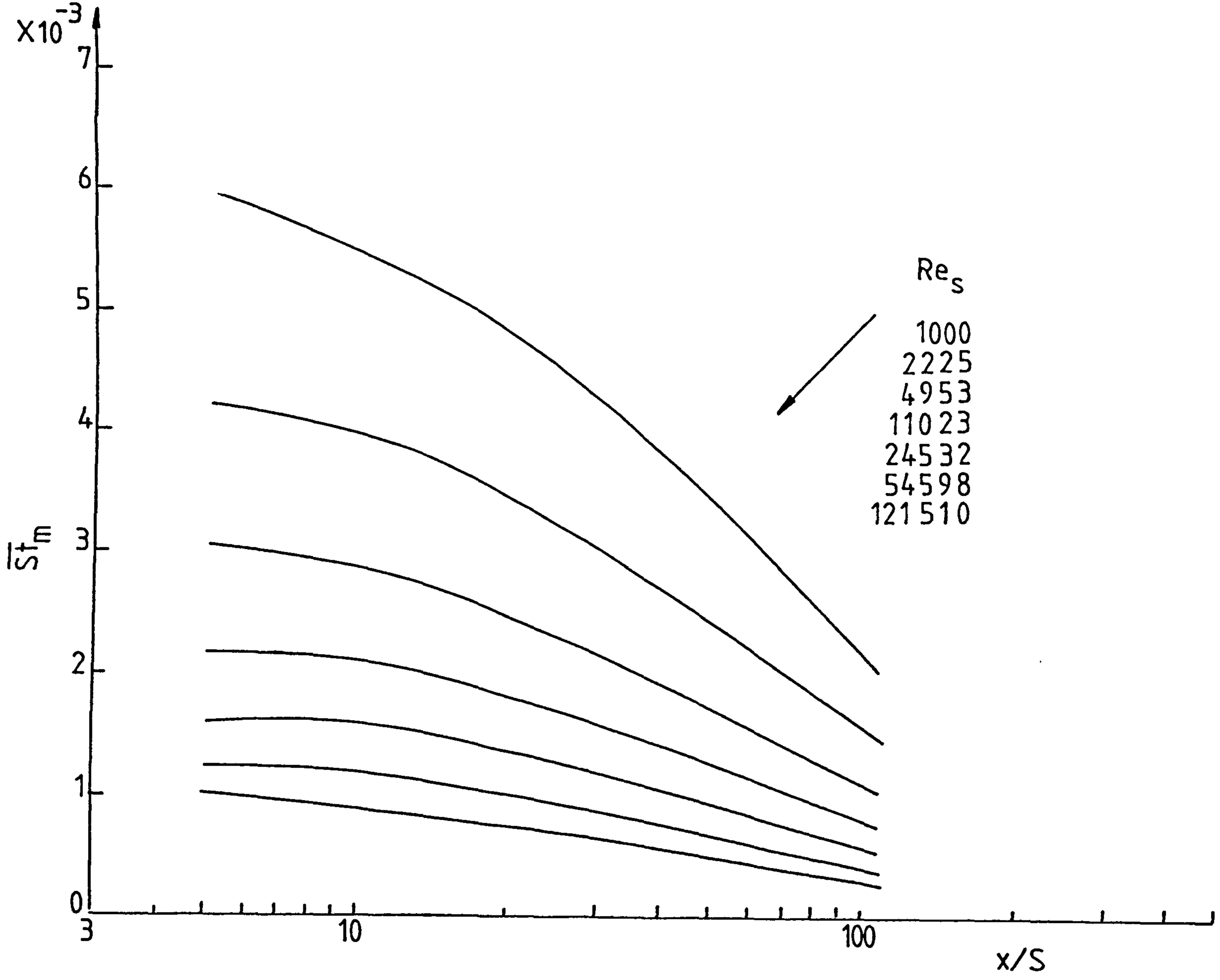

Figure 5.16 Effect of Reynolds number on the surface averaged mass Stanton number for the bluff wall-jet AR=2.0

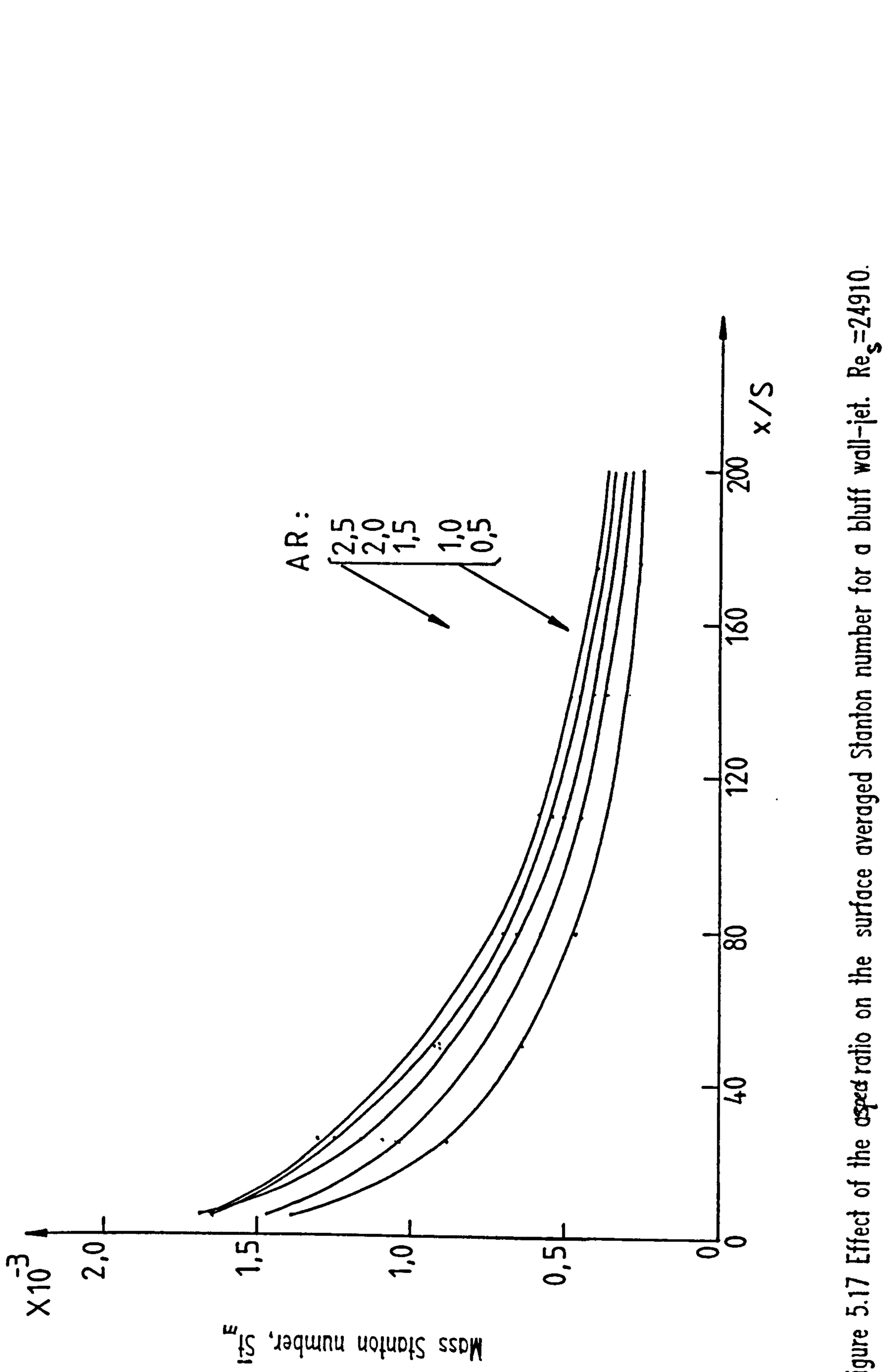

Mass Stanton number, $\overline{St}_m$

Figure 5.17 Effect of the aspect ratio on the surface averaged Stanton number for a bluff wall-jet. Re_s=24910.

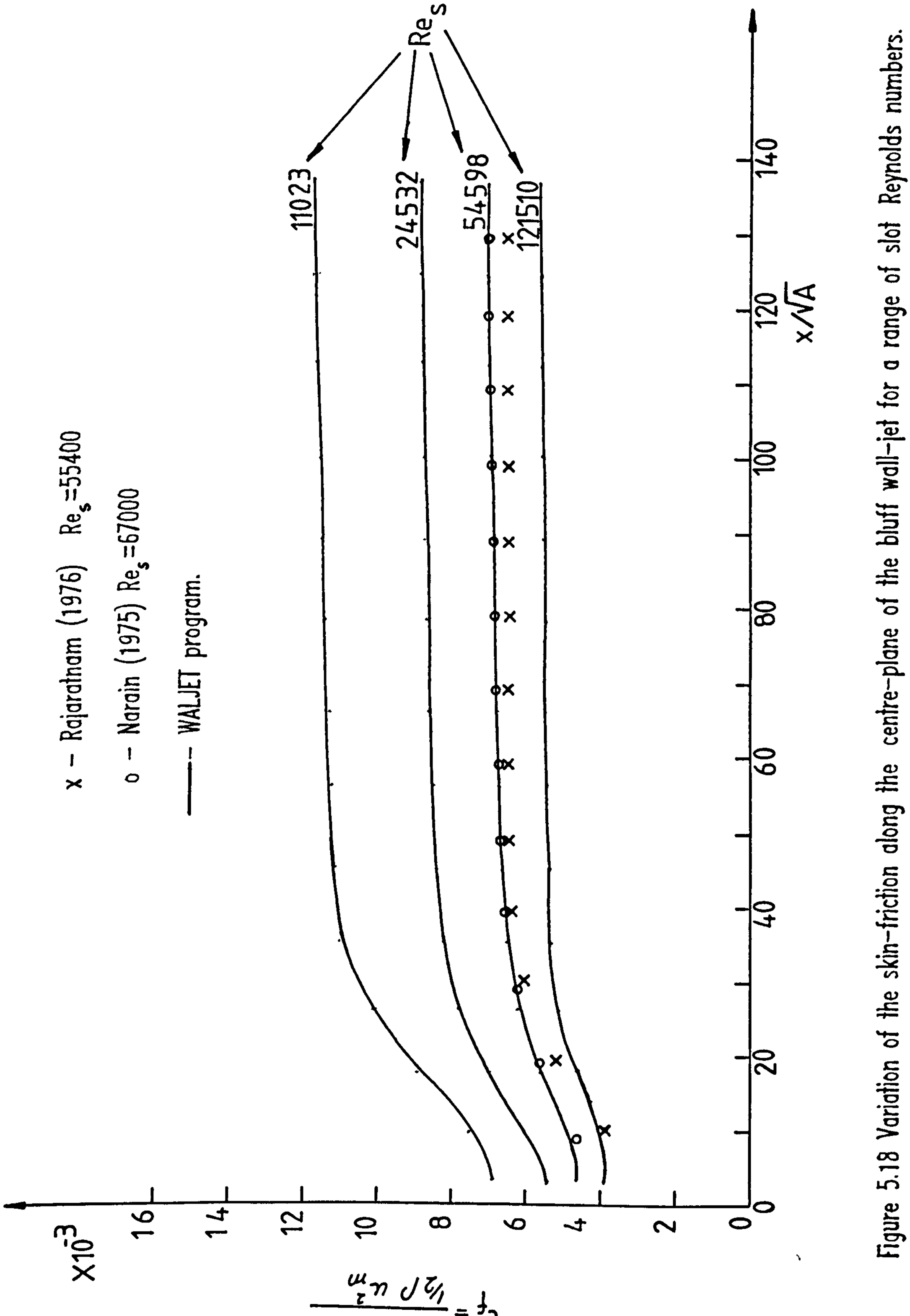

Figure 5.18 Variation of the skin-friction along the centre-plane of the bluff wall-jet for a range of slot Reynolds numbers.

CHAPTER 6

CONCLUDING REMARKS

CHAPTER 6

CONCLUDING REMARKS

Launder and Rodi (1981) in their survey of experimental research on wall-bounded jets clearly demonstrated that the most reliable group of data was obtained in studies that had been carried out over a long period of time, generally 10 years or more and covered a variety of geometrical configurations. The work reported in this thesis is similarly intended to form part of a long term study, and is associated with the work by Hammond et al (1977), Sidaway (1980) and Alamdari et al (1984). In this thesis special attention has been given to the requirements for mechanically-ventilated enclosures. Future tests coupled with improvements in computer codes, shall result in more accurate methods for determining convective heat transfer coefficients within these enclosures. It is hoped that the present test rig will enable further experimental studies, where the direction of research will be determined by the future needs for data.

In measuring convection coefficients the cost, accuracy and complication of the technique adopted, must be traded against ecconomy and simplicity. The thin-film naphthalene sublimation and phase change paint methods for heat/mass transfer measurement, examined in the present study, have both proved to be simple and economic, yet are capable of providing a reasonable degree of accuracy.

The comparison of the predictions by the 'intermediate-level' convection model of Alamdari and Hammond (1982) and the high-level 'elliptic' finite-domain flow model of Pun and Spalding (1977) with experimental results in the bound paper (Alamdari et al (1986)), as expected provided an stringent test case for accuracy of such turbulent flow models and gave valuable information regarding the flow and heat transfer behaviour of two-dimensional deflected wall-jet flows. This has shown the need and direction for further improvements in the computer codes towards a more 'realistic' prediction of the flow and transfer properties of turbulent jets when

they expand within practical geometries. The comparison has also shown the prospect which 'intermediate-level' computer codes offer, for meeting the convective heat transfer data needs of dynamic building thermal models by being more accurate, economic and user friendly.

The study of the three-dimensional parallel off-set jet provided new data for this type of flow. This work should be followed by further research on jet/plate interactions in order to provide a comprehensive set of correlating equations including more variables such as inclination angle and number of jets, than those covered in the present work. Such studies would not only be useful to the air-conditioning designer, but also to other branches of engineering such as those concerned with gas turbines and industrial furnaces.

Search for an 'appropriate' analogy factor between heat and mass transfer is still of paramont importance. The research mentioned in this thesis has resulted in a complicated relationship for the analogy factor for the wall-jets. Expansion of this method to other jet/plate interactions can increase the reliability in applying mass transfer methods to heat transfer measurements for different configurations.

REFERENCES

REFERENCES

1. Ainsworth,R.W., and Jones,T.V., "Measurements of heat transfer in circular, rectantgular and triangular ducts, representing typical turbine blade internal cooling passages using transient techniques", ASME paper, 79-GT-40, 1979.

2. Alamdari,F., and Hammond,G.P., "Time dependent convective heat transfer in warm-air heated rooms" Report SME/J/82/01 Cranfield Institute of Technology. Proc. of the Third International Symposium on Energy Conservation in the Built Environment (CIB Working Commission W-67), Dublin, 30th of March-1st April 1982.

3. Alamdari,F., and Hammond,G.P., and Melo,C., "'Appropriate' calculation methods for convective heat transfer from building surfaces", Proc. First UK national heat transfer conf., Leeds, Vol. 2, pp 1201-1211, 1984.

4. Alamdari,F., and Hammond,G.P., and Montazerin,N., "Heat/mass transfer beneath a two-dimensional wall-jet deflected by a normal, flat-plate obstruction", Proc. eighth international heat transfer conf. San Franscisco, USA, 1986. (To be published).

5. Apostolou,P., "Forced convective heat exchange over windows induced by small-aspect-ratio air-conditioning jets", Msc thesis, Cranfield Institute of Technology, 1985.

6. ASHRAE, "Hand-book of fundamentals", New York, 1977.

7. Bourque,C., and Newman,B.G., "Reattachment of a two-dimensional incompressible jet to an adjacent flat plate", Aero. Quart., 11, 201-232, (1960).

8. Butterman,H.C., and Jiji,L.M., and Hoch,J., "Theoretical and experimental studies of velocity and temperature distribution in three-dimensional turbulent wall-jets", ASME paper, 83-WA/HT-4, 1983.

9. Chandrasekhara Swamy,N.V., and Bandyopadhyay,P., "Structure of three-dimensional wall-jets", Indian Journal of Technology, Vol 19, pp 390-394, October 1981.

10. Chilton,T.H., and Colburn,A.P., "Mass transfer (absorbtion) coefficients", Ind. Eng. Chem., Vol. 26, pp 1183-1187, 1934.

11. Clark,J.A., "Energy simulation in building design", Adam Hilger, Bristol, 1985.

12. Dakos,T., and Verriopoulos,C.A., and Gibson,M.M., "Turbulent flow with heat transfer in plane and curved wall-jets", J. Fluid Mech., Vol. 145, pp 339-360, 1984.

13. Dawson,D.A., and Trass,O., "Mass transfer in turbulent radial wall-jet", Canadian Journal Chem. Eng., Vol. 44, pp 121, 1966.

14. Dixon,A.G., Dicostanzo,M.A., Sovey,B.A., "Fluid phase radial transport in packed beds of low tube to particle diameter ratio", Int. J. Heat Mass Transfer, Vol 27, No 10, pp 1701-1713, 1984.

15. Fletcher,D.F., and Maskell,S.J., and Patrick,M.A., "Theoretical investigation of the Chilton-Colburn analogy", Trans IChemE, Vol. 60, pp 122-125, 1982.

16. Hammond,G.P., (a), "Complete velocity profile and 'optimum' skin-friction formulas for the plane wall-jet", Journal of fluids engineering, Vol 104, pp 59-66, March 1982.

17. Hammond,G.P., (b), "Profile analysis of heat/mass transfer across the plane wall-jet", Heat Transfer 1982: Proc. 7th Int. Heat Transfer Conf., Munich, Vol 3, pp 349-355, Hemisphere, Washington, 1982.

18. Hammond,G.P., "Turbulent Prandtl number within a near-wall flow", AIAA Journal, Vol. 23, No. 11, pp 1668-1669, Nov. 1985.

19. Hammond,G.P., Fung,W.S., O'Callaghan,P.W., Probert,S.D., "Interferometric study of the temperature field created by a quasi-plane cold air jet and an adjacent flat plate", Journal of Mechanical Engineering Science, Vol 19, No 2, pp 47-57, 1977.

20. Hoch,J., and Jiji,L.M., (a), "Two-dimensional turbulent off-set jet-boundary interaction", Journal of Fluids Engineering, Vol 103 pp, 154-161, 1981.

21. Hoch,J., and Jiji,L.M., (b), "Theoretical and experimental temperature distribution in two-dimensional turbulent jet-boundary interaction", Journal of Heat Transfer, Vol 103, No 2, pp 331-336, May 1981.

22. Jayatillaka,C.V.L., "The influence of Prandtl number and surface roughness on the resistance of the laminar sub-layer to momintum and heat transfer", Prog. Heat Mass Transfer, Vol. 1, pp 193-329, 1969.

23. Jones,T.V., Russell,C.M.B., "Heat transfer distribution on annular fins", ASME Paper 78-HT-30, 1978.

24. Jones,T.V., Russell,C.M.B., "Efficiency of rectangular fins", ASME paper 80-HT-121, 1980.

25. Kabari,L., "Flow and heat transfer associated with impinging jets in cross-flows", PhD thesis, Cranfield Institute of Technology, 1977.

26. Kline,S.J., and McClintock,F.A., "Describing uncertainties in single-sample experiments", Mechanical Engineering, Vol. 75, pp 3-8, 1953.

27. Koso,T., and Ohashi,H., "Turbulent diffusion of a three-dimensional wall-jet", (1st report, Mean and turbulent characteristics), Bulletin of the JSME, Vol. 25, No. 200, February 1982.

28. Krieth,F., "Heat transfer", Second edition, International Text-book Company, London, 1965.

29. Kumada,M., and Mabuchi,I., and Oyakawa,K., "Generalized correlation of mass transfer by reattached jet at stagnation point on a plate", Trans. JSME, 39, 323, pp 2151-2159, 1973.

30. Launder,B.E., and Rodi,W., "The turbulent wall-jet", Prog. Aerospace Sci., Vol 19, pp 81-128, Pergamon Press Ltd., Great Britain, 1981.

31. Mahmood,M., "Heat transfer from swirling impinging jets", PhD thesis, School of Mechanical Engineering, Cranfield Institute of Technology, April 1980.

32. Mohammed,W., "Space air-conditioning of mechanically ventilated rooms: Computation of flow and heat transfer", PhD thesis, Cranfield Institute of Technology, 1986. (To be published).

33. Mok,C.K., "The flow and thermal field of wall-jets used in heating and air-conditioning applications", Msc thesis, Cranfield Institute of Technology, 1985.

34. Narain,J.P., "Three-dimensional turbulent wall-jets", The Canadian Journal of Chemical Engineering, Vol. 53, pp 245-251, June 1975.

35. Neal,S.B.H.C., "The development of the thin-film naphthalene mass-transfer analogue technique for the direct measurement of heat transfer coefficients", Int J Heat Mass Transfer, Vol 18, pp 559-567, Pergamon press, 1975.

36. Newman,B.G., and Patel,R.P., and Savage,S.B., and Tjio,H.K., "Three-dimensional wall-jet originating from a circular orifice", Aero. Quarterly, 23, 187, 1972.

37. Nizou,P.Y., "Heat and momentum transfer in a plane turbulent wall-jet", Journal of Heat Transfer, Trans. ASME, Vol 103, pp 138-140, February 1981.

38. Oladiran,M.T., "The effect of nozzle inclination on heat transfer in jet impingment systems", PhD thesis, School of Mechanical Engineering, Cranfield Institute of Technology, Oct 1981.

39. Parameswaran,V., and Alpay,S.A., "Studies on reattaching wall-jets", Transactions of the CSME, Vol 3, No 2, 1975.

40. Pun,W.M., and Spalding,D.B., "A general computer program for two-dimensional elliptic flows" Imperial College, London, Mech. Eng. Dept., Rept. HTS/76/2, Amended 1977.

41. Rajaratnam,N., "Turbulent jets" Developments in water science, Elsevier Scientific Publishing Company, 1976.

42. Rajaratnam,N., and Pani,B.S., "Three-dimensional turbulent wall-jets", Proc. ASCE J. Hydraul. Div., 100: 69-83, 1974.

43. Seban,R.A., and Back,L.H., "Velocity and temperature profiles in a wall-jet", Int J Heat Mass Transfer, Vol 3, pp 255-265, Pergamon Press, 1961.

44. SERC, "Energy in buildings specially promoted programme", Science and Engineering Research Council, Engineering Board, Environment committee, Report for the years 1979-1984, ISBN 0 901660 66 3.

45. Sfeir,A.A., "Investigatin of three-dimensional turbulent rectangular jets", AIAA Journal, Vol 17, No 10, Article No 78-1185R, pp 1055-1060, Oct 1979.

46. Sforza,P.M., and Herbst,G., "A study of three-dimensional incompressible turbulent wall-jets", AIAA Journal, Vol 8, No 2, pp 276-283, February 1970.

47. Shute,M., "Forced convective heat exchange at windows in air-conditioning enclosures", Msc thesis, Cranfield Institute of Technology, 1984.

48. Sidaway,C.S., and Hammond,G.P., and Probert,S.D., "Intermittent air injection into the rooms. The iso-thermal ceiling jet", Building Services Research and Technology, Vol 1, No 2, 1980.

49. Sparrow,E.M., and Lovell,B.J., "Heat transfer characteristics of an obliquely impinging circular jet", Trans. ASME Journal of Heat Transfer, Vol. 102, pp 202, May 1980.

50. Van Der Hegge Zijnen,B.G., "Measurements of the velocity distribution in a plane turbulent jet of air", Applied Science Research Section A, Vol 7, pp256- , 1956.

51. Ward,J., and Ideriah,F.J.K., and Probert,S.D., and Duggan,A., "Mass transfer technique for investigation of heat transfer by jet impingment systems", Journal of Mechanical Engineering Science, Vol 14, No 6, pp 389-392, 1972.

52. Ward,J., and Mohammed,M., "Heat transfer from a turbulent, swirling, impinging jet", Proc. The Seventh International Heat Transfer Conf., Munchen, Hemisphere Publishing Corporation, London, 1982.

53. White,F.M., "Fluid Mechanics", McGraw-Hill, Kogakusha Ltd, 1st edition, 1979.

54. Wilkie,D., "Development of the thin-layer naphthalene mass transfer analogy technique" PhysicoChemical Hydrodynamics, Vol. 3, No 3/4, pp 293-299, 1982.

APPENDIX A

MEASUREMENTS

APPENDIX A

MEASUREMENTS

A.1 VELOCITY AND PRESSURE

A pitot tube, using a 19 gauge hypodermic tube facing the flow and gradually expanding to a 10 gauge hypodermic leading to the manometer, was used for the velocity measurements. The tube was connected to a micro-manometer (Furness MDC FC001) with the range 0.01 to 100 mm wg.

For each jet the static pressure on the chamber was calibrated with the nozzle exit velocity. The resulting curve was used to set the rig up and also was fed to the computer for the calculations.

A.2 TEMPERATURE

Temperatures were measured using copper-constantan thermo-couples connected to a digital thermometer (Comark 5000) which was capable of reading the temperature upto 0.5 of a degree.

The 6 different channels (figure A-1) monitored temperatures:

1. At the inlet to the heat exchanger.
2. At the air leaving the heater.
3. At the air inlet to the flexible pipe.
4. Inside the settling chamber.
5. Throughout the test section (via the traversing gear).
6. In the ambient air.

Since air is not a good conductor, the readings on the termocouples fluctuated within one degree. This was not caused by any inaccuracy but was purely due to the variations in the local air temperatures. British Standard (B.S. 1041 Pt 4) suggests attaching a mass of conducting metal to the termocouple in order to stabilise the temperature. Such a mass time-averages the temperature fluctuations. The drawback to this suggestion is that it takes a fairly long time to warm the mass up to a stable temperature and therefore no stabilising mass was employed.

A.3 SURFACE PRESSURE TAPPINGS

Pressure tappings consisted of 16 gauge hypodermic tubes flush-mounted with the surface of the flat plate. These were connected via a scannivalve to the micro-manometer (see section A.1 above). The scannivalve consisted of 6 wafers, each with 24 ports. The outlets from 5 of these wafers were connected to the 6th wafer, whose outlet was directly coupled to the micro-manometer.

The following points were important in positioning the pressure tappings on the plate:

1. They should provide static pressure readings across the whole surface area.

2. A higher concentration of tappings was necessary near the nozzle.

3. The arrangement should be capable of monitoring both two- and three-dimensional flows.

A lengthwise logarithmic spread for the tappings was adopted since this ensured both closer readings near the nozzle and a better representation of the streamwise velocity variation when plotted on a logarithmic scale.

In connecting the tappings to the scannivalve the following were important:

1. The desirability of choosing a distance from the nozzle and obtaining the static pressure across the plate by only changing the switch on wafer 6.

2. the desirability of choosing a coordinate across the plate (say on the centre-line) and obtaining the static pressure along the plate by switching between the different ports on a single wafer.

3. The desirability of having an overall static pressure distribution on the plate without the necessity of making detailed measurements near the nozzle.

4. The desirability of making detailed measurements near the nozzle.

The following table shows both the positioning of the tappings and the port on the scannivalve to which each was connected. Holes were designated by their X and Z coordinates and the ports on the scannivalve were designated by row and column (5 rows and 25 columns) on the scannivalve pannel, a few of which were directly connected to the 6th wafer (see figure B-2).

plate		scannivalve		plate		sannivalve	
X	Z	Column	Row	X	Z	Column	Row
2200	-400	1	1	1550	-400	2	1
2200	-200	1	2	1550	-200	2	2
2200	0	1	3	1550	0	2	3
2200	200	1	4	1550	200	2	4
2200	400	1	5	1550	400	2	5
1050	-400	3	1	770	-400	4	1
1050	-200	3	2	770	-200	4	2
1050	0	3	3	770	0	4	3
1050	200	3	4	770	200	4	4
1050	400	3	5	770	400	4	5
540	-400	5	1	380	-400	6	1
540	-200	5	2	380	-200	6	2
540	0	5	3	380	0	6	3
540	200	5	4	380	200	6	4
540	400	5	5	380	400	6	5
270	-200	7	1	190	-400	8	1
270	-90	7	2	190	-90	8	2
270	0	7	3	190	0	8	3
270	90	7	4	190	90	8	4
270	200	7	5	190	400	8	5
135	-200	9	1	95	-400	10	1
135	-90	9	2	95	-90	10	2
135	0	9	3	95	0	10	3
135	90	9	4	95	90	10	4
135	200	9	5	95	400	10	5
65	-200	11	1	45	-400	12	1
65	-90	11	2	45	-90	12	2
65	0	11	3	45	0	12	3
65	90	11	4	45	90	12	4
65	200	11	5	45	400	12	5
35	-200	13	1	25	-400	14	1

35	-90	13	2	25	-90	14	2
35	0	13	3	25	0	14	3
35	90	13	4	25	90	14	4
35	200	13	5	25	400	14	5
15	-200	15	1	540	-300	16	1
15	-90	15	2	540	-90	16	2
15	0	15	3	540	90	16	4
15	90	15	4	540	300	16	5
15	200	15	5				
380	-300	17	1	270	-60	18	1
380	-90	17	2	270	-30	18	2
380	90	17	4	270	30	18	4
380	300	17	5	270	60	18	5
135	-60	19	1	190	-60	18	3
135	-30	19	2	190	30	19	3
135	30	19	4				
135	60	19	5				
95	-75	20	1	65	15	21	1
95	-60	20	2	65	30	21	2
95	-45	20	3	65	45	21	3
95	-30	20	4	65	60	21	4
95	-15	20	5	65	75	21	5
45	-75	22	1	35	15	23	1
45	-60	22	2	35	30	23	2
45	-45	22	3	35	45	23	3
45	-30	22	4	35	60	23	4
45	-15	22	5	35	75	23	5
25	-75	24	1				
25	-60	24	2				
25	-45	24	3				
25	-30	24	4				
25	-15	24	5				

And these tappings were directly connected to the wafer number 6 at the back of the scannivalve:

X	Z	port	X	Z	port
15	75	6	25	60	11
15	45	7	25	30	12
15	15	8			
15	-30	9			
15	-60	10			
35	-15	13	45	75	16
35	-45	14	45	45	17
35	-75	15	45	15	18
65	-30	19	95	60	21
65	-60	20	95	30	22

1) Inside the settling chamber.
2) Ambient.
3) Water inlet to the heat exchanger.
4) Temperature field in the test section.
5) Air inlet to the flexible pipe.
6) Air temperature immediately out of the heater.

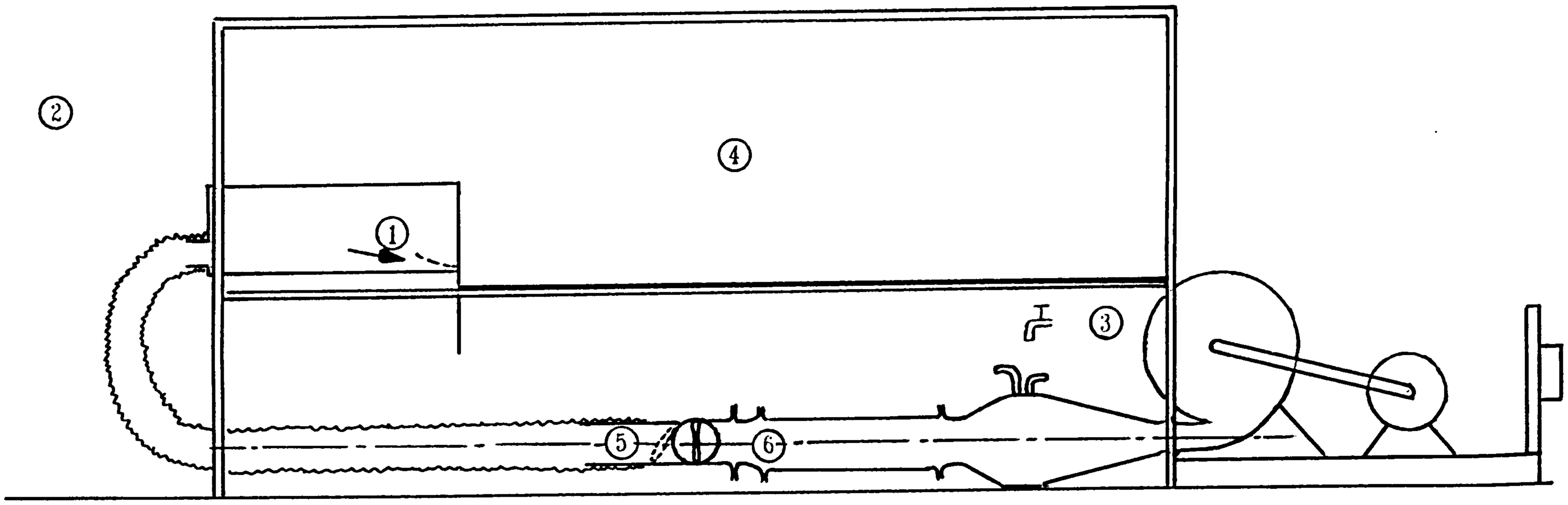

Figure A-1 : Locations of the thermocouples.

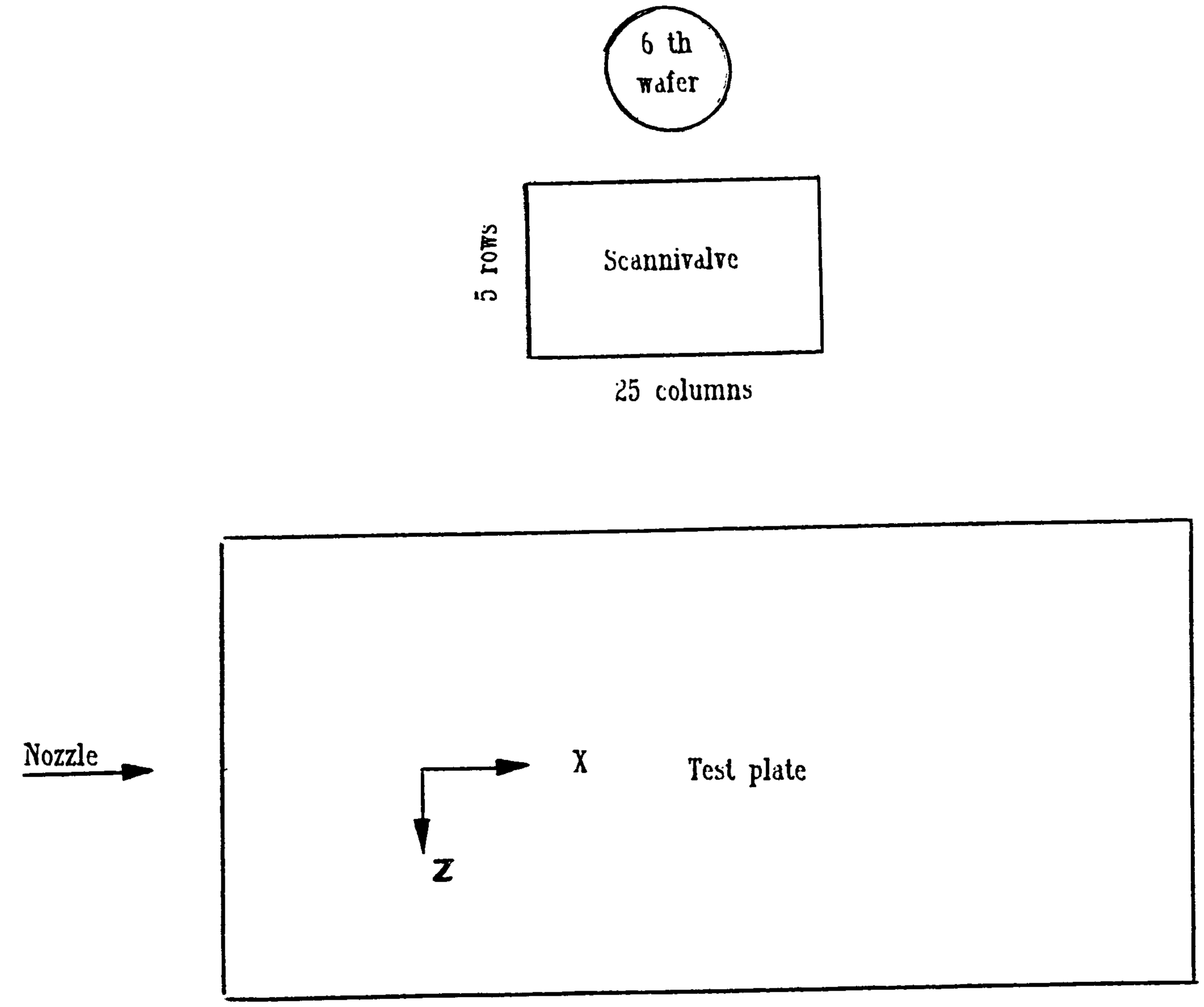

Figure A-2 Set up for the scannivalve and the test plate.

APPENDIX B

HEAT TRANSFER CALCULATIONS

APPENDIX B

HEAT TRANSFER CALCULATIONS.

The clearance time for many points along the test plate were determined at the end of each thin film naphthalene sublimation test run. A computer program was developed to use this data and calculate the respective Stanton numbers. The effect of changes in the atmospheric conditions were taken into account by including measured ambient pressures and temperatures in the calculations. The calculation method was similar to the one used by Mahmood (1980)and the highlights of the procedure were as follows:

1. Calculate the density of the naphthalene at the start of the experiment at each point. In addition to the test plate, a plug was sprayed and weighed using a balance with an accuracy of 0.001 gr. This measurement was repeated after at least 2000 secs to obtain both the quantity of naphthalene on the plate and also the loss due to natural sublimation in the time lapse between the spray and the start of the experiment.

2. The Schmidt number was calculated from expression given by Dawson and Trass(1966):

$$Sc = 7.00 * (T)^{-0.185} \qquad (B-1)$$

3. The Prandlt number was assumed constant at 0.709, corresponding to an ambient temperature of 18.5 C.

4. The naphthalene partial pressure was calculated using the equation of Sherwood and Byrant:

$$\log p_n = 11.5 * (3765 / T_n) \qquad (B-2)$$

5. The heat transfer rate was calculated (see chapter 4) from:

$$h = \left(\frac{m}{A_n t}\right) . \rho . c_p . \frac{R_n T_n}{p_n} . \left(\frac{Sc}{Pr}\right)^{2/3} \qquad (4-12)$$

6. And the Stanton number was determined from the definition:

$$St = \frac{h}{(\rho\ u\ c_p)_{slot}} \qquad (B-4)$$

7. Mass transfer Stanton numbers were recovered by reversing the Chilton-Colburn analogy factor expression:

$$St_m = St/(Sc/Pr)^{2/3} \qquad (B-5)$$

This procedure was repeated in the two-dimensional case for each clearance line and in the three-dimensional case for each recorded point.

Typical values for a test run are as follows:

Ambient pressure	= 746	mm Hg
Temperature	= 17.9	C
Static pressure on the settling chamber	= 2.44	mm Wg
Slide weight before spray	= 25.039	gr
Spray start time	= 0	secs
Spray finish time	= 3600	secs
Spray start position	= 47	cms
Spray finish position	= 0	cms
Slide weight at 1259 secs	= 25.099	gr
Slide weight at 3914 secs	= 25.088	gr
Test start at 3757 secs		
Clearance at x=7 at	5244	secs
Nozzle exit velocity	= 5.944	m/s
Spray density at the start of the test at x=7	= 0.8678	mg/cm^2
Viscosity of air	= 1.8×10^{-5}	kg/m s
Schmidt number	= 2.45	
Prandlt number	= 0.709	
Naphthalene partial pressure	= 4.886	N/m^2
Density of air	= 1.191	kg/m^3
Specific heat of air	= 1004.51	j/kg K
Reynolds number	= 1996.47	
Heat transfer rate	= 61.5	$w/m^2 C$
Stanton number	= 8.65×10^{-3}	
Mass transfer Stanton number	= 3.784×10^{-3}	

APPENDIX C

EXPERIMENTAL UNCERTAINTIES

APPENDIX C

EXPERIMENTAL UNCERTAINTIES

Two types of error were possible in the experiments. First was the error in the analysis and the assumptions. This group includes the errors such as those involved in the application of the Chilton-Colburn analogy, using a slab to measure the density of naphthalene on the plate, and the assumption that conductive heat transfer in tests using the phase change paint is one-dimensional. In every such case the source of the error is explained in the text and its possible effect on the results is as far as possible estimated.

The second type of error is the experimental error and this includes the mistakes in instruments and the readings. Method of Kline and McClintock (1953) was employed to estimate their effect on the final results. As an example their method is here applied to the calculation procedure in Appendix B. The uncertainty in calculating the heat transfer coefficient from equation B-3 may be found from:

$$\frac{w_h}{h} = \left[\left(\frac{w_{R_n}}{R_n}\right)^2 + \left(\frac{w_T}{T}\right)^2 + \left(\frac{w_{P_n}}{P_n}\right)^2 + \left(\frac{w_{c_p}}{c_p}\right)^2 + \left(\frac{w_\rho}{\rho}\right)^2 + \left(\frac{w_m}{m}\right)^2 + \left(\frac{w_t}{t}\right)^2\right] \qquad (C\_1)$$

which is written for every term of the equation and w_x/x is the possible uncertainty for the parameter x divided by the value of that parameter. In this method there would be the same odds for the uncertainty of the final result as the odds for the uncertainty of each individual parameter. (Shute 1984).

This method estimates the uncertainty in measuring the heat transfer coefficient of the example in appendix B to be at 7% at 20:1 odds.

APPENDIX D

BLUFF-JET VELOCITY PROFILES AND MASS TRANSFER

APPENDIX D

BLUFF-JET VELOCITY PROFILES AND MASS TRANSFER.

VELOCITY PROFILE MEASUREMENTS.
DIMENSIONS IN mm.
VELOCITIES IN m/S.

WALL-JET

$\frac{x=65}{z=0}$

y------ u	z=5 y------ u	z=10 y------ u	z=15 y------ u
1 30.4	2 34.2	2 26	2 13.2
4 36.1	3 35.8	3 26.3	3 12.5
5.5 37.2	4.5 36	4.5 26.3	5 11.5
7.5 37.9	6 32.5	6.5 23	6 8.1
10 34.7	8.5 27.5	8.5 17.7	10 4.1
12 29	11 21.5	12 7.6	15 0
15 20.7	12 16.7	15 4.1	
16.5 15.2	18.5 4.4	26 0	
18.5 9.1	23 2.6		
21.5 3.1			

$\frac{x=94}{z=0}$

y------ u	z=5 y------ u	z=10 y------ u	z=15 y------ u
1 27.8	1 25.7	2 21.1	1.5 13.2
3.5 31.2	3.5 29.3	4 22.2	3.5 13.2
5.5 33.7	5 30.4	5 23	5 11.8
7 34.5	7 30.7	6 21.1	7.5 10.7
9 33.7	9 27.6	9 19.9	9 9.5
11 30.9	10 24	10 17.5	11 8.1
13 27.2	12 21.5	13 13.5	13 7
15 22.6	14.5 16.7	16 10.3	15 5
17.5 17	16.5 13.8	18 8.6	18 3.4
20 13.5	19 10.6	20 5.1	20 1.8
22 8.6	21 7.6	23.5 2.6	
24 5.3	24.5 3.8		
26.5 2.7	26 1.8		

x=189
z=0

y	u
2	20.3
3	21.1
6	22.6
8	23
11	21.9
13	20.3
16	17.9
17.5	16.5
20	12.8
22	11.8
25	9.5
27	8.3
30	5.7
32	4.1
35	2.6
*	*
*	*
*	*
*	*

z=5

y	u
2	20.7
4.5	22.2
6	23
8.5	22.6
10	21.9
11.5	20.7
14	19.2
15	17.9
17	17
18	15.5
20	13.2
21.5	12.5
23.5	10.9
25	9.3
27	7.9
29	6.5
30	5.1
34.5	2.7

z=10

y	u
2	19
4	19.5
5	19.6
6	19.9
8	19.7
9.5	19
11.5	17.2
14.5	15.5
16	14.1
19	12.5
20.5	12.5
24	9.3
27	7.3
33	2.9
*	*

z=15

y	u
2	14.9
4	15.7
5.5	15.2
7	15.2
8	14.4
10	13.5
11.5	12.4
13	12.2
16	11
18	9.8
20.5	8.6
22.5	8.6
26	5.7
29	5
33	1.8

x=379
z=0

y	u
1.5	11
2	11.3
3.5	12
5	12.2
6	12.2
10	11.9
12	11.5
14	11
15.5	10.3
17.5	9.9
22.5	8.7
25	7.8
30	6.7
35	5.1
39.5	4.1
47	2.4

z=10

y	u
1	11.3
4	12.5
8	11.9
10	11.1
14	9.9
18	8.6
24	6.4
31.5	4.8
39	3.1

z=20

y	u
1	10.3
4	10.6
6	10.3
9	9.9
13.5	8.5
17.5	7.3
23	5.9
27	4.3
37.5	2.6

z=30

y	u
1	8.7
3	8.8
5	8.6
8	8.2
11	7
16	5.7
21.5	4.4
30.5	2.2

OH = 0.7

z=0
x=14

y	u
3	2.2
4	8.6
5	19
6	34
8	38.1

x=34

y	u
1.5	17.7
3	21.9
6	34
9	38.3
10.5	38.3

x=65

y	u
2	23.3
3	25.7
5	27.2
10	35.8
11	36.3

x=94

y	u
1	24
3	24.4
4	25.4
5	25.7
7	27

10	38.1	12	38.3	13	36.1	8.5	28.4
11	38.3	15	33.5	14	34.7	10	30
12.5	38.5	19	15.7	18.5	22.6	11	32
16	30.1	25	0	20	15.7	13.5	31.2
21	0	*	*	25	4.8	16	28.4
*	*	*	*	28	0	19	20.3
*	*	*	*	*	*	23	12.8
*	*	*	*	*	*	27	6.4

x=134

y------	u
1.5	21.9
3.5	23
5	23.7
8	24.9
9.5	25.3
12	25.3
14	24.4
18	20.9
21.5	17
25	11.5
31	5.4
36	0.9

x=189

y------	u
2	17.9
3	19
4	20
7	20.7
8	20.9
12	20.3
14	19.5
18	17.2
22	14.4
25	11.8
33	7
40	2.9

x=271

y------	u
1	13.5
3	14.1
4	15.2
7	15.5
9.5	15.7
13.5	14.6
18	13.1
23	11.8
28	9.5
38	5.7
46	2.6

x=379

y------	u
1	10.3
5	11
8	11.2
12	10.7
17.5	9.9
25	8.6
30	7.1
41	4.8
53	2.2

OH = 1.6

x=65

z=0

y------	u
2	8.8
3	9.9
5	13.1
8	16
10	18.6
13.5	19.9
16	29
18	33.2
21	36.8
24	35.4
26	32.5
29	21.5
32	12.8
34	7.1

z=5

y------	u
1	3.1
4	5.1
6	9.9
10	16.2
11	22.2
16	27.5
20	36.5
23	35.4
29.5	19
34	8
42	0

z=10

y------	u
1	0
3	2.2
6	5.7
9	9.5
11	13.1
17	23
23.5	24.4
26	17.7
31	5.7
38.5	0

z=15

y------	u
1	0
11	4.2
15	9.1
20.5	16
25.5	9.1
32	0

x=94

z=0

y------	u
2.5	11.8
3.5	12.3
6	13.5
8	14.1

z=5

y------	u
2	9.5
3	11.5
6	11.5
8.5	12.8

z=10

y------	u
2	7.5
4	7.6
7	7.6
10	9.1

z=15

y------	u
1.5	4.3
3	3.1
6.5	1.8
9	3.4

11	18.4	11.5	15.7	12.5	10.7	13	5.7
13.5	21.1	15	20.3	15	12.8	16	13.1
16	23.7	19	29.3	18	19.9	19.5	11.3
19.5	29.3	22.5	28.4	21	20.3	23	9.1
24	31.2	25	24.4	25	18.6	26	6.4
27	26.6	28	19.9	28	15.2	31	4.4
30	17.7	30	14.6	31	12.8	34	1.8
34	11.1	34	10.1	34	7.3		
39	4.4	37	6.3	39	1.3		
43	1.8	41	2.2				

x=134

z=0		z=5		z=10		z=15	
y	u	y	u	y	u	y	u
1	12.8	2	12.5	2	10.3	3	7.6
4	13.5	4.5	12.8	4.5	10.7	4	7.6
5	14.1	6.5	13.8	7.5	11.5	8	7
8	14.6	10	15.5	10	12.7	12	10.7
12	16.5	12	18.1	14	15.2	15	9
16	21.1	15	20.1	17.5	16	18	9.5
18.5	21.9	18	22	20	16.5	22	10.7
21	24	20	23.3	22	15.7	26	9
24	24	23	23.7	25	15.2	30	7.3
28	21.5	27	21.9	29	12.5	33.5	5.3
30	19.5	30	18.4	32	9.9	36	3.8
35	12.9	33	13.8	36	6.7	40	1.6
39	9.5	35	12.2	39	4.3		
44	5	40	7	42	3.1		
47	1.8	42	5				

x=189

z=0		z=5		z=10		z=15	
y	u	y	u	y	u	y	u
1	11.8	1.5	12.5	0.5	11.5	1	10.4
3	12.5	4	13.5	3	12.2	4	11.3
4.5	13.5	8	14.6	5	12.3	8	11.1
8	14.3	11	15.6	9	14.1	13	11.5
10	14.9	14	16.2	12	14.1	17	11.3
14	16.2	18	17.2	15	14.6	20	11.5
15	16.7	21.5	17.2	18.5	14.6	24	10.3
20	17.5	25	16.2	23	14.9	28	9.2
22.5	17.7	29	14.6	25	13.1	34.5	6.9
25	17.5	33	12.2	29	11.8	39.5	5.6
29	16	37.5	9.5	32	11.1	46	2
31.5	15.2	41.5	7.3	39	7.6		
35	13.1	47.5	4.1	45	5		
38	10.7	52.5	1.57	48	2.9		
42.5	8.1						
51	3.4						

x=379

z=0		z=5		z=10		z=15	
y	u	y	u	y	u	y	u

1	8.6	1	8.9	1	8.6	1	8.7
3.5	9.3	2	9.3	2	9.2	2.5	9.1
11	10	4.5	9.6	5	9.7	5	9.5
14	10	7	9.9	6.5	9.9	9	9.7
17.5	10.2	12	10.1	11	10	12	9.7
23	9.5	15	10.3	17	9.9	18	8.8
28.5	9.1	20	9.9	21	9.3	26.5	8.2
33	8.5	26	9.3	25	9	30	7.8
38	7.6	31	8.9	29.5	8.5	38	6.4
46	6.1	35	8.3	38	7.4	44.5	5.4
53	4.8	44	6.4	44	6.4	52	4.4
61	3.1	53	4.8	52	4.6	58.5	3.1

OH = 2.2

z=0

x=65		x=94		x=134		x=189	
y	u	y	u	y	u	y	u
1	1.3	1	4.4	1	8.1	1	8.6
8	5.7	4	5.6	3	8.3	4	8.6
12	12.2	6	7	5	9.5	5	9.5
15	15.7	9	10.3	8	10.3	8	9.9
18	19.7	12	12.5	11	12.5	9.5	10.7
22	24	18	17.2	15	14.3	12.5	11.5
25	30.7	22	21.9	18	15.5	14	12.2
29	33.2	23.5	23	20	17.9	18	13.5
30	30.6	27.5	27.5	23	19.7	20	14.6
32	27.8	32	25.3	25	21.5	23	15.7
36	16.7	37	16.5	30	22.2	26	16.7
41	5.3	42	8.1	33	21.1	30	17.2
*	*	48	1.3	38	16.2	34	16.5
*	*	*	*	43	9.9	39	14.1
*	*	*	*	49	5.7	44	12.2
*	*	*	*	55	1.3	50	7.6

X=271		X=379	
y	u	y	u
2	8.6	2	7.8
4	8.8	5	8.2
5	9.2	10	8.7
8	9.4	14	8.7
10	9.9	19	9
14	10.4	22.5	9.2
18	11.1	26	9.2
20	11.7	30	9.1
24	12.2	35.5	8.7
28	12.6	42	8.2
34	12.5	48	7.5
35.5	12.5	55	5.9
39.5	11.5	63	4.6
43.5	10.7	69	3.9
49	8.6		

54 7.3

OH = 3.1

Z=0

x=65		x=189		x=271		x=379	
y------	u	y------	u	y------	u	y------	u
2	0	2	2.9	2	4.8	2	5
18	3.4	3	2.9	4	5.1	6	5.9
23	12.3	7	3.8	5	5.2	9.5	6
26	18.1	11	4.4	8	5.3	12	6.3
30	23.7	17	6.4	11	6.1	16	6.4
32.5	28.4	20	7.6	15	6.4	22	6.5
38.5	33.2	25	9.5	19	7.5	28	7.1
40	27.5	29	12.5	25	8.4	35	7.3
43.5	20.3	36	15.2	29	9.4	42	7.9
47	12.5	42	16.2	35	10.5	48	7.3
53	1.3	48	15.2	38.5	11	56	7.1
*	*	53	13.1	46	11	64	6.4
*	*	57	11.5	53	10.5	72	5.3
*	*	67.5	5.4	62	8.5	80	4.1

OH = 3.8

x=65

z=0		z=5		z=10		z=15	
y------	u	y------	u	y------	u	y------	u
10	0	25	4.1	5	0	20	0
25	1.8	28	10.7	26	5.1	24	0.9
27	5.7	32	18.1	30	11.5	28	2.9
30.5	12.5	36	22.2	36	14.3	39.5	5.1
35	23.3	41	33.5	43	29.3	42	9
38	27.5	46	30.4	49.5	13.8	52	4.1
43	35.8	52	14.6	51	10.3	60	0.4
48	31.2	58	1.3	58	1.8		
51	22.6						
55	7.6						

x=134

z=0		z=5		z=10		z=15	
y------	u	y------	u	y------	u	y------	u
2	0	15	3.6	21.5	7.4	17	3.8
20	5.3	22	8.1	26.5	10.2	22.5	6.7
29.5	11.3	26	10.3	33	15.2	29	9.3
35	16	32	15.5	36.5	17	37	11.2
40	19.2	35.5	18.8	43	19.5	44	11.8
43.5	23.3	43	23.3	50	14.1	52	8.1
49	22.2	47	21.9	60	5.7	61	2.2
54	16.7	52	16.2	69	0		

60.5	9.9	61	6.9

x=271
z=0

		z=5		z=10		z=15	
y------	u	y------	u	y------	u	y------	u
1	3.8	3	4.1	3	5	2	4.2
5	4.2	4.5	4.6	5	5.1	5	5
9	5	9	5	8	5.4	10	5.4
15	6	14	6.3	11	6.3	15	6.4
19	7.5	19	7.6	17	7.8	20	7.9
25	9.3	25	9.9	22	8.8	24	8.7
36	12.5	33	11.8	28.5	10.3	30	9.6
45	12.8	42	12.2	36	11.3	37	9.4
53.5	11.5	45	12.2	43	11.3	45	8.4
61.5	8.9	52	10.3	50	9.9	52	7
72	4.8	58	9.1	60.5	7.6	62	5.7
79	2.9	65	6.8	65	6	70	3.4

x=379
z=0

		z=10		z=20		z=30	
y------	u	y------	u	y------	u	y------	u
2	5.9	1	5.9	1	5.9	1	6.4
5	6.4	4	7	5	6.4	3	6.4
12	7	6	7.1	7	6.5	6	6.7
17	7.7	10	7.3	10	6.7	9.5	6.7
25	8.4	18	7.8	13	7	16	6.7
32	9.2	22	8.3	18	7	22	6.9
40	9.2	27	8.7	21	7.1	28	6.9
48	8.4	33	9	26	7.3	34	6.9
58.5	6.9	40	8.8	31	7.4	42	6.5
66	6	47	8.2	36	7	49.5	5.7
74	4.4	53	7	44	6.7	56.5	5.1
84	2.9	59	6.8	55	5.9	63.5	4.2
*	*	69	5	64	5.1	75	3.1

Wall-jet

x/S=6,5

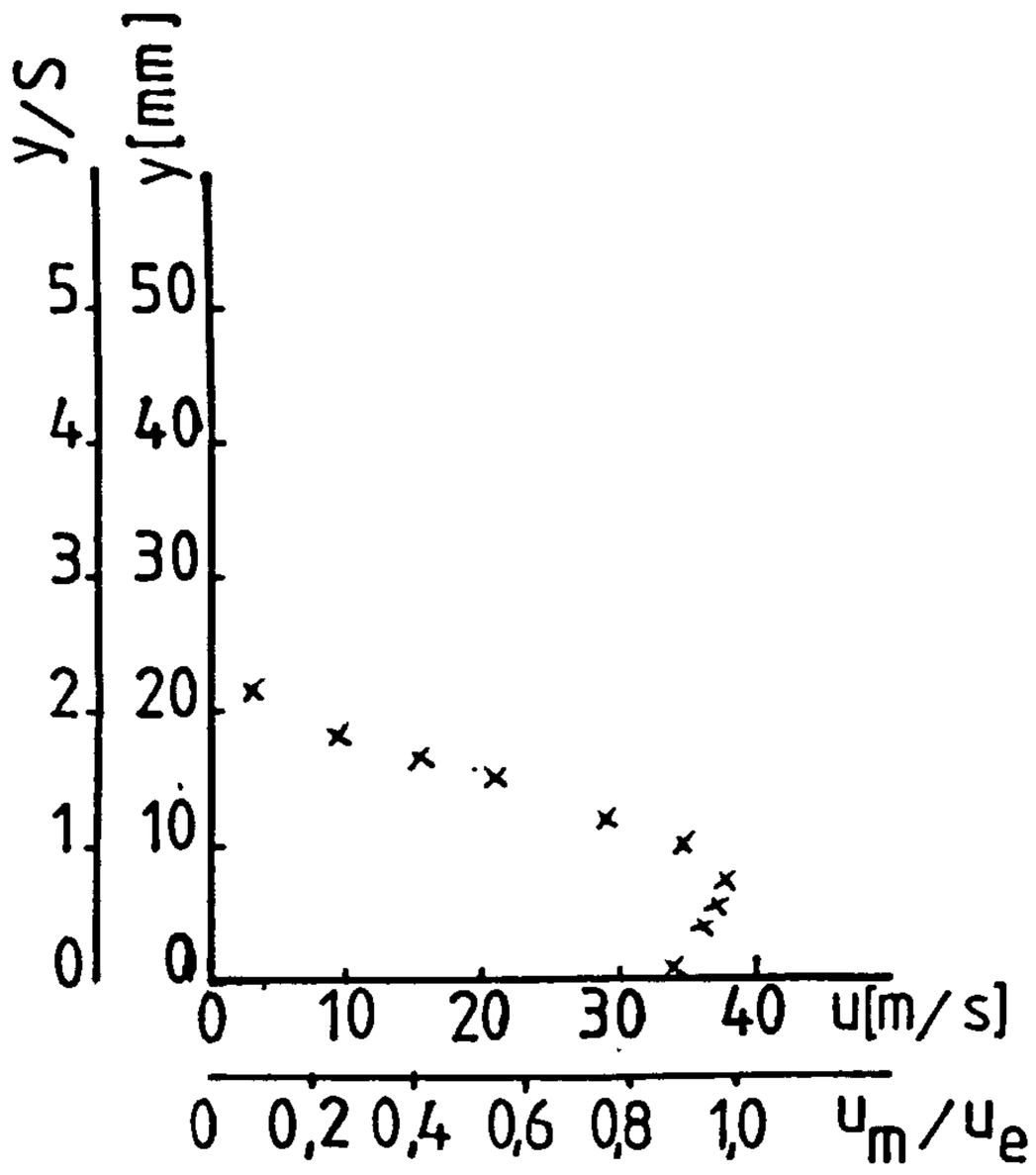

z=0

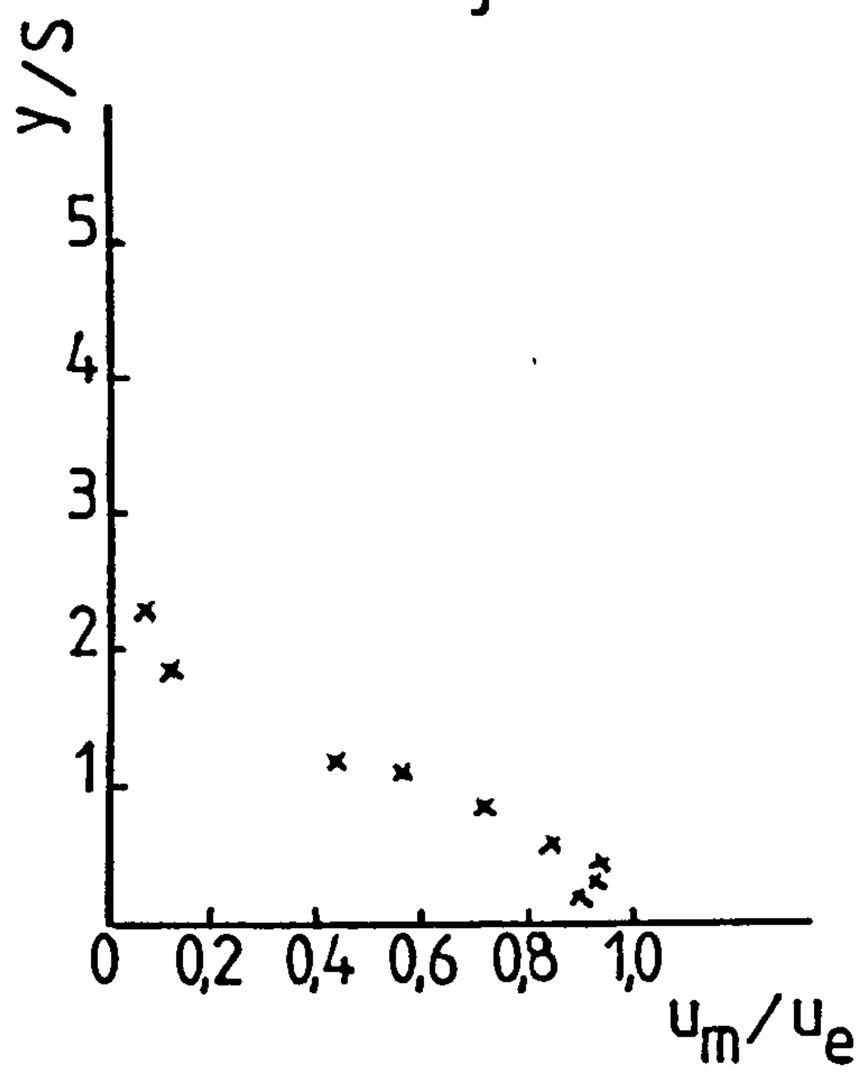

z=5 mm
z/B=0,25

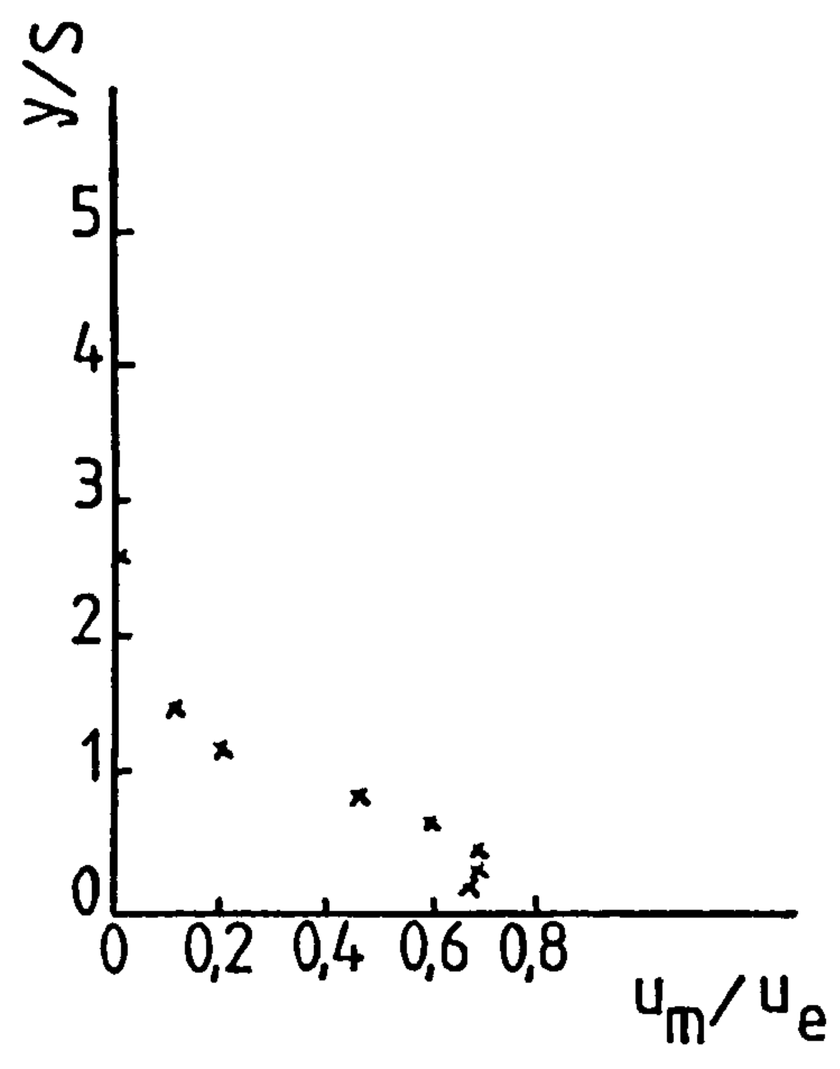

z=10 mm
z/B=0,5

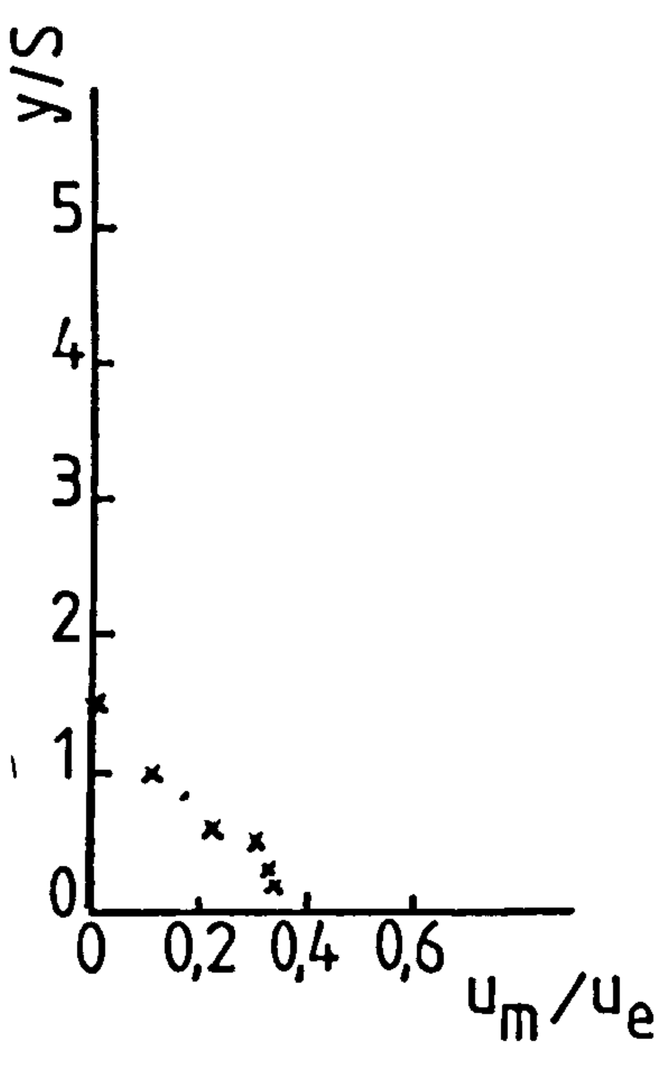

z=15 mm
z/B=0,75

Figure D-1 Three-Dimensional jet velocity profiles

Wall_jet x/S=9,4

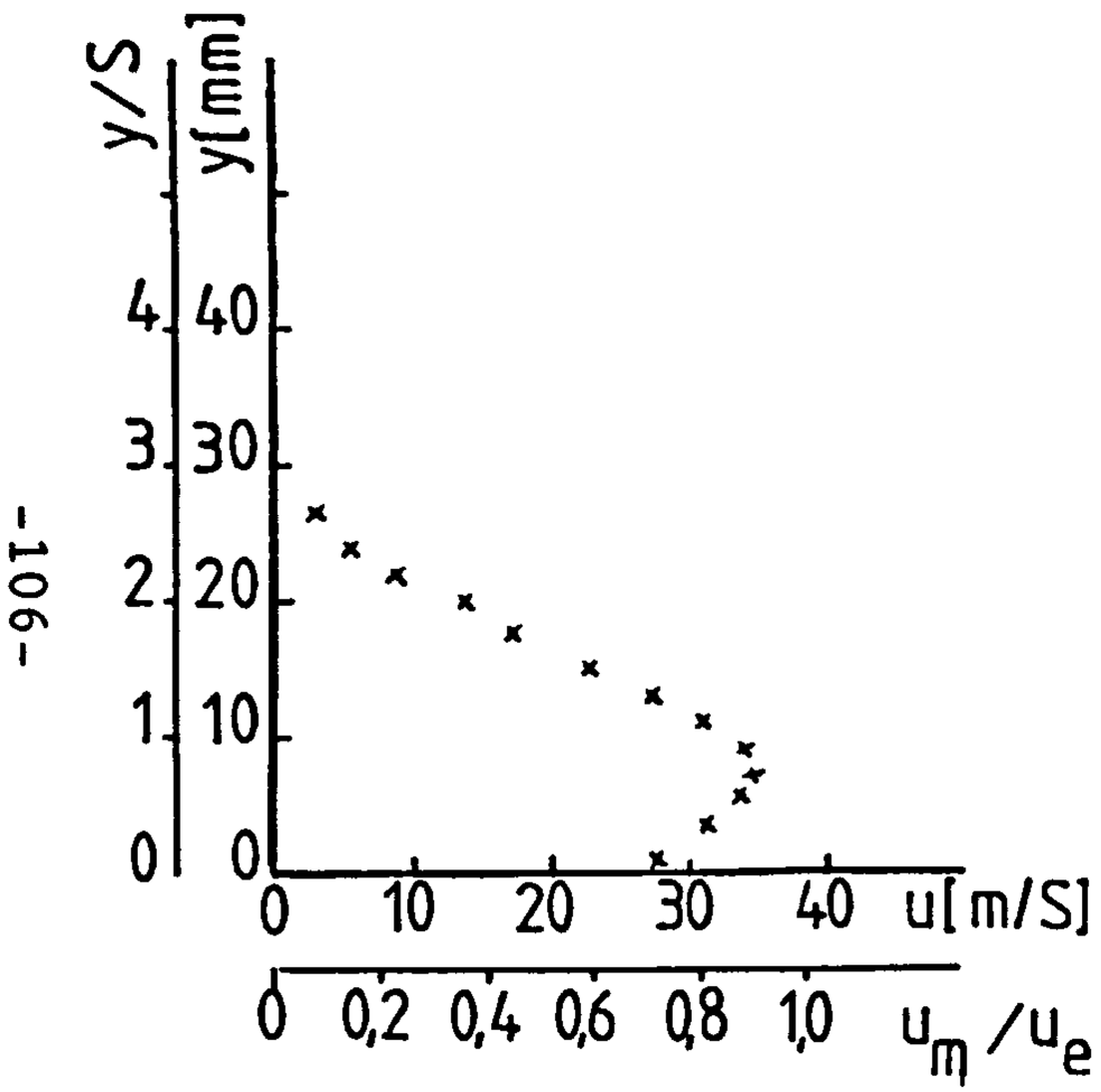

z=0

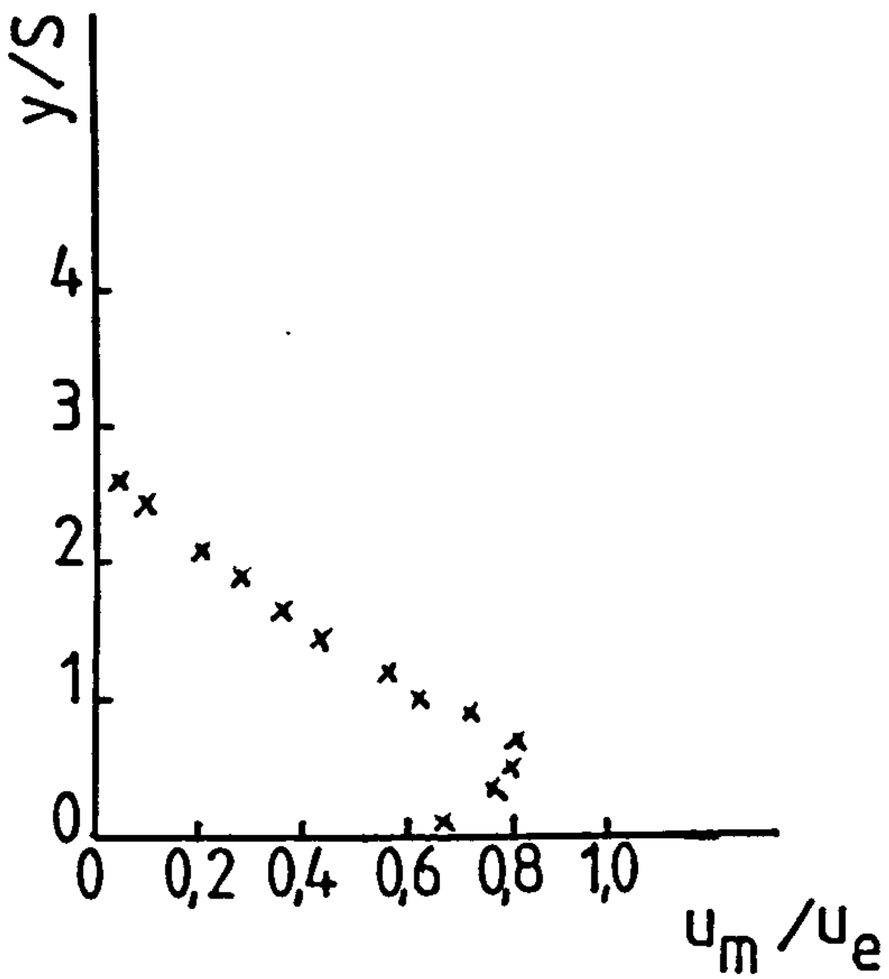

z/B=0,25

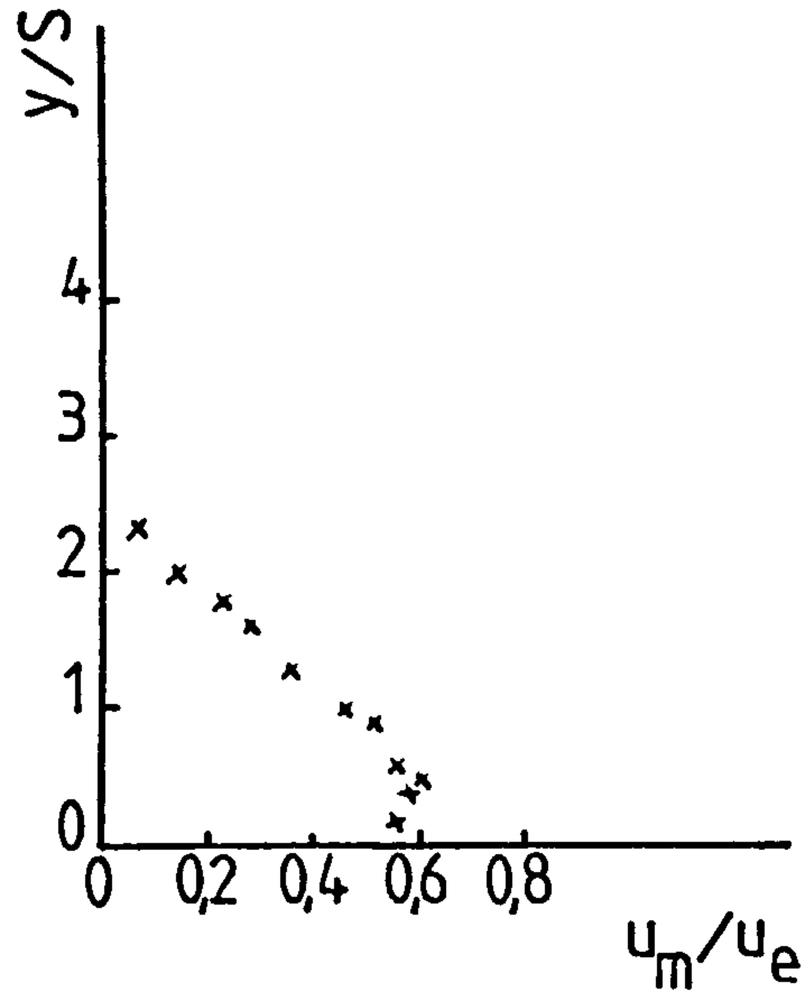

z/B=0,5

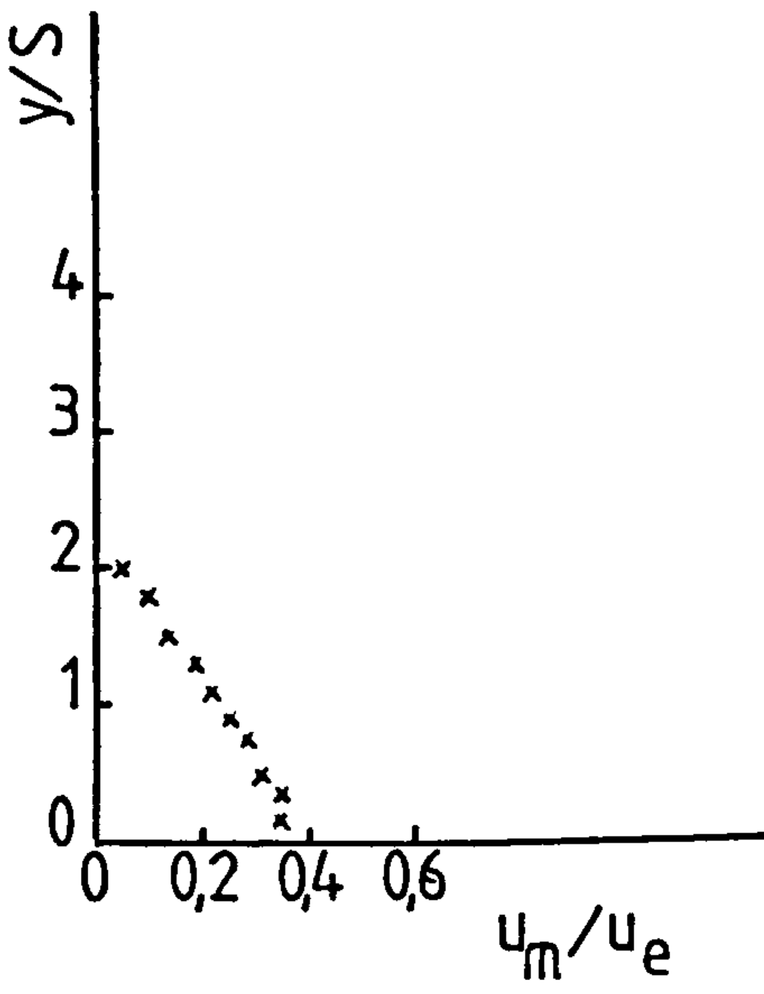

z/B=0,75

Figure D-2 Three-Dimensional jet velocity profiles

Wall_jet

x/S=18,9

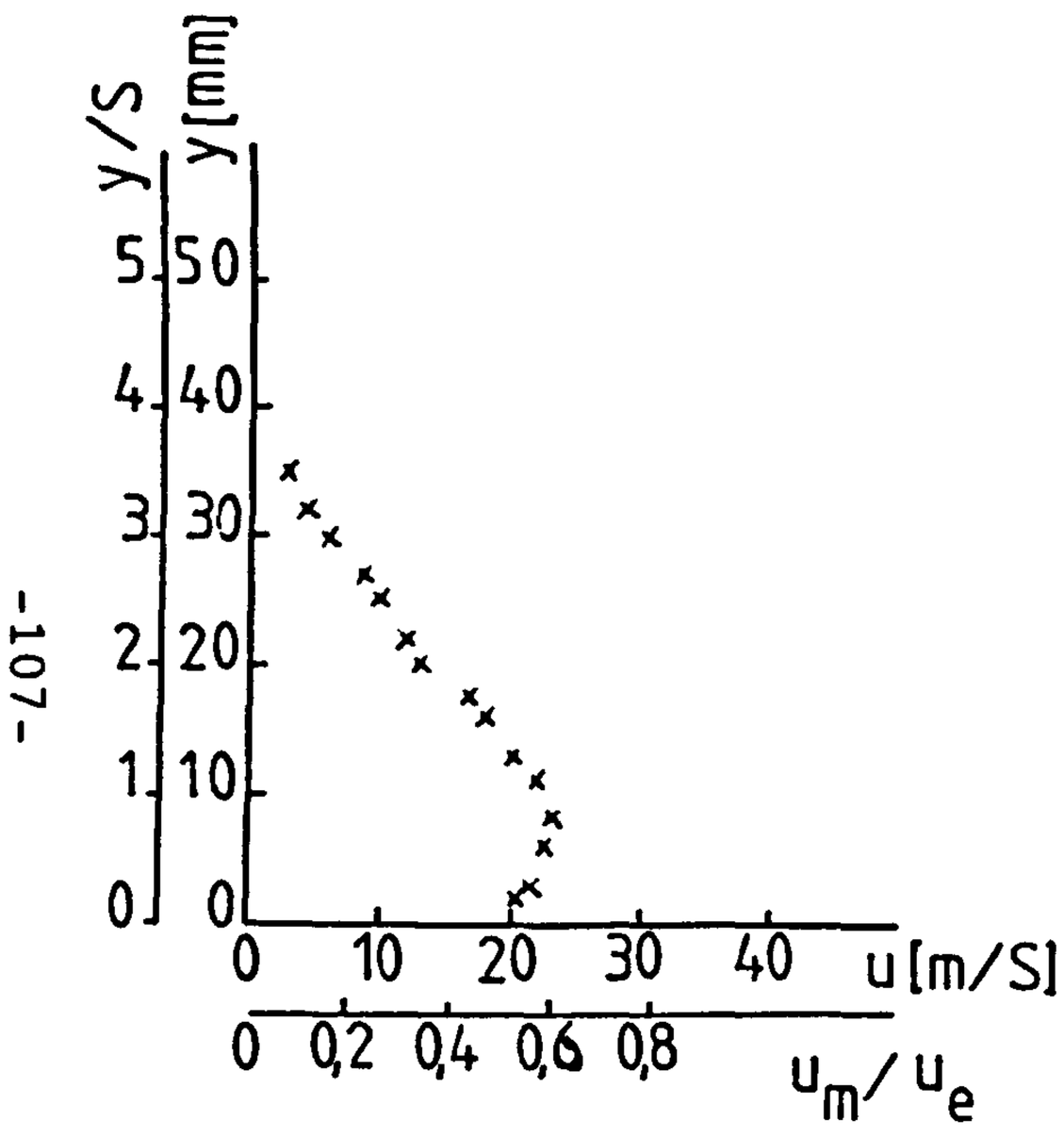

z=0

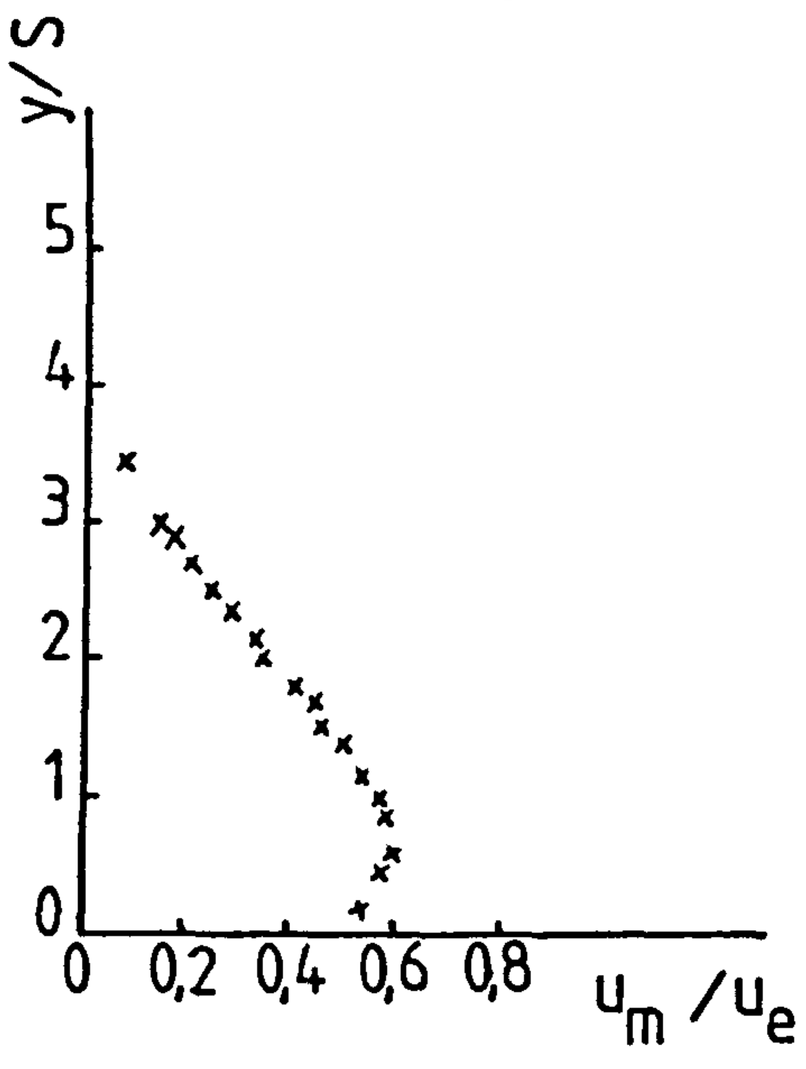

z/B=0,25

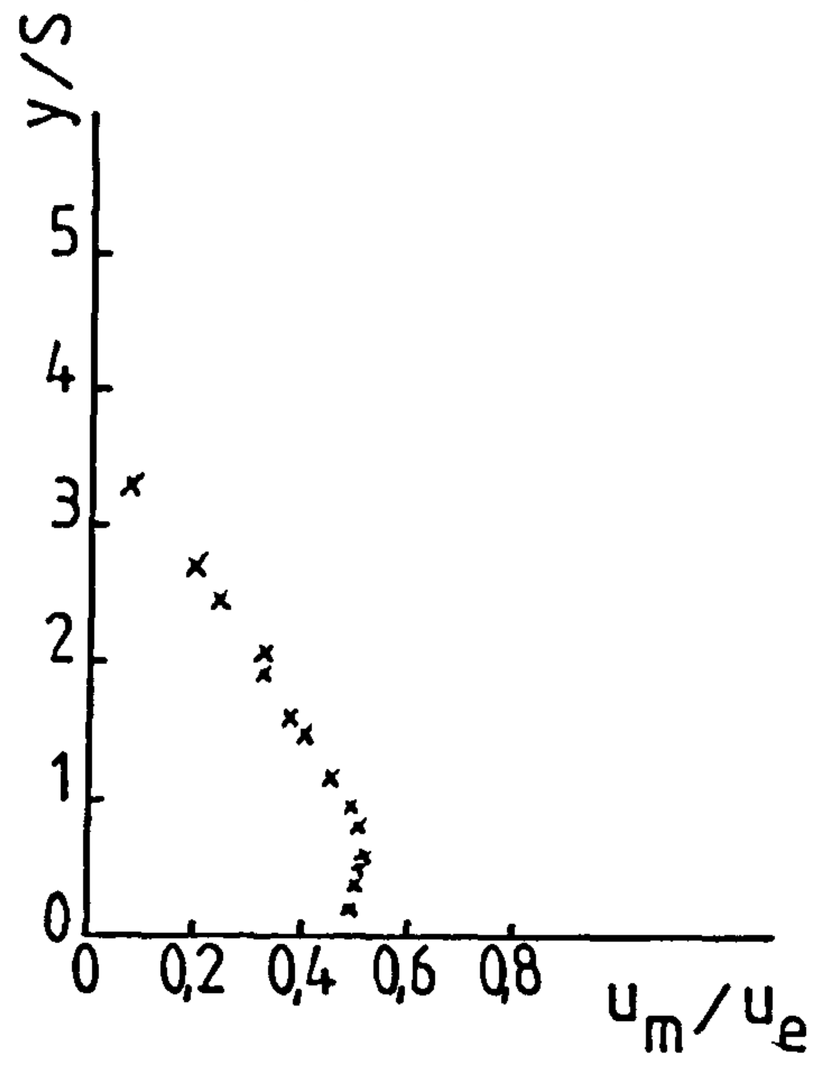

z/B=0,5

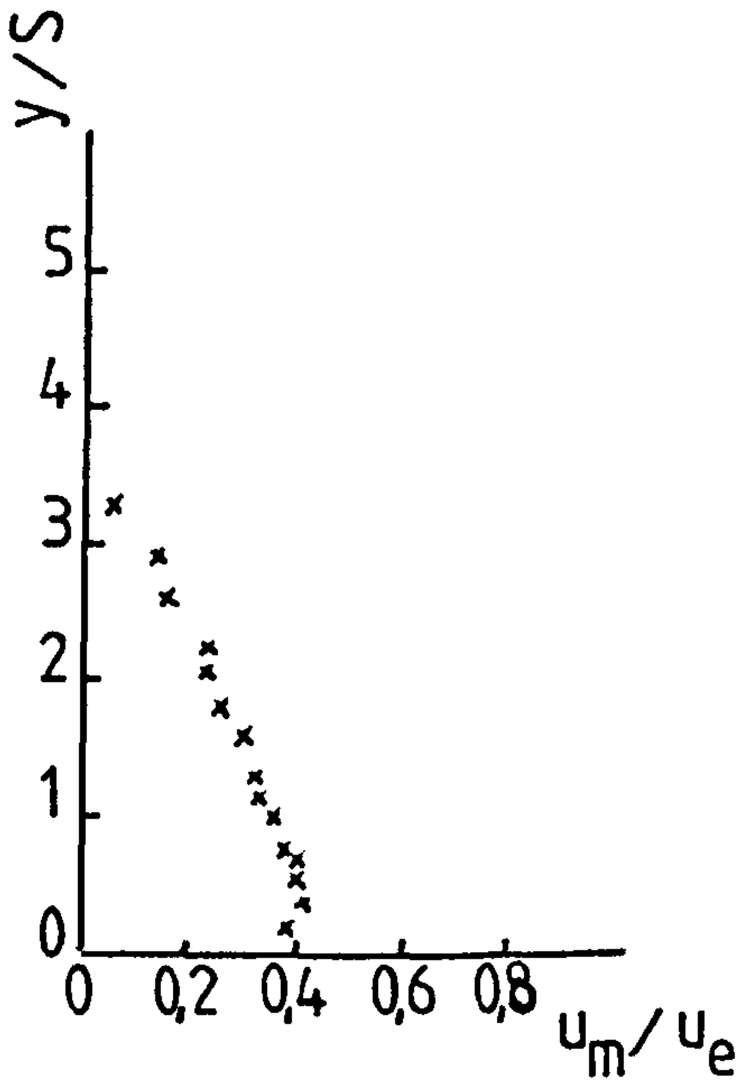

z/B=0,75

Figure D-3 Three-Dimensional jet velocity profiles

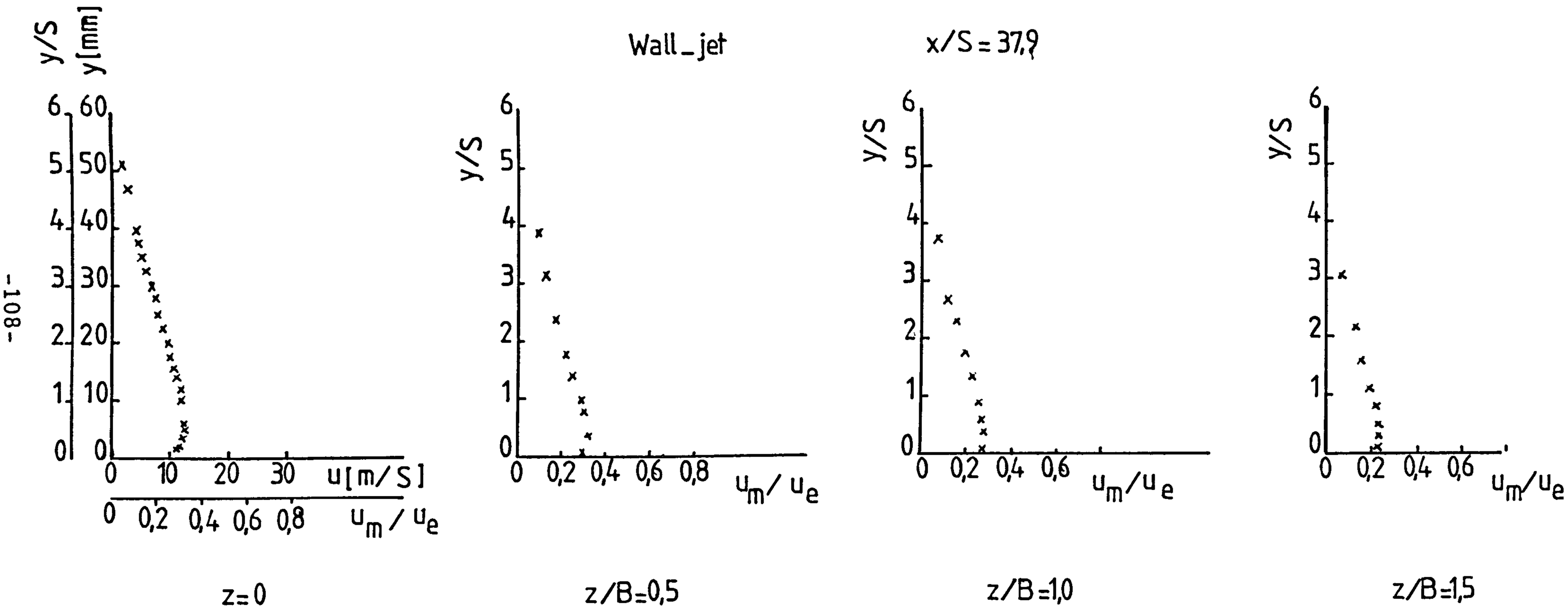

Figure D-4 Three-Dimensional jet velocity profiles

OH = 0,7

z = 0

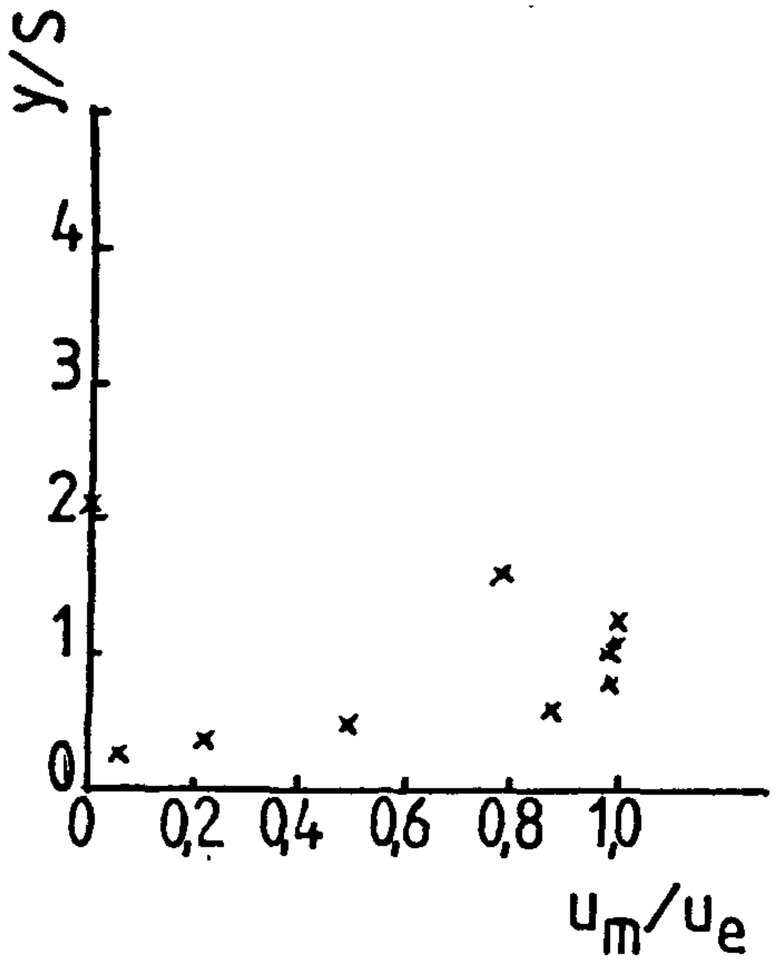

x/S=1,4

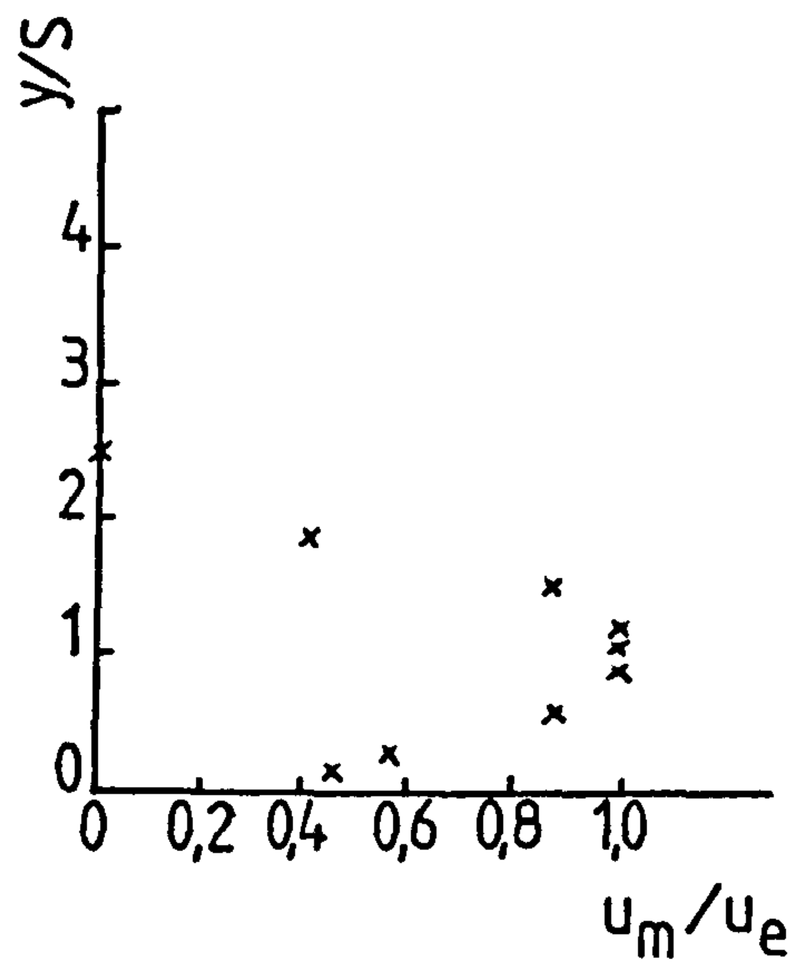

x/S=3,4

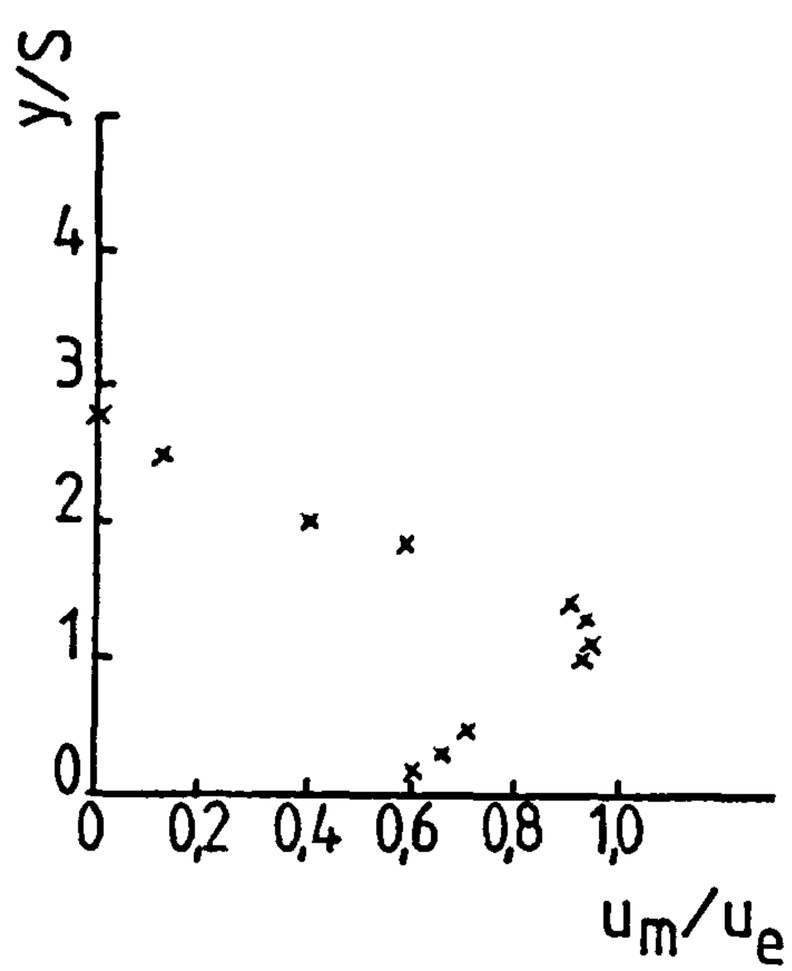

x/S=6,5

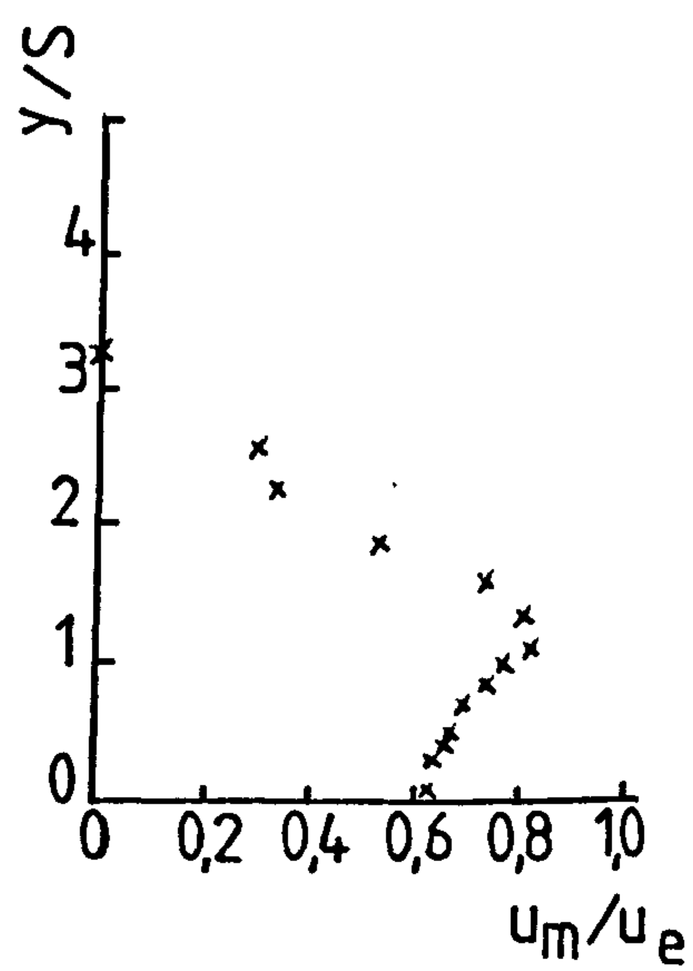

x/S=9,4

Figure D-5 Three-Dimensional jet velocity profiles

OH = 0,7

z = 0

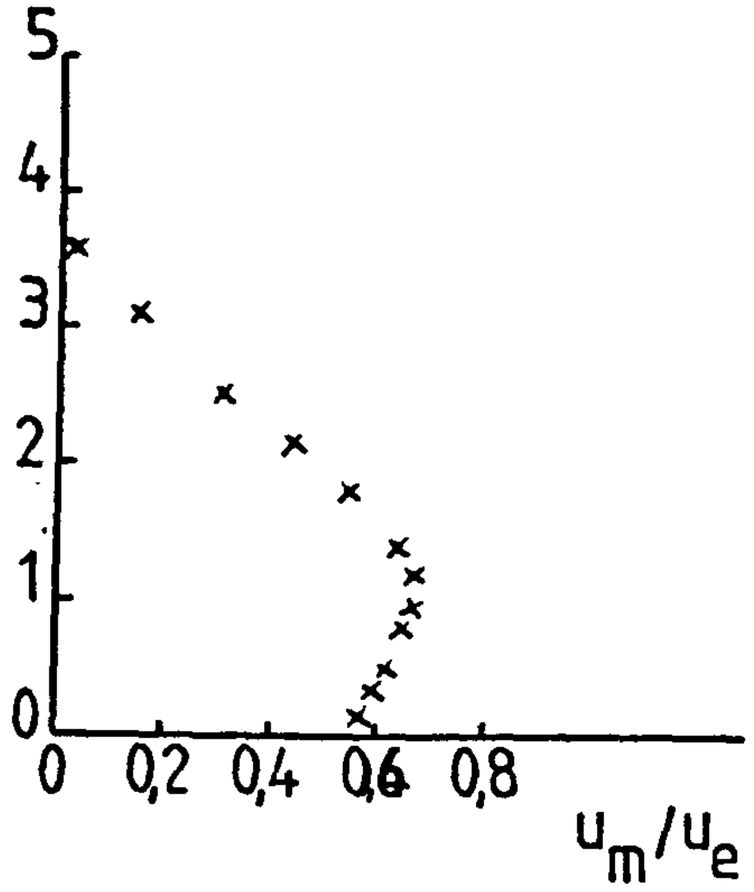

x/S = 13,4

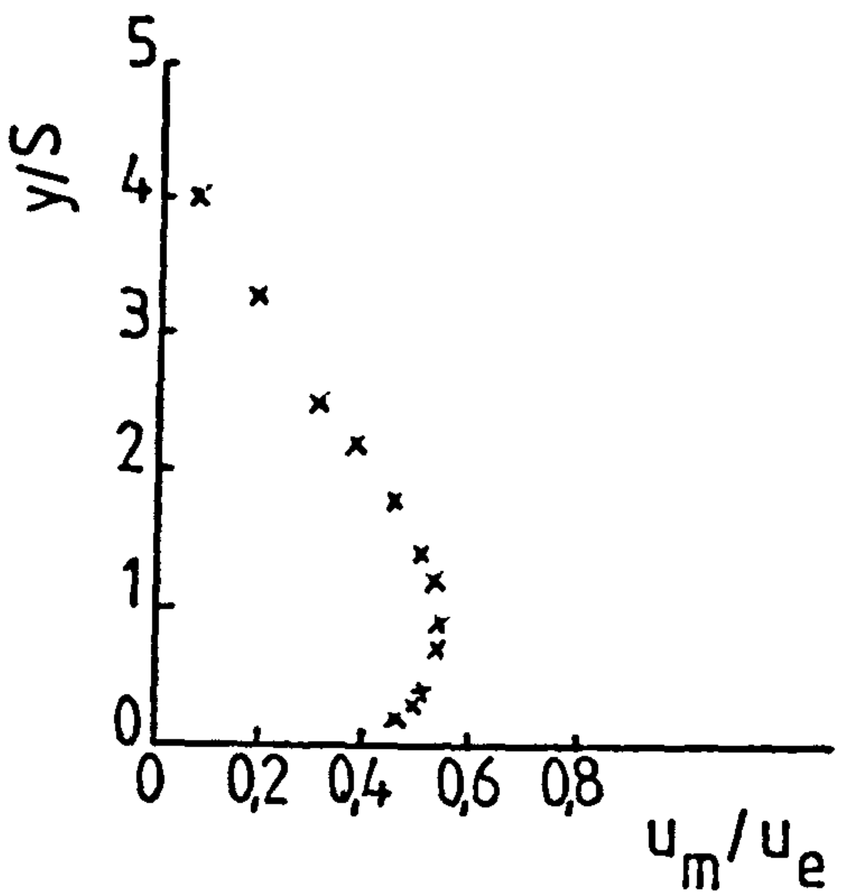

x/S = 18,9

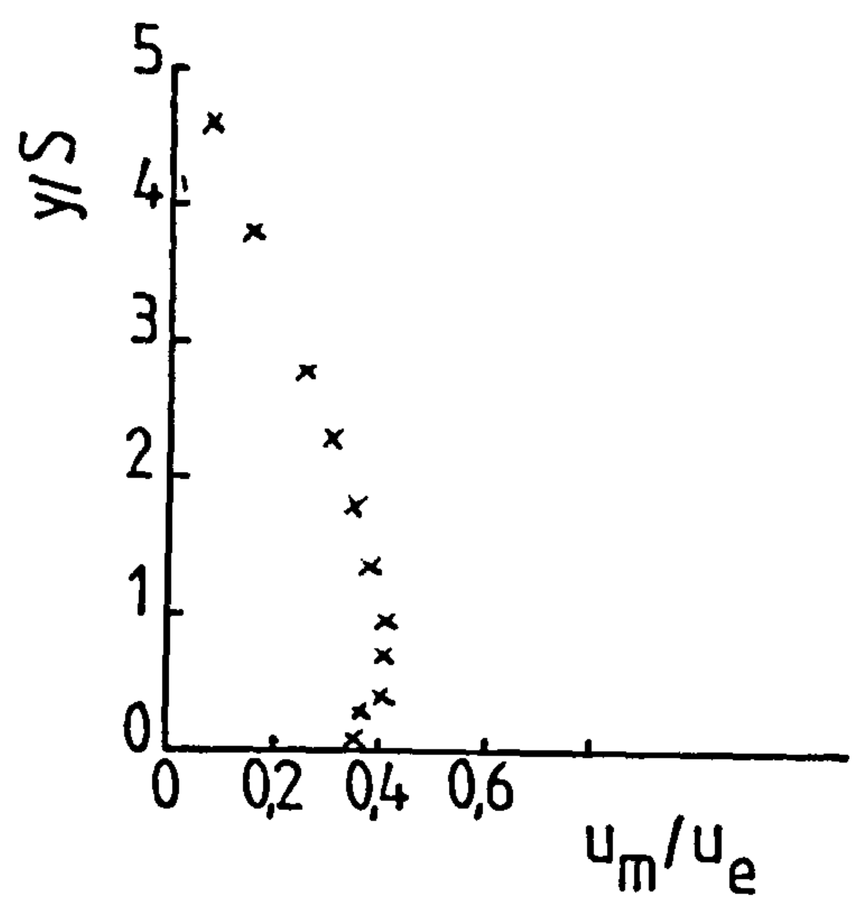

x/S = 27,1

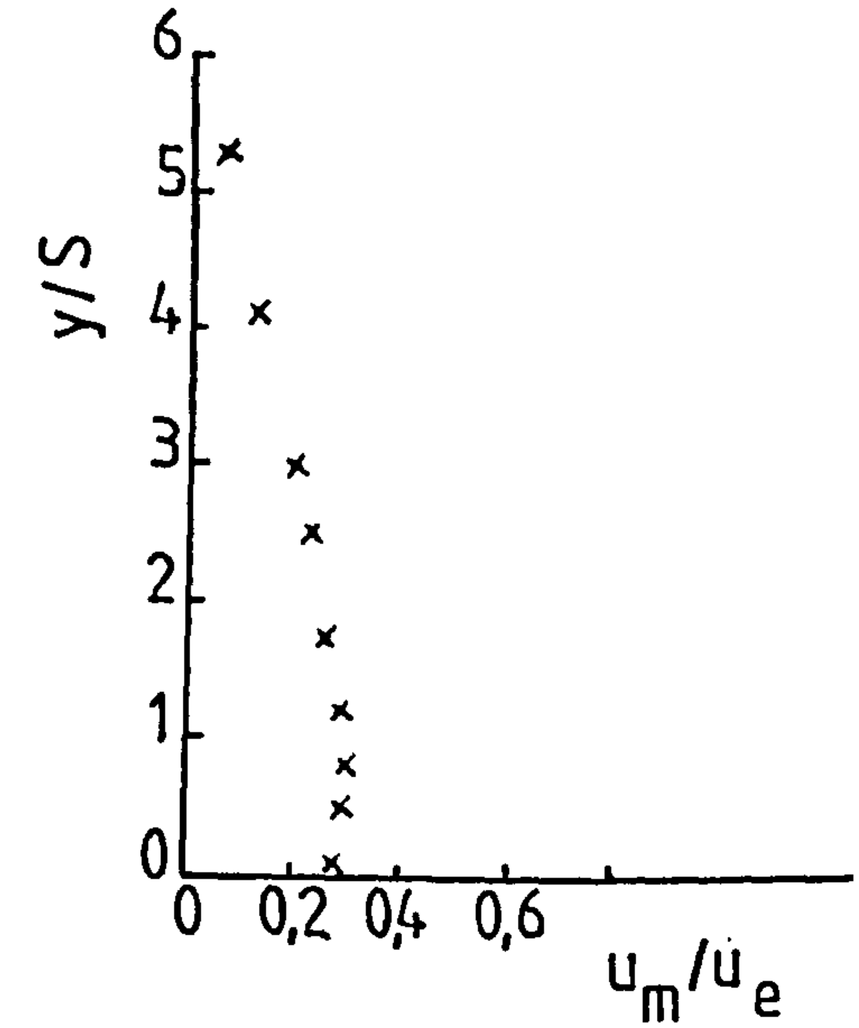

x/S = 37,9

OH=1,6

x/S=6,5

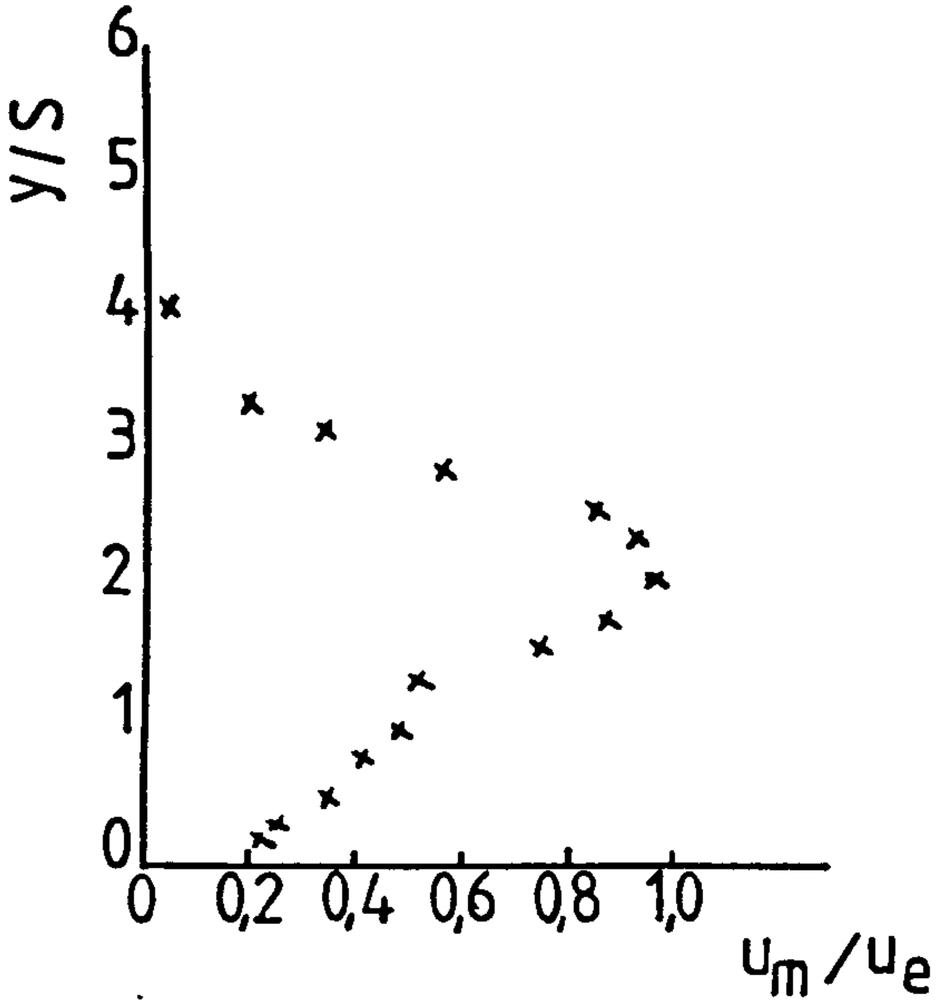

z=0

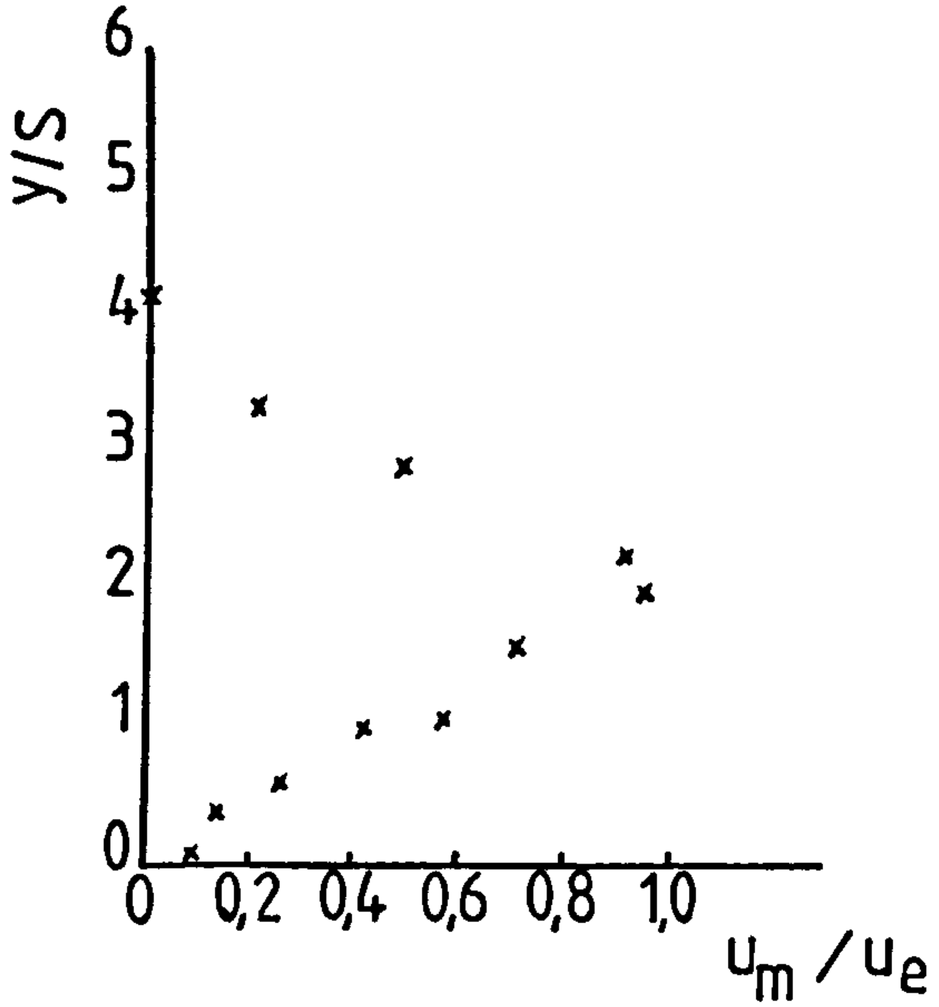

z/B=0,25

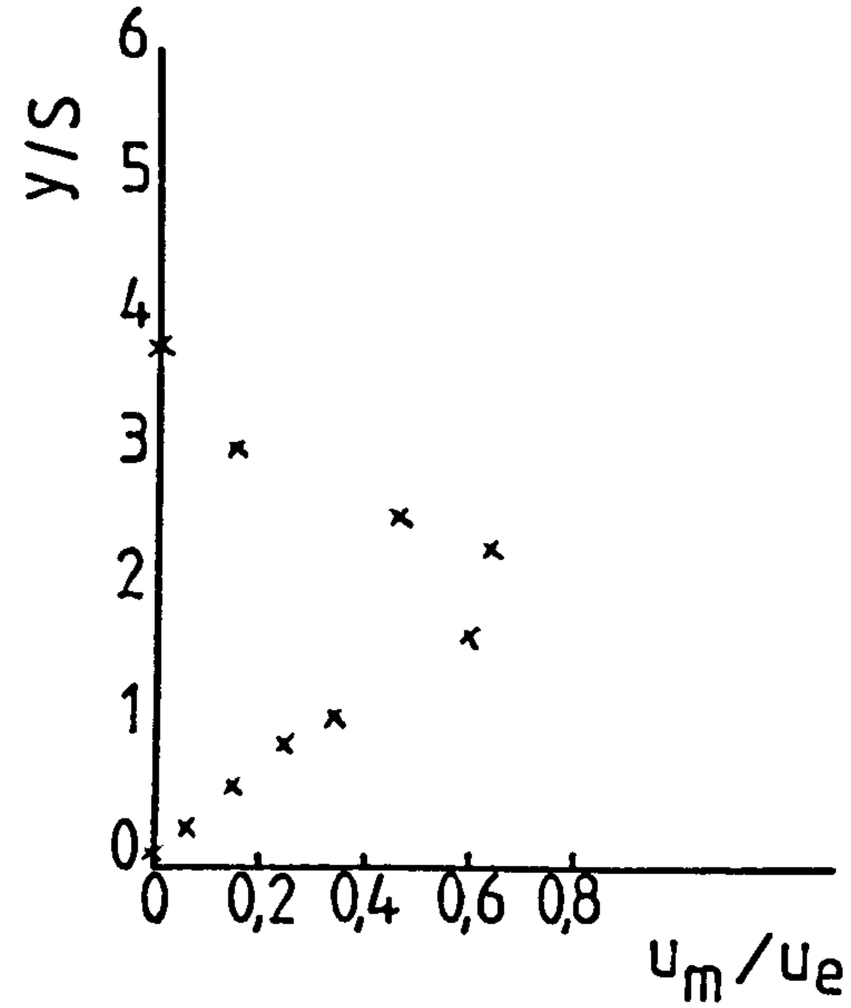

z/B=0,5

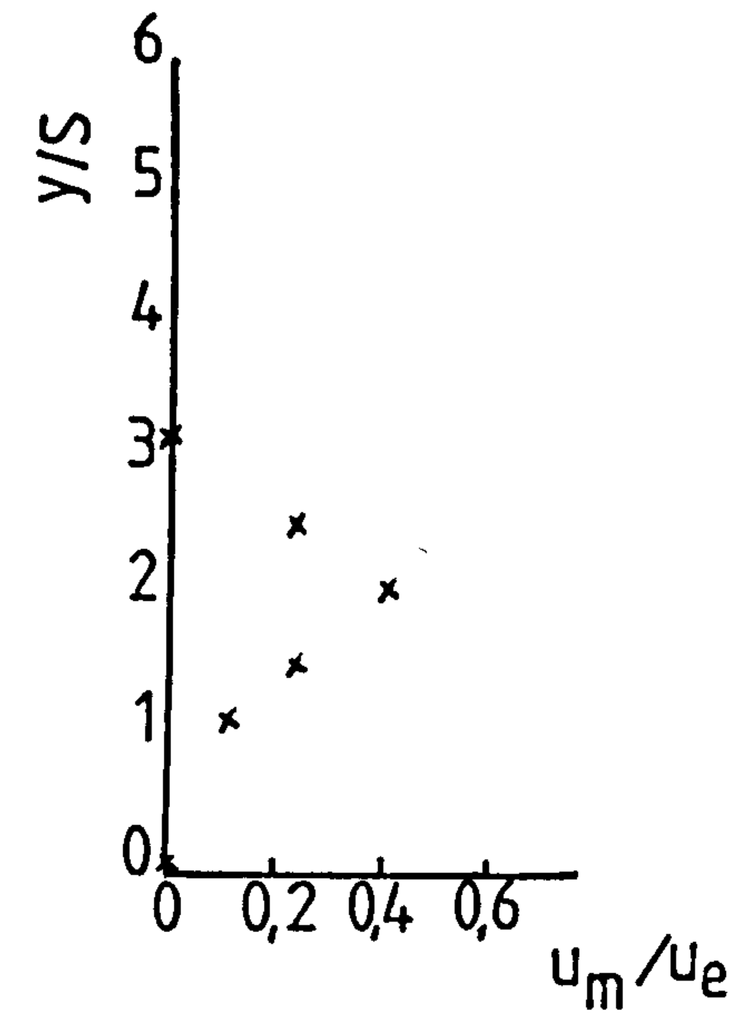

z/B=0,75

Figure D-6 Three-Dimensional jet velocity profiles

OH = 1,6

x/S = 9,4

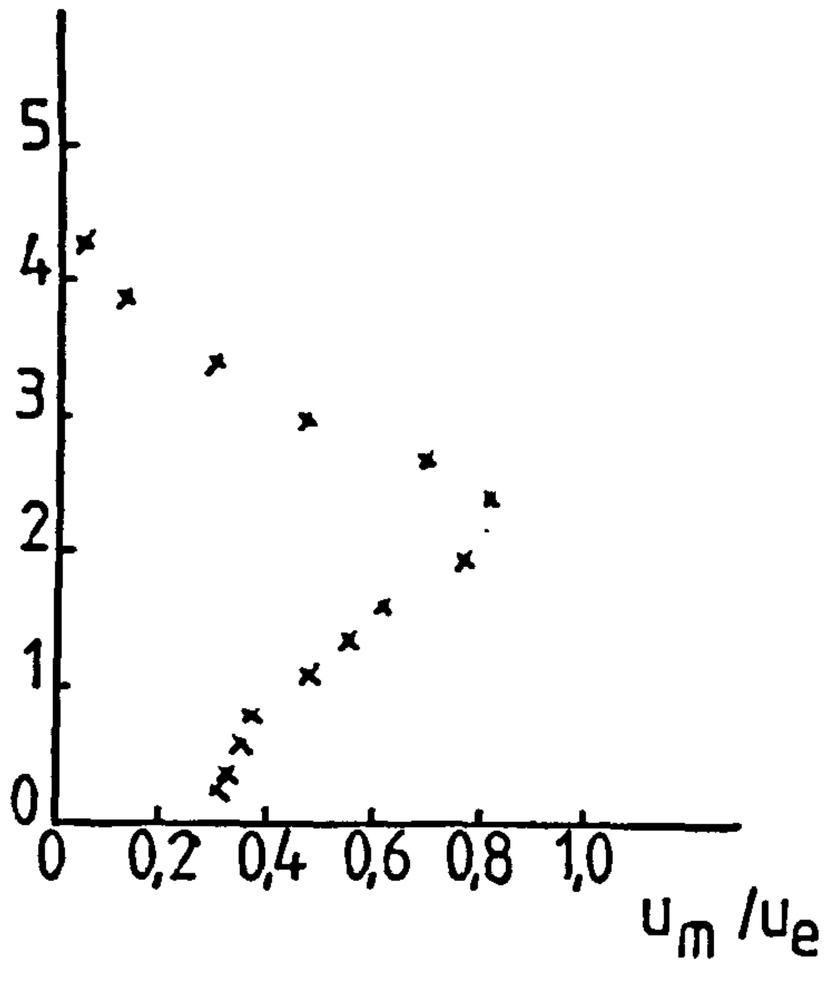

z = 0

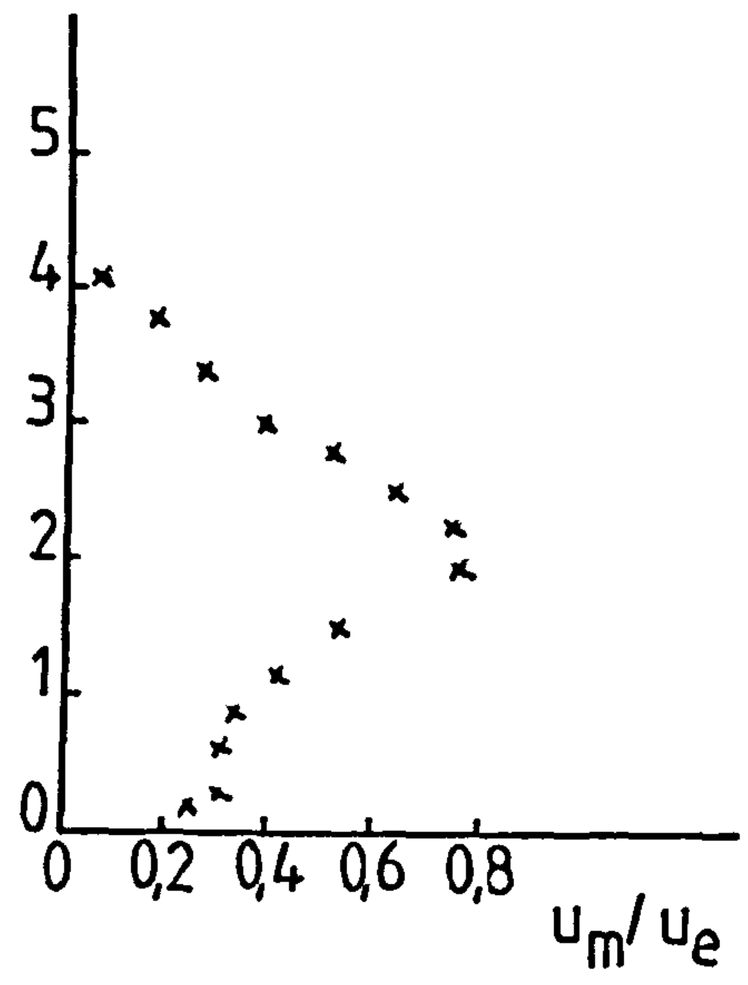

z/B = 0,25

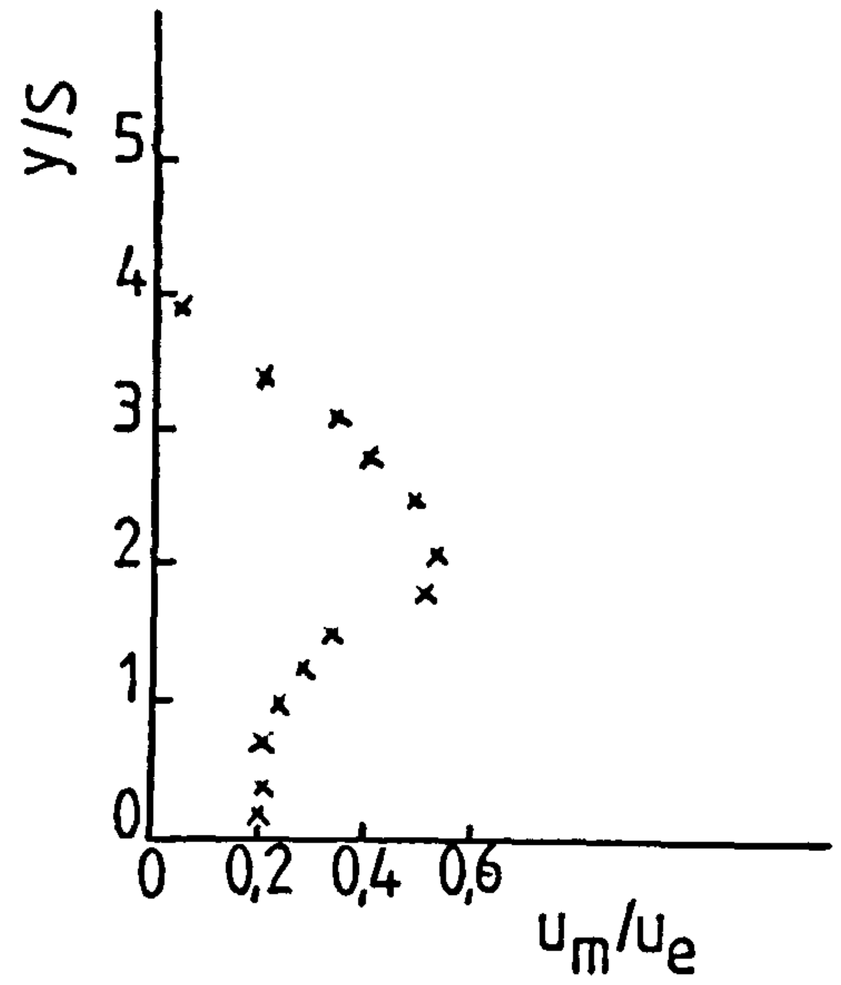

z/B = 0,5

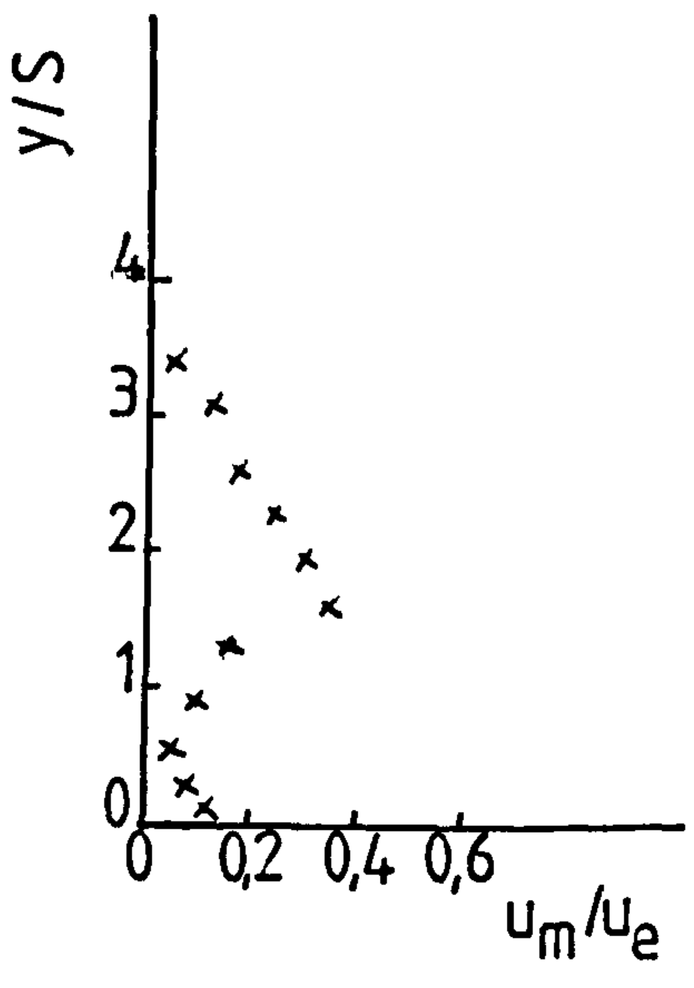

z/B = 0,75

Figure D-7 Three-Dimensional jet velocity profiles

OH=1,6

x / S = 13,4

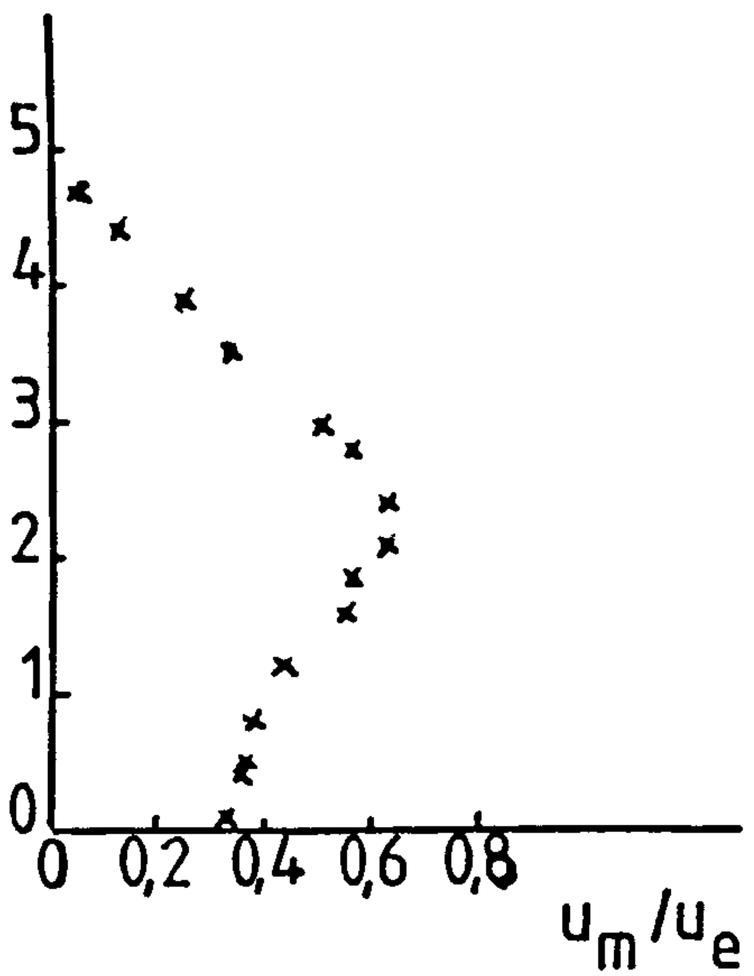

z=0

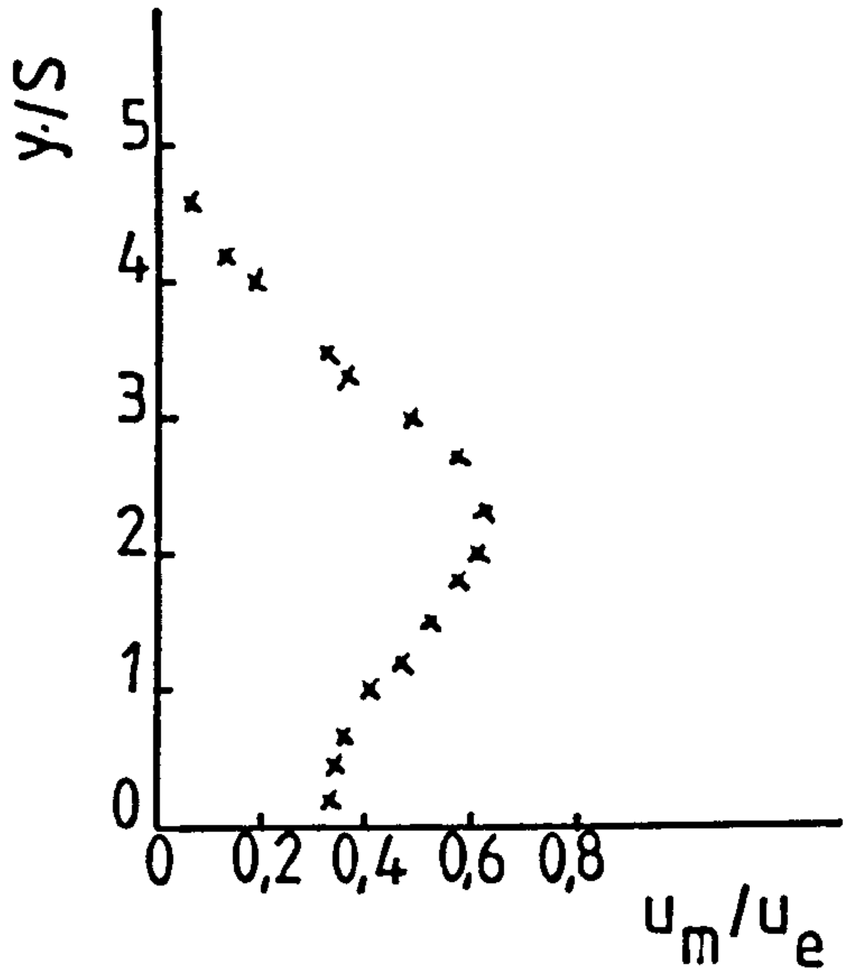

z/B = 0,25

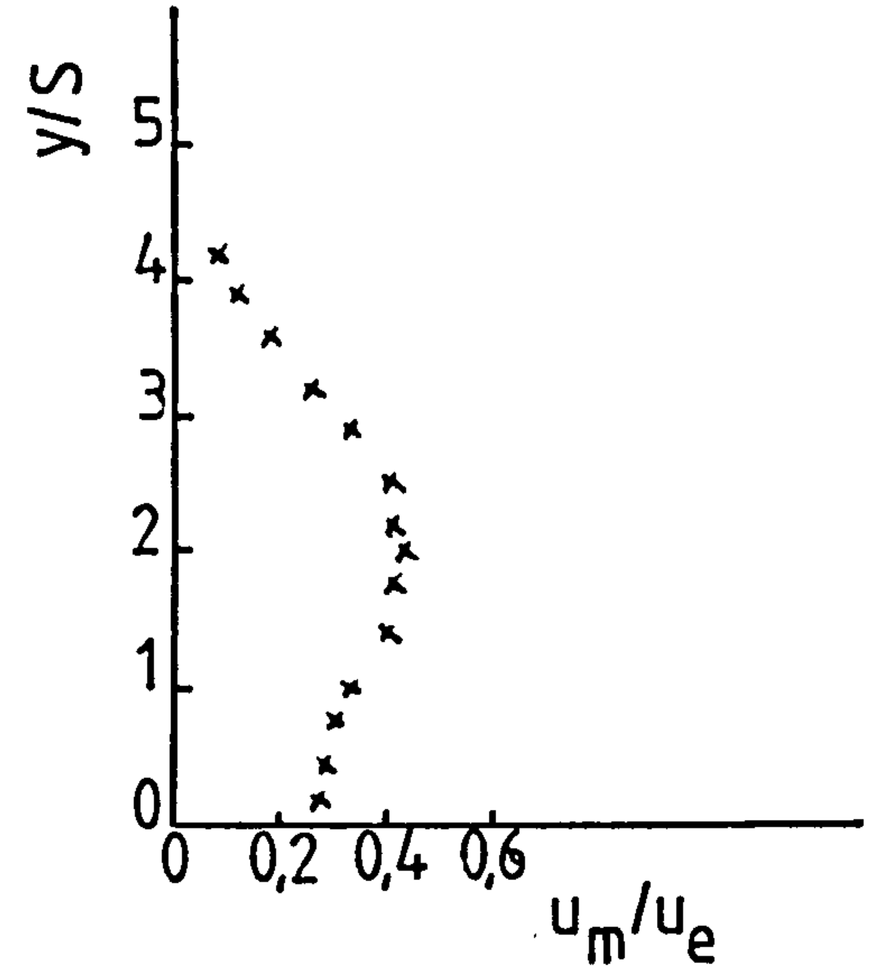

z/B = 0,5

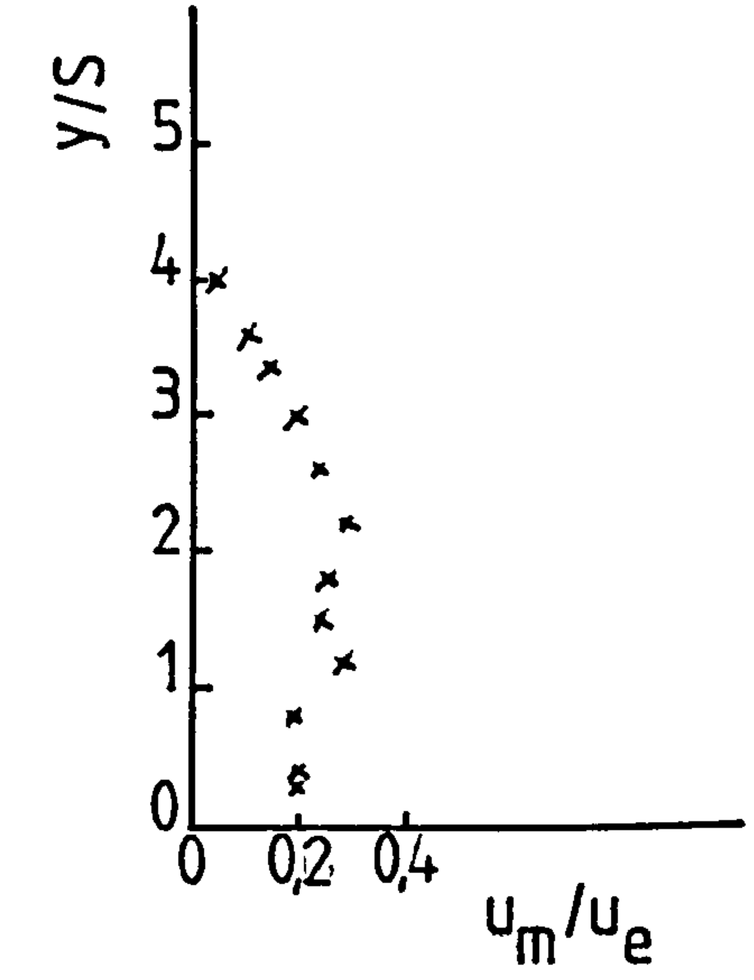

z/B = 0,75

Figure D-8 Three-Dimensional jet velocity profiles

OH = 1,6

x/S = 189

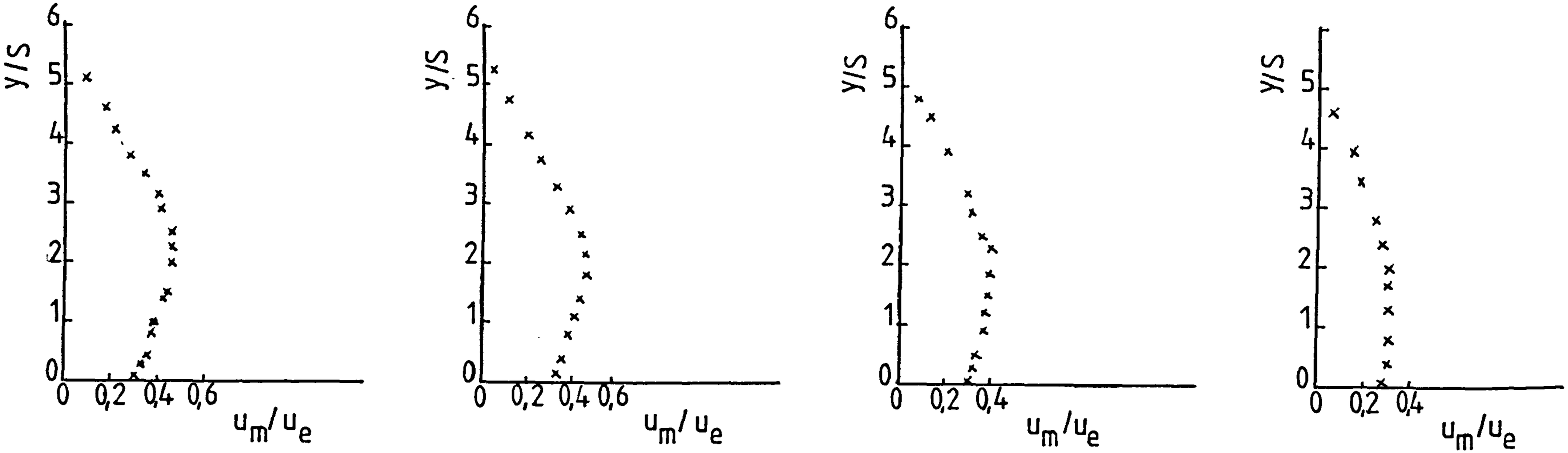

z = 0 | z/B = 0,25 | z/B = 0,5 | z/B = 0,75

Figure D-9 Three-Dimensional jet velocity profiles

OH = 1,6

x/S = 37,9

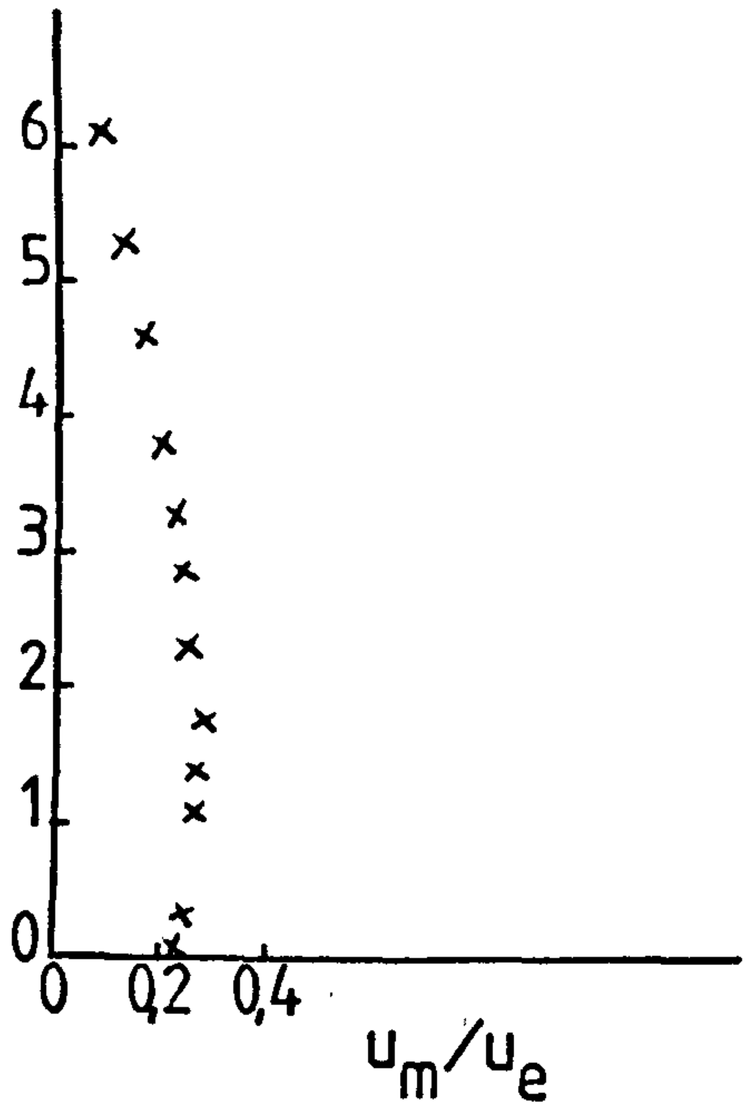

z = 0

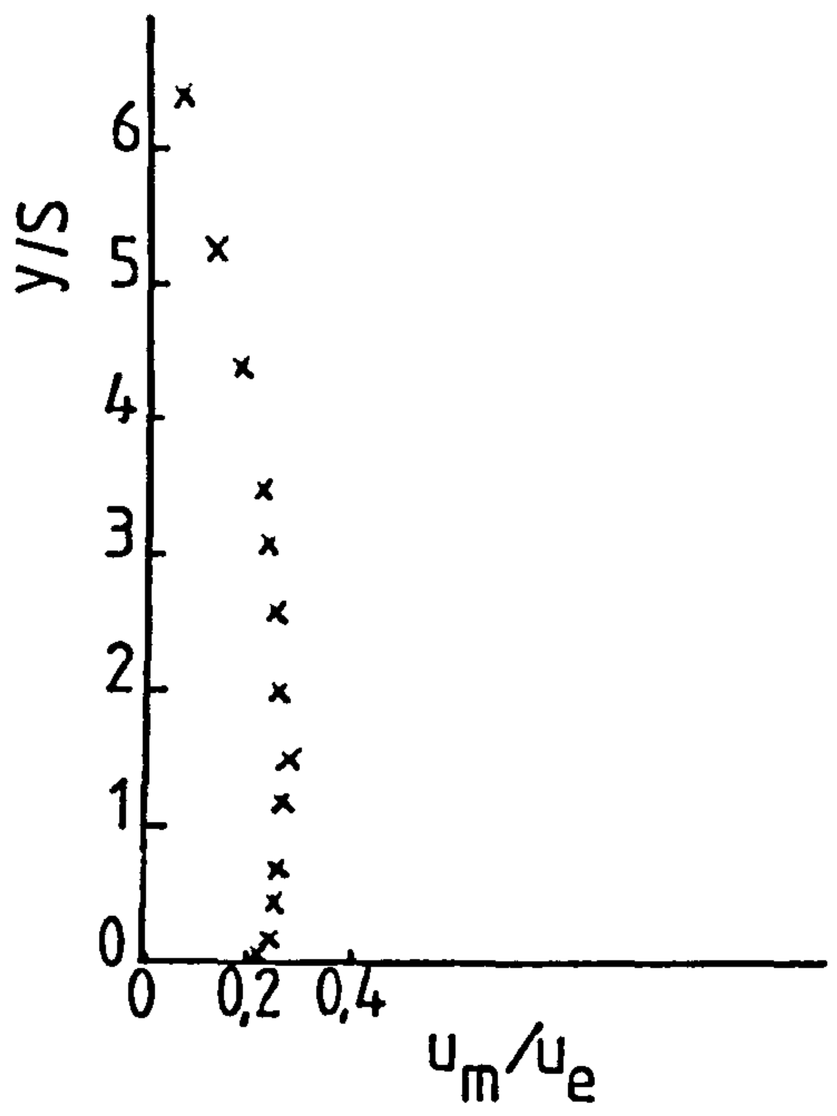

z/B = 0,25

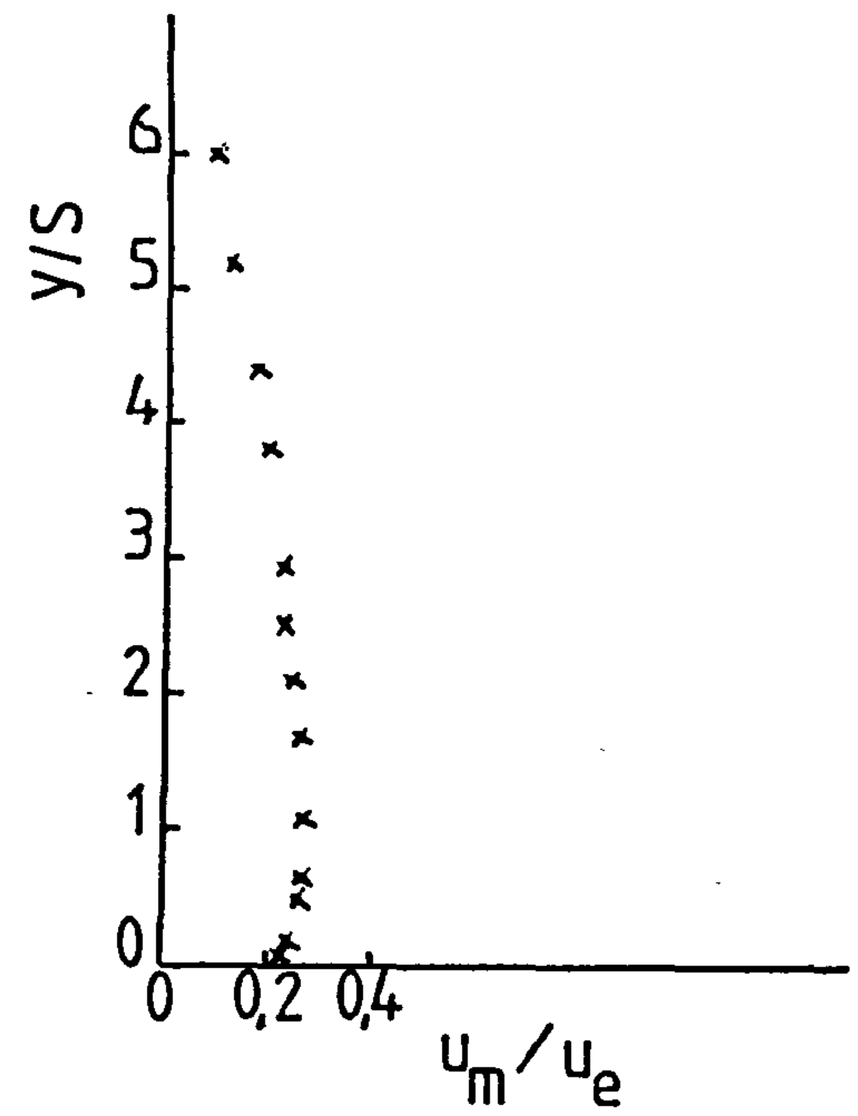

z/B = 0,5

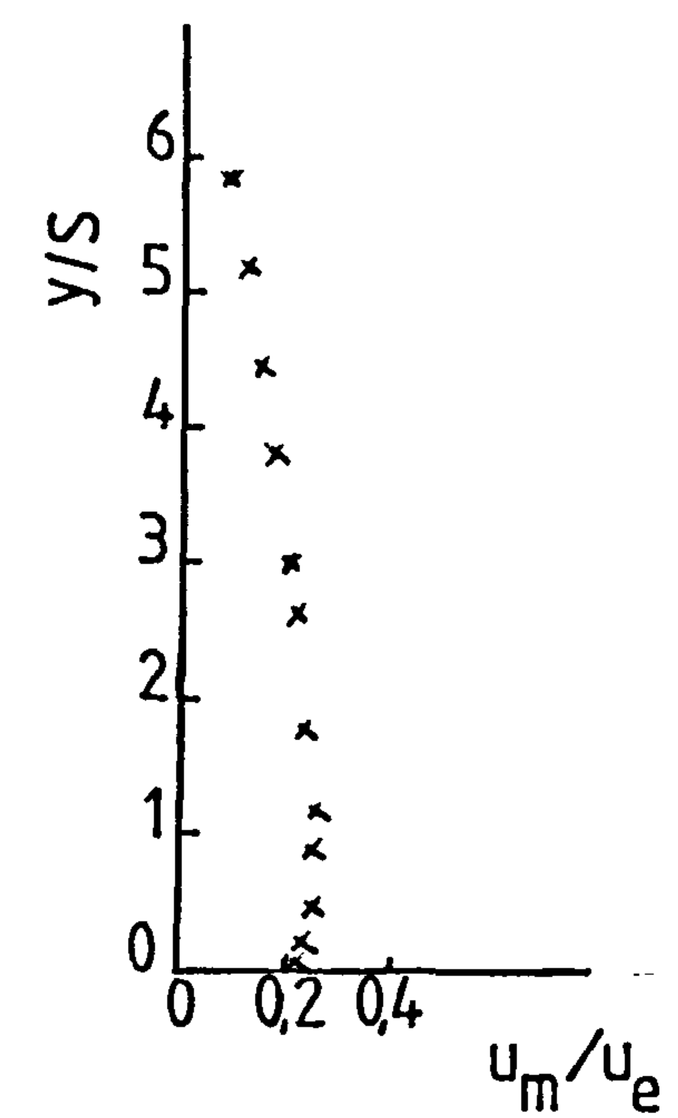

z/B = 0,75

Figure D-10 Three-Dimensional jet velocity profiles

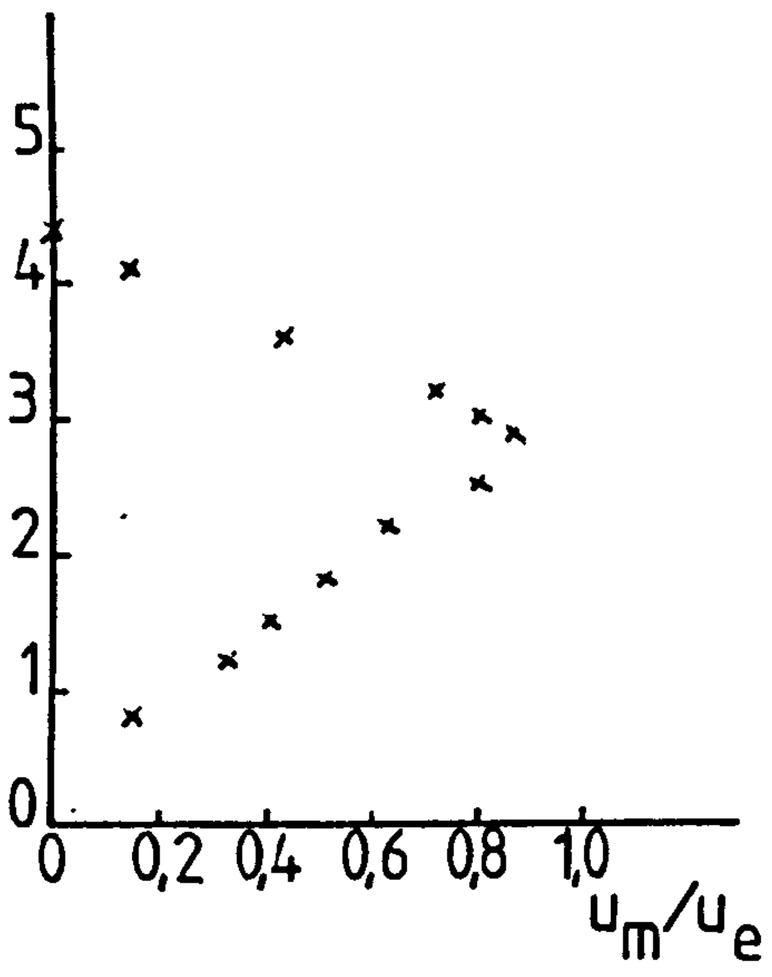

x/S=6,5

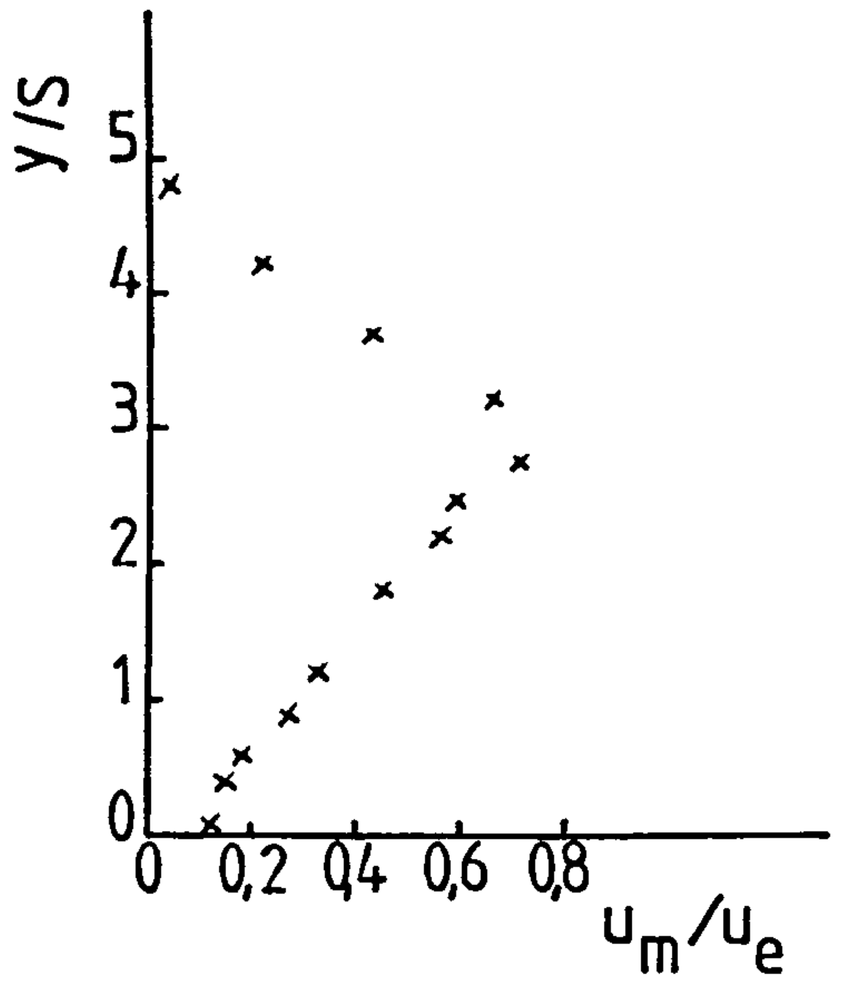

x/S=9,4

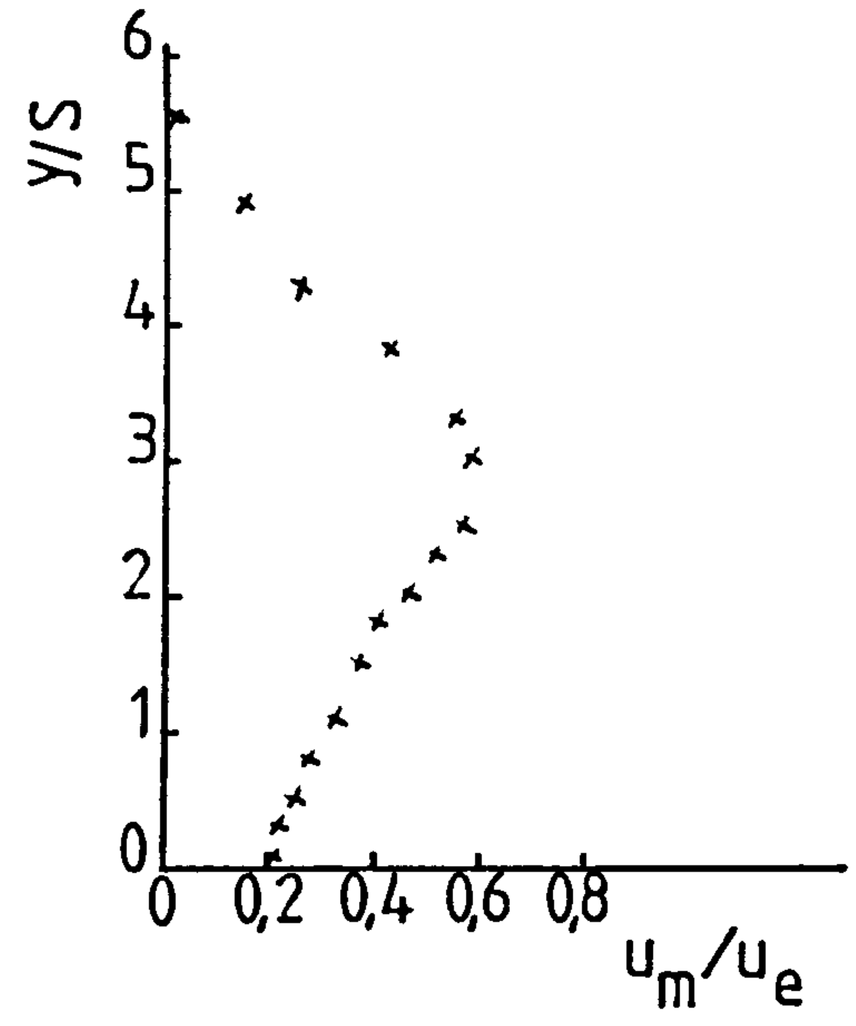

x/S=13,4

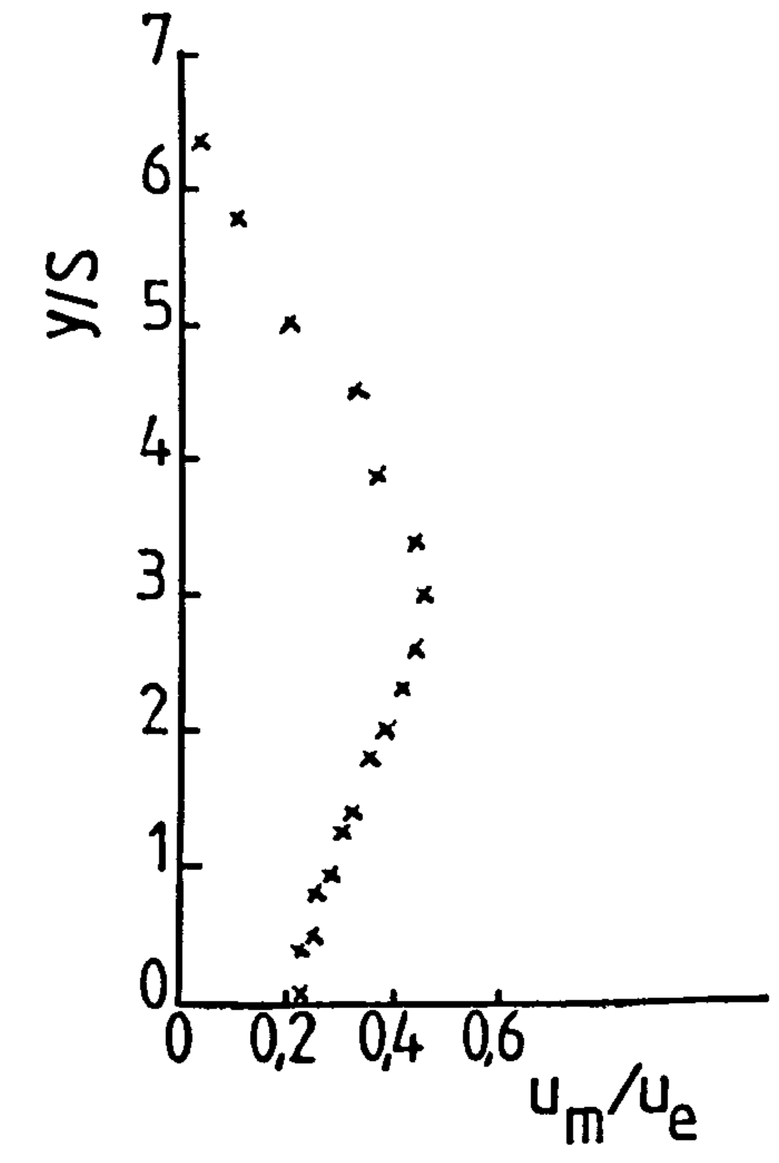

x/S=18,9

Figure D-11 Three-Dimensional jet velocity profiles

OH=2,2 z=0

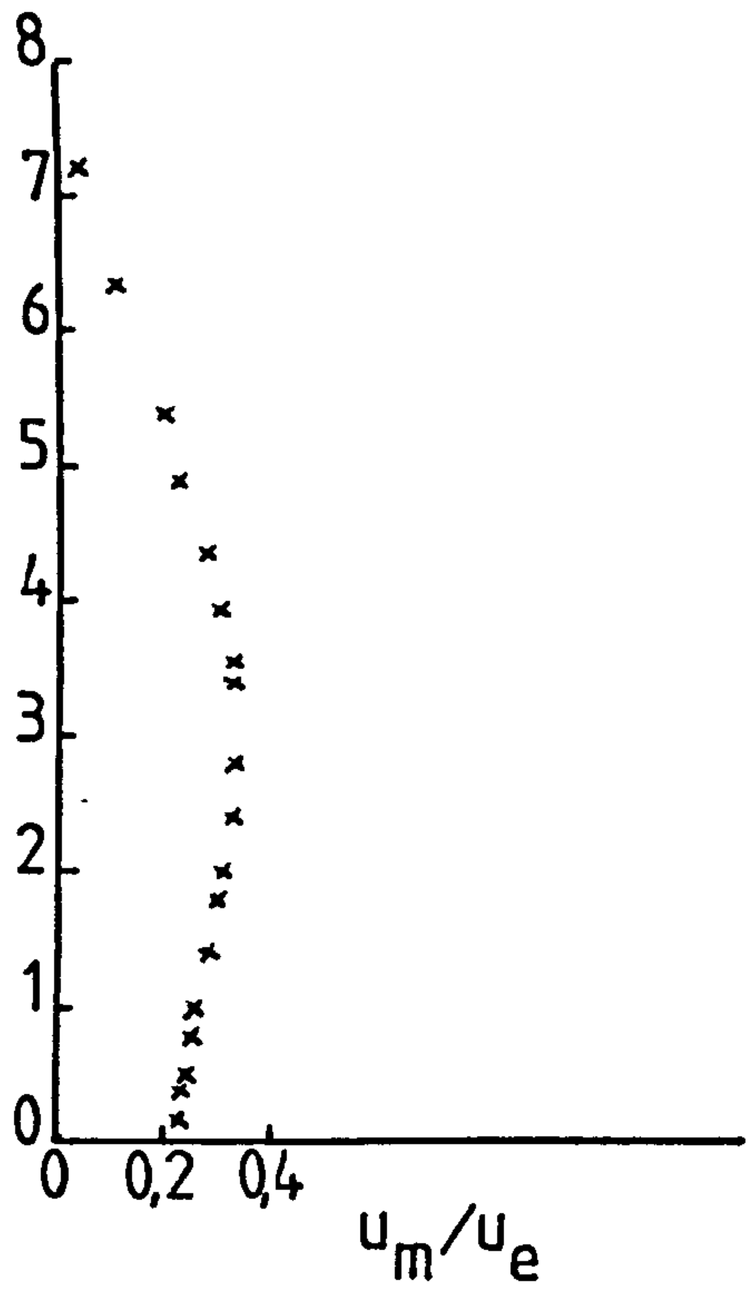

x/S=27,1

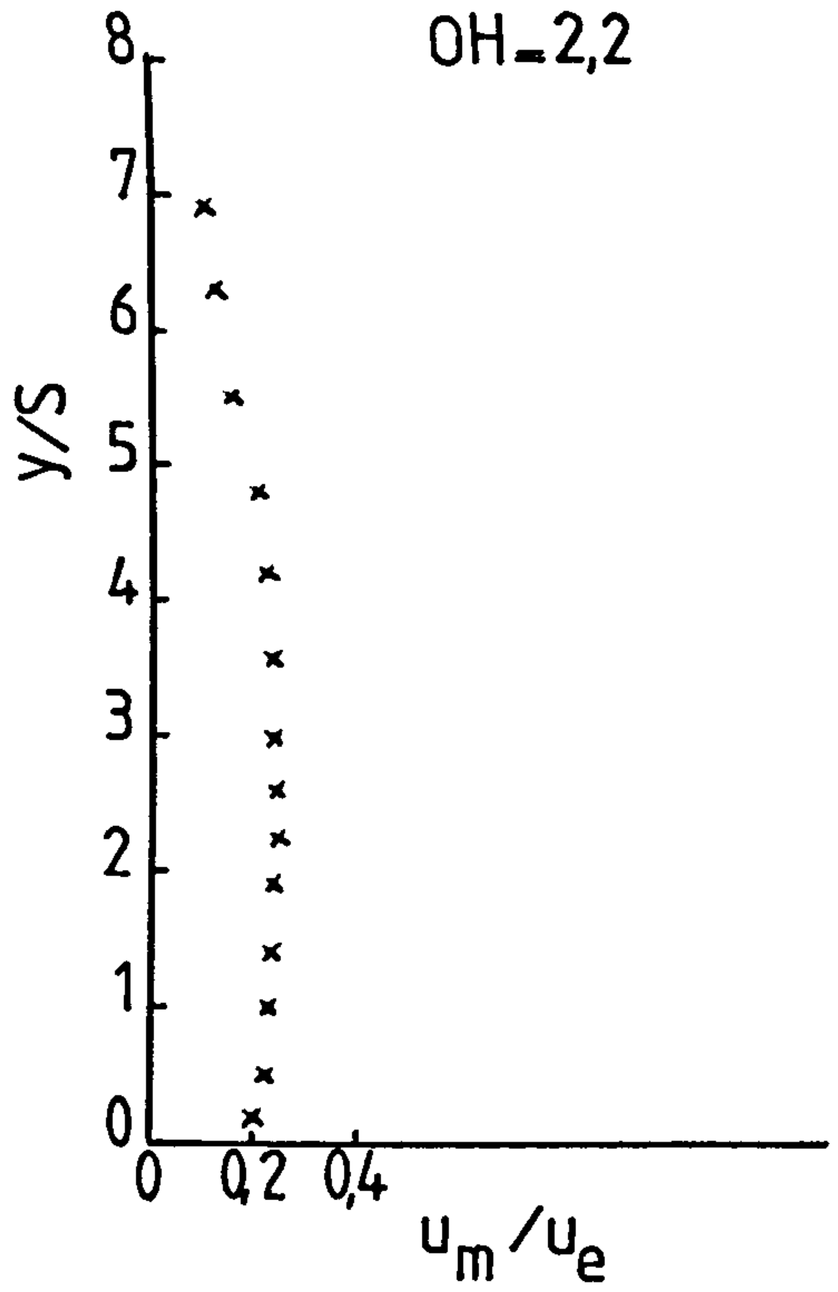

x/S=37,9

OH = 3,1

z = 0

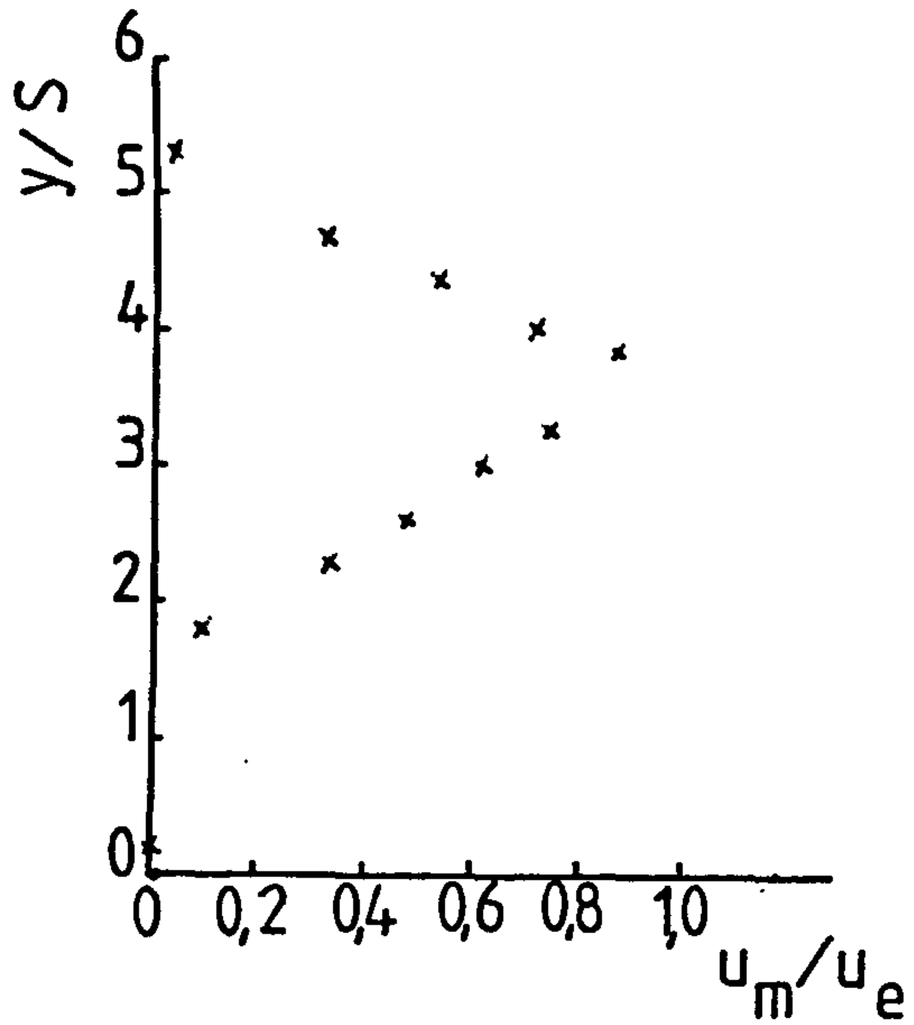

x/S = 6,5

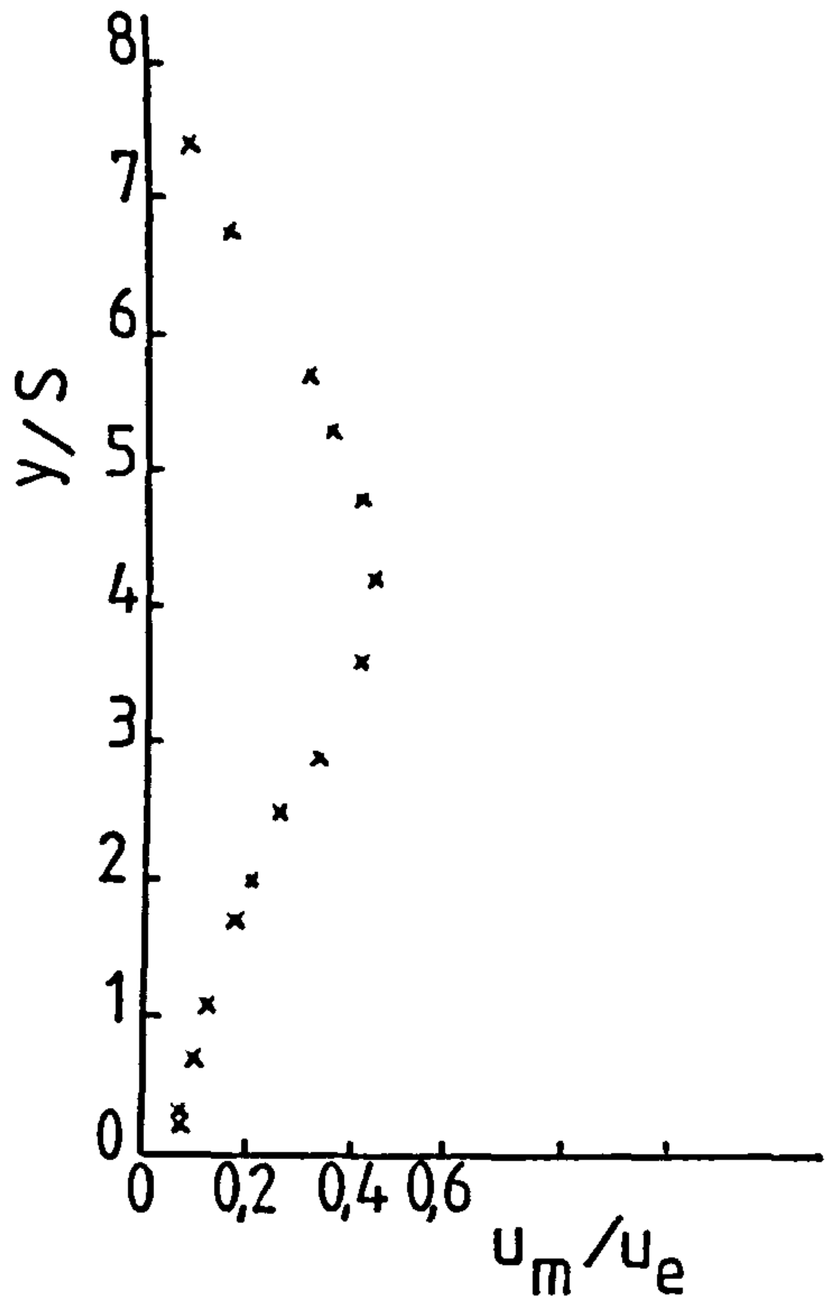

x/S = 18,9

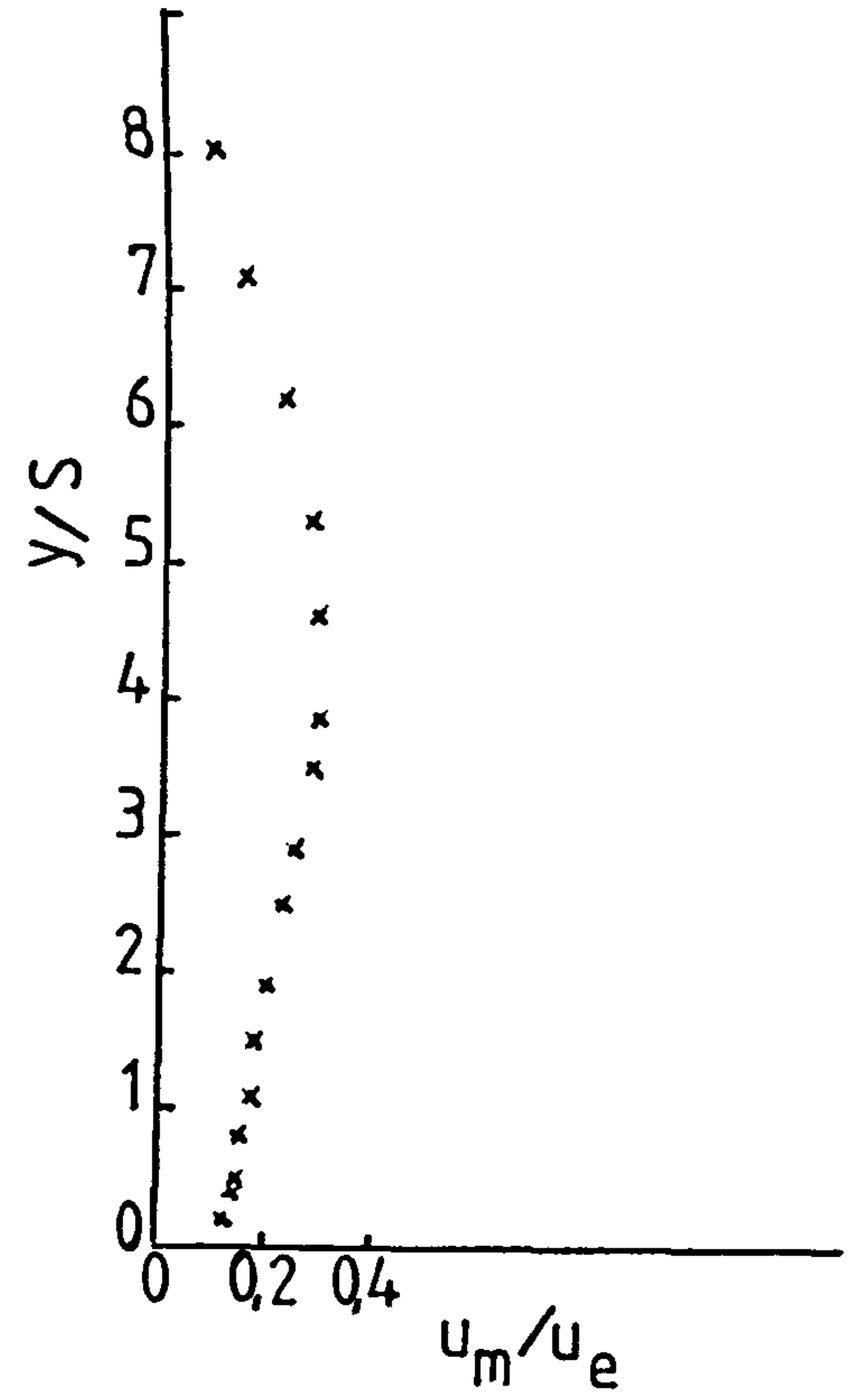

x/S = 27,1

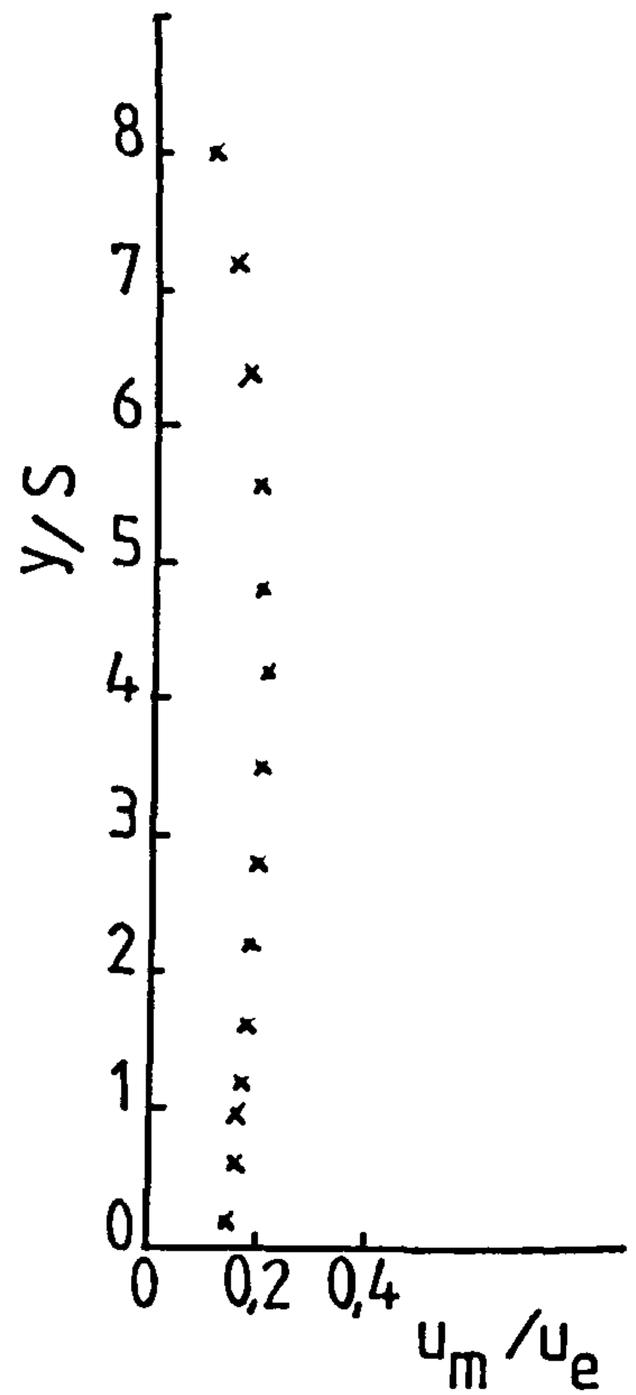

x/S = 37,9

Figure D-12 Three-Dimensional jet velocity profiles

OH = 3,8

x / S = 6,5

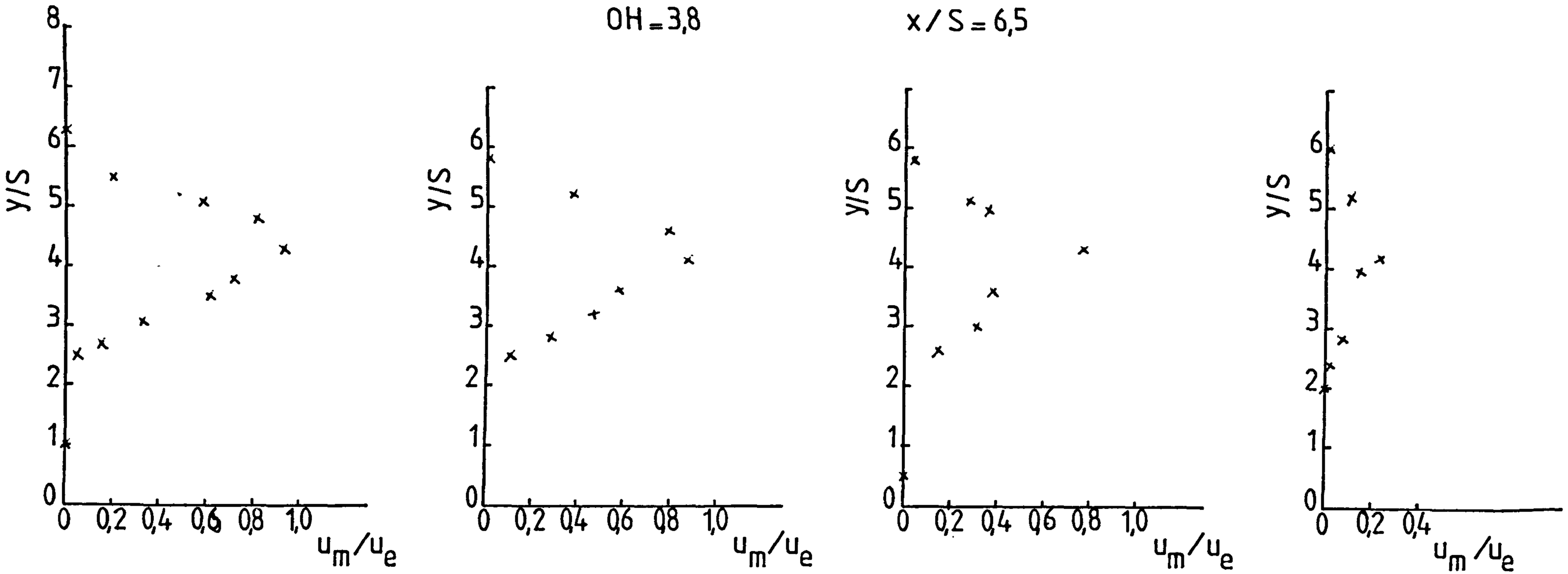

Figure D-13 Three-Dimensional jet velocity profiles

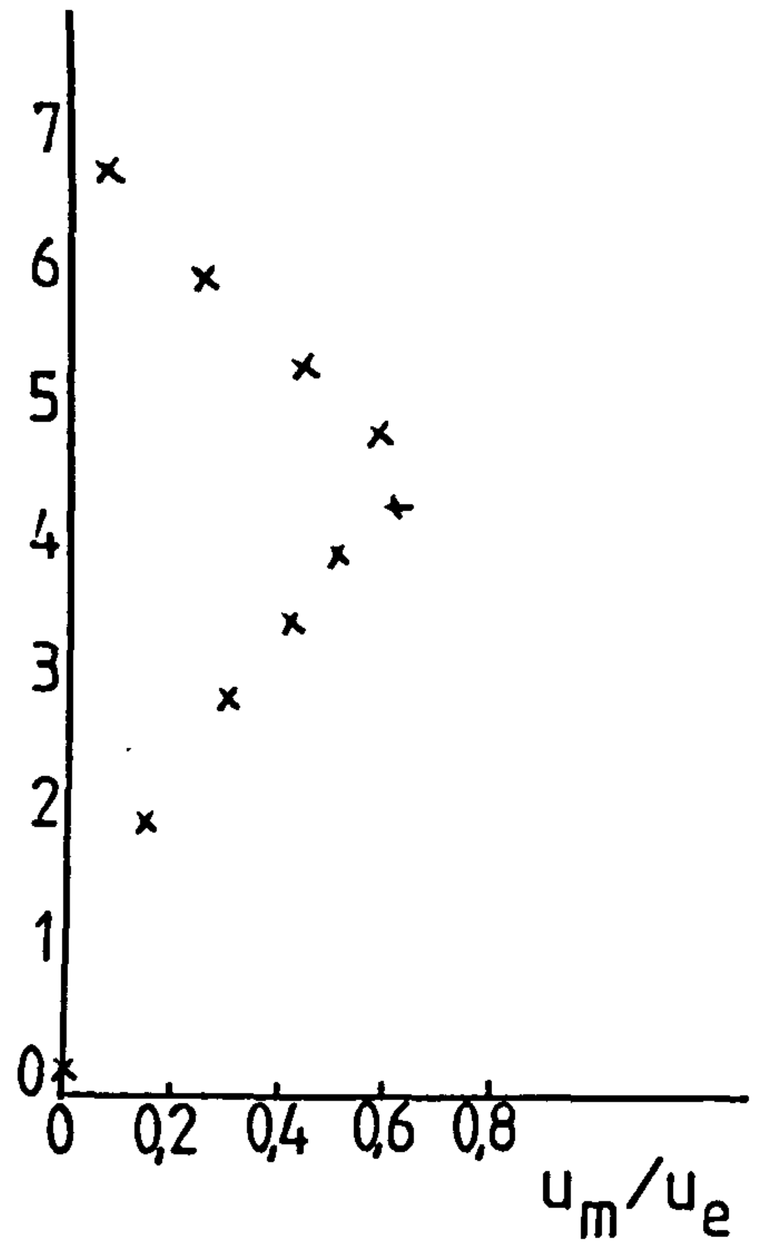

z = 0

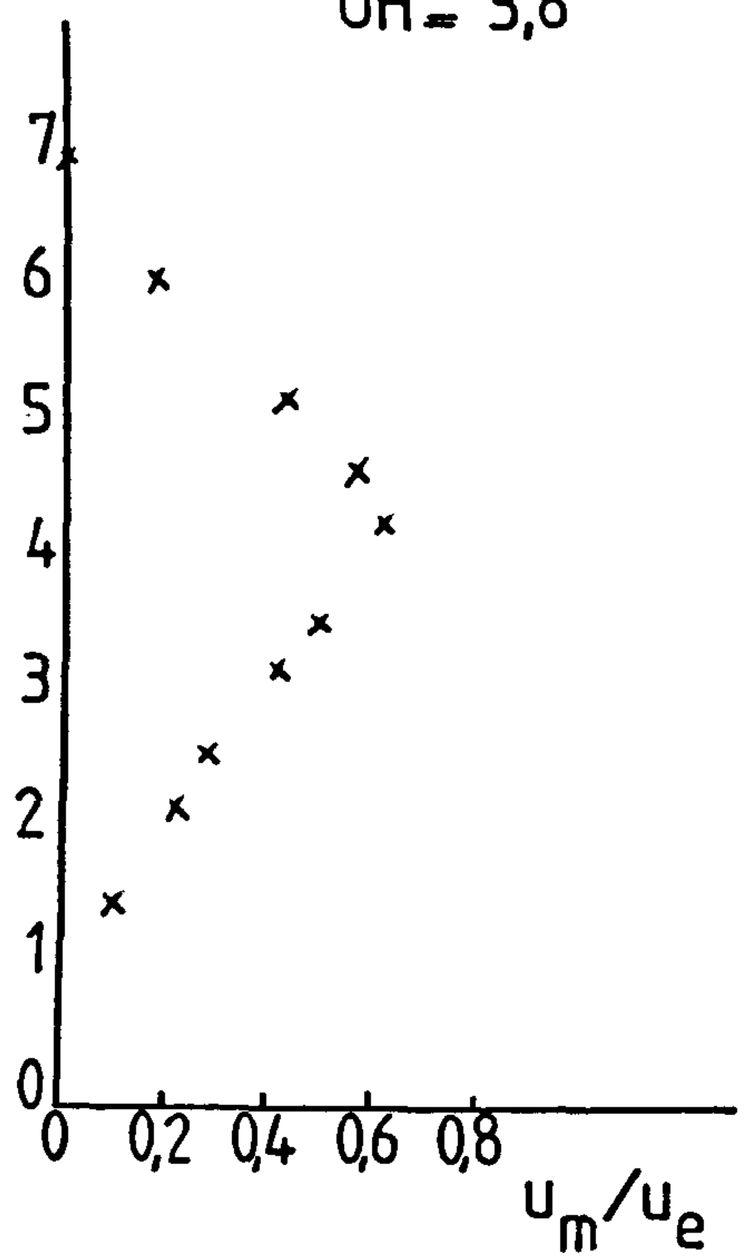

z /B = 0,25

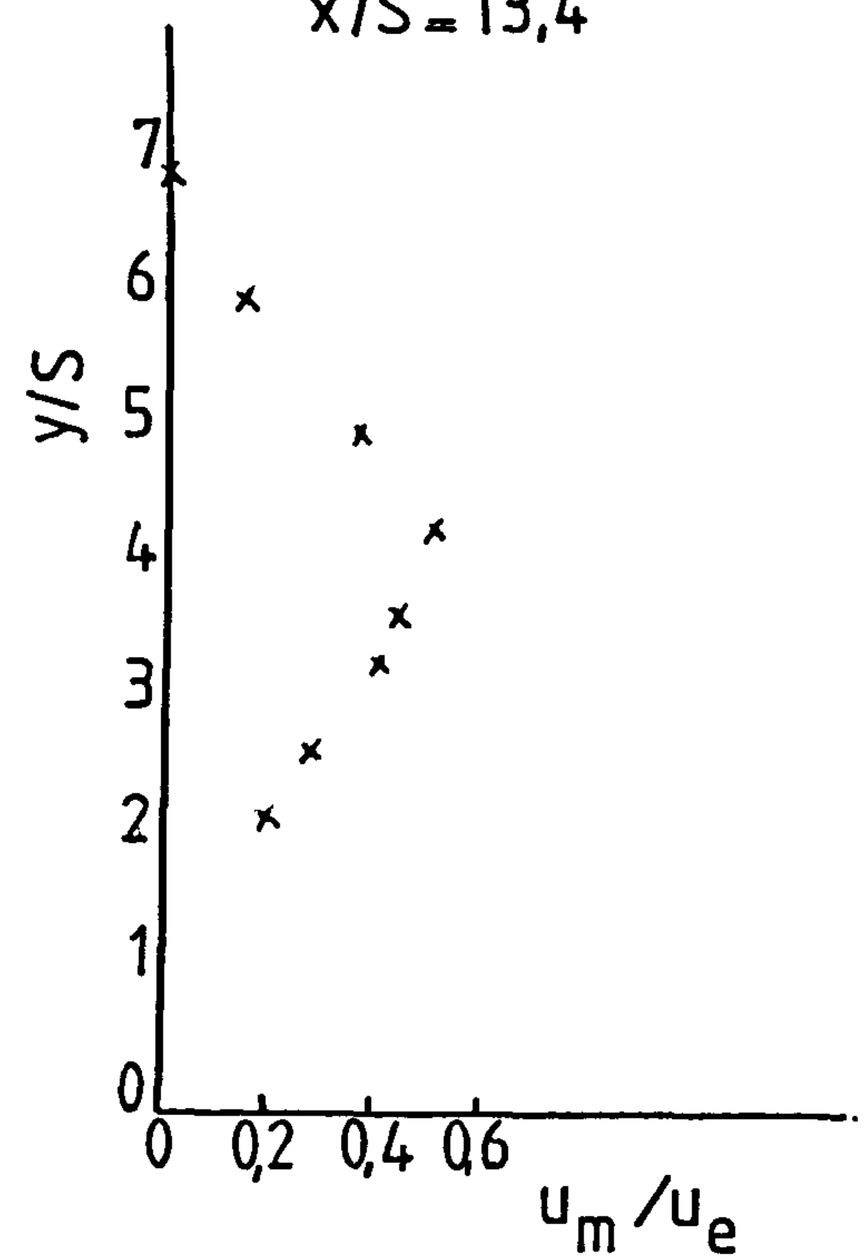

z /B = 0,5

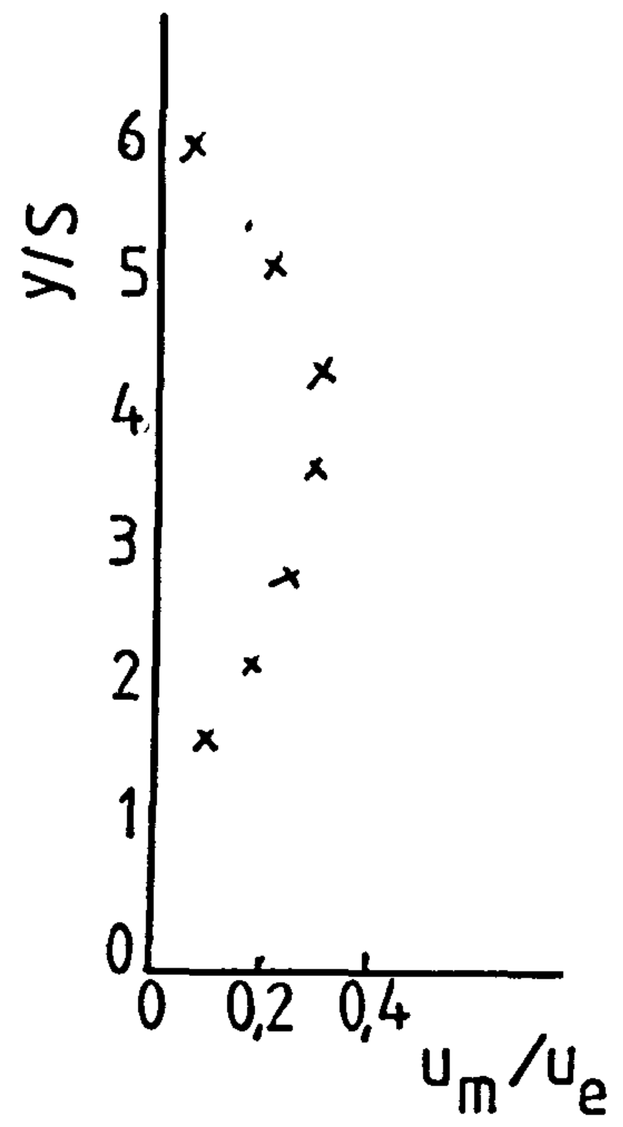

z /B = 0,75

Figure D-14 Three-Dimensional jet velocity profiles

OH = 3,8

x / S = 27,1

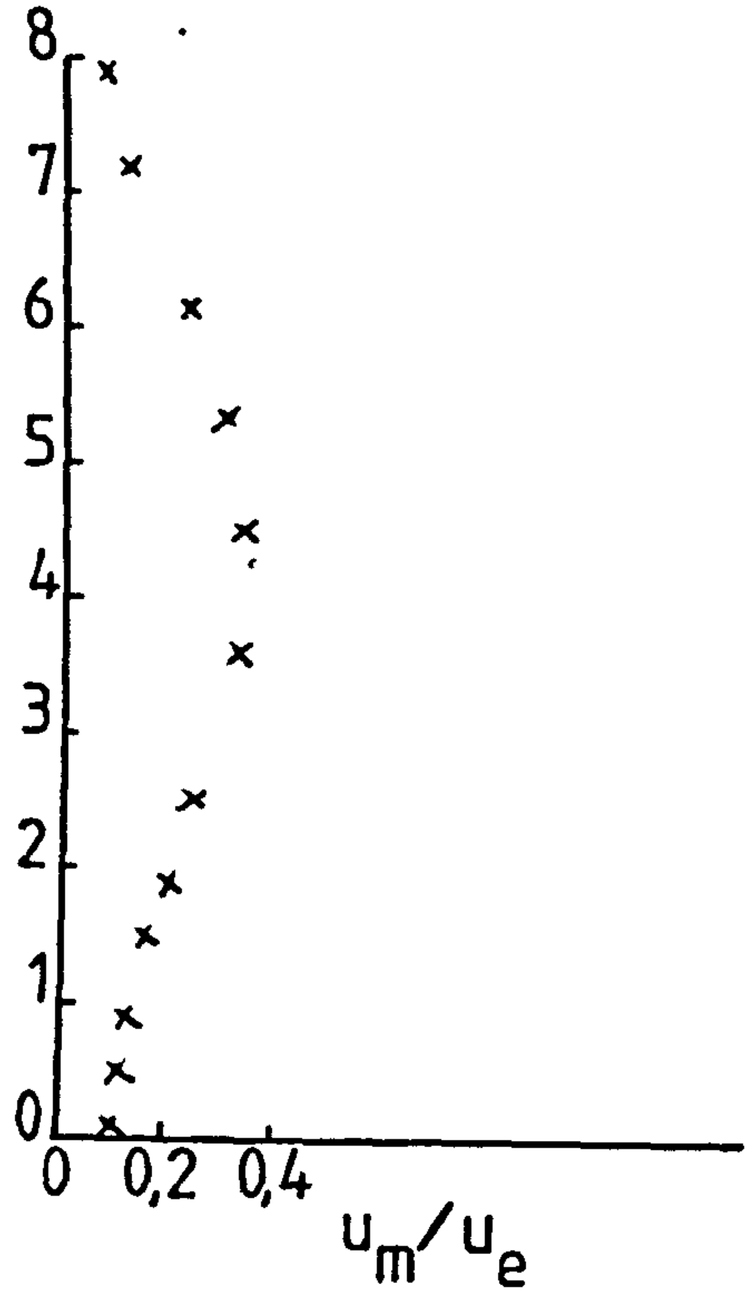

z = 0

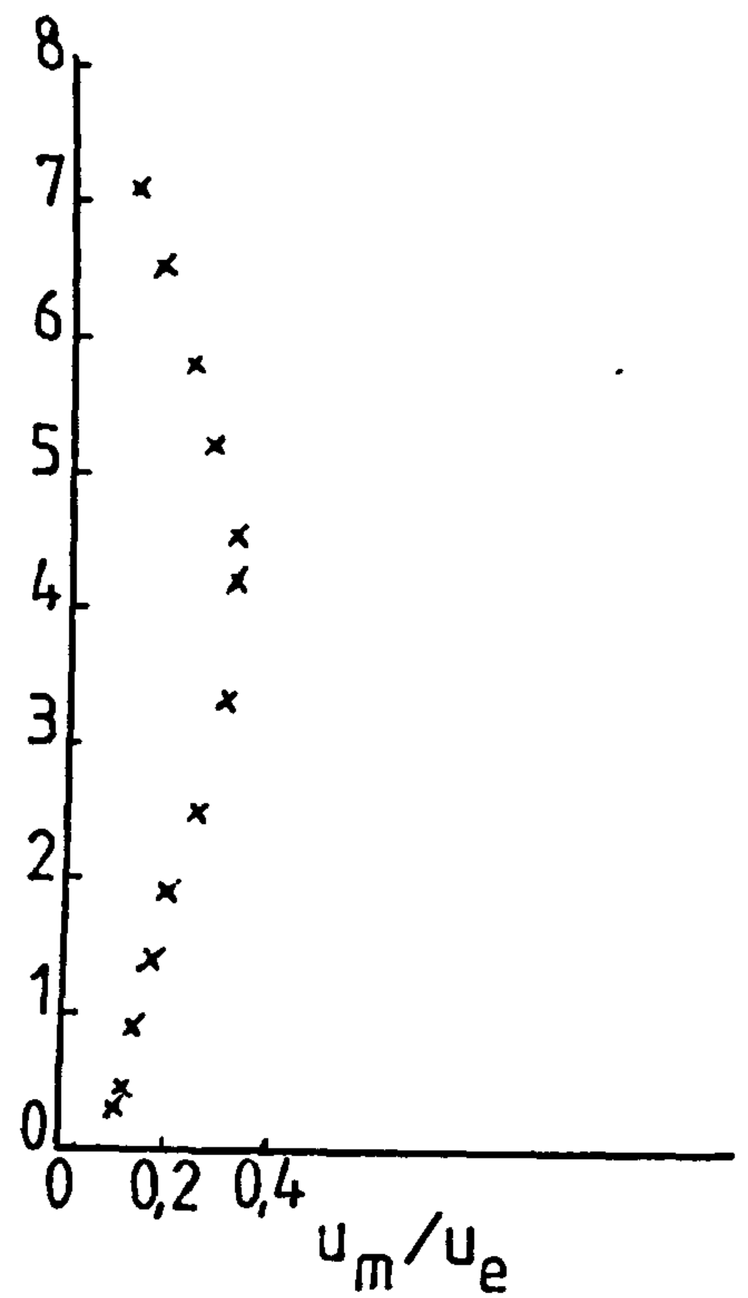

z/B = 0,25

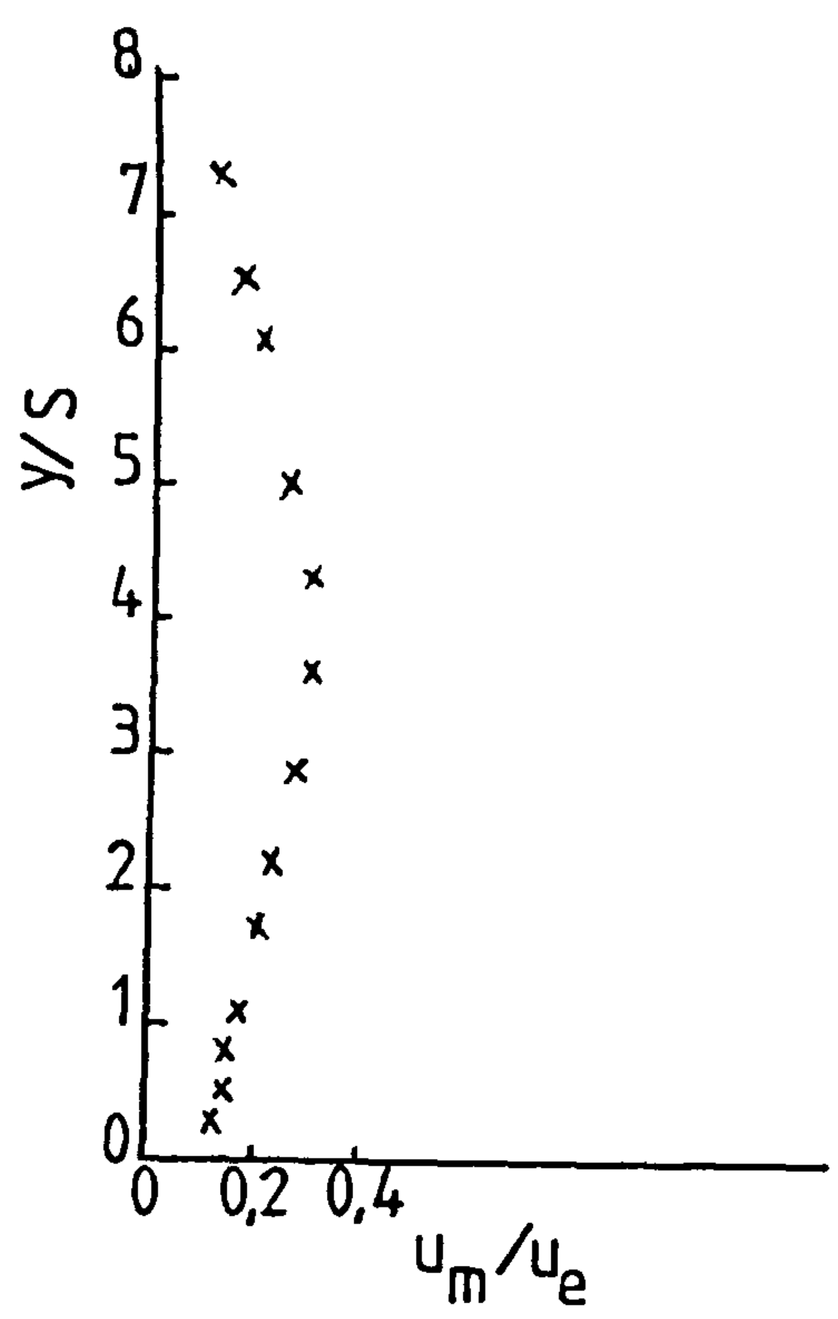

z/B = 0,5

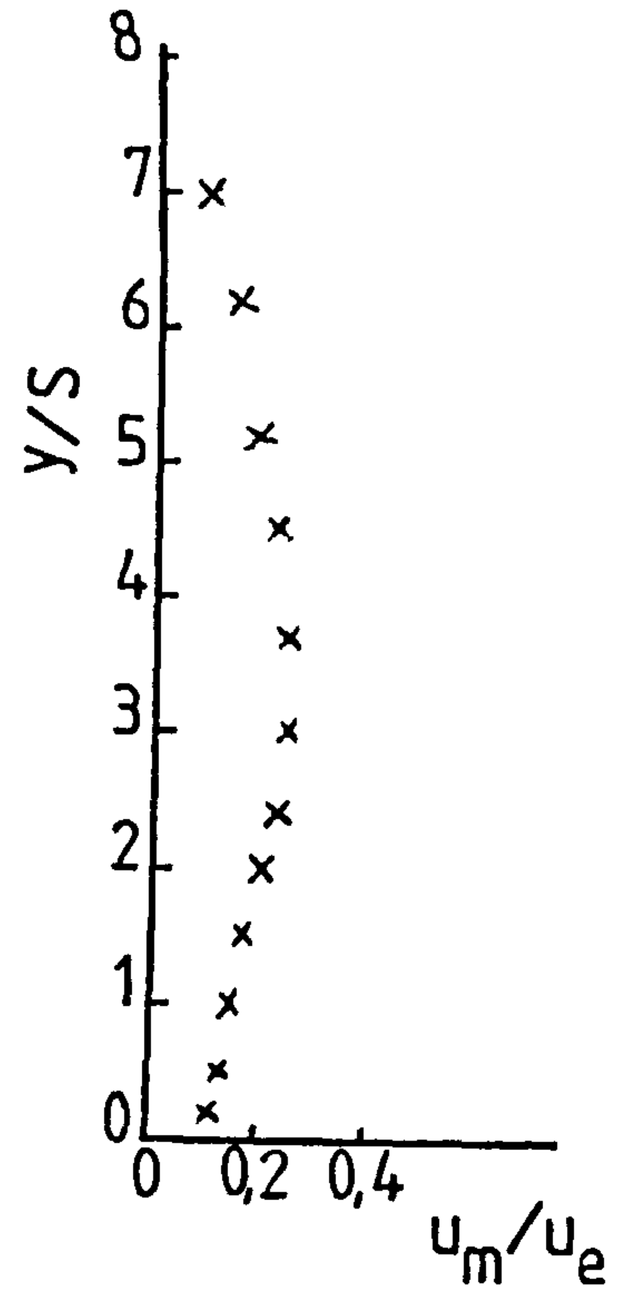

z/B = 0,75

Figure D-15 Three-Dimensional jet velocity profiles

OH = 3,8

x / S = 37,9

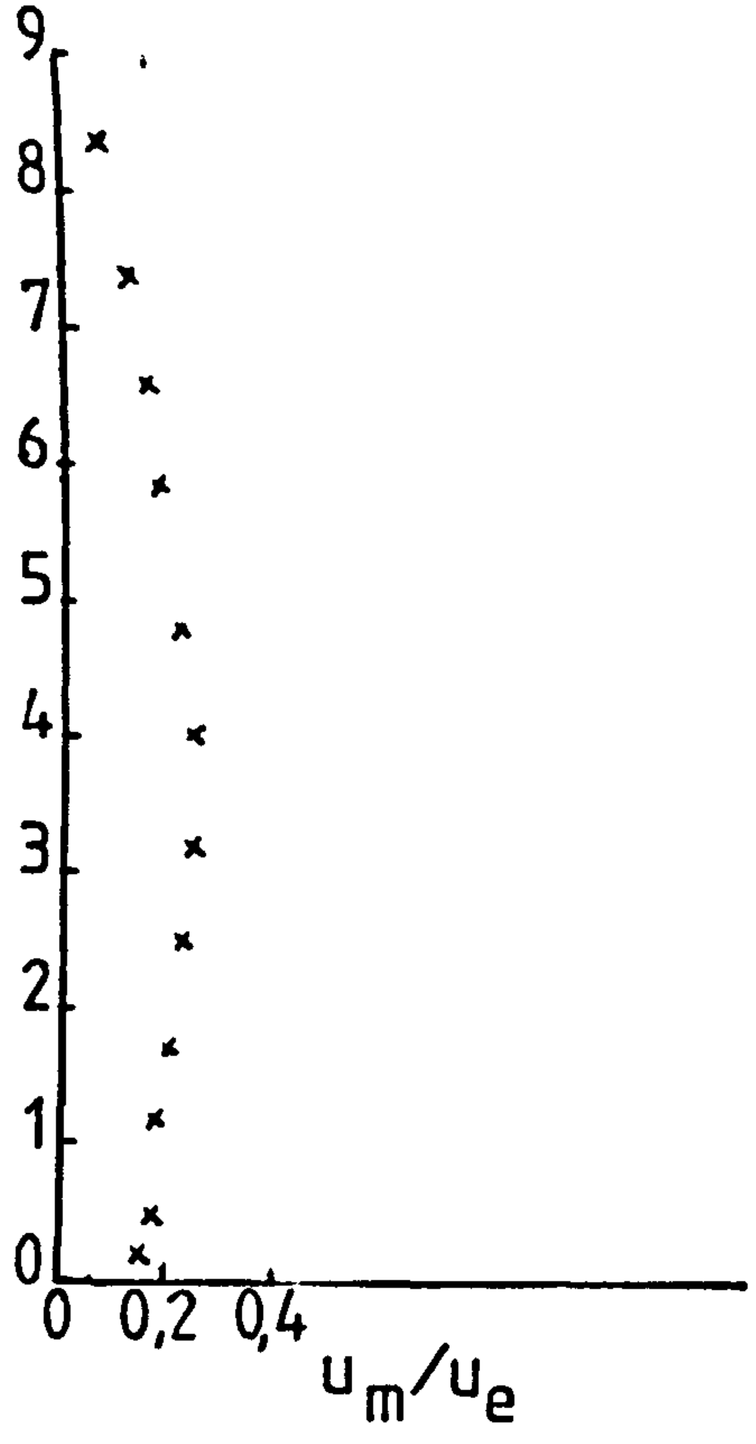

z = 0

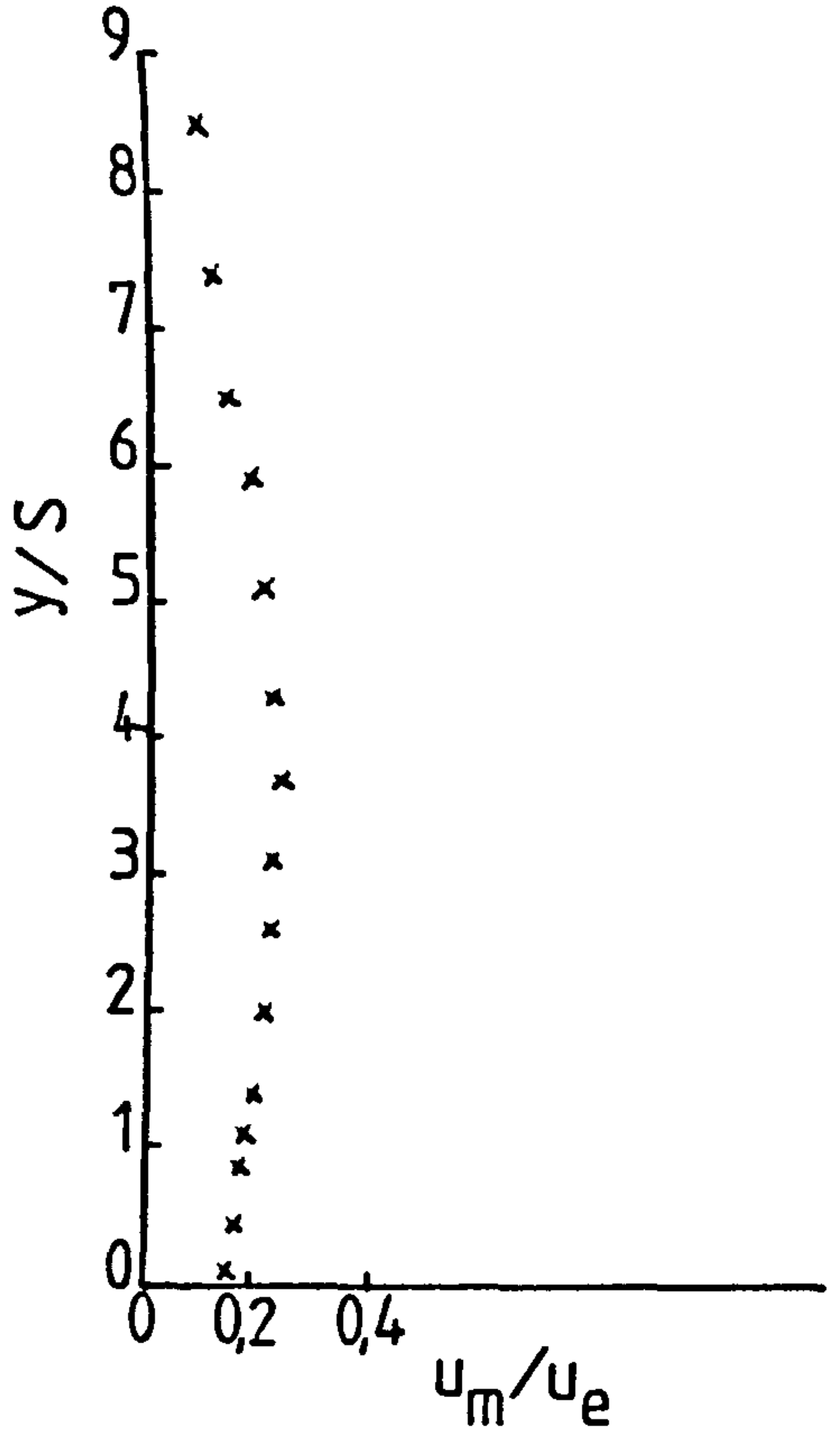

z/B = 0,25

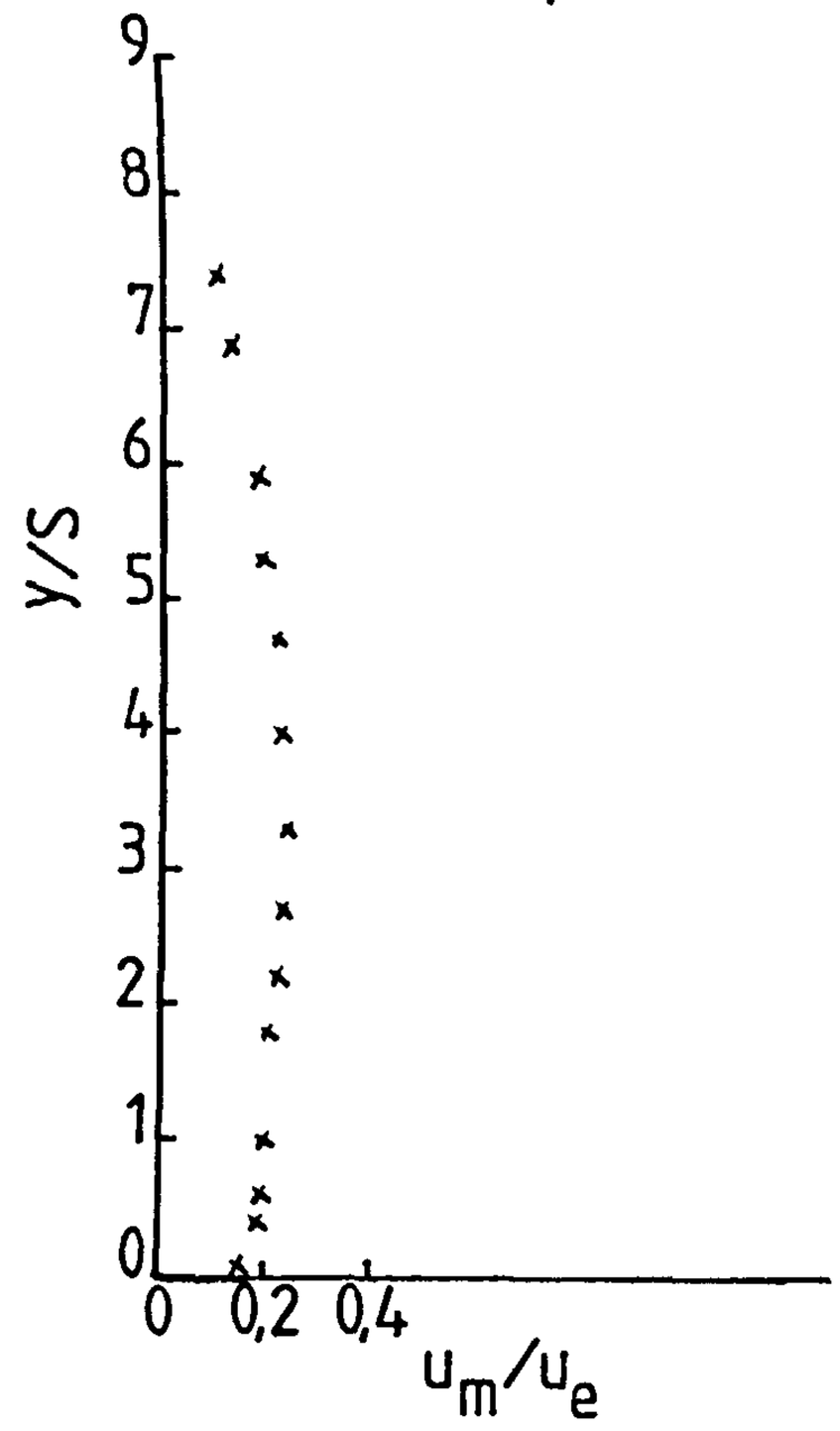

z/B = 0,5

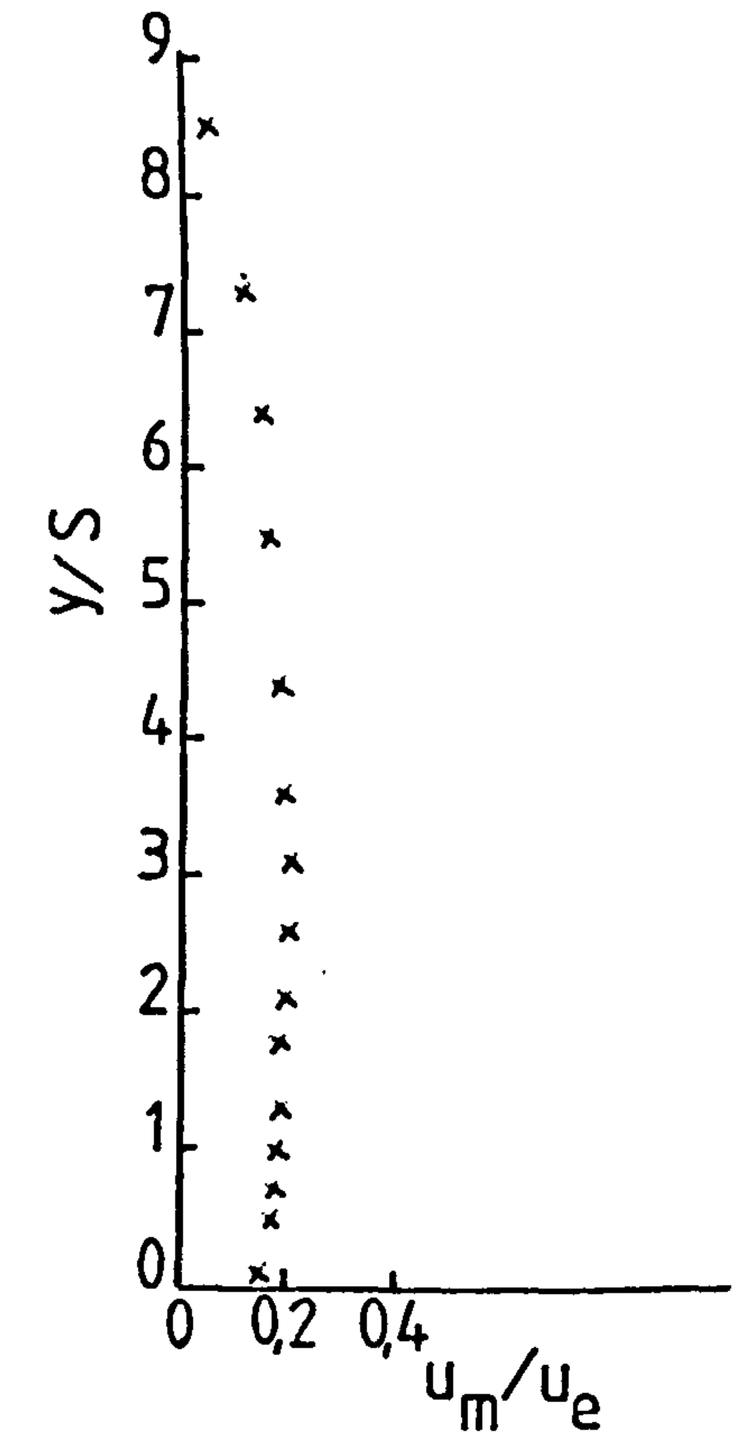

z/B = 1,0

Figure D-16 Three-Dimensional Jet velocity profiles

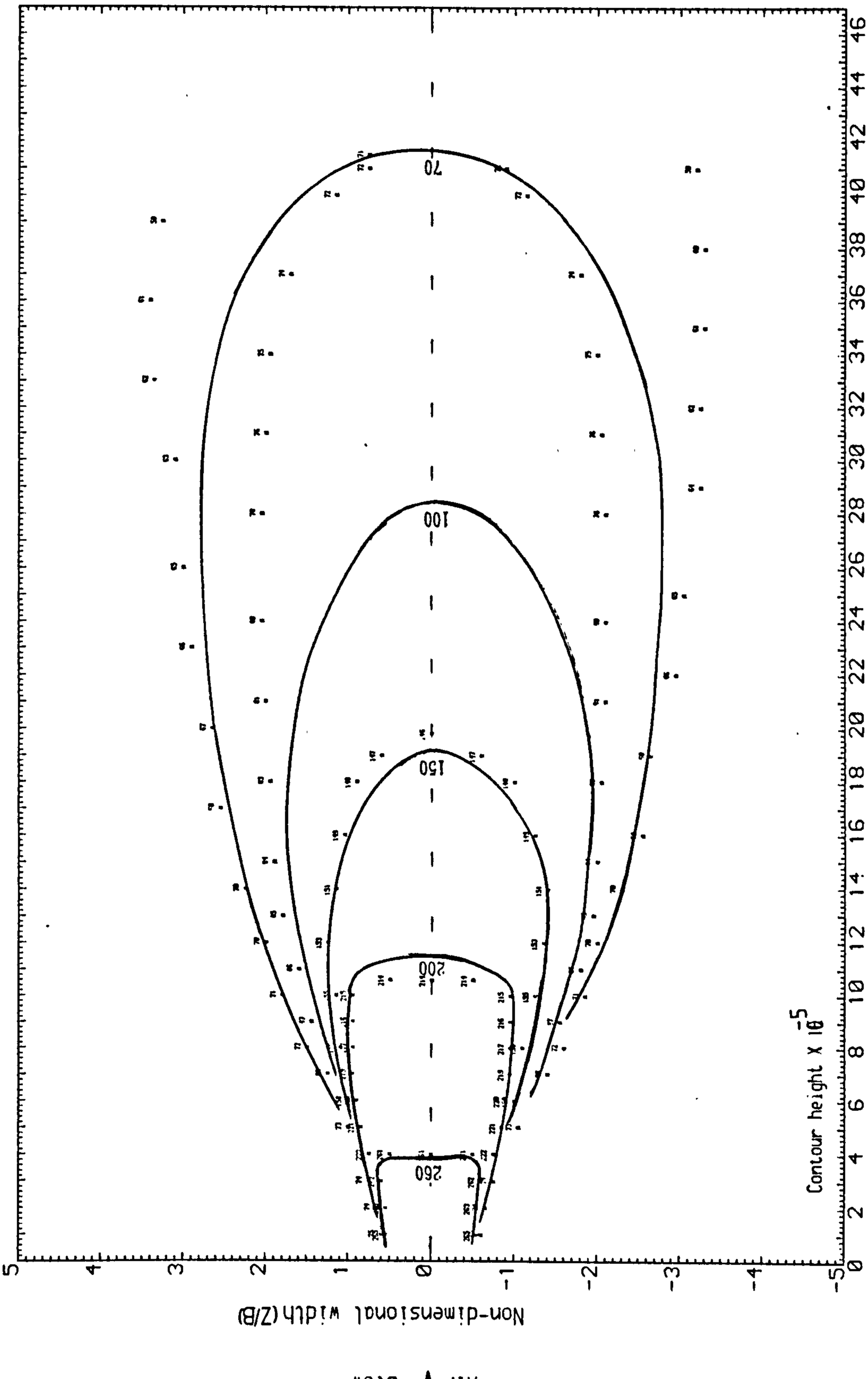

Fig. D-17 Mass transfer Stanton number contours for the non-dimensional off-set height: 0

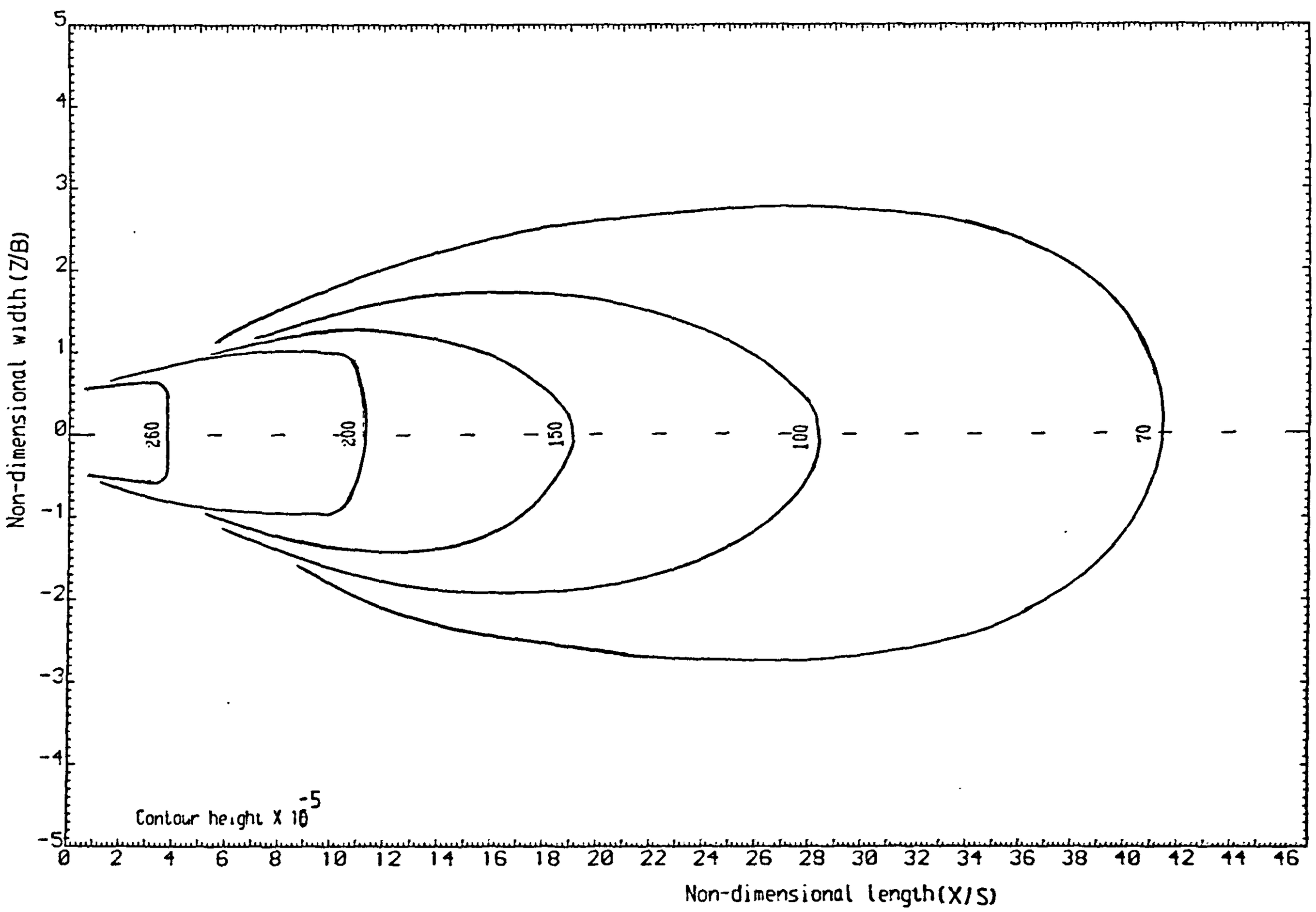

Fig. D-18 Mass transfer Stanton number contours for the non-dimensional off-set height: 0

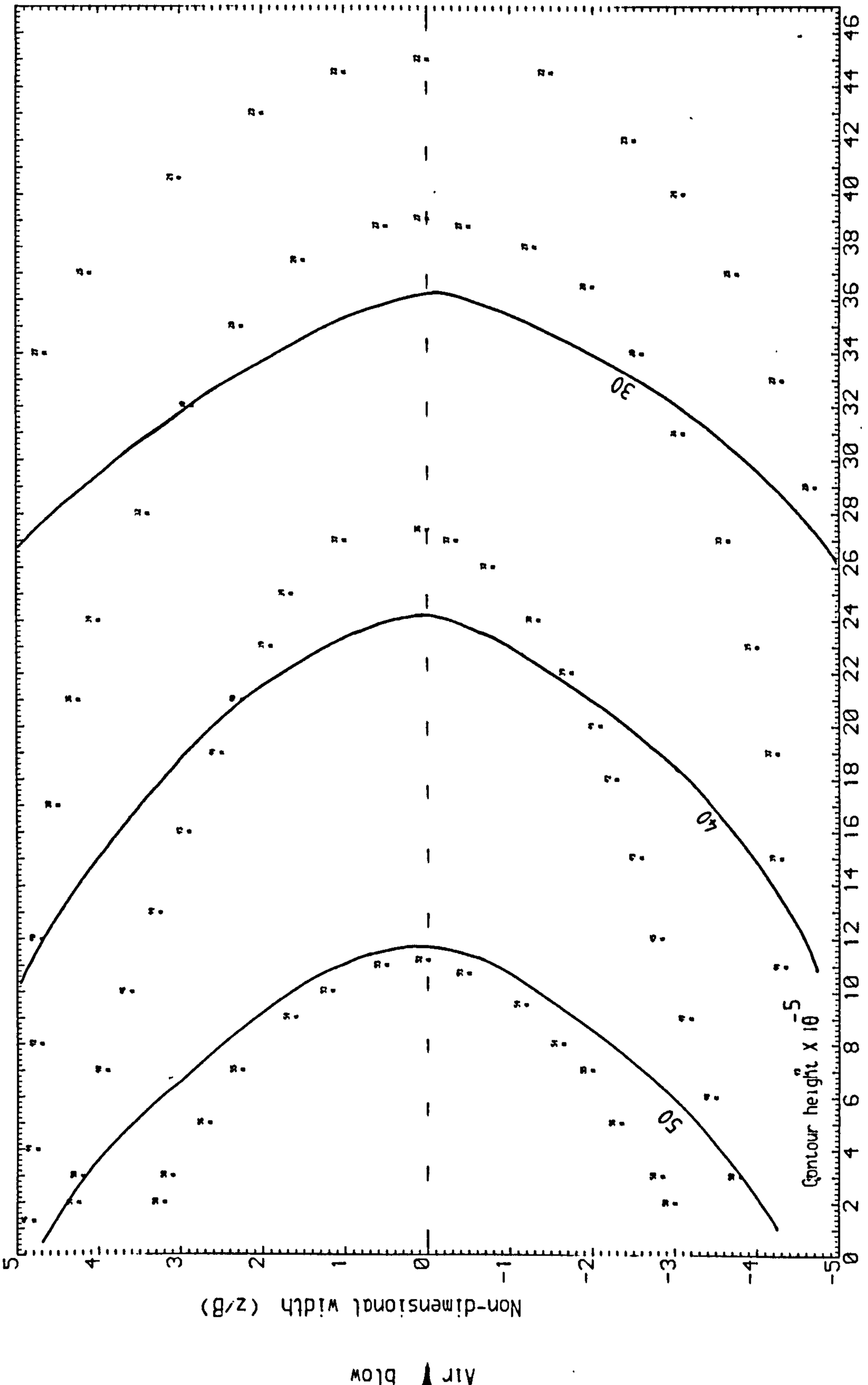

Fig. D-19 Mass transfer Stanton number contours for the non-dimensional off-set height: 0; 2nd plate

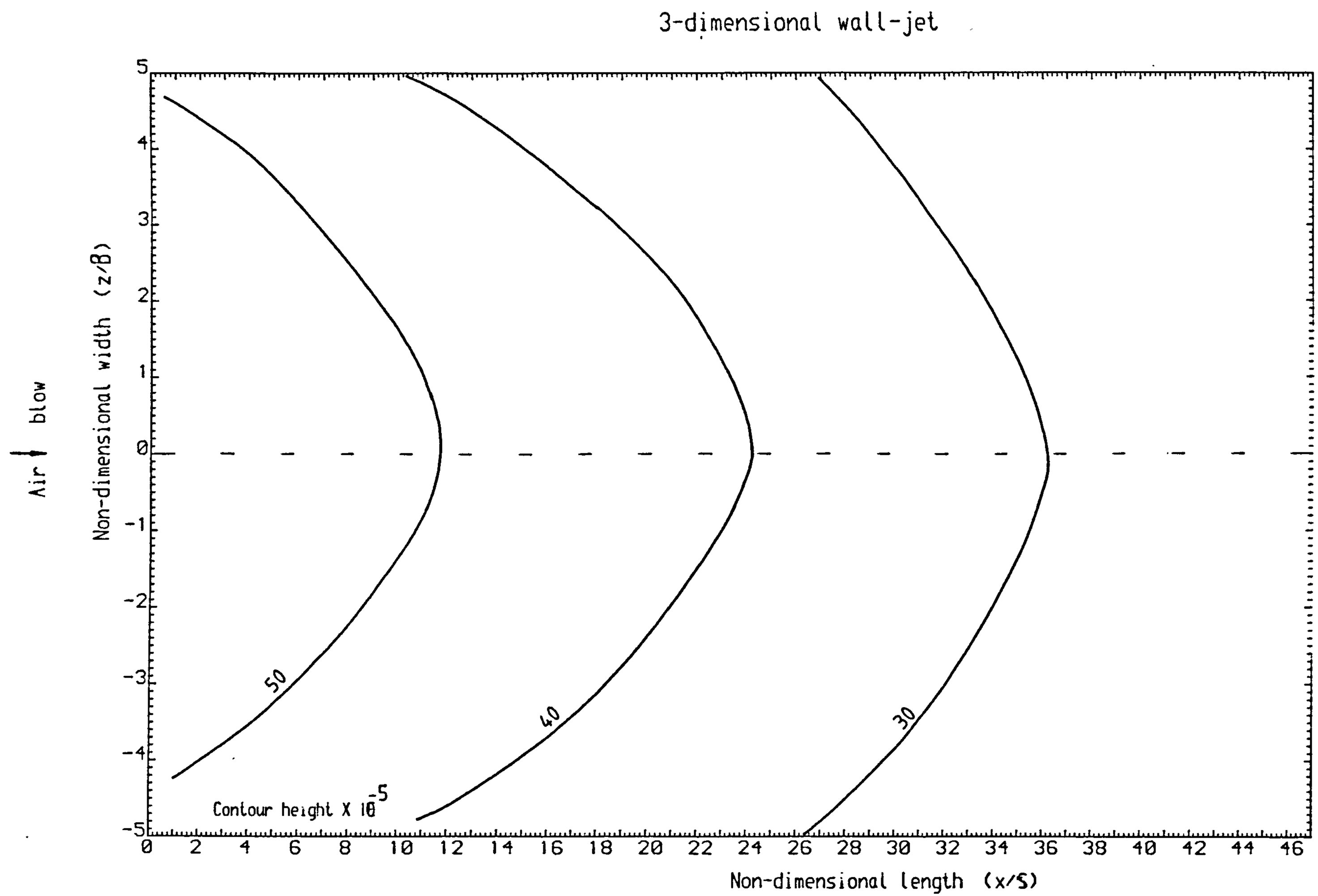

Fig. D-20 Mass transfer Stanton number contours for the non-dimensional off-set height: 0 ; 2nd plate

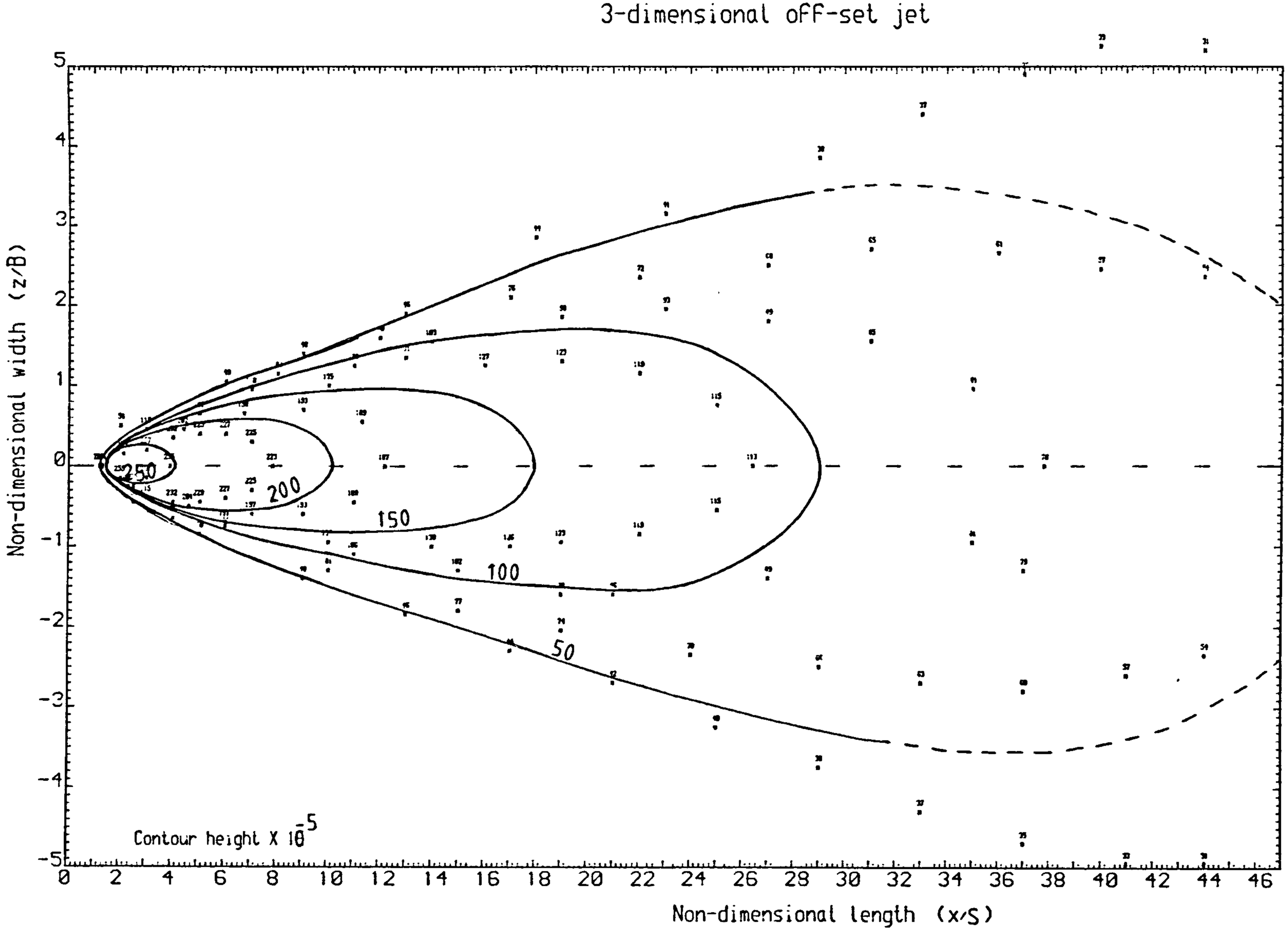

Fig. D-21 Mass transfer Stanton number contours for the non-dimensional off-set height: 0.5

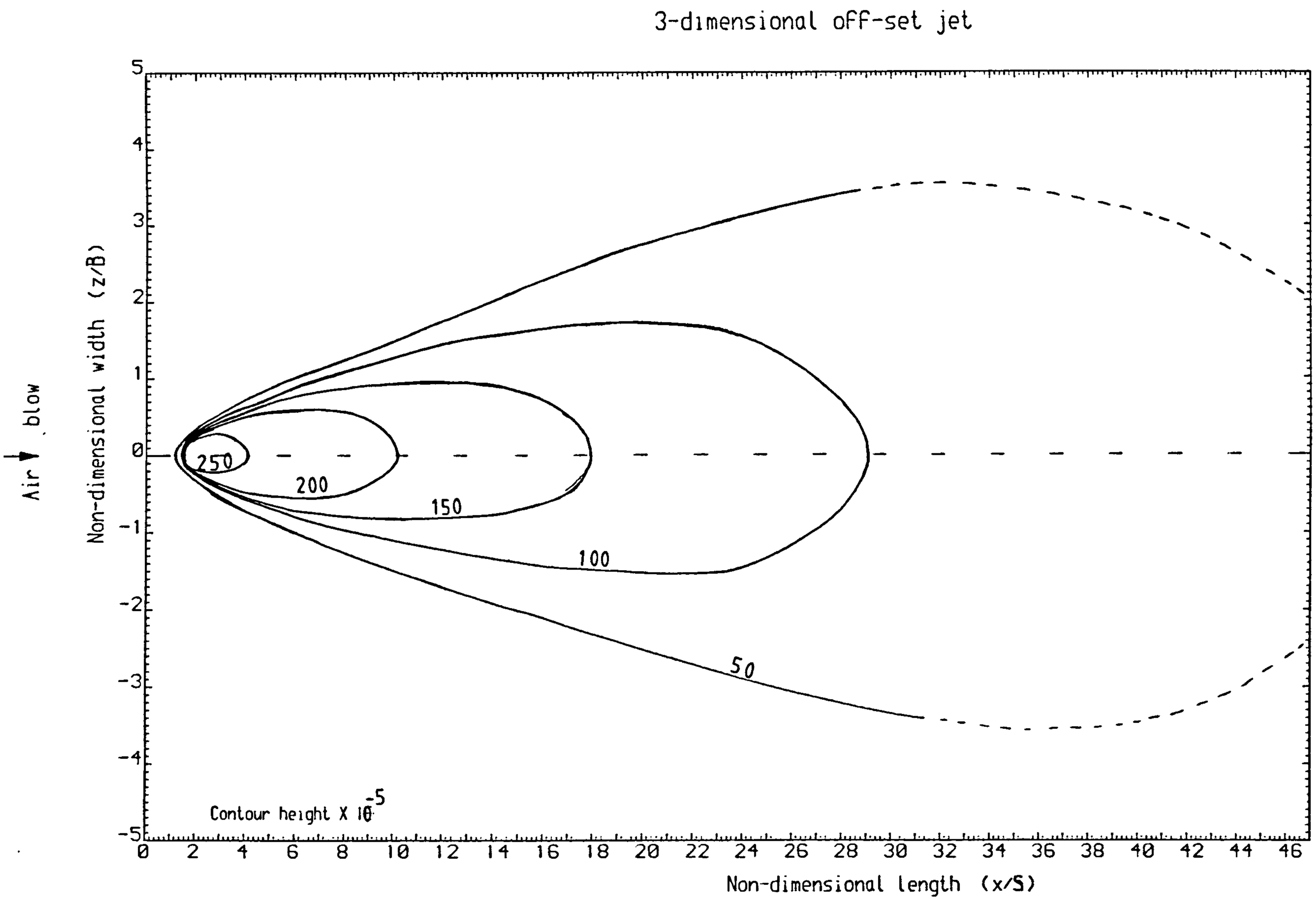

Fig. D-22 Mass transfer Stanton number contours for the non-dimensional off-set height: 0.5

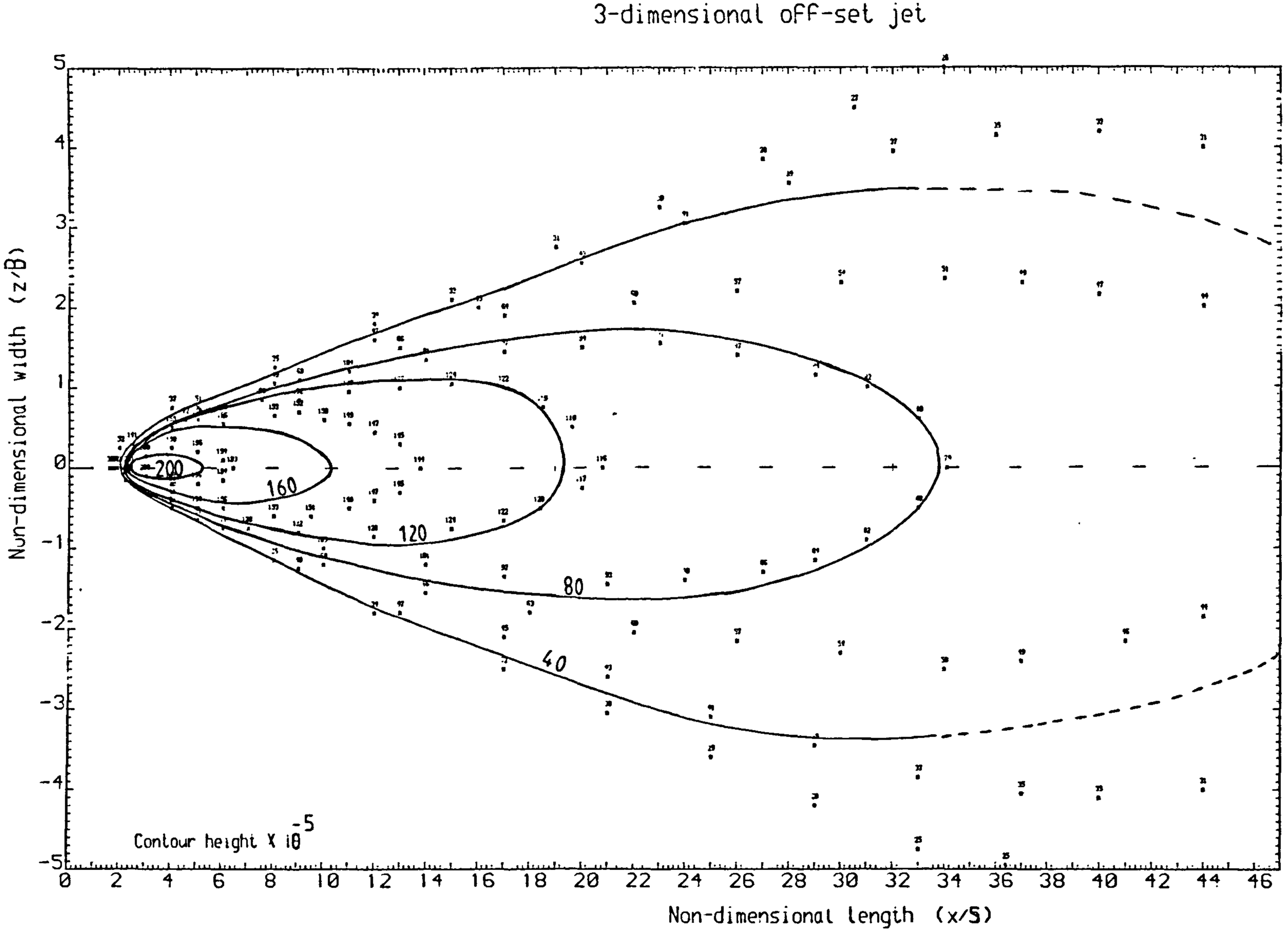

Fig. D-23 Mass transfer Stanton number contours for the non-dimensional off-set height: 0.7

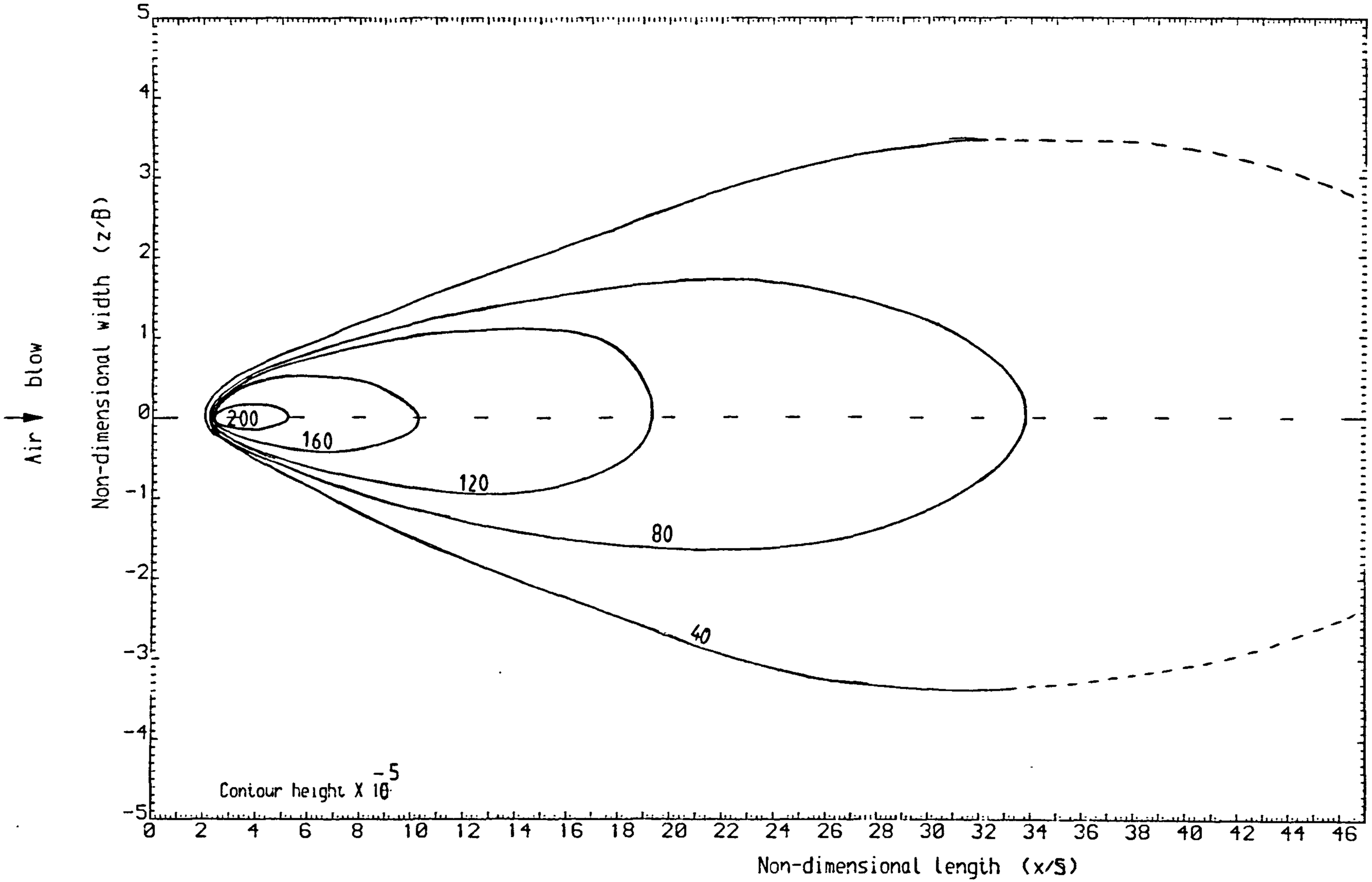

Fig. D-24 Mass transfer Stanton number contours for the non-dimensional off-set height: 0.7

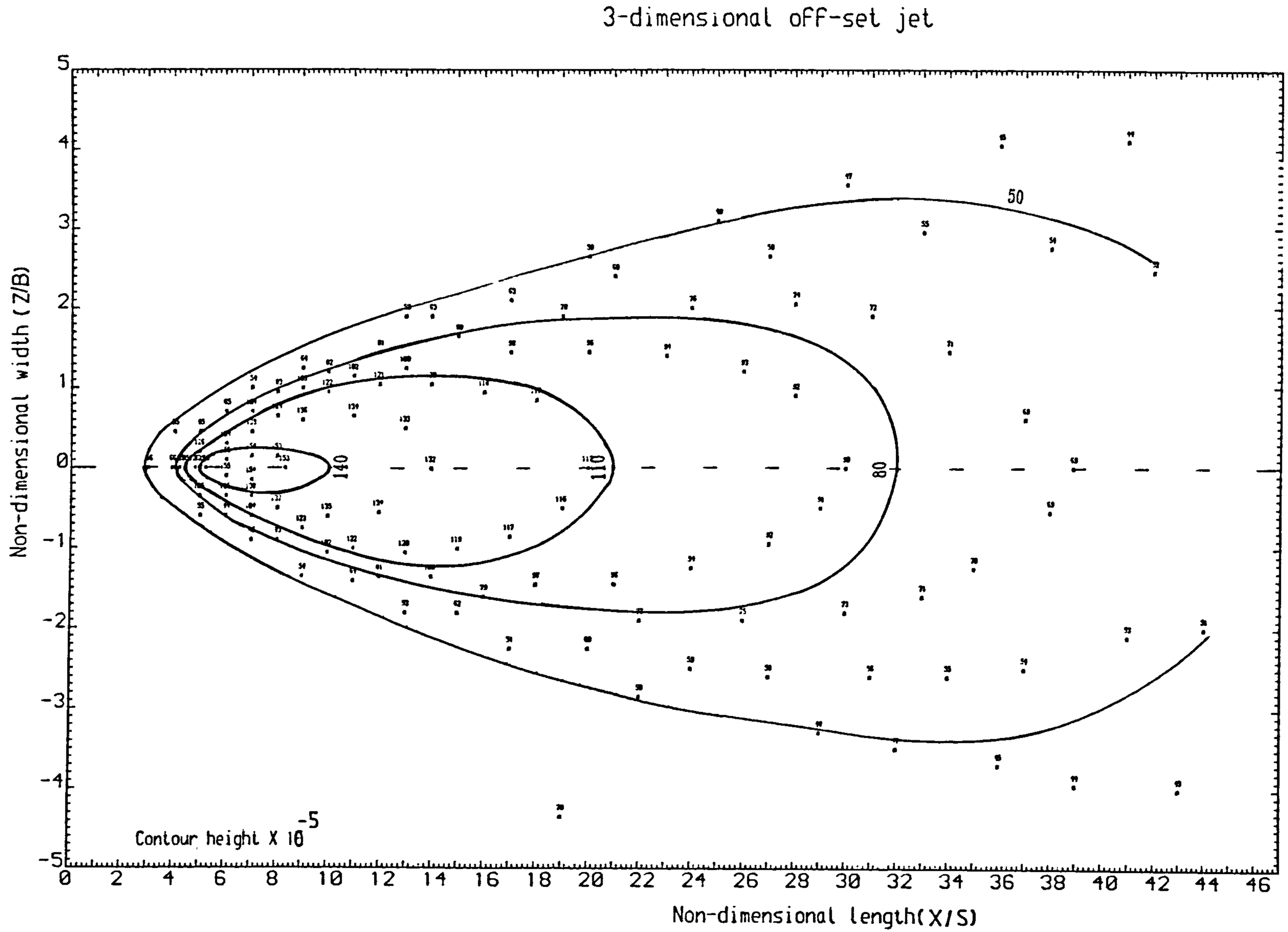

Fig. D-25 Mass transfer Stanton number contours for the non-dimensional off-set height: 1.0

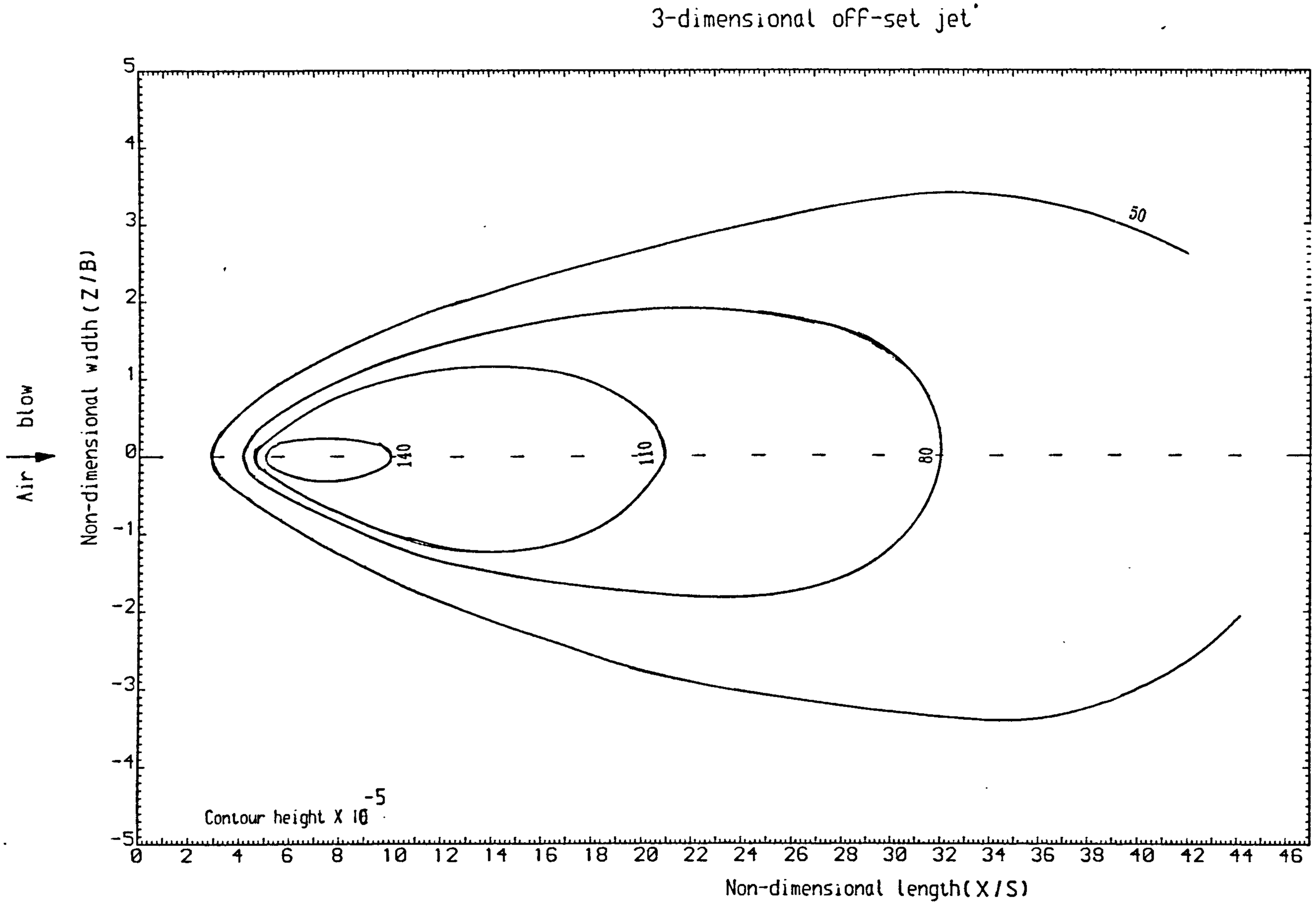

Fig. D-26 Mass transfer Stanton number contours for the non-dimensional off-set height: 1.0

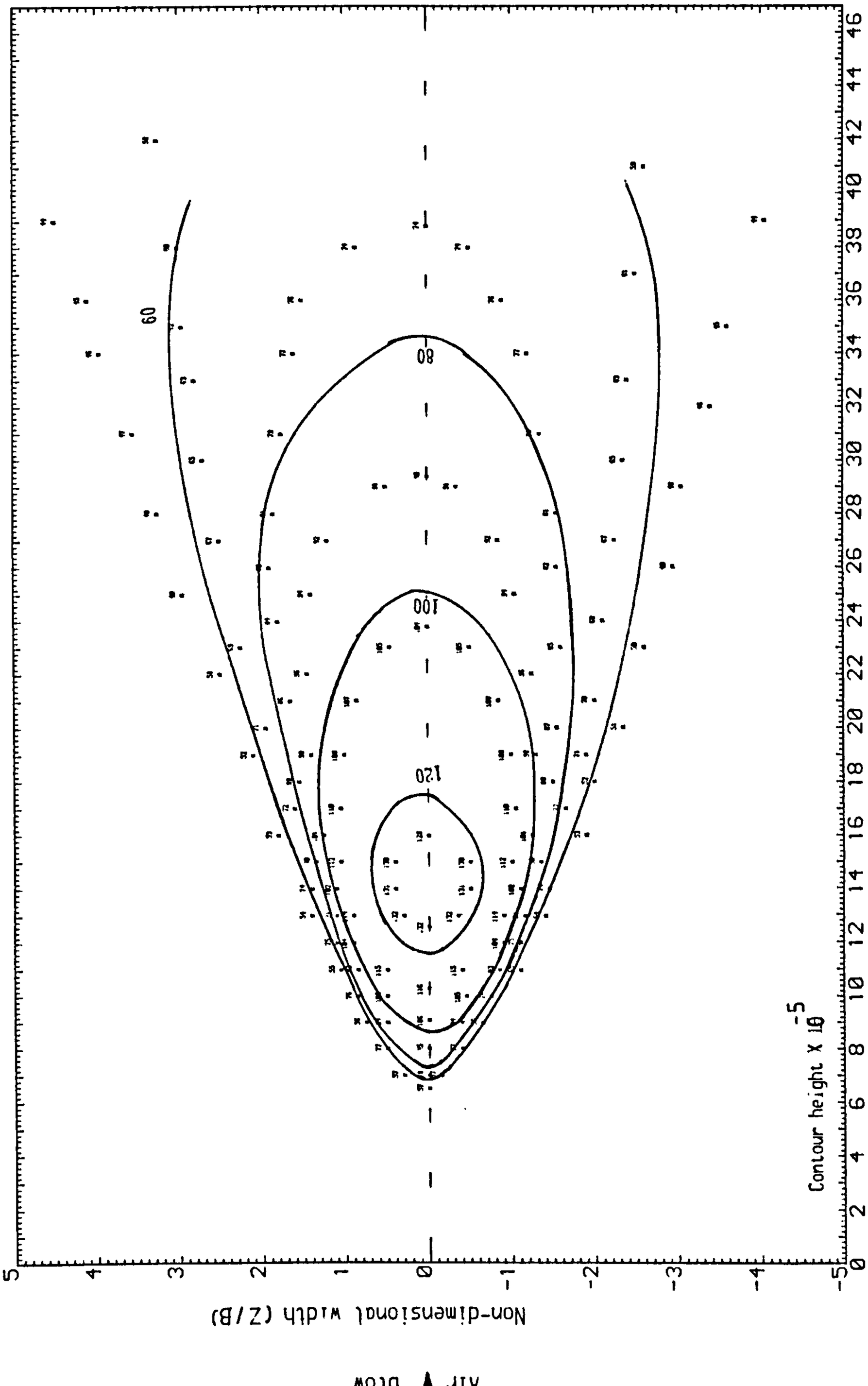

Fig. D-27 Mass transfer Stanton number contours for the non-dimensional off-set height: 1.6

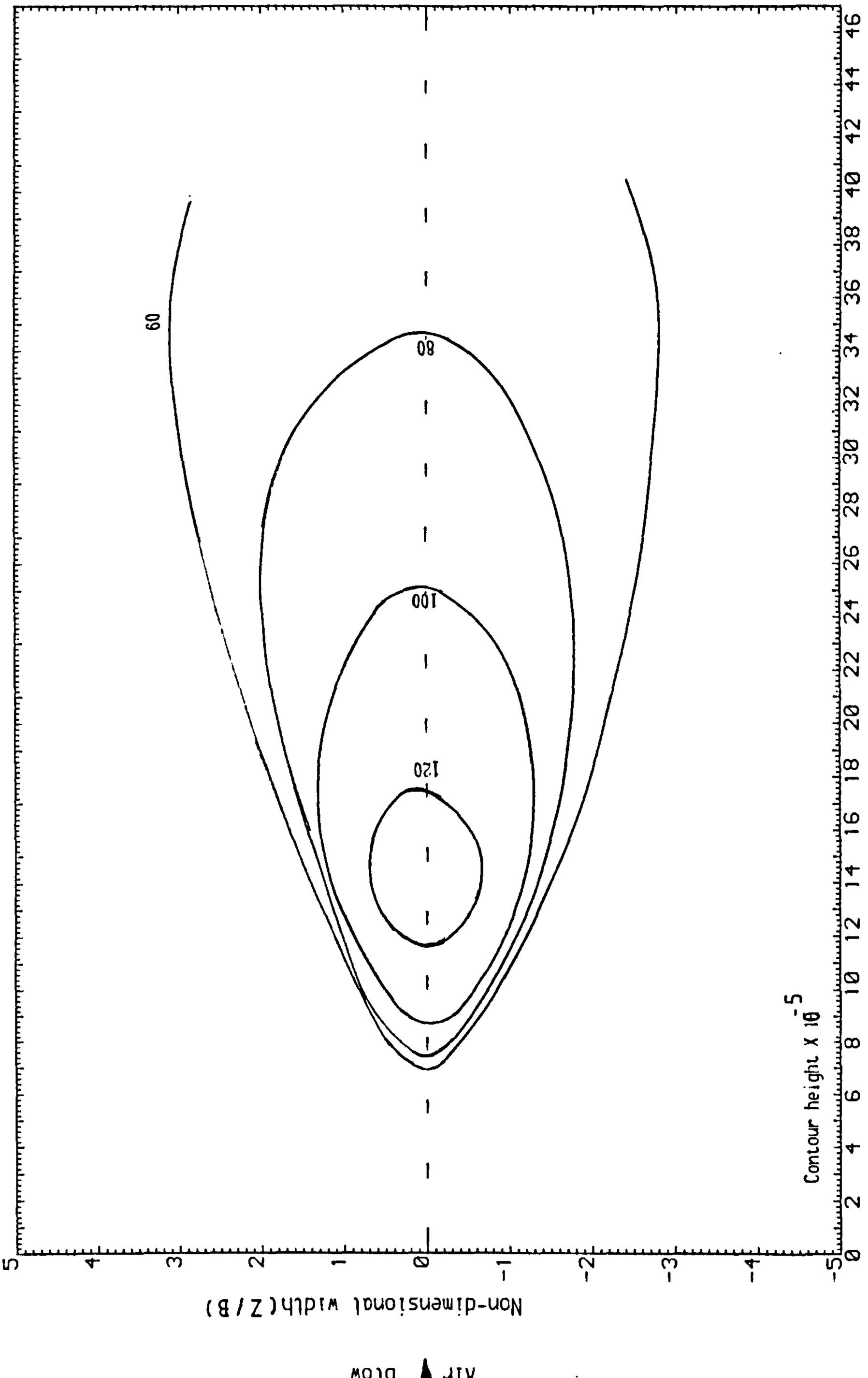

Fig. D-28 Mass transfer Stanton number contours For the non-dimensional off-set height: 1.6

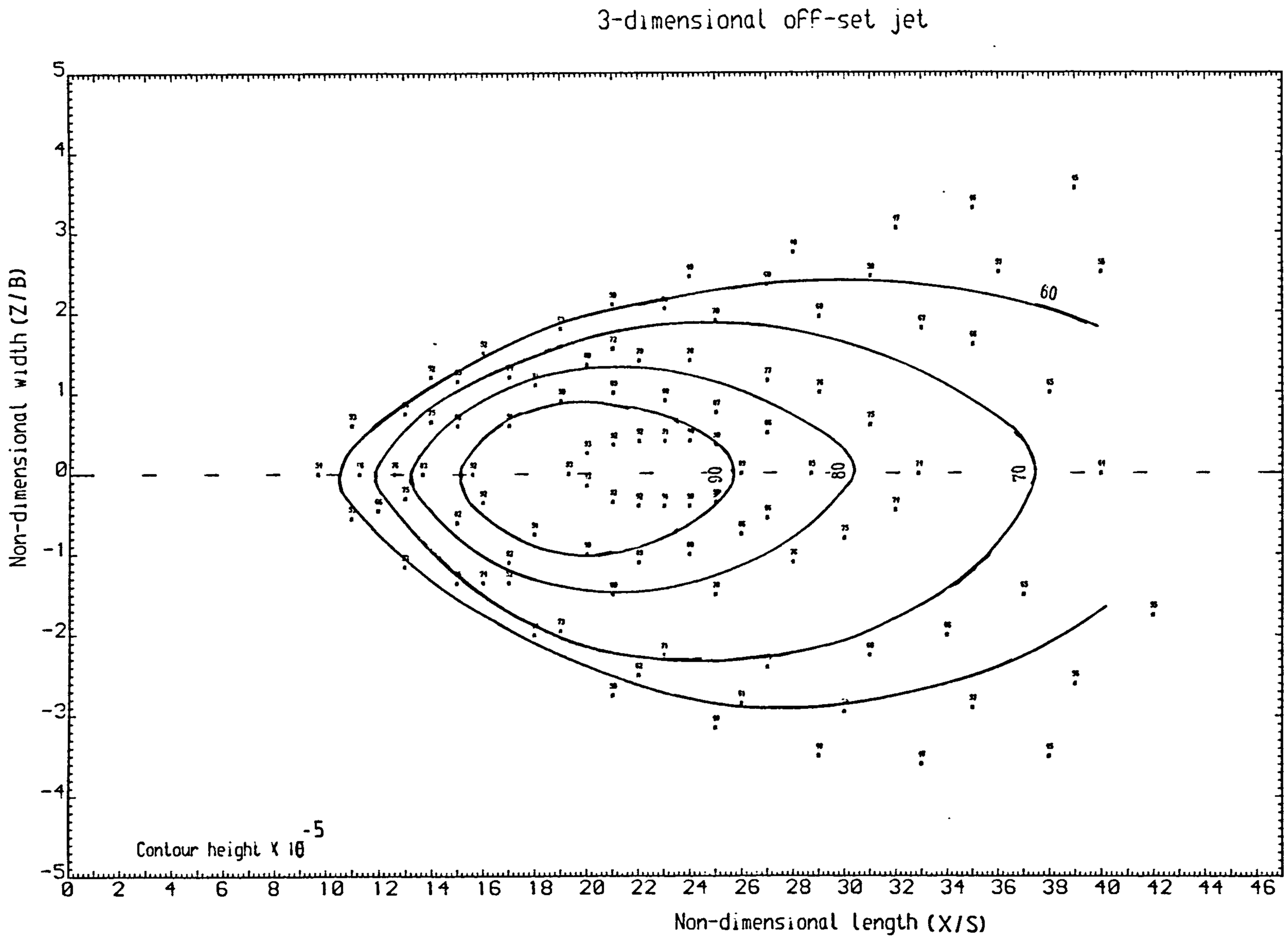

Fig. D-29 Mass transfer Stanton number contours for the non-dimensional off-set height: 2.2

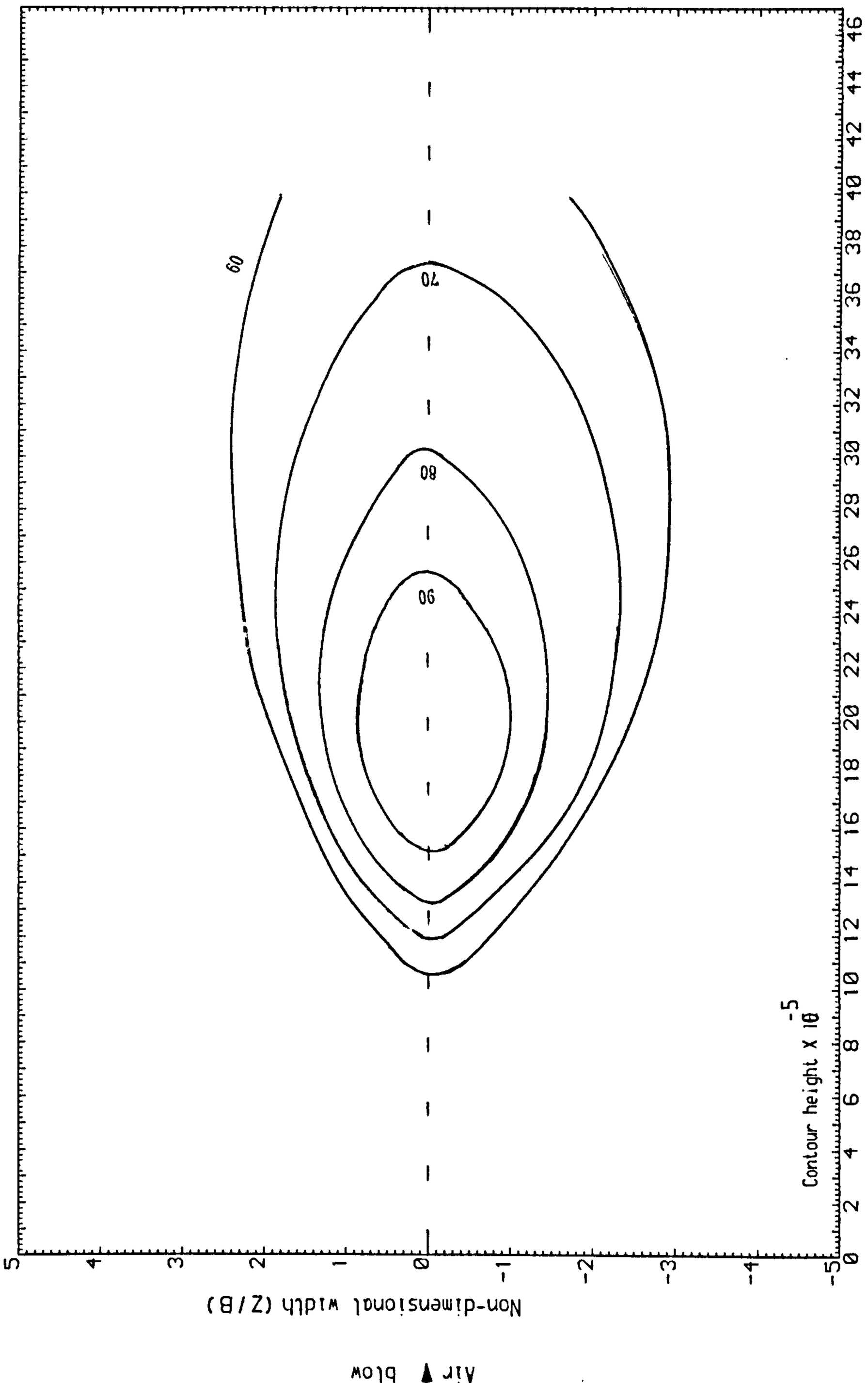

Fig. D-30 Mass transfer Stanton number contours for the non-dimensional off-set height: 2.2

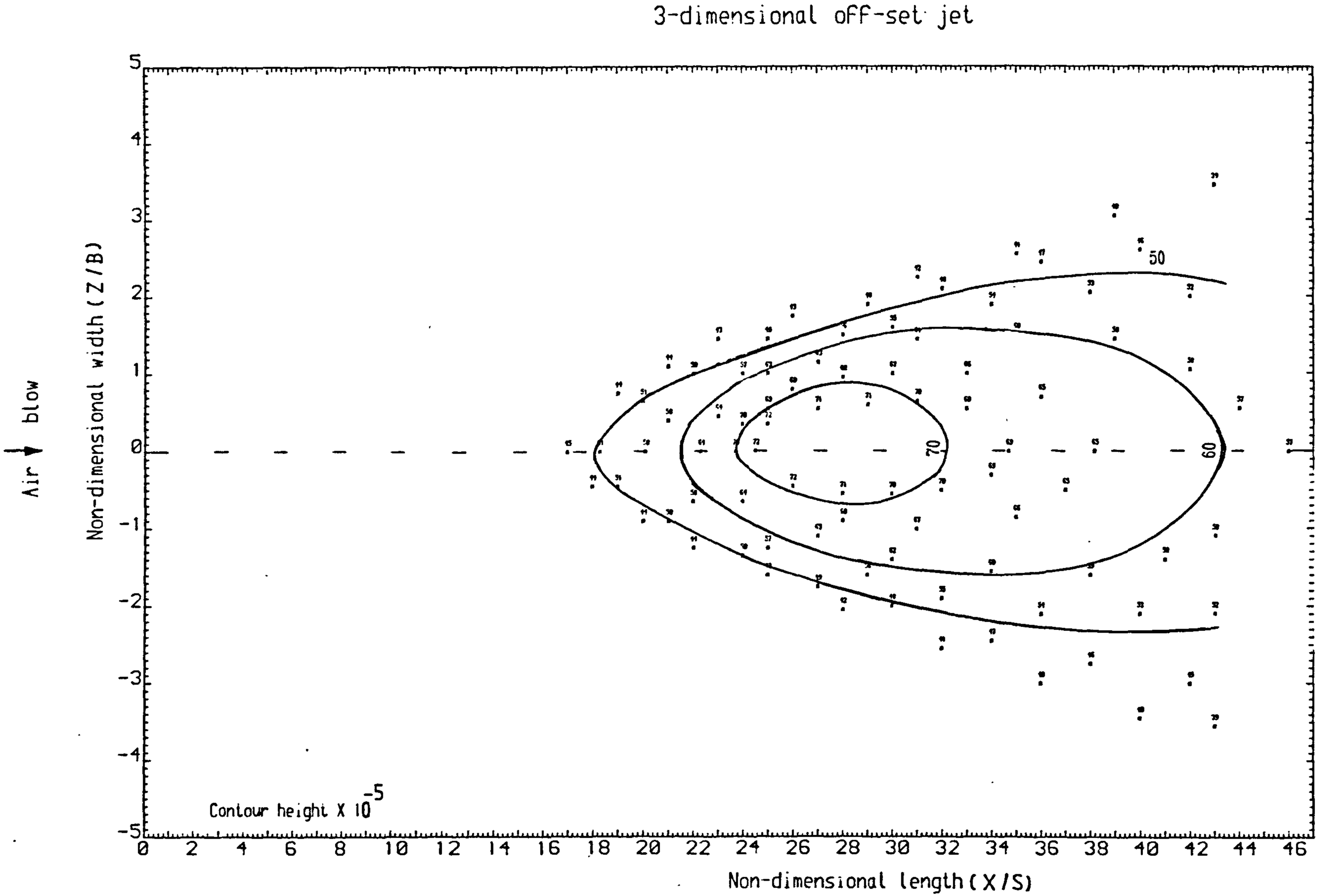

Fig. D-31 Mass transfer Stanton number contours for the non-dimensional off-set height: 3.8

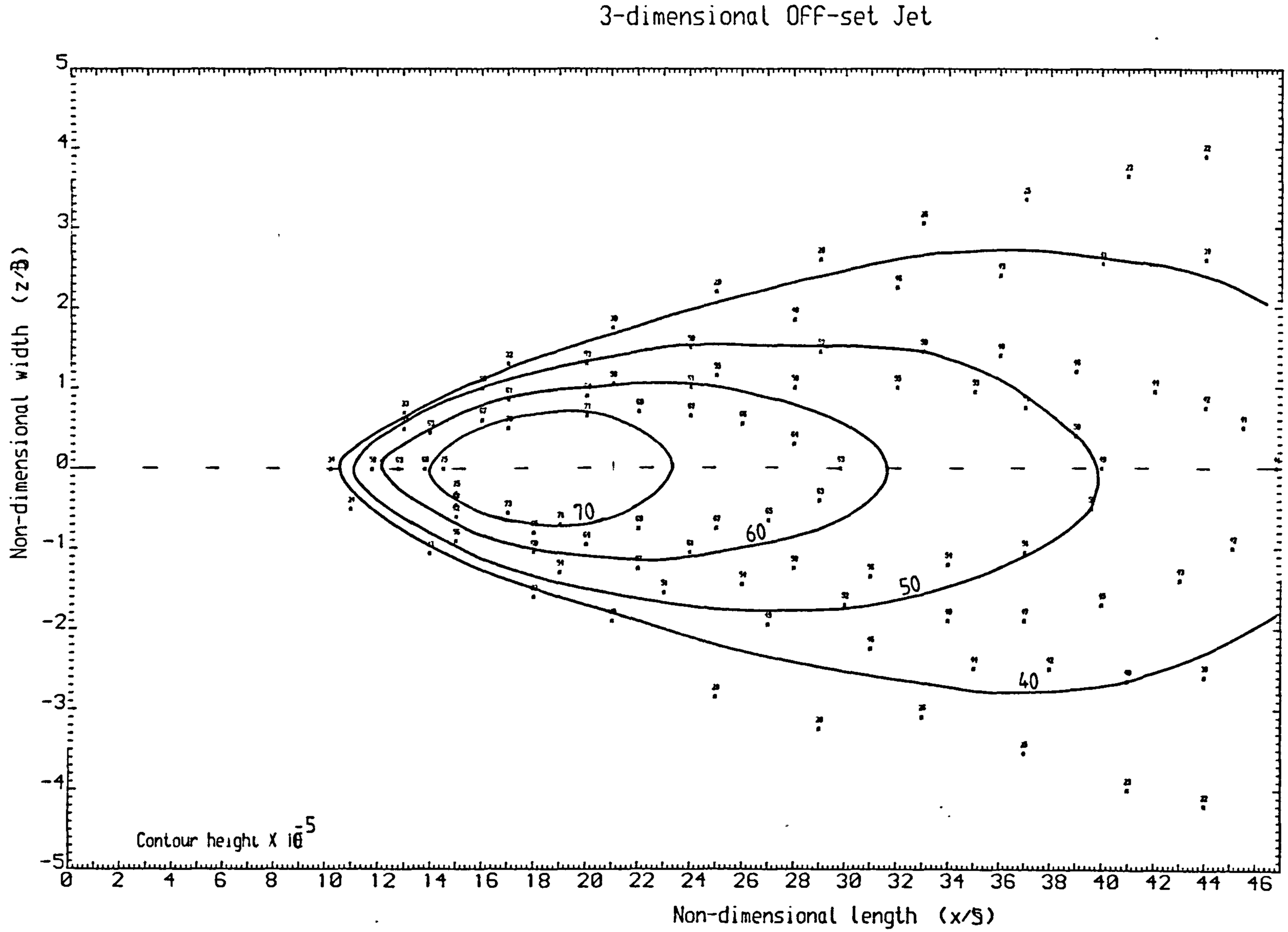

Fig. D-32 Mass transfer Stanton number contours for the non-dimensional off-set height: 3.1

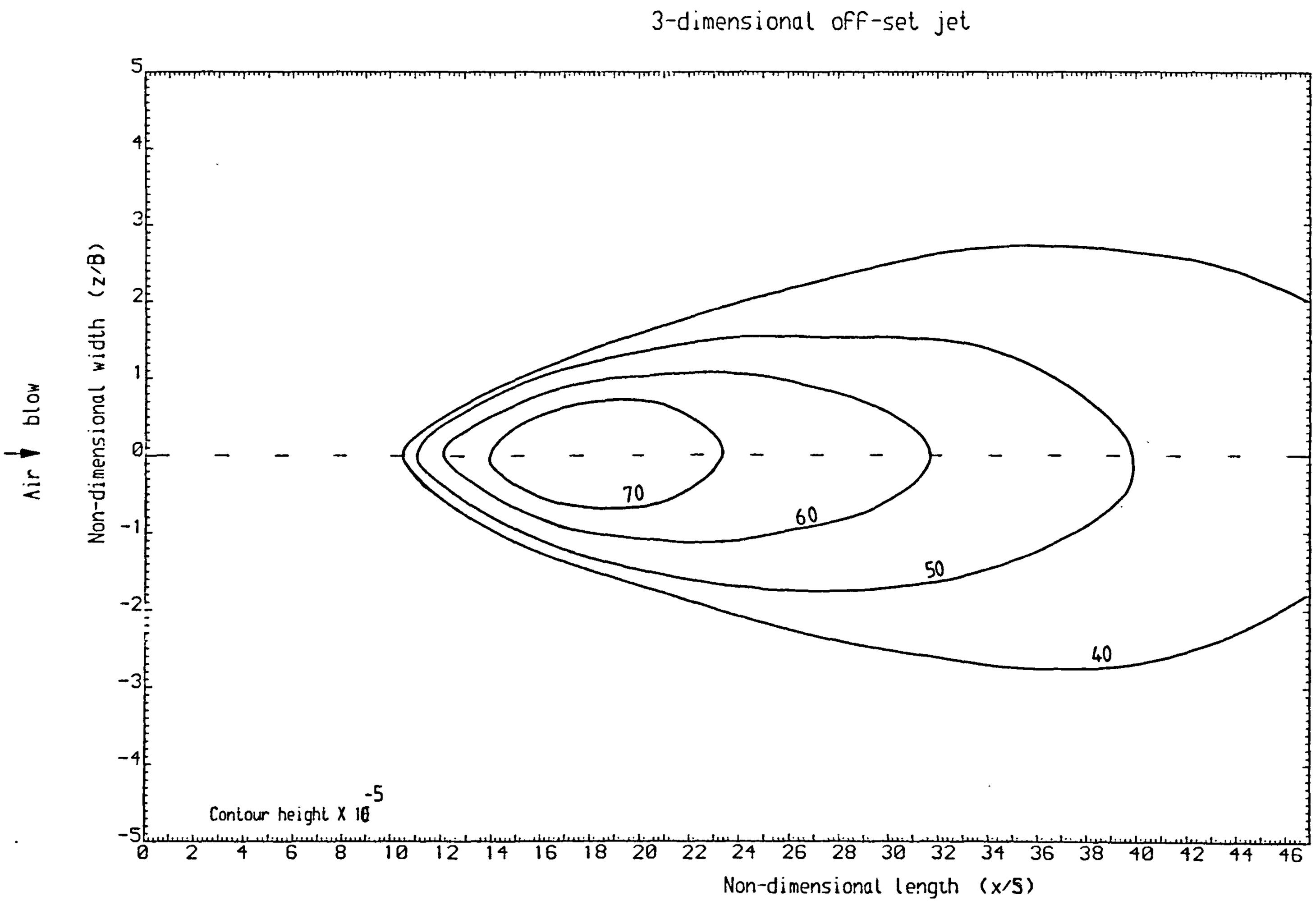

Fig. D-33 Mass transfer Stanton number contours for the non-dimensional off-set height: 3.1

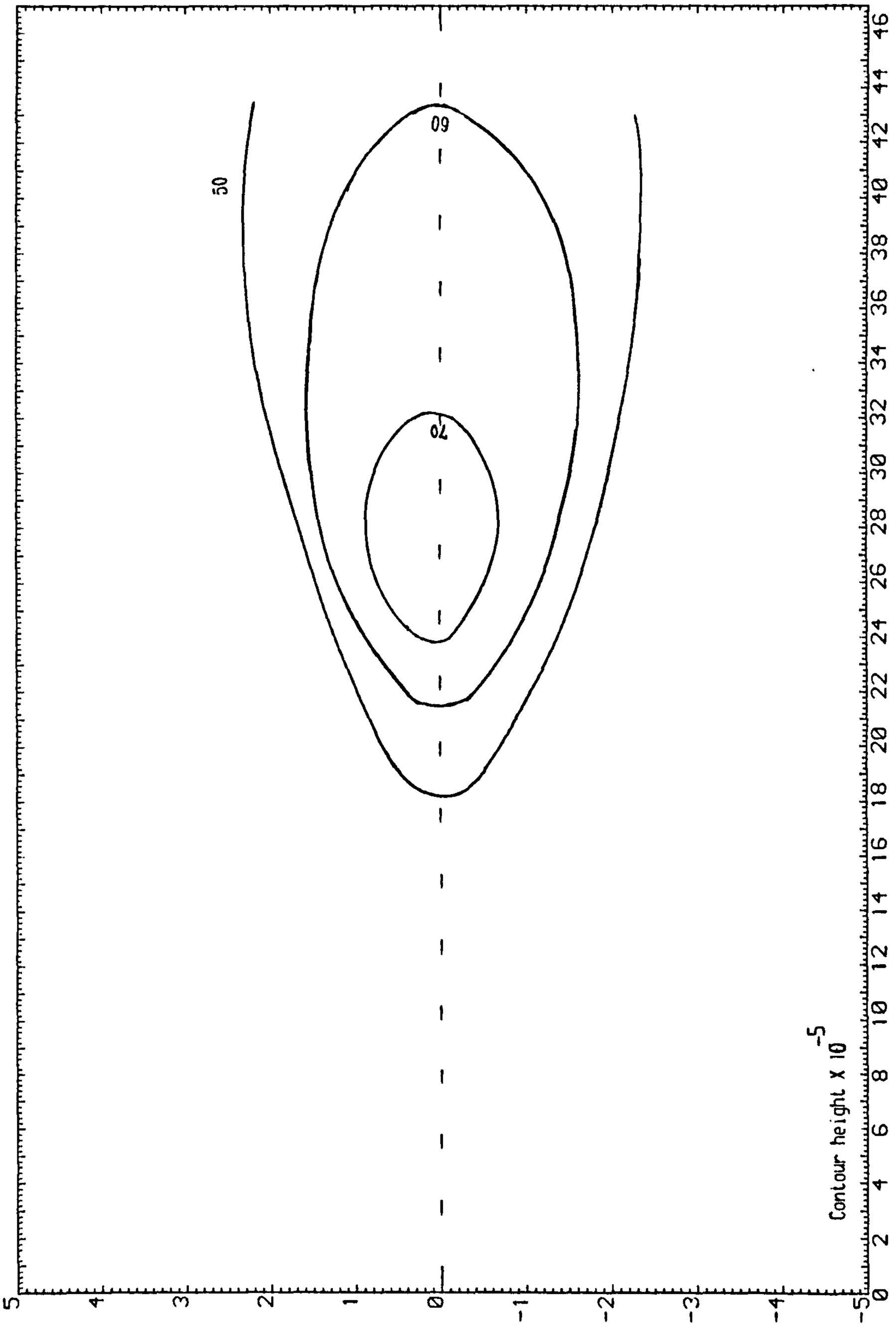

Fig. D-34 Mass transfer Stanton number contours for the non-dimensional off-set height: 3.8

APPENDIX E

THREE-DIMENSIONAL WALL-JETS: REYNOLDS NUMBER EFFECTS ON SURFACE AVERAGED MASS TRANSFER

APPENDIX E

THREE-DIMENSIONAL WALL-JETS: REYNOLDS NUMBER EFFECTS ON SURFACE AVERAGED MASS TRANSFER

The correlation presented in equation 5-16, includes the Reynolds number effects implied by wall-jet profile analysis and empirical data correlations for the jet mean-flow properties. Although both have been verified for the suggested range of Reynolds numbers, tests were carried out in order to verify the Reynolds number dependence experimentally.

Figures E-1 to E-4 show the contours of constant Stanton numbers, with and without data points, for the Reynolds numbers of 9100 and 14300. The values for a Reynolds number of 24920 are presented in appendix D. The centre-line values are compared in figure E-5 where the agreement is good. The average mass Stanton numbers for the wall-jet for the three different Reynolds numbers are compared in figure E-6, where the agreement can be seen to be fair and the disagreement may be explained similar to that in figure 5-15.

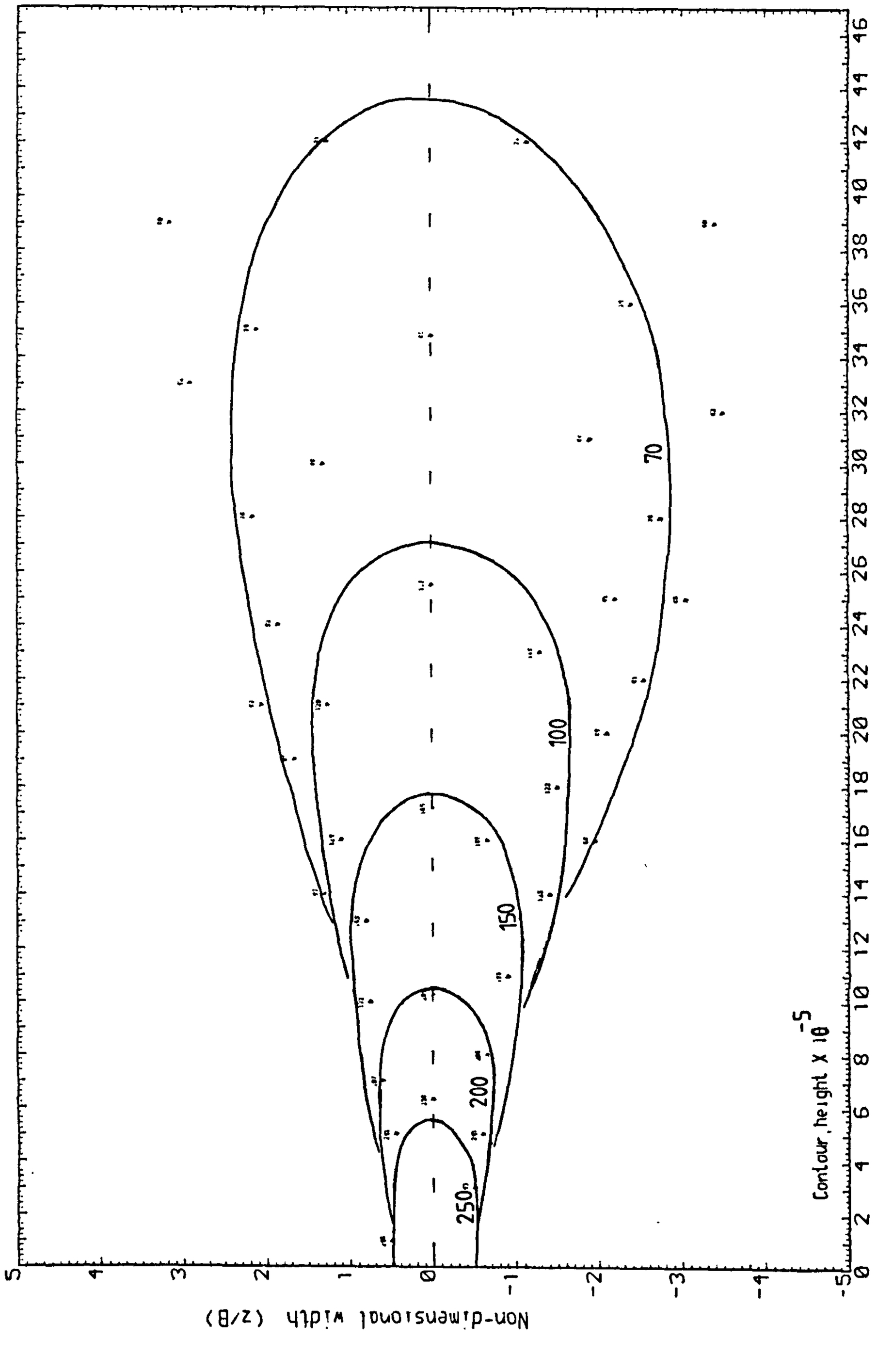

Fig.E-1 Mass transfer Stanton number contours for slot Reynolds number of 14300

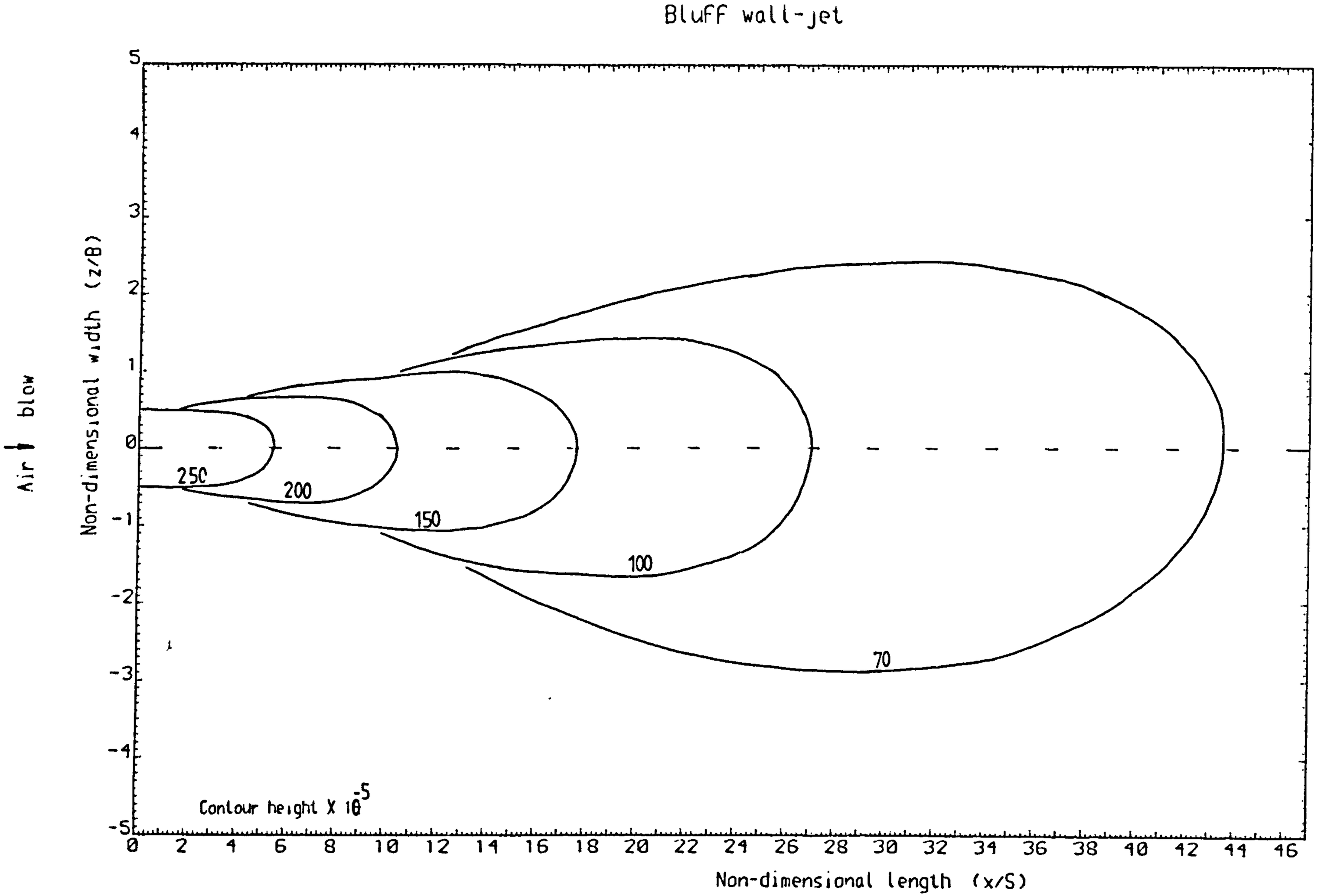

Fig.E-2 Mass transfer Stanton number contours for the slot Reynolds number of 14300

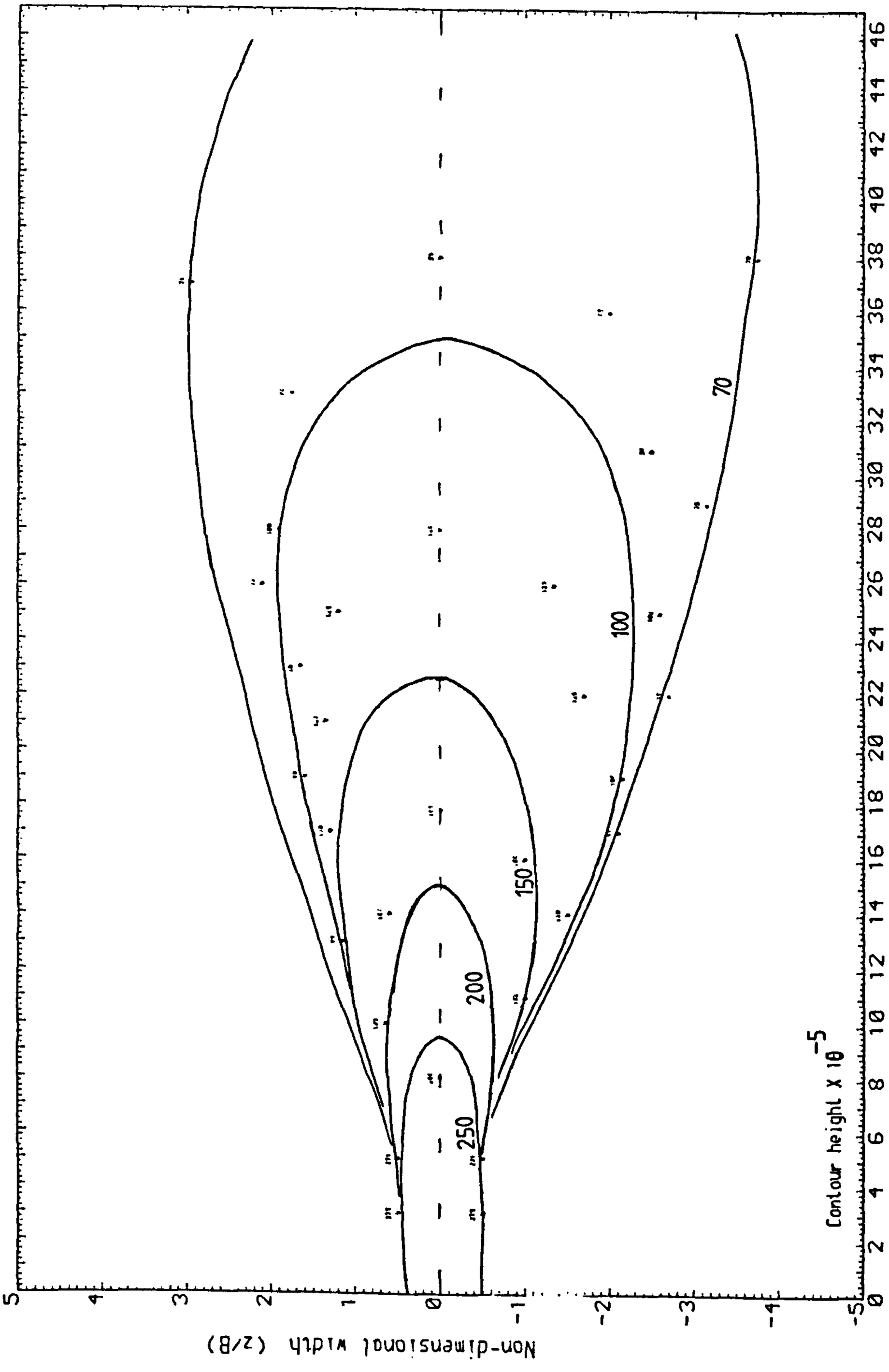

Fig.E-3 Mass transfer Stanton number contours for slot Reynolds number of 9100

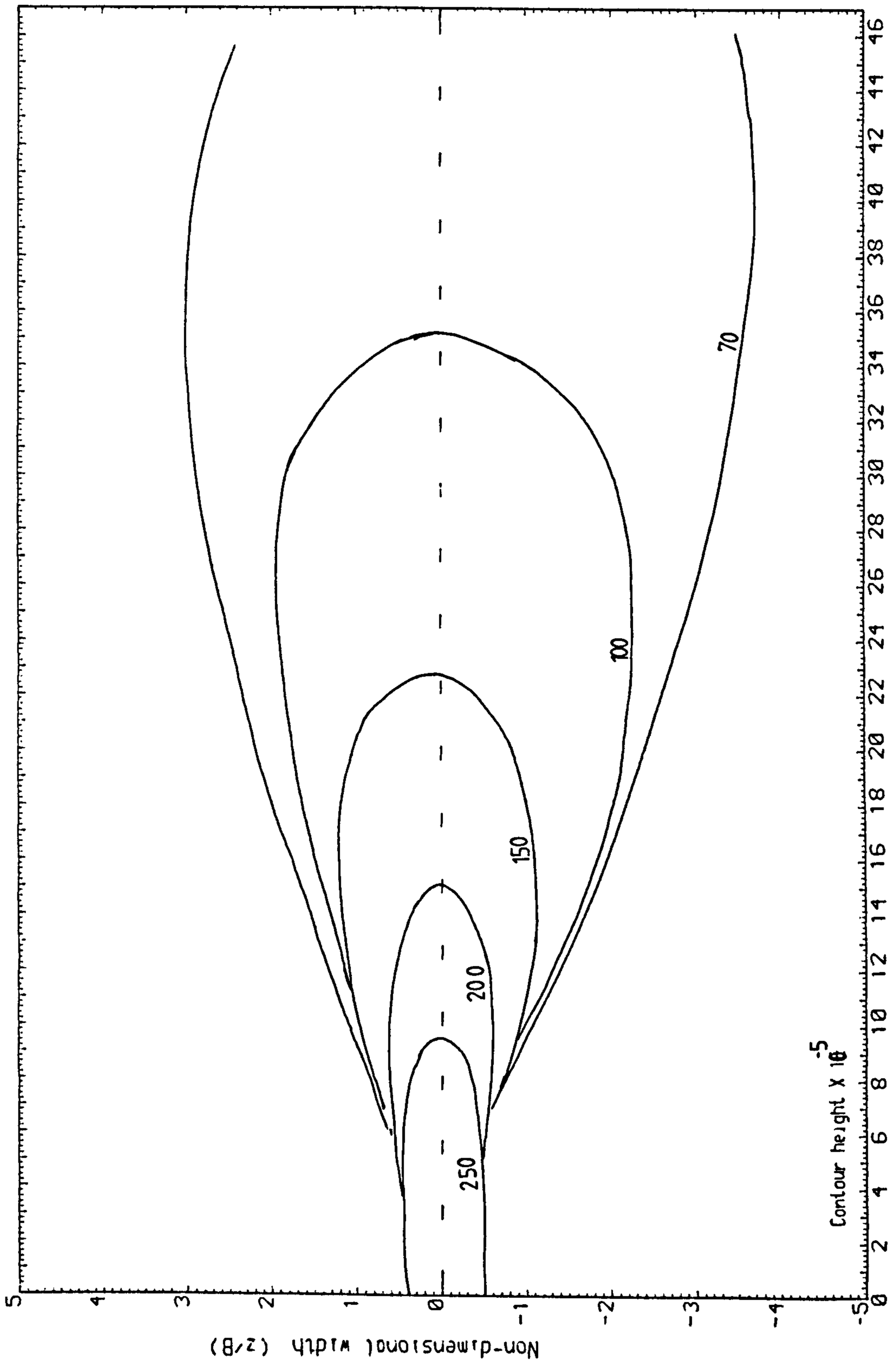

Fig.E-4 Mass transfer Stanton number contours For the slot Reynolds number of 9100

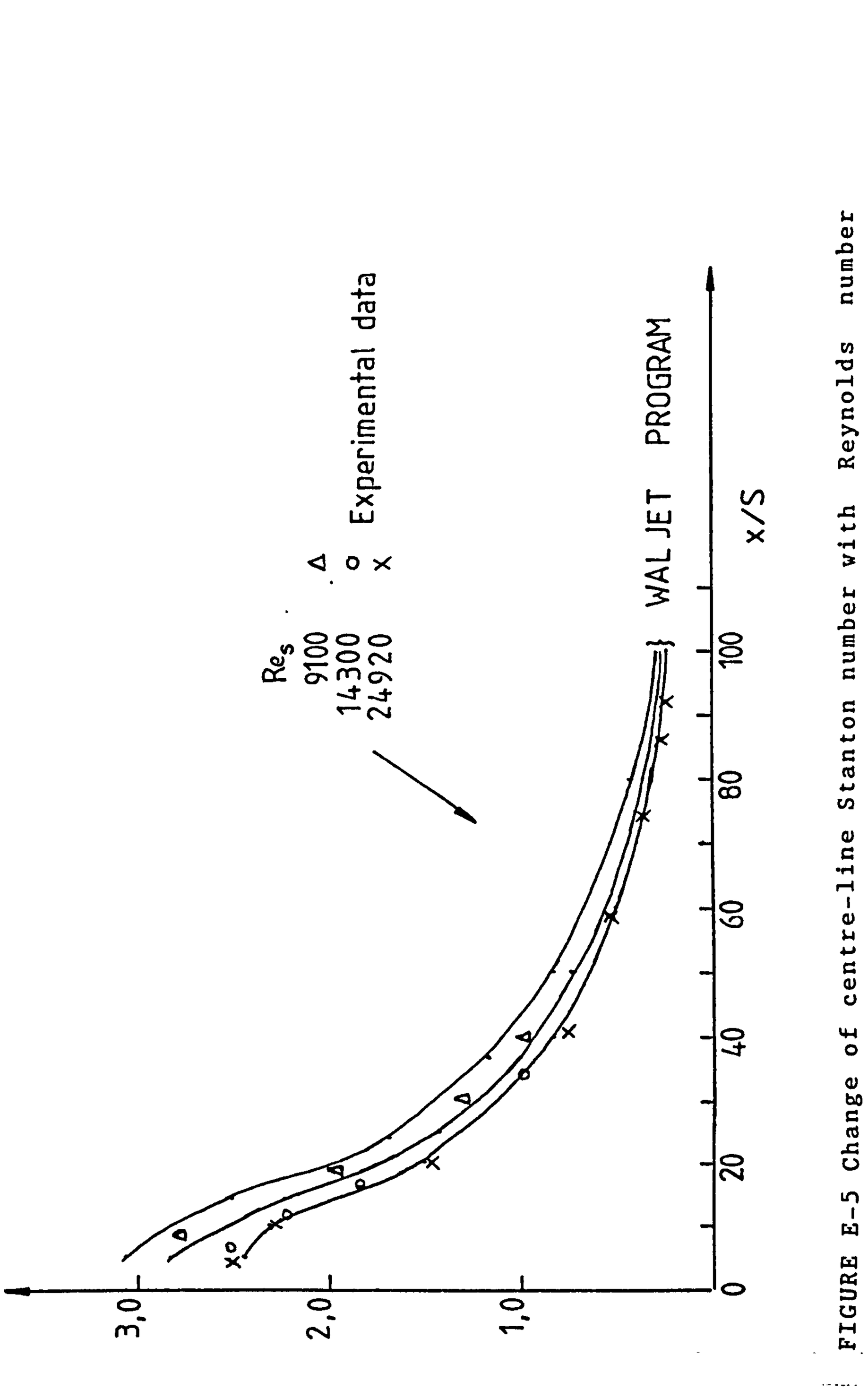

FIGURE E-5 Change of centre-line Stanton number with Reynolds number in a bluff wall-jet.

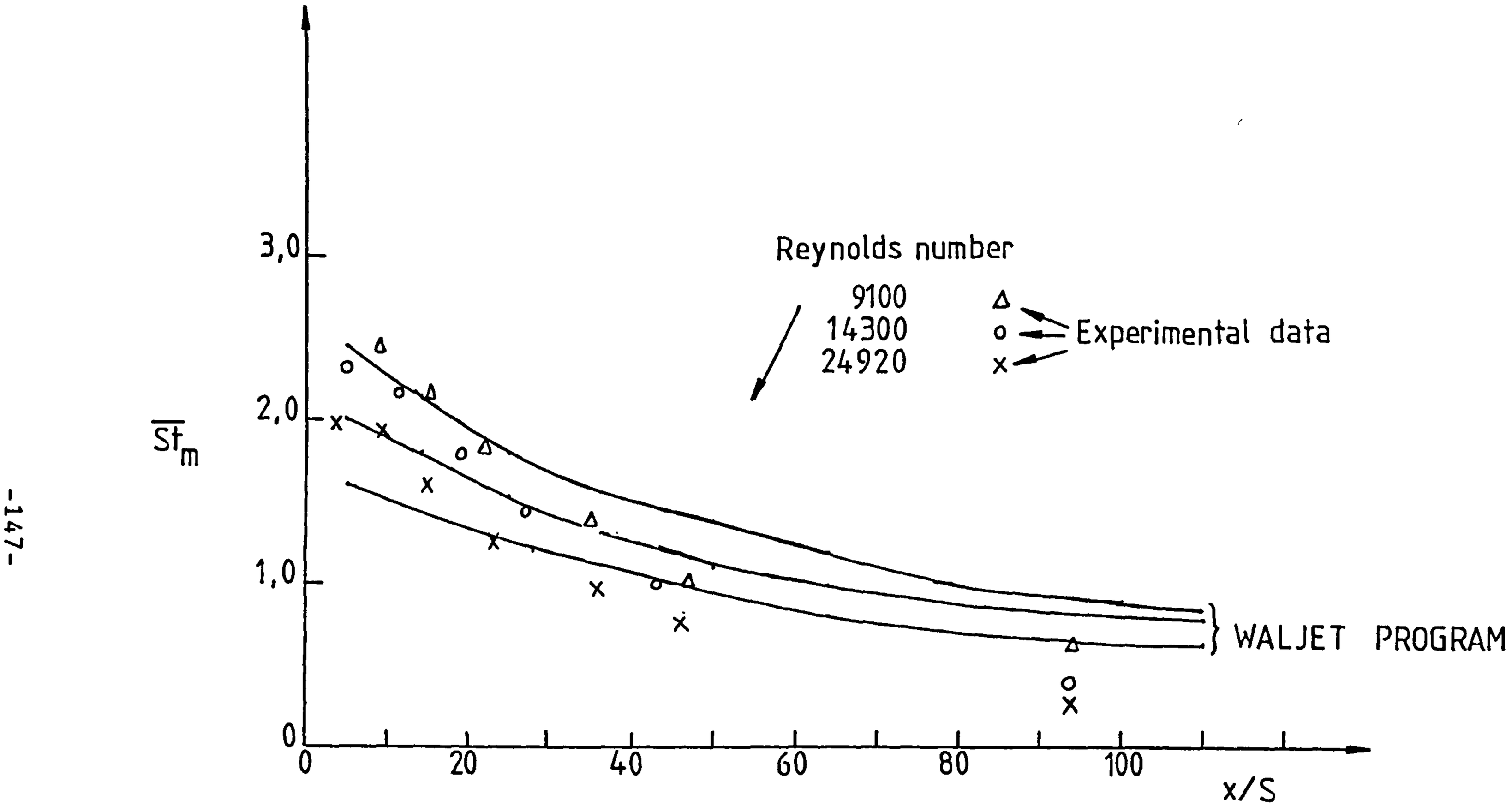

FIGURE E-6 Change of surface averaged Stanton number with Reynolds number in a bluff wall-jet.

BOUND PAPER

F.ALAMDARI, G.P.HAMMOND, N.MONTAZERIN

HEAT/MASS TRANSFER BENEATH A TWO-DIMENSIONAL WALL-JET DEFLECTED BY A NORMAL, FLAT-PLATE OBSTRUCTION

HEAT TRANSFER 1986: PROCEEDINGS OF THE EIGHTH INTERNATIONAL HEAT TRANSFER CONFERENCE, SAN FRANSCISCO, 1986 (HEMISPHERE, WASHINGTON: IN PRESS).

HEAT/MASS TRANSFER BENEATH A TWO-DIMENSIONAL WALL-JET DEFLECTED BY A NORMAL, FLAT-PLATE OBSTRUCTION

F. Alamdari, G.P. Hammond and N. Montazerin

School of Mechanical Engineering, Cranfield Institute of Technology
Bedford MK43 OAL, UK

Experimental measurements are reported of the local mass transfer distribution beneath a wall-jet emanating from a linear slot, which is deflected by a normal, flat-plate obstruction. This configuration was adopted to simulate the effect of wall-jet impingement on downstream backward - facing walls, such as occur in mechanically-ventilated enclosures. The mass transfer data was derived from the sublimation of a naphthalene thin-film on the blown surfaces. These measurements are compared with the computations of the 'intermediate-level' convection model of Alamdari and Hammond (1982) and the high-level 'elliptic' finite-domain flow model of Pun and Spalding (1977). Wall-jet profile analysis is used to aid the specification of the boundary conditions for passive scalar contaminants in these models, and to provide a rigorous expression for the heat/mass transfer analogy factor.

1. INTRODUCTION

In the aftermath of the 'oil crises' of the 1970's, the efficient use of energy in buildings has become an important priority for industrialised countries [1]. In order to assess the energy effectiveness of new building designs or evaluate the potential energy savings from alternative conservation measures for existing stock, it is necessary to accurately simulate the thermal performance of buildings. However, a weakness in all modern approaches to building thermal modelling is that emphasis is placed on simulating the transient response of the building fabric [1], while the air flow and convective heat exchange in and around the structure are modelled using only rough approximations.

In order to obtain improved ways of determining convective heat transfer data appropriate to the needs of building thermal simulation programs, a hierarchy of interacting and interdependent calculation methods have been developed by the authors and their co-workers [2]. They were originally developed for mechanically-ventilated enclosures, such as warm-air heated rooms or air-conditioned offices, in which the forced convective motion induced by the air supply jets predominates. The calculation methods themselves ranged from 'lower-level' approaches, such as wall-jet profile analysis [3,4], to the development of a 'high-level' flow model that solves finite-domain analogues to the governing 'elliptic' equations for the complex, jet-induced room airflow [2,5]. Both the higher and lower-level models have been used to develop and verify an 'intermediate-level' computer code [6], which formed the basis for generating input convective heat transfer data for dynamic building models. An apparent limitation of this intermediate-level model is that it cannot deal with the consequences of flow interactions. The model uses the known characteristics of turbulent wall-jets [3,4] to simulate air distribution systems in which the supply air jet is emitted near, and runs parallel to, one of the room surfaces. However, such wall-jets will inevitably be influenced by jet-impingement against backward-facing walls, and by 'secondary flows' or longitudinal vortices along streamwise corners. In the present contribution, experimental measurements are therefore reported of the local mass transfer distribution beneath a two-dimensional wall-jet deflected by a normal, flat-plate obstruction used to simulate the backward-facing wall situation. A schematic diagram of the flow configuration is presented in Figure 1. The measurements are compared with the computations of both the authors' intermediate-level convection code [6] and a high-level model [7].

2. EXPERIMENTAL SYSTEM

2.1 The Wall-jet Test Rig

The test rig used was designed to facilitate the experimental simulation of a wide range of wall-jet configurations. Its arrangement for the present studies is shown schematically in Figure 2. A two-stage centrifugal blower supplied air to the test section via a water-cooled heat exchanger (air cooler) and a bypass valve. The cooler extracted the energy transferred to the air stream by the blower, thereby reducing its temperature back down to that of the ambient air (~18 C). A flexible hose provides a connection between the bypass valve and the plenum chamber and air outlet nozzle. The plenum chamber was constructed from aluminium alloy sheet, with an inclined baffle plate located in the middle of the chamber to disperse the flow entering from the hose. A perforated plate traversing the chamber was also used to ensure a more uniform flow distribution before the supply air was channelled through a smooth, 4 : 1

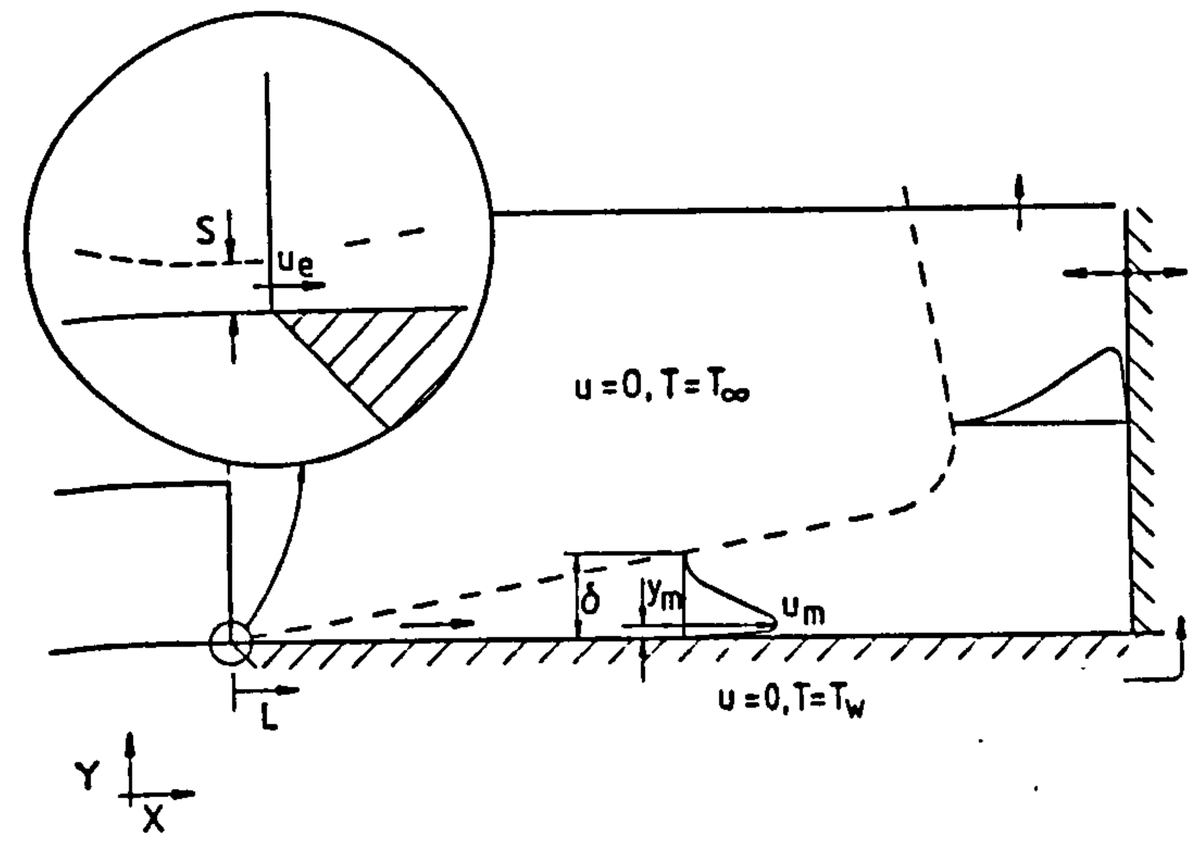

Figure 1 Flow configuration and notation.

contraction to the outlet nozzle. In the present studies, the nozzle plate was fabricated to produce a linear slot with a height (S) of 5 mm. The slot spanned the full width of the test section giving an aspect ratio (W/S) of 170. Pitot-tube traverses across the slot found essentially uniform time-averaged (mean) velocity distributions in both the transverse (Y) and spanwise directions. During the mass transfer tests, the exit velocity was determined from measurements of the total pressure in the plenum chamber, which were calibrated using the pitot-tube traverses.

The test section base plate was formed from rigid chip-board coated with a thermosetting plastic. The normal, deflection plate was made of rigid plywood, whose location in the test section could be easily adjusted as indicated in Figure 2. Perspex side walls were fitted to either side of the test section to limit spanwise dispersion of the jet flow ensuring two-dimensionality. Indeed, pitot-tube traverses within the wall-jet formed on the base plate indicated that the spanwise distribution of the peak mean velocity was essentially uniform. The jet emanating from the slot therefore flowed over the base plate as a nominally plane

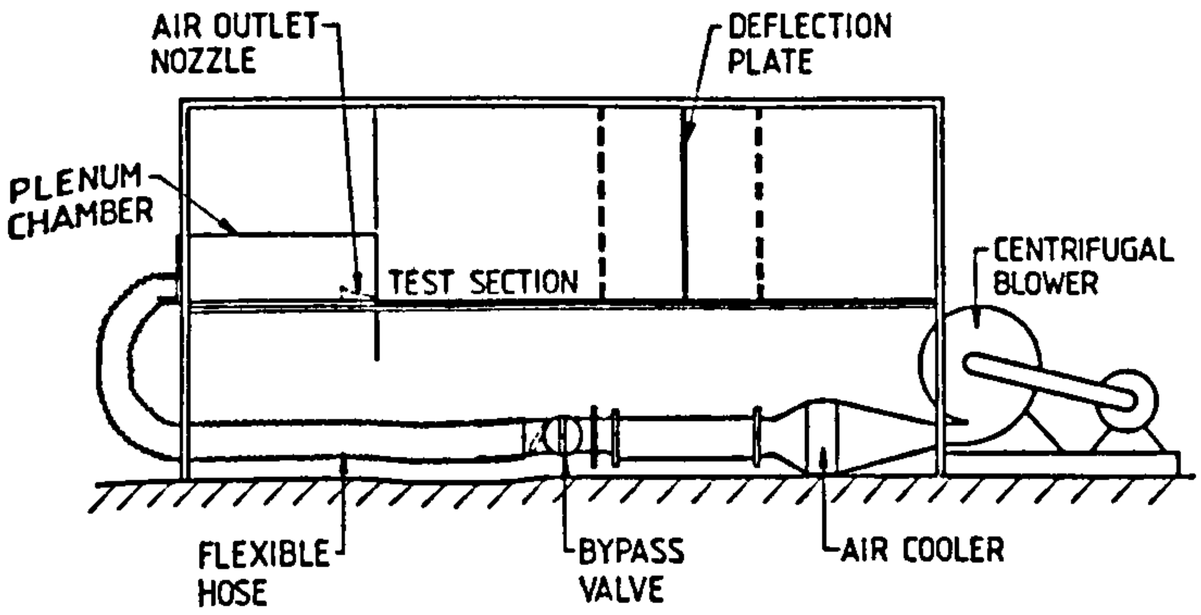

Figure 2 Schematic layout of wall-jet test rig.

wall-jet until it was deflected by the flat-plate obstruction. The deflected jet was then discharged vertically into the laboratory.

2.2. The Mass Transfer Measurement Technique

In order to determine the variation in local convective mass transfer coefficient beneath the wall-jet flow, measurements were made of the sublimation rate of naphthalene from the blown surfaces. A thin, uniform layer of naphthalene was sprayed onto perspex test plates using a spray rig similar to that originally conceived by Neal [8]. The spray rig and test procedure used in the present studies was developed by Ward and Mahmood [9], and is of rather simpler design. A removable test plug was sprayed simultaneously with each test plate, and the mass of naphthalene on this plug was then determined by accurate weighing. When conditioned air from the jet nozzle was blown over the test surfaces, the time taken for the naphthalene thin-film to clear from various points along the surface was observed. The mass transfer coefficient (β) is inversely proportional to this clearance time, and was determined from the expression [8,9]:

$$\beta = W R_n T / A t p_n \qquad (1)$$

where W is the mass of naphthalene on a test plug, A is the plug surface area, t is the clearance time, T is the naphthalene temperature, and p_n and R_n are the saturated vapour pressure and gas constant for the naphthalene respectively. The naphthalene vapour pressure is itself very sensitive to temperature [8], and the supply air temperature was therefore controlled within ± 0.5 C of the ambient.

The naphthalene-coated test plates were placed along the centreline of the jet test section, spanning a width of 42 cm (about 50 per cent of the section). The surrounding area was levelled using smooth plywood plates, in order to ensure that the blown surface was flush with both the test plate and the lower lip of the jet nozzle. Several test plates, 47 cm long, were required to cover the full streamwise length (L) for each test condition. Except for the case when the test plate was located immediately adjacent to the nozzle, a naphthalene-coated, dummy plate was always placed upstream of the test plate. This ensured a constant concentration boundary condition over the whole length of the test section. The spanwise clearance pattern was found to be essentially uniform, which provided an indirect confirmation of the two-dimensionality of the flow field.

Data for mass transfer at small concentrations may be used to yield heat transfer coefficients, provided an accurate relation for the analogy factor ($\phi \equiv St/St^*$) is available. The most widely used heat/mass transfer analogy is that due to Chilton and Colburn [10], which implies :

$$St\ Pr^{2/3} = St^*\ Sc^{2/3} \qquad (2)$$

Neal and others have recognised that this simple analogy factor [$\phi = (Sc/Pr)^{2/3}$] cannot adequately account for the differences in the effective diffusivities of heat and mass transport. Nevertheless, the use of this relation in connection with the thin-film naphthalene technique has been shown to give accurate heat transfer data for turbulent pipe-flow and for impinging jets by Neal [8] and Ward and Mahmood [9] respectively. The attraction of the method for the present authors is that it is free of surface conduction effects and of the complication of radiative exchange normally associated with the direct measurement of convective heat transfer.

3. HIGHER-LEVEL MATHEMATICAL MODEL

The high-level flow model employed in the present study was based on the CHAMPION computer code of Pun and Spalding [7]. The code solves finite-domain approximations to the governing partial-differential equations formulated in terms of 'primitive' pressure-velocity variables. Closure of these equations is obtained through an isotropic 'eddy' viscosity, or turbulent exchange coefficient for momentum, calculated via transport equations for both the turbulence kinetic energy and its dissipation rate. The transport of heat is modelled using the effective Prandtl number approach, while 'wall functions' are employed to bridge the steep property gradients in near-wall regions. The 'elliptic code' solves 'upwind' finite-domain equations for a two-dimensional, predetermined size, staggered grid in an iterative, 'line-by-line' manner using the SIMPLE algorithm of Patankar and Spalding [11]. In the present case a nonuniform grid of 21x21 nodes was employed. The jet inlet conditions were specified using wall-jet empirical data and the results of profile analysis [3,4] in a similar manner to that employed by Alamdari et al [2]. A 'block-correction' procedure, was applied in a line-by-line manner, after each iteration, in order to ensure mass conservation. Full details of the code, including the measures taken to ensure grid-independent solutions, are reported by Alamdari [5].

4. INTERMEDIATE-LEVEL MATHEMATICAL MODEL

In order to calculate the surface heat transfer within mechanically - ventilated enclosures, Alamdari and Hammond [6] developed an intermediate-level model in the form of a computer program they called the ROOM-CHT (Room Convective Heat Transfer) code. The program prescribes the flow and thermal field using the known characteristics of wall-jets [3,4], which are the normal means of air distribution in buildings with forced convective heating or cooling systems. Once the mean-flow field has been determined, the corresponding local heat transfer distribution across the surfaces is computed using the 'optimum log-law' devised by Hammond [4], on the basis of wall-jet profile analysis. The equations which constitute the ROOM-CHT program are generally explicit, algebraic ones, except for this heat transfer log-law which is implicit and is solved using the Newton-Raphson iterative method. Nevertheless, initial values for the flow field parameters are estimated from experimental data [3], and this enables a convergent solution to be obtained very rapidly; typically in about three iterations. The computational grid normally employs around 10 uniformly-spaced calculation points per metre length of surface. The mathematical details of the ROOM-CHT program are given in the previous papers of the authors [2-4, 6], and they are also set out in full in Alamdari's thesis [5].

5. HEAT/MASS TRANSFER BOUNDARY CONDITIONS

The earlier simulations performed using the intermediate-level, ROOM-CHT program [2,6] and higher-level, elliptic code [2] were for enclosures with forced convective heating or cooling systems. The thermal boundary conditions for a heated wall-jet [4] are $T_m > T_w = T_\infty$, where the suffices denote the peak (maximum), wall (surface), and free-stream conditions respectively. In this case, the thermal conditioning of the supply air takes place before it is discharged into the enclosure, and the wall-jet shear layer and thermal field thicknesses are nominally the same; $\delta = \delta_\theta$. However, the uniform naphthalene concentration boundary condition prevailing with the thin-film mass transfer technique is analogous to that of a heated plate of uniform temperature ($T_m = T_w > T_\infty$). Here the thermal field grows from the jet slot, and its thickness is always less than that of the shear layer; that is $\delta > \delta_\theta$. The wall-jet profile analysis of Hammond [4] for a heated or cooled jet must therefore be modified in order to enable the two computer codes to simulate the conditions for which the experimental data was obtained.

The wall-jet temperature profile outside the 'diffusive sublayer' may be closely represented by an expression, using conventional near-wall scaling of the form [4]:

$$T^+ = \frac{1}{\kappa_\theta} \ln y^+ + B_\theta + g_\theta \left[\pi_\theta, \frac{y^+}{\delta_\theta^+} \right] \qquad (3)$$

Hammond [4] adopted values of $\kappa_\theta = 0.48$ and $B_\theta = 12.5\ Pr^{2/3} - 5.8$ for the thermal log-law constants, and employed a quartic wake function, for the heated wall-jet which gave the cross-stream temperature profile shown in Figure 3. This profile was found to be dependent on both the molecular Prandtl number (Pr) and the local Reynolds number ($R_m \equiv u_m y_m / \nu$, see Figure 1). Guidance on the form of the wake function that would be appropriate in the heated plate situation may be obtained from the experimental data reported by Nizou [12]. His temperature profile measurements in an airflow resemble those for a turbulent boundary-layer. It can therefore be represented by the thermal analogue of the cubic

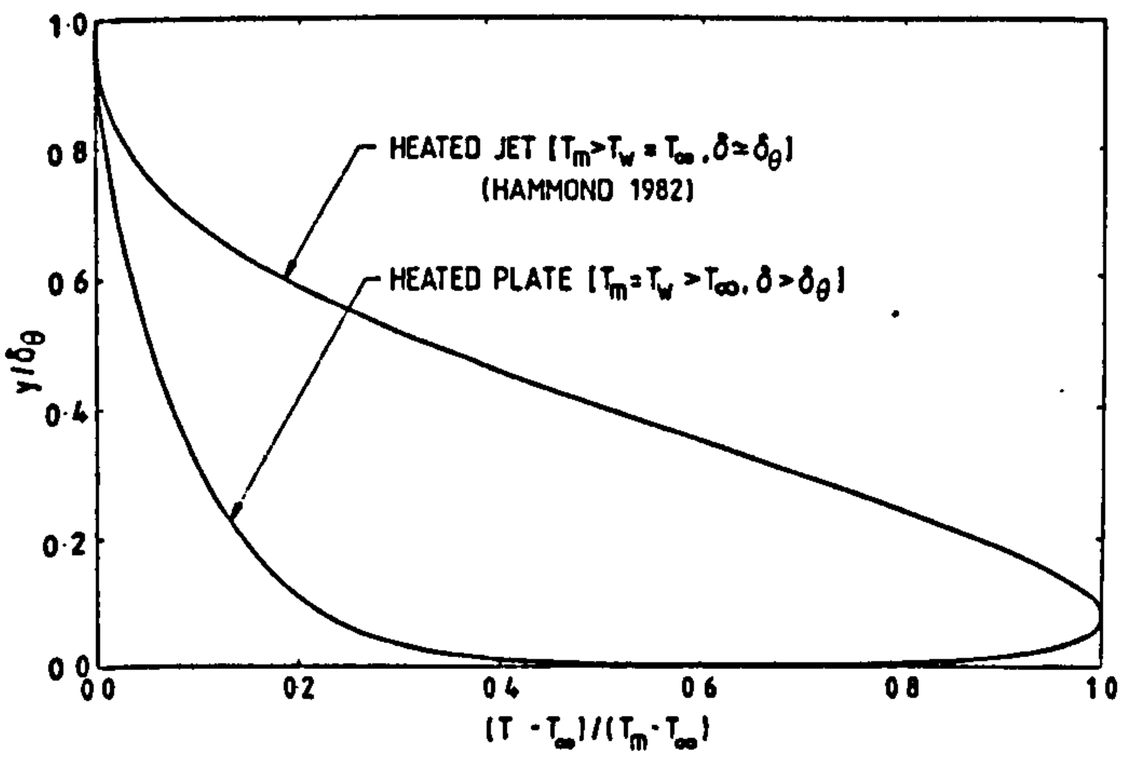

Figure 3 Wall-jet temperature distributions according to profile analysis ($R_m \simeq 10^4$ and Pr = 0.7).

velocity wake function derived by Dean [13] and others for the latter flow:

$$g_\theta\left(\pi_\theta, \frac{y^+}{\delta_\theta^+}\right) = \frac{1}{\kappa_\theta}(1+6\pi_\theta)\left(\frac{y^+}{\delta_\theta^+}\right)^2 - \frac{1}{\kappa_\theta}(1+4\pi_\theta)\left(\frac{y^+}{\delta_\theta^+}\right)^3 \qquad (4)$$

where Nizou's data [12] suggests that the thermal 'wake strength', π_θ, is effectively zero. The resulting temperature profile for the heated plate case (computed using the 'friction velocity' given by the previous wall-jet analysis [4]) is again displayed in Figure 3.

The heated plate temperature profile formula, equations (3) and (4), may be used to derive an expression for the Reynolds analogy factor ($St/0.5C_f$, where $C_f \equiv \tau_w / \frac{1}{2}\rho u_m^2$ is the 'skin friction' coefficient [3, 4]). This involves transforming the temperature formula at its free-stream boundary, and combining it with the previous velocity profile expression [4] transformed at the peak velocity location (y_m). Arranging in the most convenient form gives:

$$St / 0.5\, C_f = \qquad (5)$$

$$1 + \left[\frac{\ell n\{(\delta_\theta/\delta)(\delta/y_m)\} + \kappa_\theta B_\theta - \kappa B - \kappa g(y_m/\delta)}{\kappa}\right]\left(\frac{C_f}{2}\right)^{\frac{1}{2}}{}^{\kappa_\theta/\kappa}$$

where Hammond [4] adopts $\kappa = 0.41$ and $B = 5.2$ for the velocity log-law constants. This expression can be readily solved for given values of the wall-jet thickness ratio δ_θ / δ, if the previous analysis [4] is used to determine the ratio y_m / δ, the wake function at the velocity peak $g(y_m/\delta)$, and the skin friction coefficient, C_f.

In order to enable the above results to be incorporated into the ROOM-CHT and elliptic computer codes, it is necessary to determine an appropriate value for the wall-jet thickness ratio δ_θ / δ. This was obtained by using the elliptic code to compute the flow field development of an unobstructed, plane wall-jet, starting from the slot exit. The thickness ratio δ_θ / δ was found to be about 0.3 for the uniform concentration boundary condition and a Schmidt number (Sc) of 2.45, applicable to the naphthalene-air sublimation tests.

6. COMPUTATIONS AND MEASUREMENTS

6.1 Flow Field

Mean-flow data on the peak velocity decay and spread respectively of plane wall-jets may be presented in the form [3]:

$$\frac{u_m}{u_e} = K_u \left(\frac{x}{S}\right)^{-\frac{1}{2}} \quad \& \quad \frac{b_u}{S} = K_b \left(\frac{x}{S} + \frac{x_o}{S}\right) \qquad (6)$$

where b_u is the cross-stream distance from the wall to the point in the outer layer for which $u = 0.5\, u_m$. In a survey of published experimental data, Hammond [3] found mean values for the empirical constants (and their standard deviations) to be $K_u = 3.73$ ($\sigma = 0.57$), $K_b = 0.073$ ($\sigma = 0.007$), and $x_o/S = 8.10$ ($\sigma = 2.20$). Cross-stream pitot-tube traverses made in the undeflected region of the present wall-jet indicated that, at the slot Reynolds number prevailing in the mass transfer tests ($Re_s \equiv u_e S/\nu = 3330$), $K_u = 3.35$, $K_b = 0.084$, and $x_o/S = 11.0$. Although these values are not outside the range found in the above survey, they suggest a rather more rapid development than is the norm. However, at higher Reynolds numbers ($Re_s \simeq 1.5 \times 10^4$) the empirical constants were found to approach the mean values quite closely.

6.2. Surface Mass Transfer

The experimental mass transfer distributions obtained with the wall-jet test rig and the thin-film naphthalene technique are presented in Figure 4. Here the results for three streamwise locations of the deflection plate are shown, although only at a single slot Reynolds number ($Re_s = 3330$) as the qualitative behaviour is insensitive to this parameter. The experimental uncertainty in the mass transfer Stanton number ($St^* = \beta / u_e$) was found to be ± 7.5 per cent. The monotonic decay in the undeflected wall-jet region is characteristic of that found in plane wall-jets [6]. However, the augmentation in the mass transfer rate on the deflection plate is more reminiscent of the behaviour observed beneath a two-dimensional impinging jet. Locally high values are exhibited near the corner stagnation line, followed by another monotonic fall towards wall-jet values. The apparent dip in the transfer rate close to the corner is presumably due to the influence of the low velocity, inner layer in the wall-jet as it approaches the deflection plate.

The thin-film mass transfer data are compared with the computed results of the ROOM-CHT program and the elliptic code in Figure 4. Generally good agreement is displayed for the

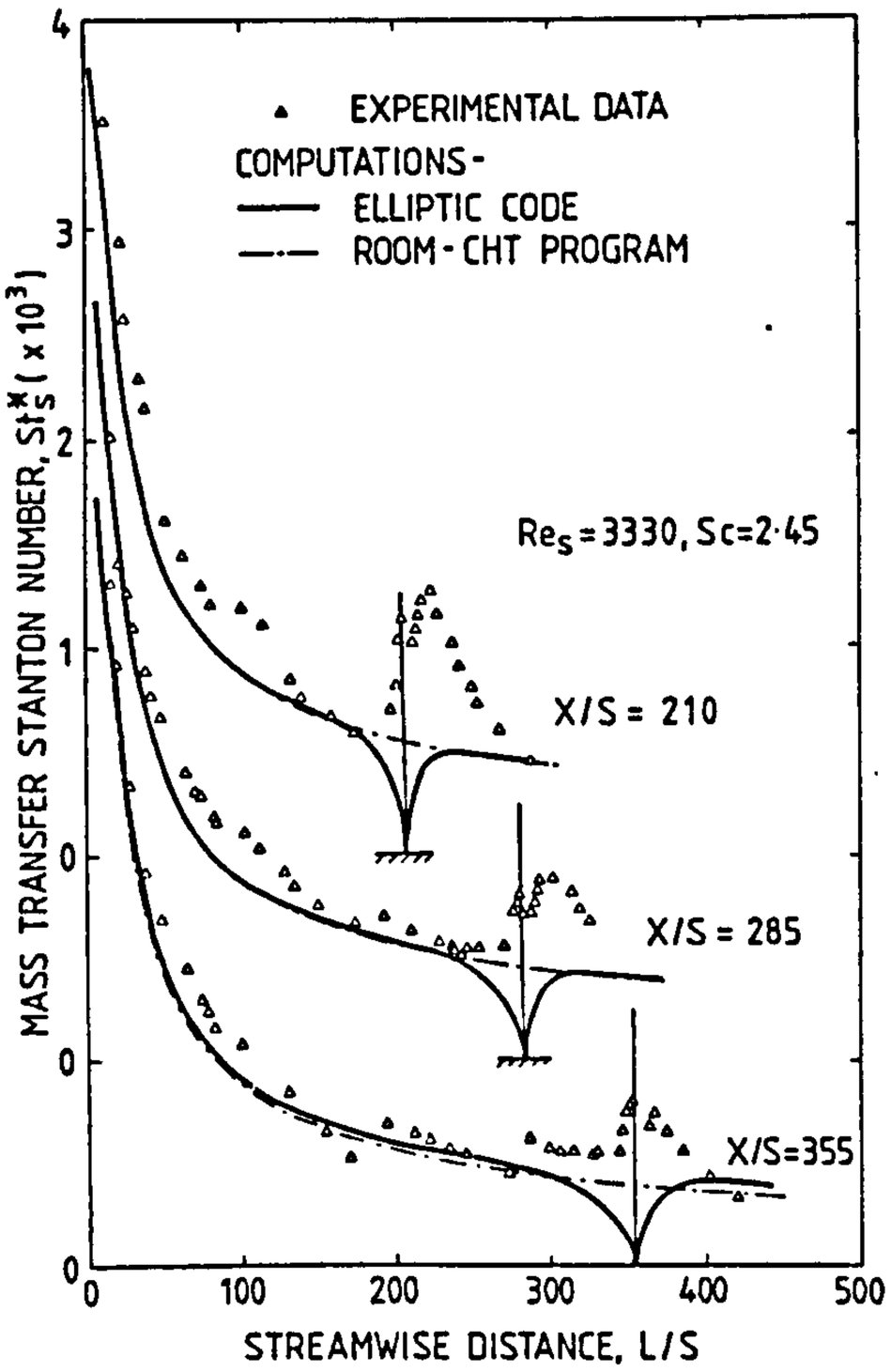

Figure 4 Wall-jet mass transfer distribution induced by a normal, flat-plate obstruction.

undeflected wall-jet flow along the base plate. However, appreciable differences are observed around the corner stagnation flow. The ROOM-CHT program displays a monotonic decay in mass transfer rate from the jet inlet onwards. In contrast, the more sophisticated elliptic code is better able to simulate the complex flow field, and correctly displays a stagnation line at the corner. Unfortunately, the turbulence model and wall functions [7,14] that are employed in the present version of the elliptic code imply $St^*/0.5\ C_f = f(Sc)$. The skin friction coefficient is zero along the stagnation line, and therefore the code yields $St^* = 0$ there. This may simply be regarded as a consequence of the current state-of-the-art, and future improvements in turbulence modelling will hopefully eliminate the direct coupling of momentum, heat and mass transfer in stagnation flows.

6.3. Heat/Mass Transfer Analogy Factors

In order to convert mass transfer measurements into equivalent heat transfer data, it is necessary to adopt an accurate expression for the analogy factor ($\phi \equiv St/St^*$). The popular Chilton-Colburn analogy, equation (2), is compared in Fig. 5 with the expressions used in the ROOM-CHT program and the elliptic code for the case of a plane wall-jet. The wall function for passive scalar contaminants used in the elliptic code is based on Jayatillaka's P-function [14]. This can easily be rearranged to display the variation shown in Fig. 5, if the skin friction coefficient is calculated via wall-jet profile analysis [4]. The 'standard' version of the ROOM-CHT program [2,6] uses the analogy factor for a heated wall-jet [4], while the present version employs that for the heated plate case from equation (5). The influence of the jet thickness ratio, δ_θ / δ, with the latter flow can be clearly seen in Figure 5. In common with the turbulent pipe-flow results of Neal [8], the simple Chilton-Colburn analogy is found to deviate significantly from the more rigorous expressions for wall-jets. The latter formulations require a knowledge of the skin friction coefficient, but they may be readily incorporated into higher- and intermediate- level computer codes, which normally calculate C_f simultaneously.

Building thermal models require convective heat transfer coefficients that are averaged over individual surfaces. Such data are presented in Table 1, along with the corresponding values computed by the ROOM-CHT program and the elliptic code. It can be seen that the data obtained using the Chilton-Colburn analogy is more that 30 per cent higher than that generated via the more rigorous wall-jet profile analysis for the heated plate case with $\delta_\theta / \delta = 0.3$. Good agreement is observed between the latter data and both sets of computations for the surface-averaged convection coefficient over the base plate. Not surprisingly in view of their failure to simulate the jet-impingement effect, the computations for the deflection plate are lower than the profile-analysis-converted experimental data. Fortunately, such disparities would have rather smaller impact when used in conjunction with building thermal models for practical geometries. This is because the relative length of far walls [6] (corresponding to the deflection plate) would be longer, and the jet-impingement effect would consequently have less influence on the surface-averaged coefficient over this surface. In any case, the convective exchange within an enclosure is coupled with the thermal radiation heat transfer,

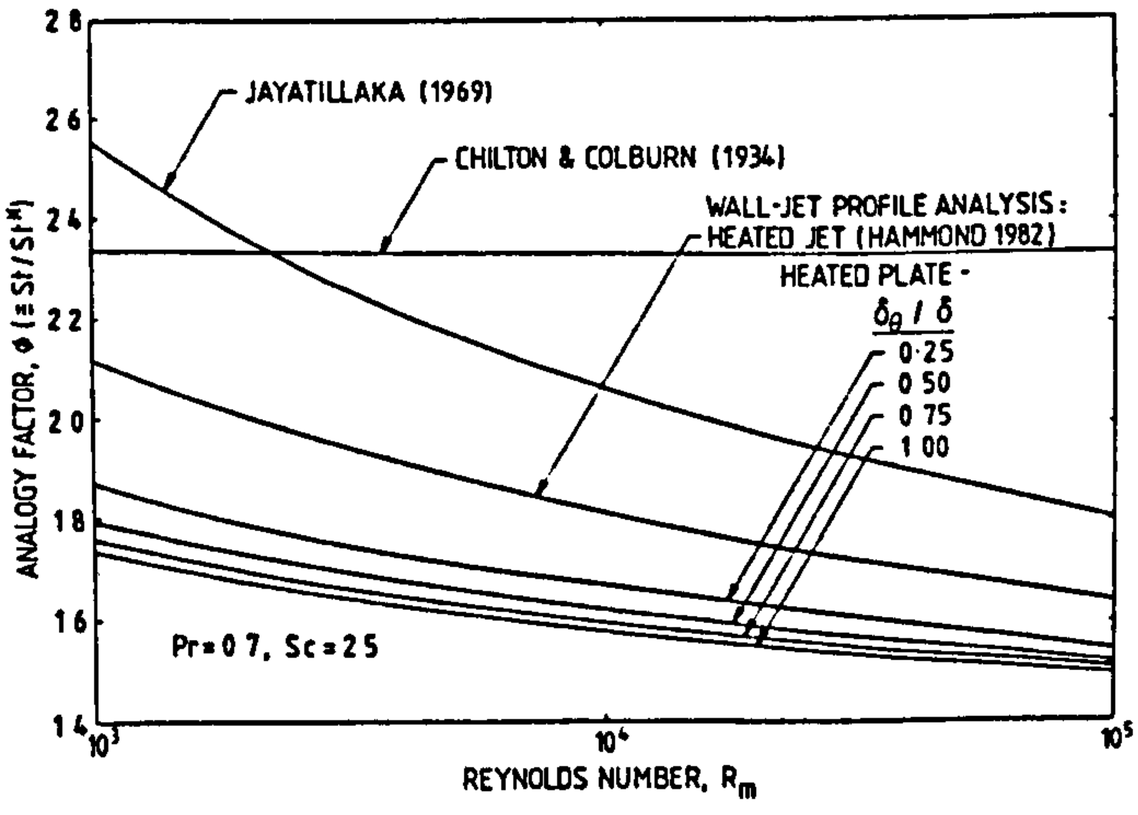

Figure 5 Heat/mass transfer analogy factors for plane wall-jets.

Table 1. Surface-averaged Convective Heat Transfer Coefficients ($\bar{h}$, W/m^2K)

	Base Plate			Deflection Plate		
Deflection Plate Location, X/S	210	285	355	210	285	355
Experiment :						
Chilton-Colburn Analogy	35.2	27.9	25.3	23.3	19.1	14.5
Wall-jet Profile Analysis	27.5	21.4	19.2	17.7	14.5	10.9
Computations:						
ROOM-CHT Program	27.7	24.0	20.5	9.6	8.3	7.2
Elliptic Code	28.1	25.4	22.4	10.7	10.7	10.1

and this will further reduce the real impact of errors in the former.

7. CONCLUDING REMARKS

The computations presented here support the ascertion by Alamdari et al [2] that intermediate-level computer codes offer the best prospect for meeting the convective heat transfer data needs of dynamic building thermal models in terms of accuracy, economy and user friendliness. The ROOM-CHT program took 1/15th of the central processor time used by the elliptic code to compute the heat/mass transfer beneath the present deflected wall-jet flow. Despite the fact that the former code contains both two- and three-dimensional versions, it only utilised two-thirds of the computer storage capacity of the two-dimensional elliptic code. Indeed, it would not be realistic in computational terms to directly couple a high-level flow model to a building thermal simulation program, whereas it has already been demonstrated that the authors' intermediate-level computer codes can be fairly readily incorporated into these programs as subroutines [2].

The experimental local mass transfer data obtained in the present study can, in addition to aiding the verification of the particular models used here, be employed to assess other numerical calculation procedures for complex turbulent flows. Such data provides a stringent test case, which requires accurate simulation of both the outer and near-wall flow regimes.

ACKNOWLEDGEMENTS

The work reported here was supported by the UK Science and Engineering Research Council Grant GR/C/2419.0, and forms part of the Council's specially promoted programme on 'Energy in Buildings'. The authors are grateful to Mr. C.K. Mok, who made some of the mean-flow measurements. They are also appreciative of the care with which Mrs. A. Stalley prepared the camera-ready typescript, and Mrs. K. O'Connell traced the figures.

The authors' names appear alphabetically.

REFERENCES

1. Clarke, J.A., Energy Simulation in Building Design, Adam Hilger, Bristol, 1985.
2. Alamdari, F., Hammond, G.P., and Melo, C., 'Appropriate' Calculation Methods for Convective Heat Transfer from Building Surfaces, Proc. First UK National Heat Transfer Conf., Leeds, vol. 2, pp 1201-1211, 1984.
3. Hammond, G.P., Complete Velocity Profile and 'Optimum' Skin Friction Formulas for the Plane Wall - jet, ASME J. Fluids Eng., vol. 104, pp 59-66, 1982.
4. Hammond, G.P., Profile Analysis of Heat / Mass Transfer Across the Plane Wall - jet, Proc. 7th Int. Heat Transfer Conf. Munich, vol. 3, pp 345-355, 1982.
5. Alamdari, F., Convective Heat Transfer within Mechanically - ventilated Building Spaces, Ph.D. Thesis, Cranfield Institute of Technology, UK, 1984.
6. Alamdari, F., and Hammond, G.P., Time-dependent Convective Heat Transfer in Warm-air Heated Rooms, Proc. 3rd Int. Symp. Energy Conservation in the Built Environment, Dublin, vol. 4, pp 209-220, 1982.
7. Pun, W.M., and Spalding, D.B., A General Computer Program for Two-dimensional Elliptic Flows, Imperial College (London) Mech. Eng. Dept. Rept. HTS/76/2, Amended 1977.
8. Neal, S.H.B.C., The Development of the Thin-film Naphthalene Mass Transfer Analogue Technique for the Direct Measurement of Heat Transfer Coefficients, Int. J. Heat Mass Transfer, vol. 18, pp 559-567, 1975.
9. Ward, J., and Mahmood, M., Heat Transfer from a Turbulent Swirling, Impinging Jet, Proc. 7th Int. Heat Transfer Conf., Munich, Vol. 3, pp 401-407, 1982.
10. Chilton, T.H., and Colburn, A.P., Mass Transfer (Absorption) Coefficients, Ind. Eng. Chem., vol. 26, pp 1183-1187, 1934.
11. Patankar, S.V., and Spalding, D.B., A Calculation Procedure for Heat, Mass and Momentum Transfer in Three - dimensional Parabolic Flows, Int. J. Heat Mass Transfer, vol. 15, pp 1787-1806, 1972.
12 Nizou, P.Y., Analogy Between Heat and Momentum Transfer in Plane Turbulent Wall-Jet, Int. J. Heat Mass Transfer, vol. 27, pp 1737-1748, 1984.
13. Dean, R.B., A Single Formula for the Complete Velocity Profile in a Turbulent Boundary Layer, ASME J. Fluids Eng., vol. 9 8 , pp 723-727, 1976.
14. Jayatillaka, C.V.L., The Influence of Prandtl Number and Surface Roughness on the Resistance of the Laminar Sub - layer to Momentum and Heat Transfer, Prog. Heat Mass Transfer, vol. 1, pp 193-329, 1969.

Table 1. Surface-averaged Convective Heat Transfer Coefficients ($\bar{h}$, W/m^2K)

	Base Plate			Deflection Plate		
Deflection Plate Location, X/S	210	285	355	210	285	355
Experiment :						
Chilton-Colburn Analogy	35.2	27.9	25.3	23.3	19.1	14.5
Wall-jet Profile Analysis	27.5	21.4	19.2	17.7	14.5	10.9
Computations:						
ROOM-CHT Program	27.7	24.0	20.5	9.6	8.3	7.2
Elliptic Code	28.1	25.4	22.4	10.7	10.7	10.1

and this will further reduce the real impact of errors in the former.

7. CONCLUDING REMARKS

The computations presented here support the ascertion by Alamdari et al [2] that intermediate-level computer codes offer the best prospect for meeting the convective heat transfer data needs of dynamic building thermal models in terms of accuracy, economy and user friendliness. The ROOM-CHT program took 1/15th of the central processor time used by the elliptic code to compute the heat/mass transfer beneath the present deflected wall-jet flow. Despite the fact that the former code contains both two- and three-dimensional versions, it only utilised two-thirds of the computer storage capacity of the two-dimensional elliptic code. Indeed, it would not be realistic in computational terms to directly couple a high-level flow model to a building thermal simulation program, whereas it has already been demonstrated that the authors' intermediate-level computer codes can be fairly readily incorporated into these programs as subroutines [2].

The experimental local mass transfer data obtained in the present study can, in addition to aiding the verification of the particular models used here, be employed to assess other numerical calculation procedures for complex turbulent flows. Such data provides a stringent test case, which requires accurate simulation of both the outer and near-wall flow regimes.

ACKNOWLEDGEMENTS

The work reported here was supported by the UK Science and Engineering Research Council Grant GR/C/2419.0, and forms part of the Council's specially promoted programme on 'Energy in Buildings'. The authors are grateful to Mr. C.K. Mok, who made some of the mean-flow measurements. They are also appreciative of the care with which Mrs. A. Stalley prepared the camera-ready typescript, and Mrs. K. O'Connell traced the figures.

The authors' names appear alphabetically.

REFERENCES

1. Clarke, J.A., Energy Simulation in Building Design, Adam Hilger, Bristol, 1985.
2. Alamdari, F., Hammond, G.P., and Melo, C., 'Appropriate' Calculation Methods for Convective Heat Transfer from Building Surfaces, Proc. First UK National Heat Transfer Conf., Leeds, vol. 2, pp 1201-1211, 1984.
3. Hammond, G.P., Complete Velocity Profile and 'Optimum' Skin Friction Formulas for the Plane Wall - jet, ASME J. Fluids Eng., vol. 104, pp 59-66, 1982.
4. Hammond, G.P., Profile Analysis of Heat / Mass Transfer Across the Plane Wall - jet, Proc. 7th Int. Heat Transfer Conf. Munich, vol. 3, pp 345-355, 1982.
5. Alamdari, F., Convective Heat Transfer within Mechanically - ventilated Building Spaces, Ph.D. Thesis, Cranfield Institute of Technology, UK, 1984.
6. Alamdari, F., and Hammond, G.P., Time-dependent Convective Heat Transfer in Warm-air Heated Rooms, Proc. 3rd Int. Symp. Energy Conservation in the Built Environment, Dublin, vol..4, pp 209-220, 1982.
7. Pun, W.M., and Spalding, D.B., A General Computer Program for Two-dimensional Elliptic Flows, Imperial College (London) Mech. Eng. Dept. Rept. HTS/76/2, Amended 1977.
8. Neal, S.H.B.C., The Development of the Thin-film Naphthalene Mass Transfer Analogue Technique for the Direct Measurement of Heat Transfer Coefficients, Int. J. Heat Mass Transfer, vol. 18, pp 559-567, 1975.
9. Ward, J., and Mahmood, M., Heat Transfer from a Turbulent Swirling, Impinging Jet, Proc. 7th Int. Heat Transfer Conf., Munich, Vol. 3, pp 401-407, 1982.
10. Chilton, T.H., and Colburn, A.P., Mass Transfer (Absorption) Coefficients, Ind. Eng. Chem., vol. 26, pp 1183-1187, 1934.
11. Patankar, S.V., and Spalding, D.B., A Calculation Procedure for Heat, Mass and Momentum Transfer in Three - dimensional Parabolic Flows, Int. J. Heat Mass Transfer, vol. 15, pp 1787-1806, 1972.
12 Nizou, P.Y., Analogy Between Heat and Momentum Transfer in Plane Turbulent Wall-Jet, Int. J. Heat Mass Transfer, vol. 27, pp 1737-1748, 1984.
13. Dean, R.B., A Single Formula for the Complete Velocity Profile in a Turbulent Boundary Layer, ASME J. Fluids Eng., vol. 9 8 , pp 723-727, 1976.
14. Jayatillaka, C.V.L., The Influence of Prandtl Number and Surface Roughness on the Resistance of the Laminar Sub - layer to Momentum and Heat Transfer, Prog. Heat Mass Transfer, vol. 1, pp 193-329, 1969.